Development of a Lignin Substituted Thermoset for Fiber Reinforced Polymers

Entwicklung von Lignin–substituierten Duroplasten für faserverstärkte Kunststoffe

TECHNISCHE UNIVERSITÄT DARMSTADT

Vom Fachbereich Chemie der Technischen Universität Darmstadt
zur Erlangung des akademischen Grades eines

Doktor-Ingenieurs (Dr.–Ing.)

genehmigte

Dissertation

vorgelegt von

Dipl.–Ing. Sabrina Mehlhase

aus Rüsselsheim

Referent: Prof. Dr. Matthias Rehahn
Korreferent: Prof. Dr. Markus Biesalski
Tag der Einreichung: 16. März 2016
Tag der mündlichen Prüfung: 02. Mai 2016

Darmstadt 2016
D 17

Development of a Lignin Substituted Thermoset for Fiber Reinforced Polymers
Entwicklung von Lignin–substituierten Duroplasten für faserverstärkte Kunststoffe

Vom Fachbereich Chemie der Technischen Universität Darmstadt zur Erlangung des akademischen Grades eines Doktor-Ingenieurs (Dr.–Ing.) genehmigte Dissertation vorgelegt von Dipl.–Ing. Sabrina Mehlhase aus Rüsselsheim.

Referent: Prof. Dr. Matthias Rehahn
Korreferent: Prof. Dr. Markus Biesalski

Tag der Einreichung: 16. März 2016

Darmstadt — D 17

Die vorliegende Arbeit wurde am Ernst-Berl-Institut für Technische Chemie und Makromolekulare Chemie der Technischen Universität Darmstadt unter der Leitung von Herrn Prof. Dr. Matthias Rehahn und Herrn Dr. Roland Klein in der Zeit von Oktober 2011 bis April 2015 durchgeführt.

Danksagung

Meinem Doktorvater Prof. Dr. Matthias Rehahn möchte ich herzlichst für die Möglichkeit in seinem Arbeitskreis zu promovieren danken. Desweiteren möchte ich meinem Betreuer Dr. Roland Klein für die stete Unterstützung und anregenden Diskussionen danken sowie die Möglichkeit auf diesem sehr spannenden Themengebiet forschen zu können.

Herrn Prof. Dr. Markus Biesalski möchte ich für die freundliche Übernahme des Korreferats und die Betreuung im Rahmen des TUD–UPM Lab Projekts danken.

Nicht nur für die finanzielle Unterstützung, sondern auch für die Bereitstellung der Lignine sowie die gute Zusammenarbeit und hilfreichen Diskussionen, möchte ich mich bei UPM und speziell bei Frau Valkonen, Frau Dr. Trellenkamp, Herrn Dr. Duetsch und Herrn Dr. Ringena bedanken. Dies gilt auch für alle weiteren Kooperationspartner des UPM-TUD Lab–Projekts: den Arbeitskreisen von Prof. Dr. Biesalski, Prof. Dr. Schabel der TU Darmstadt, der Papiertechnischen Stiftung sowie dem Fraunhofer LBF. Hierbei möchte ich Matthias Baaske, Jennifer Dietz, Henri Kröling, Johanna Fleckenstein und Narmin Nubbo für die Zusammenarbeit und hilfreiche Diskussionen danken.

Besonders möchte ich mich bei meinem Arbeitskreis bedanken. Ihr seid meine zweite Familie und ein großartiger Haufen. Der F–Turm Gang Christopher, Daniel, Elmo, Tschiffy und Steffen danke ich für den sehr unterhaltsamen (Büro–)alltag. Conny danke ich für alle Ratschläge und Gespräche und die Fähigkeit alles positiv zu sehen.

Meinen Bachelor–Studenten Tamara Winter, Jens–Kai Reuter und Sunna Möhle möchte ich für das Produzieren toller Ergebnisse und die gute Zeit bedanken die ich mit Ihnen hatte.

Da das Wichtigste zum Schluss kommt, möchte ich mich nun bei meiner Familie bedanken. Meinen Eltern danke ich dafür, dass sie mir diesen Weg ermöglicht haben und immer für mich da sind. Dies gilt natürlich auch für meine Oma Karola. Meinem Onkel Mathias möchte ich für wichtige Lektionen des Lebens bedanken, vor allem die mit dem Schwan. Ich danke auch meinen Schwiegereltern, und meinen “Schwestern” Katrin und Britta.

Meinem Mann Stephan danke ich dafür, dass du mein Fels in der Brandung bist und nie aufhörst an mich zu glauben. Ohne dich wäre das nicht möglich gewesen.

Contents

Abbreviations

α	Conversion of the reaction
A	Pre exponential factor
acKL	Acetylated kraft lignin
awKL	Acid washed kraft lignin
cf.	see also
CFC	Carbon fiber reinforced composite
CYDDGE	1,6-cyclohexanedimethanol diglycidyl ether
ΔH_{tot}	Total heat of reaction
DoC	Degree of cure
DSC	Dynamic scanning microscopy
DMTA	Dynamic mechanical thermal analysis
DGEBA	Digylcidyl ether of bisphenol A
DETA	Diethylene triamine
DICY	Dicyandiamide
νDICY	Micronized dicyandiamide
ϵ_b	Strain at break
E_a	Activation energy
E	Young's modulus
EHL	Enzymatic hydrolyzed lignin
EEW	Epoxy equivalent weight
FRP	Fiber reinforced polymer
FT-IR	Fourier transform infrared spectroscopy
G'	Storage modulus
G"	Loss modulus
GC	Gel chromatography
GFC	Glass fiber reinforced composite
GPC	Gel permeation chromatography
HDDGE	1,6–hexandiole diglycidyl ether
HPPDGE	Polypropyleneglycol diglycidyl ether
IPDA	Isophorondiamine
k_1	Rate constant of the initial reaction
k_2	Rate constant of the autocatalytic reaction
KL	Kraft lignin
KL 1	Kraft lignin 1
KL 2	Kraft lignin 2
KL 3	Kraft lignin 3
μ	Dynamic Viscosity
m	Reaction order of the initial reaction

M_n	Number average molar mass
M_w	Mass average molar mass
m_f	Mass of the fibers
m_L	Mass of lignin
$m_{Composite}$	Mass of the composite
MI	Methyl imidazole
MS	Mass spectroscopy
v_R	Reaction rate
N	Number of Monomers
n	Reaction order of the autocatalytic reaction
NMR	Nuclear magnetic resonance
Φ	Bio-content
Ψ	Fiber mass fraction
PDI	Polydispersity index
p	Degree of consersion
P_n	Degree of polymerization
q	heat flow
q_T	Maximum heat flow at maximum conversion
R	Tensile strength
σ_b	Strength at break
SEM	Scanning electron microscopy
$\tan\delta$	Loss factor
TGA	Thermogravimetric analysis
T_g	Glass transition temperature
TMPTGE	Trimethylopropane triglycidyl ether
UR	Urone
xpKL	extra–pure kraft lignin

1 Introduction

Due to rising oil prices, changing consumption habits, increased awareness about CO_2 emissions, recycling and the lack of landfills, the demand for environmental awareness and friendliness is growing worldwide. Biodegradable plastics and bio–based polymer products from renewable resources can form eco–friendly and sustainable products. Those can compete in markets dominated today by petroleum-based products. By now, for high–volume applications, such as packaging, these products are mainly based on biomass derived raw materials with typical utilized bioplastics such as polylactic acid (PLA), polyhydroxyalkanoates (PHA) and cellophane. [1,2]

The soaring price for raw materials has forced the use of natural materials for development and fabrication of polymer composites. [3] Biofiber reinforced polymers based on agricultural products have appealing properties: they are at least partially recyclable, offer a solution for waste disposal and reduction in agricultural residues. The re-use of residues offers an economical solution for farming and rural areas in developing countries. [4]

Natural fibers such as flax, hemp, straw, kenaf and jute offer excellent properties at low cost and are easily available. Therefore, natural fiber reinforcement has gained much impetus to substitute synthetic fibers like glass, carbon and aramid fibers in various applications, especially in car manufacturing. Today, a new car is constructed with an average of 4.5 kg of natural fiber reinforced polymer composite. In some particularly eco–friendly brands the amount of composite material reaches 50 kg. Especially the use in parts such as door paneling, dashboards, glove and luggage compartments, rear shelves and autoskies has already advanced to large-scale production. [5,6]

Among the fiber reinforced polymers the application as fillers has a significant importance. The development of starch fillers, coconut-shell particle fillers, keratin derived from chicken feathers and wood flour have been actively pursued. [7–9] A wood derived alternative is presented by lignin which is a highly abundant biopolymeric material that constitutes along with cellulose as a major component of higher vascular plants. [10]

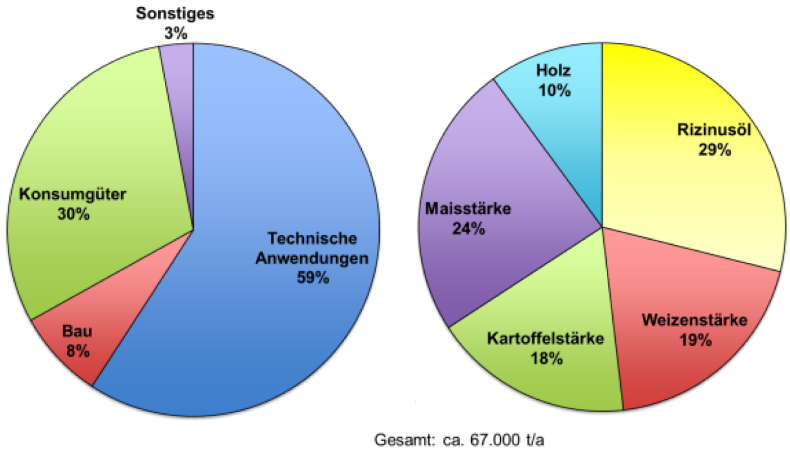

Figure 1.1.: Application areas of natural fiber reinforced plastics (left) and the demand of raw materials for the production of biobased plastics (right) in Germany. [5]

Lignin is one of the most abundant renewable resource amid cellulose and plant oils. It is available throughout the year from numerous pulping processes such as biorefinery and paper manufacturing.[11–13] In Germany, wood occupies an agricultural area of 11.1 million hectare which is roughly 31 % of Germany's total territory. Only around 10 % of biobased plastics are created from wood.[5] Taking into account that applications such as packaging materials build the majority of demand for natural fiber reinforced plastics (cf. Figure 1.1), one can presume a great growth potential.

Lignin can be attained from a great variety of origins and pulping processes. One major disadvantage of lignin is its complex and undefined structure, which limits its utilization. However, the abundance and its highly functional character makes lignin (predominantly lignosulfonates) an excellent raw material for industrial applications.[14]

It is possible to introduce lignin chemically either modified or unmodified in its raw form. Chemical modification of lignin can be broken down into three groups:

1. Fragmentation of lignin into its aromatic compounds for fine chemistry.[15,16]
2. Synthesis of new chemical active sites to impart new reactivity including amination, sulfonation, halogenation.[17,18]
3. Functionalization of the hydroxyl groups with propylene oxide, ethylene oxide and chloroacetic acid for increasing reactivity.[19,20]

In its unmodified form lignin has been introduced to thermoplastic compounds already. Blends of lignin with the recyclable polymers polyethylene terephthalate (PET) and polypropylene (PP) have been spun to fibers followed by carbonization leading to biobased carbon fibers.[21] Building panels using lignocellulosic particles in thermoplastic binders such as polyurethanes and polypropylene are known under the trademark Nadura®.[22] Ziegler et al.[23] developed a lignin based thermoplastic with hemp fibers as reinforcement material which was easily processable in typical plastic processing technologies such as injection moulding, extrusion moulding and compression moulding. Their approach has since resulted in the ARBOFORM® products which has great potential in sustainable and fire resistant applications.[24,25] It is used in various applications such as cabinet material, housing material for loudspeakers and in electronic devices such as circuit boards.[26] Also, further processing via carbonization to porous carbon materials for filters, absorbents, precursors for infiltration with silicon to produce silicon–carbon ceramics and even lignin–derived nanoporous carbon for supercapacitor applications is possible.[27–29]

Thermosetting polymers (thermosets) play an important role in industrial applications due to their high flexibility for tailoring desired ultimate properties such as high Young's modulus, strength, durability, thermal and chemical resistance provided by high cross–linking density.[30] Although there are several applications for lignin in thermoplastics, application of lignin in unsaturated thermosets are virtually nonexistent. This is caused by the poor solubility of lignin in industrial polyester and vinyl ester resins as well as the ability of lignin to inhibit free–radical polymerization by forming quinonic structures which are stabilized by resonance over the whole molecule.[31,32] These obstacles were overcome by introducing chemically modified lignin into thermosets for instance as compatibiliser in hemp/epoxy composites to increase fiber–matrix adhesion,[33,34] or epoxidized lignin/aminated lignin as active resin components,[19,35] however, rarely as non-reactive additive.

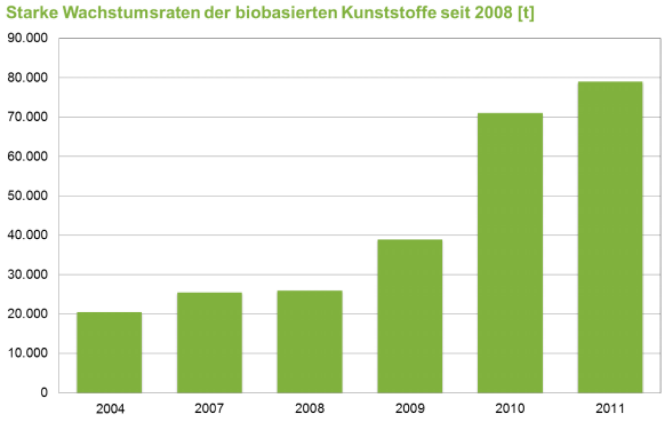

Figure 1.2.: The rapidly growing demand for biobased materials which increased by almost 55 % since 2008.[5]

The demand for biobased materials is growing rapidly (cf. Figure 1.2). Taking this economic aspect into consideration, substitution of expensive thermosets with cost–effective filler would provide an opportunity to establish an innovative biomaterial. In this work, a lignin filled epoxy formulation is developed for the use in lightweight materials. Therefore, a brief survey of sustainable resources and resins with their use in fiber–reinforced materials is given. Further, the characterization of lignins and their introduction in epoxy resins is addressed followed by the validation, optimization and application in fiber–reinforced polymer based composite materials. Moreover, lignin as a possible reactive component in the epoxy system is investigated.

1.1 Sustainable Resources

The pressure of a growing population and urbanization are globally affecting the environmental change. They are key factors in the increasing demand for energy, water and food resulting in depletion and degradation of natural resources. In 2005 the World Summit on Social Development expressed the goals necessary for sustainable development as three pillars of sustainability[36,37]:

Economic viability demands a reasonable lifestyle for generations to come. A sustainable economic model proposes an equitable distribution and efficient allocation of resources. The approach is to develop a profitable business with the idea, that the business operations won't create social and environmental issues.

Social justice seeks for sustainable solutions of pressures like social tension to guarantee a peaceful and respectful life together. It focuses on the balance between the needs of an individual with the needs of the group. Companies are committed to address issues like worker safety, recovery programs as well as the health and water scarcity around their factories.

Environmental conservation addresses the exploitation of resources like the global oil deposits, which is basically the main source for base chemicals. Further, environmental initiatives include the goal of zero waste, the reduction of the carbon footprint by managing energy consumption and greener packaging.

Figure 1.3.: Examples for wood based products and different applications for lignin in polymer chemistry: as dispersants[39–41], composites[9,42] and in polyurethanes[43–45].

As a consequence, it is crucial to find replacements for current materials by natural alternatives. The most popular renewable resources are:

Plant oils: Due to their world–wide availability and relatively low prices plant oils are an attractive and feasible alternative for the production of polymeric materials. In addition, only minor modification of the plant oils lead to a large variety of monomers for different applications. The potential is noticeable in the growth of the oleochemistry industry. The main components are triacylglycerols, which are the product of esterification of glycerol with three fatty acids.[11]

Wood and plants: Being available from renewable agricultural and forestry feedstocks like wood, wood wastes and residues as well as grasses and crops, wood and plant parts are highly promising renewable resources. Biofibers like hemp, flax, pineapple leafs or kenaf consist of cellulose and are a viable alternative for glass fibers. Additionally, a large industrial sector is devoted to the conversion of biomass into fuel ethanol. Therefore cellulose is fermented enzymatically into ethanol.[38]

Lignin is one of the most important bio–resources for base materials and environmentally compatible polymers. The introduction of lignin into formaldehyde–based wood resins, or exploitation of its ubiquitous aliphatic and phenolic hydroxyl groups began to emerge only in the last quarter of the 20th century. Another interesting research topic is the conversion of lignin via carbonization into carbon fibers, which result in either its graphitized form as structural carbon fibers or with an activator in activated carbon fibers.[21,46,47]

It is evident that the application of lignin is a promising alternative in polymer chemistry compared with traditional resources. Figure 1.3 summarizes the wood based products cellulose, plant oils and lignin

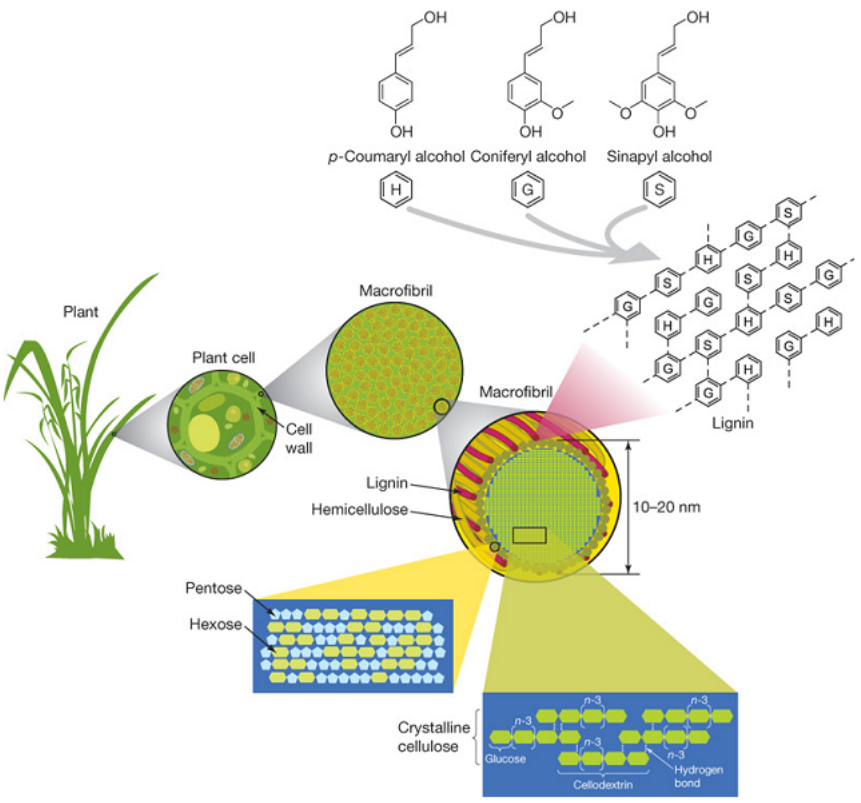

Figure 1.4.: Composition of a vascular plant. The cell wall consists of microfibers and can be divided into four different layers. Each layer contains cellulose, which is embedded in a matrix of lignin and hemicellulose.[51]

and gives a perspective on the multiple ways lignin can be used. The following sections address in detail the chemistry and extraction of lignin and cellulose as raw materials.

1.1.1 Lignin

Lignin is a highly abundant biopolymer and is considered as the main aromatic renewable resource these days. Along with cellulose and hemicellulose, lignin is a major component in higher vascular plants.[10,48,49] It fills the cavities in the cell wall between cellulose, hemicellulose and pectin. The schematic structure of a vascular plant is shown in Figure 1.4. The cell wall consists of microfibrils and microfibers which resemble hollow tubes and can be divided into four different layers (one primary and three secondary walls). Each layer contains cellulose, which is embedded in a matrix of lignin and hemicellulose. Therefore, these components, as well as minor components like resin, fat and waxes, build up a bio composite material on their own. Lignin is covalently linked to the hemicellulose and different polysaccharides—in a process called lignification—to increase mechanical strength as well as to form a continuous system. Further, lignin proves to be important as part of the water absorption system making it possible for the plant tissue to conduct water efficiently throughout the network and plays a role in protecting plants against diseases.[50]

The amount of lignin in plants depends on the type of wood. Ranging from 28–30 % for softwoods like spruce and larch to 20–25 % for hardwoods like poplar and birch. The structural elucidation of lignin started in 1928 through contributions of the working group around Freudenberg.[52] With his co–workers

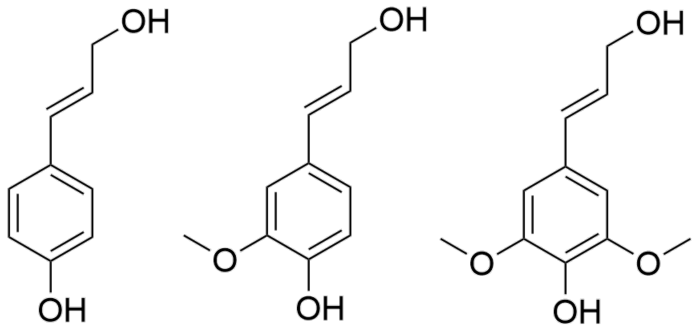

Figure 1.5.: Monomer species of lignin: *p*–coumaryl alcohol (1), coniferyl alcohol (2) and sinapyl alcohol (3).

he investigated several methods for isolating lignin from cellulose and hemicellulose and characterized it by careful analytical methods. On the basis of oxidative dehydrogenation experiments, it was revealed that lignin's main linkages are between carbon–carbon and ether, with the latter preferentially alkyl–aryl ether linkages.[53] Later on, much more accurately structures of lignin based on NMR studies have subsequently been published by Ludwig and Nimz.[52,54] With the recent trend in sustainability and renewable resources, the interest in the research on lignin increased tremendously resulting in major advances for the structural elucidation of lignin, most notably the work of Glasser and Sarkanen.[55–57]

In detail, Lignin is characterized by a complex amorphous macromolecular structure composed of highly branched aromatic–aliphatic moieties. It is derived from mainly three phenylpropanoid units as shown in Figure 1.5: *p*–coumaryl alcohol (1), coniferyl alcohol (2) and sinapyl alcohol (3). These react like a classical chain polymerization in combinatorial phenolic coupling reactions induced by enzymatically generated free radicals with the growing macroradical as shown in Figure 1.6.[14] Figure 1.7 illustrates a hypothetical large fragment of lignin composed of the completely arbitrary sequence of phenylpropanoid units.

Lignin accumulates as a by–product in the paper–making process and has been considered until recently as waste that serves as fuel to recover energy for paper mills. Nearly 70 million tons of lignin accrue yearly.[58] The process to extract lignin to separate it from cellulosic fibers is called chemical pulping. There are several methods used for chemically pulping, but only three play a major role in industry: kraft, soda and sulfite pulping. The choice of the pulping process is determined by the type of wood and the desired product.

Sulfite Process

The sulfite process is historically the oldest pulping process invented from Tilghman in 1866.[59] In this process, wood chips are cooked with a solution of hydrogen sulfite and sulfites. When exceeding SO_2 in the hydrogen sulfite solution exists, the process is called acidic bisulfit process, otherwise it is just called bisulfit process. The main reaction step is the sulfonation of the phenylpropanoid structure which increases the hydrophility as shown in Figure 1.8a. This results in the increase of its solubility. To cleave the phenolether

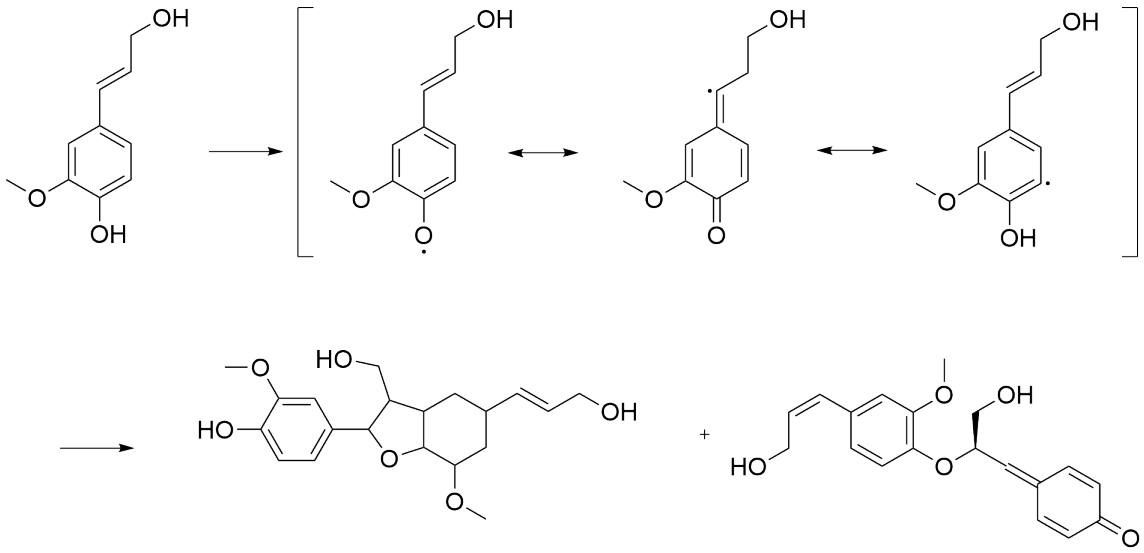

Figure 1.6.: The synthesis of lignin. The monomer species react in a classical chain polymerization in combinatorial phenolic coupling reactions induced by enzymatically generated free radicals with the growing macromolecule.

linkages, additional SO_2 in neutral environment is added as shown in Figure 1.8b. Additionally, the reduction of the cross-linking density results in small fragments of lignin further increasing the solubility.

The disadvantages of this process is that the pulping process is limited to a few types of wood but no grasses. Moreover, the delignification is very slow and the chemicals used cannot be regained in all cases. As an advantage, high conversions can be achieved.

To improve the sulfite process, several enhanced processes are available. The *alkaline sulfite process* uses sodium as base and takes places in a pH-range of 9–13 making it comparable with the kraft process. Albeit the process is technically difficult and the recovery of educts is elaborate. The *multi-stage sulfit process* separates the whole process into partial steps to avoid the specific disadvantages. The most common process is the *Stora process* which performs the first steps in neutral environment slowly increasing the SO_3^- concentration. Through the preferred sulfonation of lignin in the neutral stage the reactive sides will be blocked, so that in the next stage recondensation is prevented. [60,61]

Soda Process

The soda process is the first chemical digestion process and the first partial pulping process for hardwoods. It is also the predecessor for the kraft process. In contrast to the sulfite process, the delignification takes place in an alkaline environment. As base a sodium hydroxide solution is used, whereas OH^- actually cares for the cleavage of the lignin. Since OH^- shows less reactivity than the sulfur compounds in the sulfite and kraft process towards the lignin, the delignification proceeds partially. To obtain a better conversion, higher temperatures of around 180 °C and pressure are necessary. These conditions unfortunately increase undesirable side reactions. Figure 1.9 illustrates the individual steps of the soda process.

Due to the alkaline environment phenolate moieties form which contribute to the solubility in water. After hydrolytic cleavage of the ether bonds the β–C–atom is acidic by means of the activated adjacent

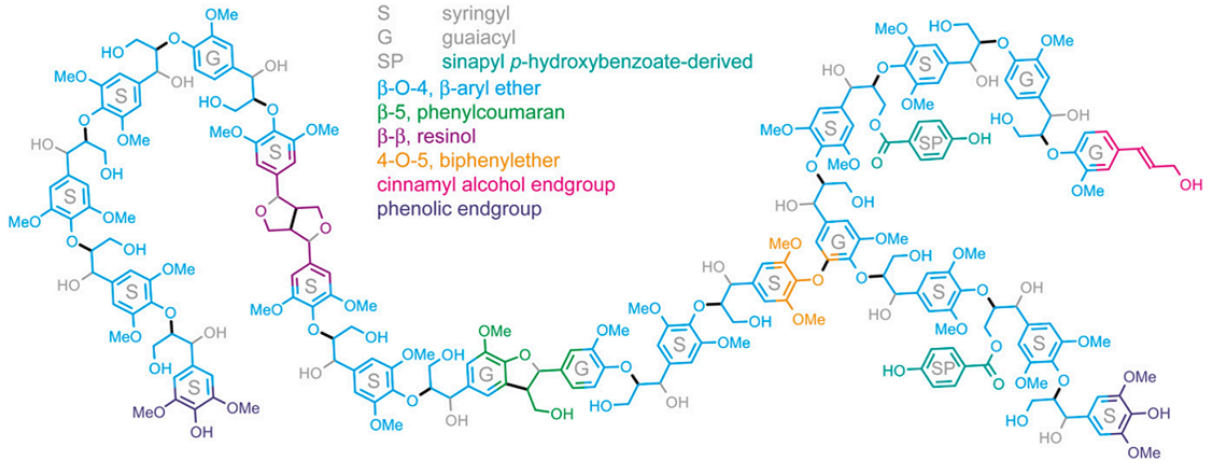

Figure 1.7.: Hypothetical structure of the macromolecule lignin with its assignment to its monomeric species and chemical functionalities.

oxygen-atoms and can be abstracted as well. This results in the shift of negative charge and the cleavage of the lignin–O–C–linkage. Additionally, the methoxy moieties can also be cleaved into phenolates. The resulting methanol is a very good solvent for lignin and its fragments which supports the dissolving of lignin.

Kraft Process

The kraft pulping process originates to two U.S. patents granted to Eaton in 1871 for the delignification of wood with a mixture of sodium hydroxide and sodium sulfide.[62,63] However, industrial application was first made possible by discovering of sodium sulfate to recover sulfide from the alkaline pulping liquor by Carl Ferdinand Dahl.[64] The new process called the sulfate process was adopted at one for pulping wood in Scandinavia. This led to "super" strength paper which therefore was called kraft papers, with *kraft* the Swedish expression for strength. The word kraft has by then become the standard for identifying the sulfate pulping process.[65]

In 2009 kraft pulping was almost 90 % of the total chemical pulping worldwide.[66] In addition, all lignins used in this work originate from the kraft process. During the kraft process, wood chips are cooked in a continuous fashion with NaOH and Na_2S to achieve a nucleophilic cleavage of lignin by means of the sulfide anion as shown in Figure 1.10. The effectiveness results from the NaOH as well as the Na_2S, which almost entirely is hydrolized to NaSH:

$$Na_2S + H_2O \longrightarrow NaOH + NaSH$$

In this form lignin is soluble in the sodium hydroxide solution. The resulting black liquor contains the main share of lignin in its partially degraded form as well as degradation products of the polysaccharides in hydroxy acids as well as low molecular weight fragments of lignin. The residual lignin (10–15 %) is going to be removed subsequently from the pulp after various stages of washing, screening and bleaching. The kraft process is illustrated in Figure 1.11.

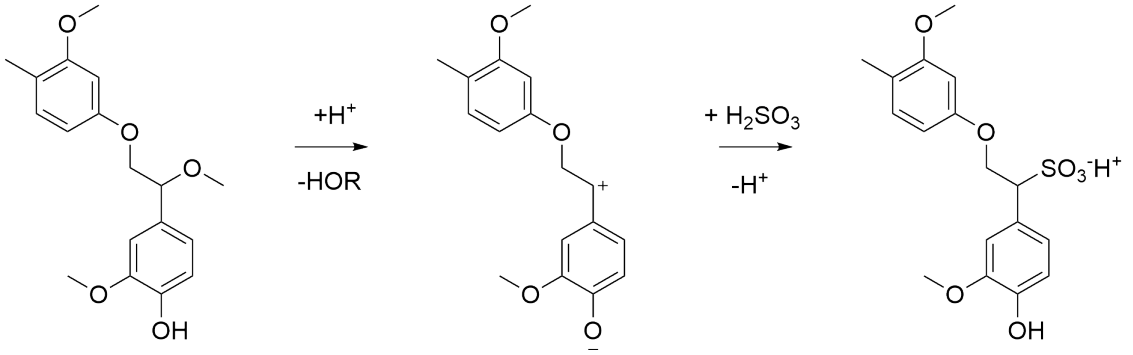

(a) First step of lignin extraction in the sulfite process: sulfonation of lignins phenylpropanoid structure to increase its hydrophility.

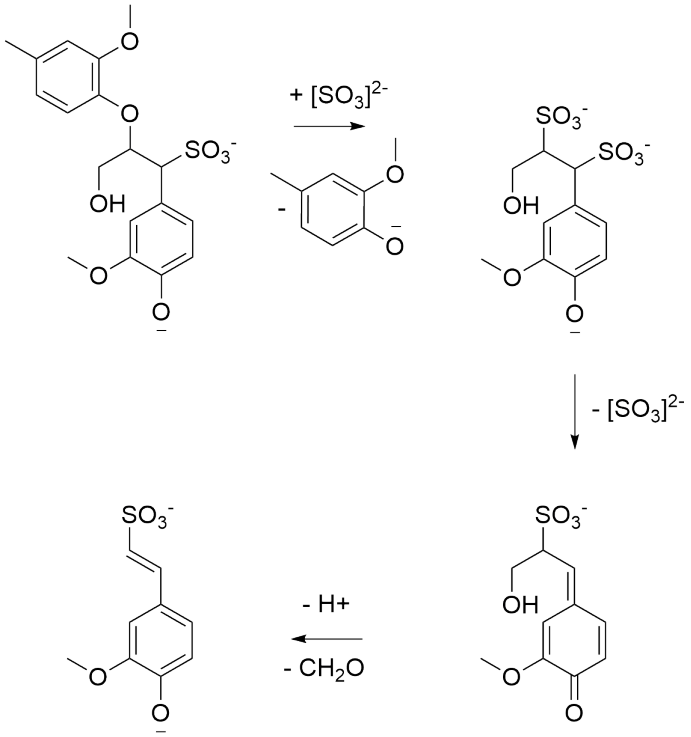

(b) Second step of lignin extraction: Cleaving the phenolether linkages with the addition of SO_2 in neutral environment is added. As a consequence, the reduced cross–linking density results in small lignin fragments which further increases its solubility.

Figure 1.8.

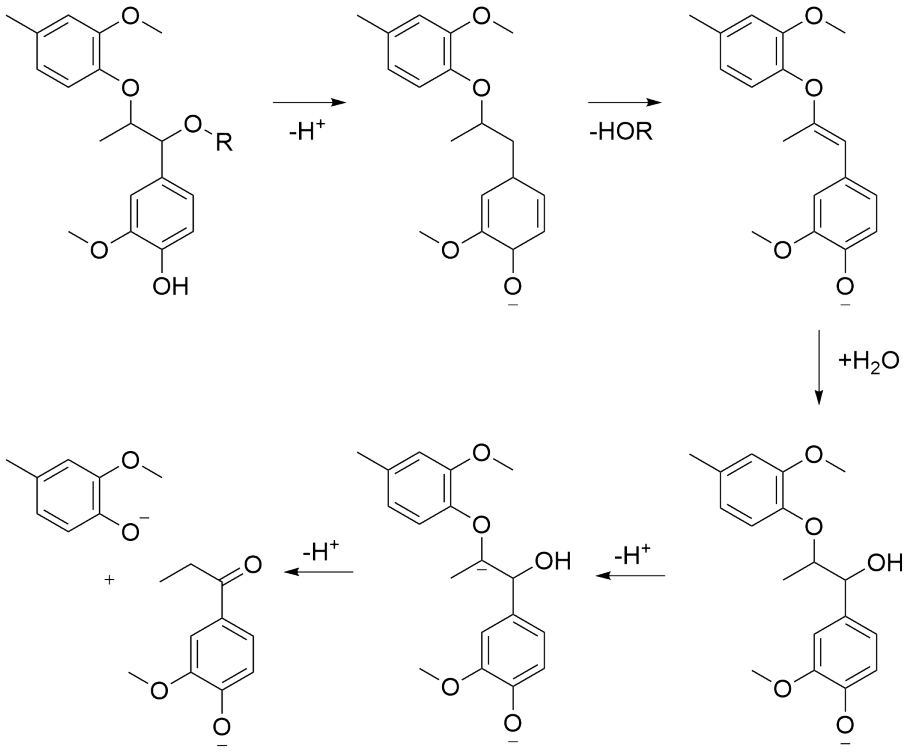

Figure 1.9.: Contrary to the sulfite process, delignification takes place in alkaline environment. Sodium hydroxide solution is added, in which OH^- cleaves the lignin at temperatures of around 180 °C under pressure.

Compared to the other pulping processes, the kraft process has some major advantages making it appealing for industrial use. With the kraft process, nearly every sort of wood is processable. Further, the pulp shows superior strength properties with very low lignin content. Also the digestion times are fast making it even more profitable. However, the pulp requires vigorous bleaching due to the lack of whiteness. Additionally, only low yields in softwoods are achieved and the final product contains residues of H_2S and mercaptans. Table 1.1 summarizes the advantages and disadvantages of the kraft process.

New Technologies in Lignin Pulping

Altogether, the traditional pulping processes with sulfur compounds still dominate the market. Table 1.1 compares the advantages and disadvantages of the kraft process (and therefore Soda process) to the sulfite process.

Newly developed technologies provide delignification and lignin fragmentation with the use of less energy and more accessible structures in terms of lower molecular weight and higher solubility.

The Organosolv pulping process uses organic solvents for delignification. The simplest method is the Alcell process. It uses a mixture of ethanol and methanol which hydrolizes lignin at higher temperatures.[67] In the acid digestion process, organic acids are able to partially esterify lignin in order to solve the obtained acetylated lignin. Typically used are acetic acid (Acetocell process) and formic acid (Formacell process).[68,69] In the steam explosion process, mechanical degradation of the fibrous micro structure takes place through relaxation of the steam–lignin mixture to normal pressure. At least, the aquasolv process soakes wood with superheated water to achieve plasticizing of the lignin. With relaxation to

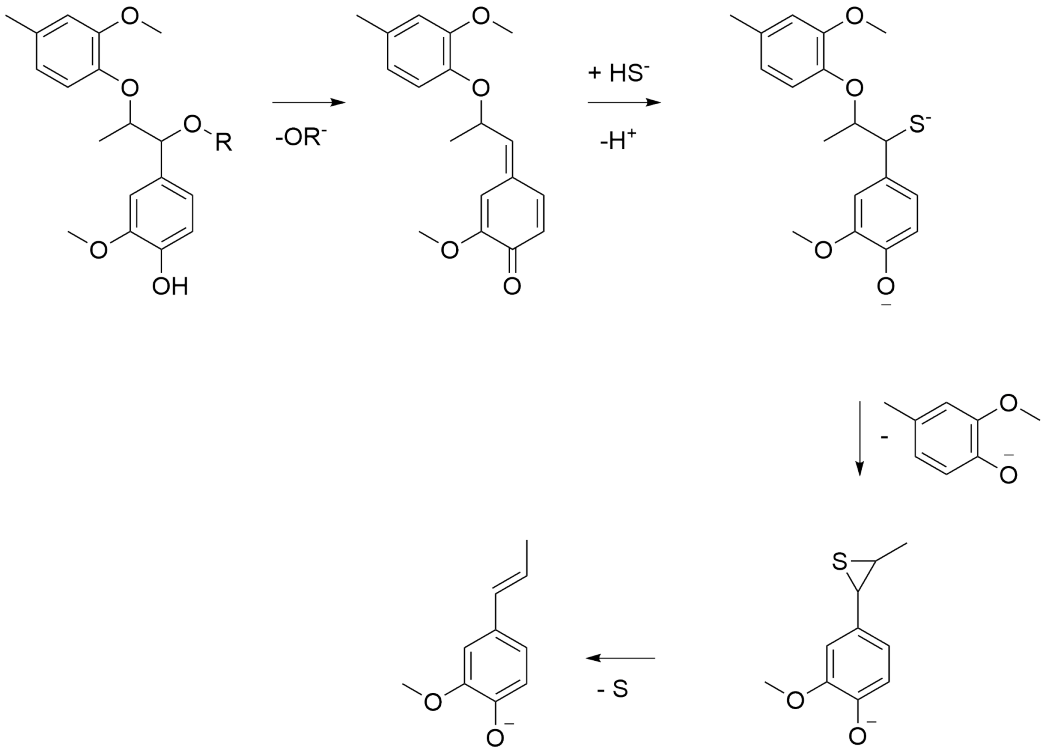

Figure 1.10.: During the kraft process wood chips are cooked with NaOH and Na_2S to achieve a nucleophilic cleavage of lignin by means of the sulfide anion.

normal pressure the fibrils degrade and after extraction with hot water a highly purified lignin with low cross-linking density is obtained. [70]

1.1.2 Natural Fibers

In 1997, around 20 million tons of natural fibers were produced worldwide. Agricultural plant-based fibers include seed hair, bast and hard fibers as shown in Figure 1.12. [71]

Flax is a commodity crop grown in Europe as well as in diverse agricultural systems like Russia, India and Canada. It has a number of unique properties, however only 2 % of its world consumption is used in

Table 1.1.: Advantages and disadvantages of the traditional lignin pulping processes, the kraft process and the sulfite process.

Process	Advantages	Disadvantages
Kraft process	no restrictions in sort of wood high paper strength low lignin content in the pulp fast digestion times	disturbing H_2S and mercaptans low yield in softwoods low degree of whiteness requires vigorous bleaching
Sulfite process	increased process flexibility high conversion with softwoods well bleachable pulp no odor nuisance	resin-rich woods process poorly low conversion with hardwoods sensitive to heartwood, branches and bark low paper strength

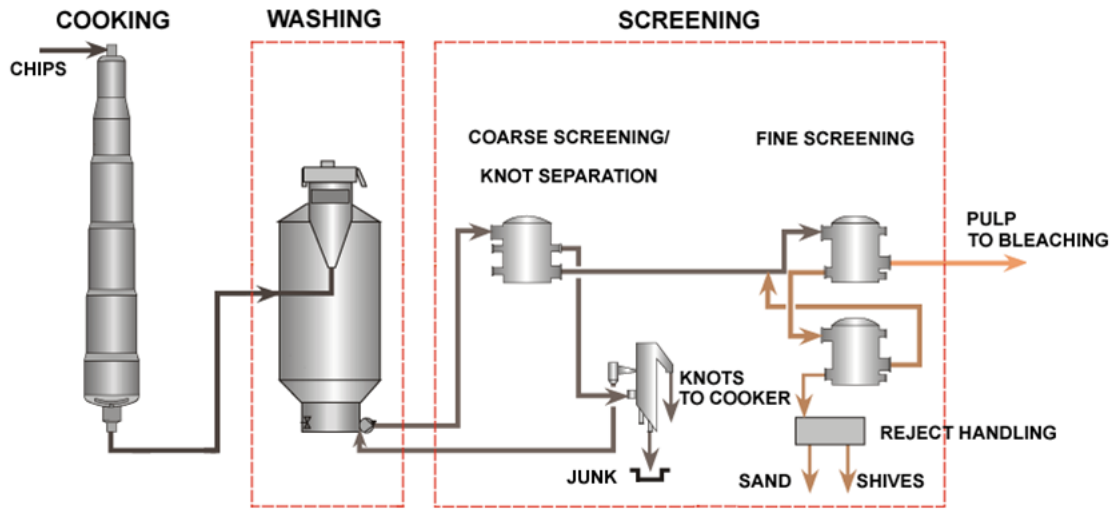

Figure 1.11.: Overview about the extraction of lignin in the kraft pulping process. Delignification occurs in the cooking vessel in which lignin accrues in the so called black liquor.

industrial applications. Ramie fibers are the strongest and also longest fibers. Currently, those non-wood fibers are being used commercially in biocomposites. The major chemical composition of these fibers is similar to wood fibers and includes cellulose, lignin and pentosan. Wood fibers contain about 40–45 % cellulose, 26–34 % lignin and 7–14 % hemicellulose. In contrast, fibers like flax, hemp and jute contain almost 25–32 % hemicellulose. [72]

Natural fibers can be used as harvested, as raw material for cellulose production or can be modified into cellulose esters, which are mainly used as major components of thermoplastics. Cellulose is the most abundant polymer worldwide with an estimated annual production of $1.5 \cdot 10^{12}$ tons and is assumed as an inexhaustible source of raw material. Cellulose is a polysaccharide consisting of linked *D*–Glucose units as illustrated in Figure 1.13. It occurs in nature largely in crystalline forms made up of partially aligned or oriented polymer chains, which consist of up to 10 000 β–1–4–linked anhydroglucose units. Higher plants use cellulose to establish high-strength tissue. Cellulose is especially suitable since it consists of long linear polymer chains which are stabilized via hydrogen bonds. Due to its molecular structure cellulose is predestined to build up highly tensile fiber structures. [73]

1.2 Resins

The term resin is commonly associated with the sticky liquid found inside or segregated by plants. It is composed mainly of volatile fluid terpenes such as bicyclic terpenes like alpha– and beta–pinene, the monocyclic terpenes limonene and terpinolene and small amounts of tricyclic terpenes as well as resin acids. Historically, the use of natural resin dates back to the stone age and found since then its application in art, medicine and construction materials. Today the term resin is applied to a component which sets into a hard lacquer or enamel–like finish. Also casting and synthetic resins fall within this concept since they solidify the same way as traditional plant resins do.

Synthetic resins found their way into technical applications with the invention of the phenol-formaldehyde resin Bakelit by Leo Baekeland in 1907. [74] These are formed by condensation of phenol

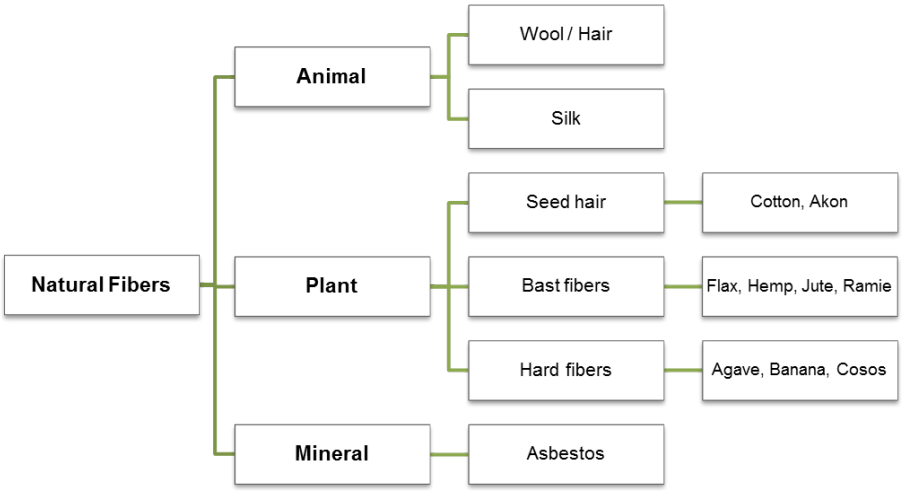

Figure 1.12.: The three main sources of natural fibers: Animal, plant and mineral based natural fibers with the several fiber compounds produced of those.

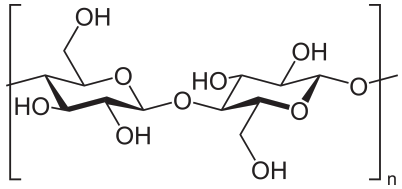

Figure 1.13.: Molecular structure of cellulose derived from D–glucose units which consists of condensed $\beta(1\rightarrow4)$-glycosidic bonds.

with carbonyl compounds, especially formaldehyde, which is by far the most important phenolic resin. Using acid– or base–catalyzed condensation results in end products with differing properties. In an acid medium the condensation products are essentially linked by methylene groups in ortho– and para–positions which are soluble with an average molecular weight between 600 and 1 500. While heating, no further condensation occurs unless suitable di– or polyfunctional compounds are added whereas hexamethylenetriamine (urotropine) is the most important. These are called novolacs. In alkaline environment soluble hydroxymethylphenols called resoles are obtained with a molecular weight between 300 and 700, which contain one or more benzene nuclei. In contrast to novolacs, resoles are able to cross-link through their reactive groups on heating. Figure 1.14 shows the structures of novolac and resol.[75,76]

Another class of synthetic resins are aminoplasts which are composed of melamine and formaldehyde. These resins show a better stability towards water and high temperatures. The condensation reaction is carried out in alkaline environment yielding in a precondensate consisting of *N*–[tris– and hexakis–(hydroxymethyl)] compounds of melamine. Cross-linking of the precondensate occurs with further condensation under elimination of water. Typical applications for melamine-formaldehyde resins are moldings, adhesives for chipboards and textiles as well as paper additives.[77,78]

The class of epoxy resins is one of the most important synthetic resins. They are generally synthesized with a polyfunctional hydroxy compound with 1–chloro–2,3–epoxypropane (epichlorohydrin) in an alkaline environment. The most simple, and commercially most important, epoxy resins are bisphenol A

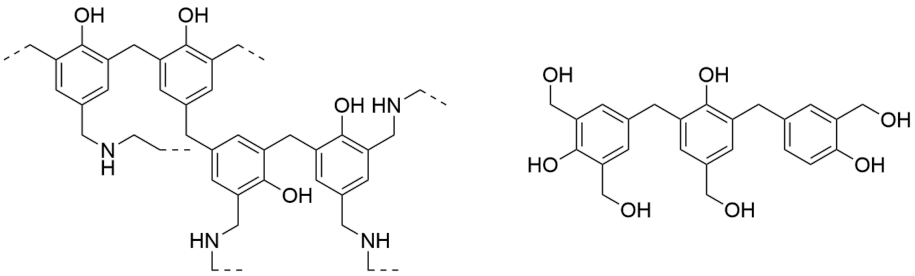

Figure 1.14.: Chemical structures of novolac (left) and resol (right) which are the most important phenolic resins. Differing only using either acid– or base–catalyzes condensation which results in end products with different properties.

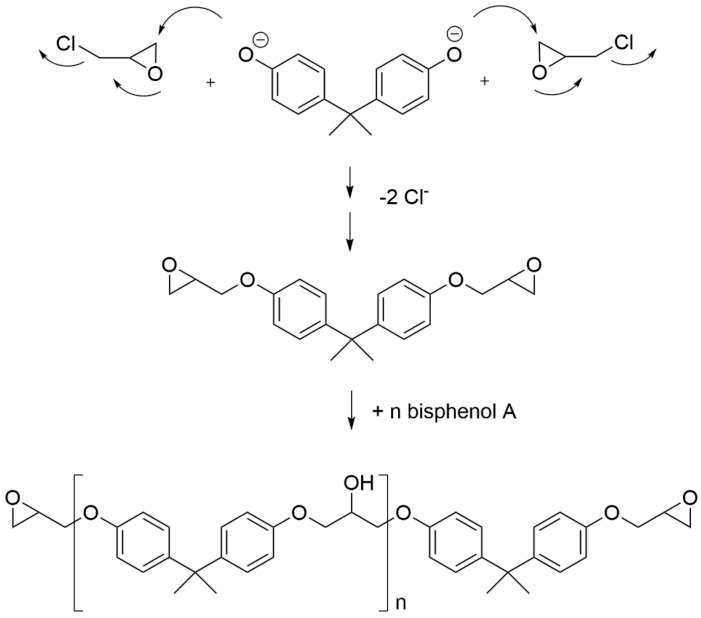

Figure 1.15.: Synthesis of DGEBA: reaction of bisphenol A with epichlorohydrin to bisphenol A diglycidyl ether. Further addition of bisphenol A increases the molecular weight of the resin.

diglycidyl ethers (commonly abbreviated to DGEBA). They are prepared from bisphenol A and epichlorohydrin as shown in Figure 1.15. Further addition of bisphenol A increases the molecular weight of the products. Depending on the repetition units molecular weights vary between 340 and 4 000 ($n = 0 - 12$) with melting points between −15 °C and 155 °C. Besides epoxy resins based on bisphenol A, bisphenol F is also frequently used due to its lower viscosity.

Aliphatic epoxy resins are divided in two groups: glycidylic epoxy resins and cycloaliphatic epoxides. Glycidylic epoxy resins are usually synthesized by the reaction of aliphatic alcohols or polyols with epichlorohydrin resulting in monofunctional (e. g. dodecanol glycidyl ether) and difunctional (diglycidyl ester of hexahydrophthalic acid) resins, although higher functionalities are possible. In general, glycidylic epoxides show a low viscosity at room temperature which makes them mainly useful as reactive diluents. They are able to reduce the viscosity of other epoxy resins as an additive and, at the same time, act as cross-linking agents. Cycloaliphatic epoxides contain cycloaliphatic rings which are directly connected to the oxirane. They show a high temperature resistance and better electrical properties which makes them

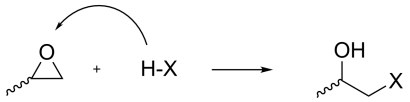

Figure 1.16.: Addition mechanism of the curing agent with the epoxy ring. The oxiran ring opens under formation of a hydroxyl–group, in which the required proton is transferred from the adjacent molecule resulting in a free valence. Therefore, the addition of the corresponding group takes place.

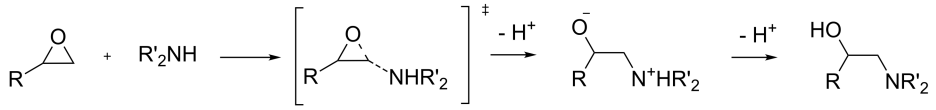

Figure 1.17.: The epoxy–amine curing process follows a S_N2–type II mechanism with a nucleophilic attack of the nitrogen on the terminal carbon atom of the oxiran ring. The primary amine reactions twice with an epoxy molecule resulting in a tertiary amine.

useful for electronic applications like the encapsulation of light emitting diodes. However, curing occurs at elevated temperatures which makes them useless for applications cured at room temperature.[79,80]

For the addition on the oxirane ring (curing) a di– or multifunctional compound with a mobile hydrogen atom is necessary. This includes amines, carboxylic acids as well as aminoamides and thiols. The cross–linking reaction is of exothermic nature with a heat of reaction of $22-26$ kcal per mole epoxy groups.[77] Figure 1.16 shows the simplified reaction scheme of the addition mechanism.

The oxiran ring opens under formation of a hydroxyl–group, in which the required proton is transferred from the adjacent molecule resulting in a free valence. Therefore, the addition of the corresponding group takes place. A crucial factor for the reaction time is the mobility of the transferred proton. This is influenced by the binding properties of the reaction partner. This allows to tailor the pot life and curing time for the desired application. In the following, the curing reaction with amino–based curing agents and its detailed mechanism will be explained.

1.2.1 Epoxy Resins Using Amino–based Curing Agents

The detailed mechanism of the epoxy–amine curing process is thoroughly investigated. The fundamental understanding of the reaction is crucial for the development of new materials. The reaction follows a S_N2–type II mechanism with a nucleophilic attack of the nitrogen on the terminal carbon atom of the oxiran ring. The primary amine reacts twice with an epoxy molecule which results in a tertiary amine. The reaction obeys a 2^{nd} order kinetic as shown in Figure 1.17 in which the first step is assumed to be rate determining since the proton transfer is fast compared to the nucleophilic attack. The reaction can be catalyzed by hydroxyl groups.

Various possible pathways of the reaction on molecular level have been suggested in literature. The most important pathways are: uncatalyzed, self–promoted and alcohol–catalyzed. Each reaction pathway has two possible routes with an acyclic and a cyclic transmission state. The acyclic pathway shows the attack of the amine on an epoxy which is stabilized by both a hydrogen bond between the amine hydroxy and the ether oxygen and a hydrogen bond between epoxy oxygen and a hydrogen donor. This lowers the

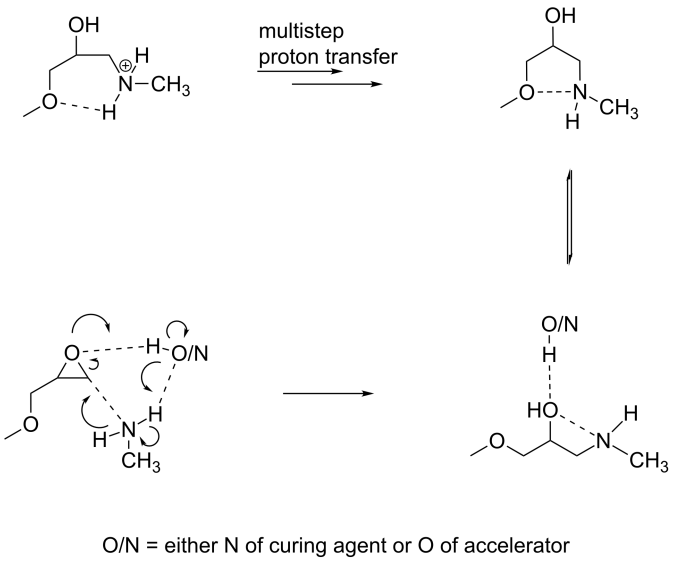

Figure 1.18.: The comparison of the cyclic and acyclic transition states during epoxy–amine reaction. The bond cleavage and formation of the epoxy–amine occurs simultaneously with a hydrogen transfer in a concerted manner leading to the product. The acyclic pathway is a step–wise process involving one or more intermediates.

activation barriers. The alcohol–catalyzed reaction has a 14.6 kJ/mol lower activation energy compared to the self–promotion reaction. The cyclic transition states lower the activation energy and provide stabilizing effects. Figure 1.18 shows that the reaction pathway via a cyclic transition state is different compared to its acyclic counterpart. In particular, the bond cleavage and formation of the epoxy–amine occurs simultaneously with a hydrogen transfer in a concerted manner leading to the product, whereas the acyclic pathway is a step–wise process involving one or more intermediates. [81]

1.3 Thermosets

Conventionally, polymers are classified by the way they act when they are heated. This results in three main categories of polymers: Thermoplastics, elastomers and thermosets. Thermoplastics flow when heated beyond a particular temperature, whereas thermosets remain in the solid state until the ceiling temperature is reached or degradation of the material takes place. Elastomers are elastic polymers with weak intermolecular interactions which are generally used above their glass transition temperature.

The different behavior of polymers arises from their chemical structure (cf. Figure 1.19). Thermoplastics are linear polymers that are in their solid state either semicrytalline or amorphous glasses. When they are heated to their melting point or glass transition temperature respectively, polymers chains are free to move and flow takes place. In constrast, thermosets are closely cross–linked polymers with minimal deformability unless the covalent chemical bonds are destroyed. A further major difference to thermoplastics is their insolubility in all organic solvents. Some linear polymers like poly(tetrafluoroethylene) will not flow when heated because of strong non–covalent forces which hold the polymer chains together. Poly(phenyle oxide) degrades before it can flow. However, they are still classified as thermoplastics due to their structure. On the other hand, cross-linked polymers like LDPE are also thermoplastics since they can flow or dissolve in an adequate solvent. In a thermoset, only a fraction (the sol fraction) will eventually dissolve, while the

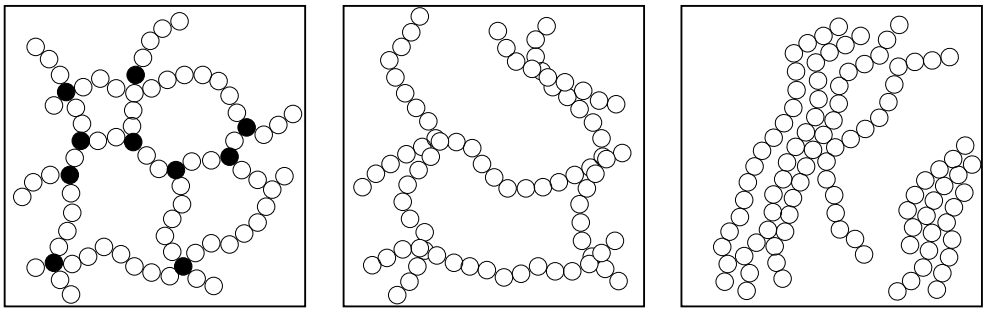

Figure 1.19.: Comparison of the chemical structure of amorphous thermosets as well as amorphous and semicrystalline thermoplastics.

Table 1.2.: Advantages and disadvantages of thermoplastics and thermosets.

	Advantages	**Disadvantage**
Thermoset	higher T-stability high flexibility in design high levels of dimensional stability cost-effective	Non-recyclable cannot be remolded / reshaped difficult to surface finish
Thermoplastic	highly recyclable high-impact resistance (ABS, polyamides) remodeling / reshaping possible most polymers chemical resistant superior finishes	typically more expensive temperature sensitive

cross-linked structure (the gel fraction) only swells. For this reason, a thermoset can also be defined as a cross-linked polymer network by covalent bonds which percolates through the whole bulk.

Thermoplastics and thermosets have advantageous and disadvantageous aspects in different applications. Table 1.2 compares those advantages and disadvantages between thermosets and thermoplastics to emphasize the qualities of a thermoset for the aspired goal of a biobased thermosetting resin. The most important aspects are the high flexibility in the design of the final product which makes it easier to discover the most suitable application for the biobased thermoset. The cost–effectiveness of thermosets is a crucial aspect as well. The fundamentals of the polymerization leading to a highly cross–linked network of a thermoset is described hereafter.

1.3.1 Fundamentals of Network Formation in Thermosets

To achieve a cross–linked network resulting in a thermoset several polymerization techniques can be applied:

- Step–growth polymerization
- Chain–growth polymerization
- Combination of Step- and Chain-growth
- Controlled polymerization

Chain–growth polymerization occurs in a free radical co-polymerization which requires an activated species (radical) which reacts with the functional group generating a new active species until termination occurs and the chain becomes deactivated. In order to generate a network one of the monomers must contain two or more functional groups.

The combination of step– and chain–growth methods is typically achieved by the polymerization of a linear backbone in a free radical manner followed by the cross–linking of functional groups present in the backbone by the step-growth reaction. Another prominent example are systems were both mechanisms take place in a competitive way. This is the case for epoxy–amine formulations which contain Lewis acid or Lewis base based accelerators. The accelerator initiates the chain-growth of the epoxy that occurs parallel to the step-growth epoxy–amine reaction.

Controlled polymerization techniques like atom transfer radical polymerization (ATRP), nitroxide mediated free radical polymerization (NMP) and reversible addition fragmentation chain transfer polymerization (RAFT) which are typically used to synthesize polymers with narrow molecular weight distribution is surprisingly a subject of great interest for example to control the “chain–growth condensation” of para-substituted AB–type aromatic monomers.

Due to its importance in this work the step–growth polymerization, especially the polyaddition, will be addressed in the following section in more detail.

Step–growth polymerization

Step–growth polymerization includes techniques like polycondensation and polyaddition.[77,78] The polymer network is generated by the reaction of monomers providing type A functional groups (nA) with a second monomer providing functional groups of type B (nB) as present in a co-monomer or curing agent as shown in Equation 1.1.

$$n\mathrm{A}-\mathrm{A}+n\mathrm{B}-\mathrm{B}\longrightarrow -(-\mathrm{A}-\mathrm{A}-\mathrm{B}-\mathrm{B}-)_n- \tag{1.1}$$

The step–growth can also take place in a homopolymerization of a monomer featuring both functional groups A and B (nA–B) (Equation 1.2)

$$n\mathrm{A}-\mathrm{B}\longrightarrow -(-\mathrm{A}-\mathrm{B}-)_n- \tag{1.2}$$

From this point of view, a multitude of reactions seems imaginable. However, besides the presence of the functional groups A and B, the most important factor is that the reaction yields in high conversion. Network formation takes place in consecutive steps starting from the monomers: any A–functional group can react with any B–functional group independently of the molecular weight of the monomers. This generates branched structures of increasing size as the reaction progresses leading to the situation that the largest branched structures contain more unreacted A and B groups. The larger reaction probability of this large branches in contrast to the smallest species, the monomers, leads to the sudden formation of a fully cross-linked polymer network.

High conversion is not only affecting the cross-linking density, it has a significant impact on the degree of polymerization. The degree of conversion p is defined as:

$$p = \frac{(N_0 - N)}{N_0}$$

Where N_0 is the number of monomers (equivalence assumed) at the start of the reaction and N the number of monomers at time t. The degree of conversion can accommodate values between 0 and 1. With the number average of the polymerization degree defined as

$$P_n = \frac{N_0}{N}$$

and therefore the relationship between p and P_n results in

$$P_n = \frac{1}{1-p} \tag{1.3}$$

Figure 1.20 shows the relationship between conversion, degree of conversion p and degree of polymerization P_n. P_n ascends with increasing conversion leading to $P_n = \infty$ with 100 % conversion.

A further prerequisite is a high reaction time, which can be achieved by using energy–rich compounds or the addition of catalysts. Assuming a first–order reaction regarding the monomer concentrations follows

$$-\frac{d[A]}{dt} = k \cdot [A][B] \tag{1.4}$$

When the monomers are exactly equivalent then $[A] = [B]$, (1.4) can be simplified to

$$-\frac{d[A]}{dt} = k \cdot [A]^2$$

Integration results yields

$$\frac{1}{[A]} - \frac{1}{[A]_0} = k \cdot t$$

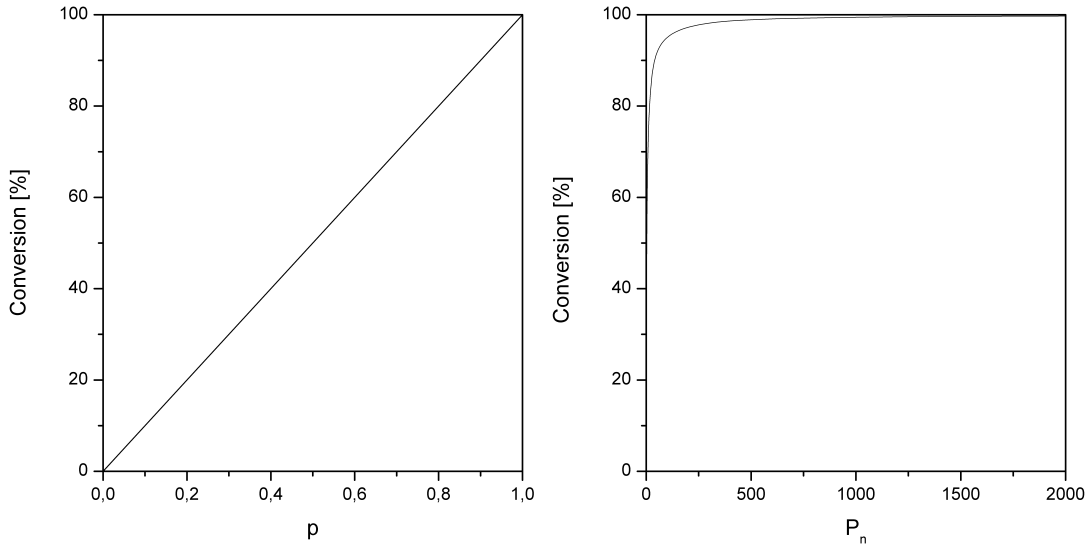

Figure 1.20.: Relationship between Conversion, degree of conversion p and degree of polymerization P_n in step-growth polymerization. P_n ascends with increasing conversion leading to $P_n = \infty$ with 100 % conversion.

The temperature–independent rate constant k ranges between 0.3 and 100 000 and is dependent on the degree of polymerization. With

$$P_n = \frac{[A_0]}{[A]}$$

and

$$[A] = [A_0] \cdot (1 - p)$$

follows

$$\frac{1}{[A_0](1-p)} - \frac{1}{[A_0]} = k \cdot t \tag{1.5}$$

Combining (1.3) and (1.5) results in

$$\frac{P_n}{[A_0]} - \frac{1}{[A_0]} = k \cdot t$$

Therefore, P_n can anticipated with the initial concentration and time when k is known as shown in

$$P_n = [A_0] \cdot k \cdot t + 1$$

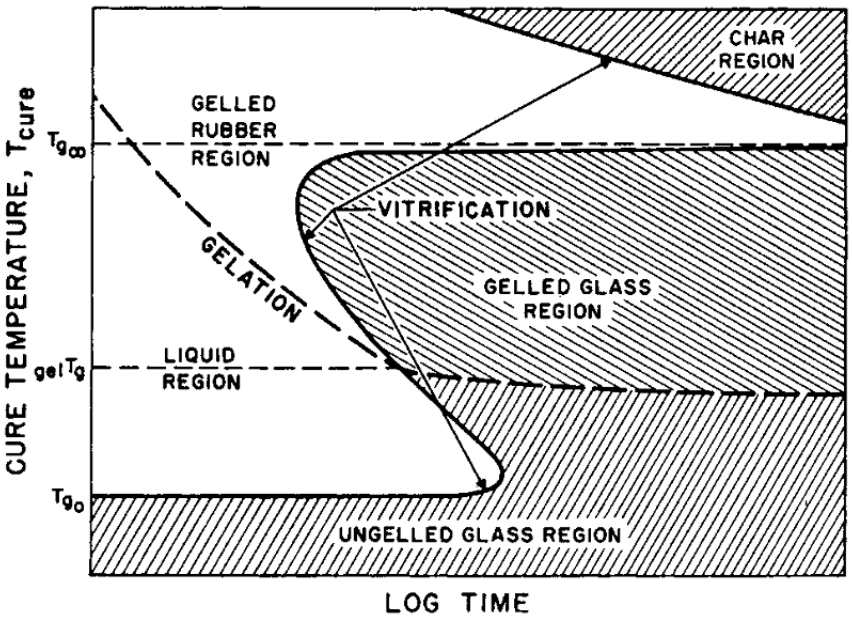

Figure 1.21.: Time–Temperature–Transformation (TTT) cure diagramm which plots the time required to reach gelation and vitrification.[82]

The relationship of the degree of polymerization for a A–A, B–B type of reaction with the numbers of monomers N_A and N_B and the stoichiometric ratio $r = N_{A,0}/N_{B,0}$ results in the carothers equation:

$$P_n = \frac{N_r}{N} = \frac{1+r}{r+1-2\cdot r\cdot p}$$

Time–Temperature–Transformation Diagram

The cross–linking reaction of thermosets is quite complicated due to the interaction of curing kinetics and the accompanying changing properties. To understand curing phenomena the time–temperature–transformation (TTT) diagram (Figure 1.21) plots the time required to reach gelation and vitrification.

The isothermal cure of a thermoset is generally characterized by two effects.

Gelation corresponds to the initial formation of an infinite network of cross–linked polymer which percolates throughout the whole bulk. The polymer shows an abrupt increase in viscosity transforming the mass from a liquid into a solid. This is quite important for the processability of the resin since this curing step should take place in the final desired shape of the material as no reshaping is possible at this point. In step–growth polymerization gelation occurs at high conversions and depends primary on the functionality of the monomers. The gel conversion for a stoichiometric reaction of A with B is given by (1.6) showing that the gelation is time–independent.

$$x_{gel} = \left[\frac{1}{(A-1)\cdot(B-1)}\right]^{0.5} \tag{1.6}$$

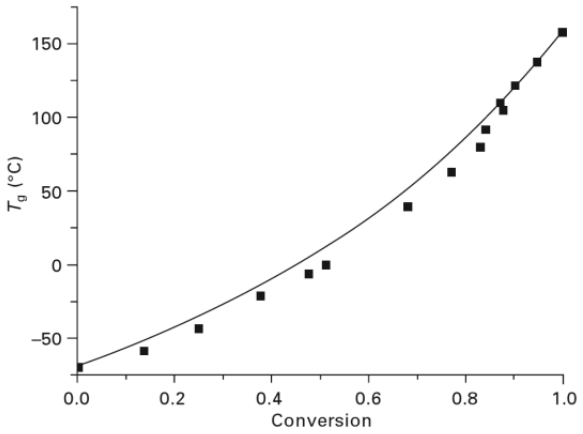

Figure 1.22.: Relation between T_g with increasing conversion.[82]

Vitrification describes the increasing molecular weight resulting in the transition from a liquid or rubbery state into a glassy state. This is characterized by the glass transition temperature T_g, which is a second–order thermodynamic transition which correlates to the discontinuity of the first derivative of enthalphy or specific volume. Equation 1.7 shows the dependency of T_g with increasing conversion. The parameter λ specifies the ratio of changes of the specific heat at the T_g for the fully cross–linked network and for the initial blend.[82]

$$\frac{T_g - T_{g,0}}{T_{g,\infty}} = \frac{\lambda \cdot x}{1-(1-\lambda)\cdot x} \tag{1.7}$$

The knowledge of the specific T_g for a thermoset is important for its application since the properties change dramatically when reaching this transition. For example the Young's modulus drops by 2–3 orders of magnitude from the range of GPa to MPa. Figure 1.22 shows the relation between T_g and increasing conversion.

Below $T_{g,\infty}$ the temperature of the thermoset remains ungelled, it remains processable and meltable. Below $T_{g,0}$ is the glass transition temperature of the freshly prepared uncured resin, basically no reaction occurs since the reactive species are immobilized in the glassy state. Above $T_{g,\infty}$ the resin will not vitrify on isothermal cure. Curing will proceed as it will not be quenched beforehand as it would be below $T_{g,\infty}$, although 100 % conversion is impossible since some reactive sites are isolated by the network.[82]

1.4 Fiber–reinforced Polymer Composites

Fiber–reinforced polymer (FRP) composites are materials where two entirely different components are combined to result in an enhanced material with new properties. FRPs are characterized by fibers with a reinforcing effect resulting in increasing strength and Young's modulus of the material and a polymer matrix which acts as a support for the fibrous structure.[83] Due to the many possibilities to combine different fibers and matrices, tailor-made properties for particular applications makes FRP a class of materials with huge future potential.

Crucial is an optimal interaction of fiber and matrix: fibers are able to absorb extremely high tensile forces, but cannot provide form stability. Whereas polymer materials are unreinforced either too brittle like thermosets or too flexible as seen in thermoplastics. However, to obtain a reinforced material certain rules of thumbs have to be considered in the development of an FRP for optimum benefit:

1. The Young's modulus E of the fibers longitudinal has to be higher than E of the matrix.
2. The tensile strength R of the fibers longitudinal has to be higher than R of the matrix.
3. The elongation at break ϵ_b of the matrix has to be higher than ϵ_b of the fiber

Through the restriction, that Young's modulus and tensile strength are dependent on the fiber orientation it is obvious that the mechanical properties are anisotropic. The optimal mechanical properties are achieved when the fibers are continuous and directed. However, it is impossible to engineer each structural element with directed and continuous fibers. In addition, the manufacturing method is limited for this kind of fibers as well. In order to compensate those aspects, short fibers are used. These fibers show a reinforcing effect with a length of just 1 mm.

The most popular FRP composites today are reinforced with carbon, glass and aramid fibers whose properties are shown in Table 1.3. Compared to traditional materials like steel, carbon fiber reinforced composites have a Young's modulus at the same level but a higher tensile strength. Similar results are obtained for aramid fiber reinforced polymers. However, the manufacturing process for carbon and aramid fibers is expensive, which makes glass fibers a cost-effective alternative.

In thermosets the amount of fiber content can be increased up to 80 %. Due to the alignment the enhancement of the properties is tremendous. In thermoplastics the amount of fiber content is limited by the processability such as extrusion and injection molding. The fiber orientation in the composite is random and yields enhancements of the properties not as high as observed in thermoset composites.

1.4.1 Natural Fiber Polymer Composites

In recent decades, natural fibers emerged as a feasible alternative as reinforcing material due to their advantages compared to conventional fibers. Compared to glass and carbon fibers, natural fibers have a low density and cost. They show comparable specific tensile strength properties, are non–abbrasive to the equipment. Also, they show a lower environmental impact regarding their renewability, recyclability and bio–degradability. Natural fibers are grouped into three different types depending on their source: seed hair, bast fibers and lead fibers. Some examples are cotton (seed hairs), ramie, flax and jute (bast fibers)

Table 1.3.: Mechanical properties of carbon, aramid and glass fiber reinforced polymers compared to steel. [84]

Material	E [GPa]	R [MPa]
Steel	200	700
Carbon FRP	150	1 500
Aramid FRP	127	2 900
Glass FRP	44	900

as well as sisal and abaca (leaf fibers). Of these fibers, jute, flax, ramie and sisal are the most commonly used fibers for FRPs and their properties compared to conventional glass fibers are shown in Table 1.4.

As already described above, natural fibers themselves are cellulose fiber reinforced materials which consist of microfibrils in an amorphous matrix of lignin and hemicellulose (see Chapter 1). Hydrogen bonds as well as other linkages provide the necessary strength and stiffness to the fibers. The hemicellulose is responsible for the biodegradability, thermal degradation and moisture absorption whilst lignin is thermally stable but degrades in UV light.

There are many factors which influence the performance of natural fiber reinforced polymers. Due to the hydrophilic nature of the fibers, it is necessary to modify the fiber surface to improve the adhesion between fiber and the hydrophobic matrices. Furthermore, a high fiber content is required to achieve high tensile strength. Since most thermoplastics are processed at high temperatures, those temperatures must be carefully selected regarding the decomposition temperatures of natural fibers. Pyrolysis of the cell walls contributes to char formation with increasing processing temperature. These charred layers help to prevent the further thermal degradation of the lignocellulose. For instance the thermal degradation of jute fibers starts at 220 °C which can be difficult to cope with in high temperature applications. Regarding the fibers, this results in the decrease of the mechanical properties whereas in the composite, due to the emerging volatile degradation products, a porous polymer matrix forms which leads to density loss and inferior mechanical properties. Another challenge is the hygroscopic nature of the cellulosic fibers. Fibers absorb moisture resulting in a water content between 5 and 10 %. This can lead to dimensional variations in the composite and poor processability resulting in porous materials with low mechanical properties. The moisture uptake can be reduced by sizing the fibers or by grafting of vinyl monomers onto the fiber surface.

Improved mechanical properties are achieved by a number of parameters like the volume fraction of the fibers, the fiber aspect ratio, fiber–matrix adhesion, orientation of the fibers as well as the stress transfer at the interface. The Young's modulus depends on the fiber properties whereas the tensile strength is sensitive to the matrix properties. Tensile strength can be improved by low stress concentration and strong interface adhesion. High fiber aspect ratio and fiber concentration have a strong influence on the modulus.

Table 1.4.: Mechanical properties of natural fibers compared to glass fibers determined by the zero span method.

Fiber	Specific Weight	Tensile Strength [MPa]	Young's Modulus [GPa]	Specific Young's Modulus
Glass fiber	2.5	3400	72	28
Flax	1.5	344	27	50
Jute	1.3	393	55	38
Sisal	1.3	510	28	22
Pineapple leaf	1.6	170	62	40

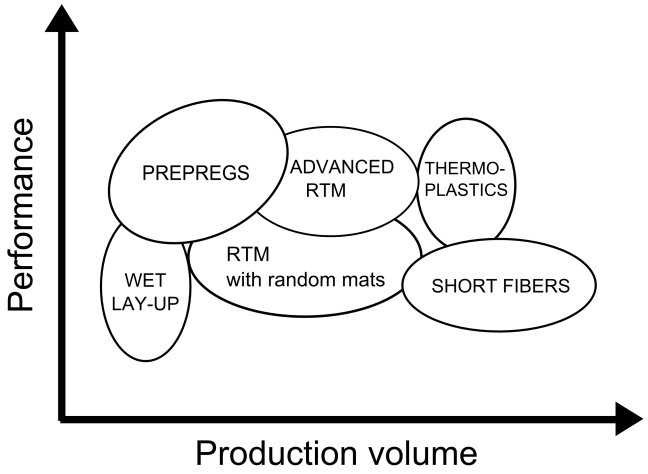

Figure 1.23.: Relation between performance and production volume for fiber reinforced polymers.

In general, in short–fiber composites a critical fiber length is required to achieve its full stressed condition in the matrix. Fibers below the critical length show debonding at the interface at lower load resulting in failure. For high impact strength, it is important that an optimum bonding between fibers and matrix is reached. This is achieved by the degree of adhesion, fiber pullout and the energy absorption mechanism. The properties improve linearly with increasing fiber content to a maximum of around 80 %, at this stage the wetting of the fibers is compromised leading to premature failure.

1.4.2 Manufacturing of Fiber Reinforced Thermosetting Composites

The key to an ideal product is to determine which strengths and weaknesses come with particular types of processes. In general, the basic requirement of all manufacturing processes is to ensure constant pressure and temperature throughout the composite over the required period of time. There are several widely used methods for manufacturing conventional composite parts: wet lay–up, pultrusion, resin transfer molding (RTM) or vacuum assisted resin transfer molding (VARTM) and autoclave processing. Furthermore, an already pre–impregnated (prepreg) composite material often referred to as *advanced composite* can be chosen before the composite is molded. Those are gone through a vacuum assisted wet lay–up process and cured to a minor degree of polymerization. The methods of wet lay–up and the further processing through prepreg lay–up will be discussed further due to its relevance in this work.

Wet Lay–Up Process

The widely applied wet lay–up is a simple method compared to other composite manufacturing methods (cf. Figure 1.24): the resin is impregnated by hand into the fibers. Fibers in form of fiber mats or wovens are positioned in a mold. The mats are impregnated layer–by–layer until the reinforcement thickness is achieved. To ensure easy removal of the FRP, a release agent, which is often a gel coat, is applied to the mold beforehand.

The disadvantages of materials manufactured by this process are the poor mechanical properties due to non-uniformity and the presence of voids. In order to avoid this problem, the use of a vacuum bagging

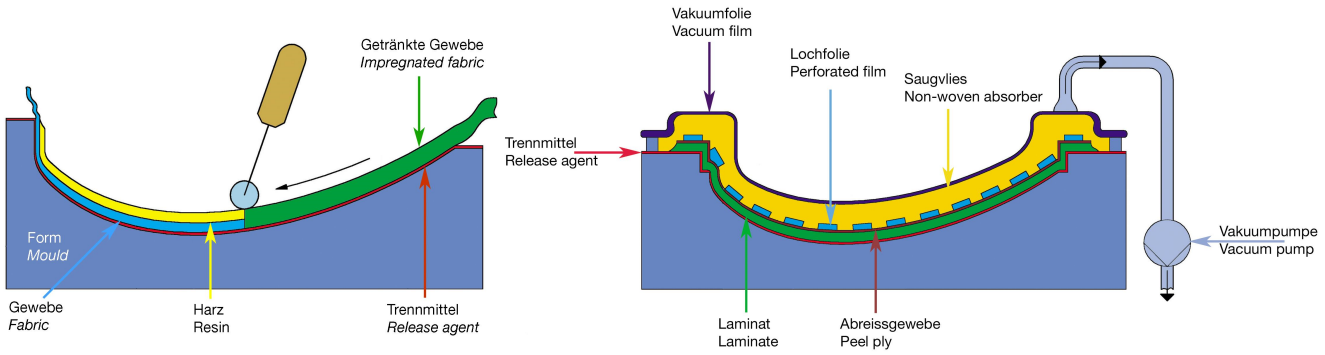

Figure 1.24.: Wet lay-up process for low-production applications. Lamination of the fibers in the mold (left) and further processing with vacuum technique for the reduction of voids (right).[85]

process is necessary as shown on the right hand picture in Figure 1.24. Therefore, the fibers and matrix are sandwiched between peel ply, a non–woven absorber and a vacuum bag. The peel ply is placed immediately on top the FRP to ensure a smooth surface. The non–woven absorber absorbs excess resin from the FRP during cure to achieve the desired fiber volume. After the hand lay–up, vacuum is drawn which reduces the void content tremendously and increases the fiber wet–out due to pressure.

The wet lay–up is beneficial for low–volume production such as motor sport components and core–bonding in production boats due to its low cost and easy processing.

Prepreg Process

Preimpregnated materials (prepregs) are fiber mats or woven which are already laid up and pre–cured to a minor degree of polymerization by the materials manufacturer. The curing agent is latent, which means that the prepreg is storable for weeks and sometimes months at ambient temperatures. Considering the rheological properties, the prepreg is at ambient temperatures nearly solid with a light sticky feel to it comparable to adhesive tape. Generally for industrial use, the prepreg is stored frozen to prolong the shelf life even more.[86]

In further processing prepregs are laid up by hand or machine onto a mold, vacuum bagged and then heated to $120-180\,^{\circ}C$ to allow the resin to reflow and to cure. Typically this is done in an autoclave to provide additional pressure up to 5 bar to the FRP. There are several advantages using pre–impregnated FRPs. Resin/curing agents ratios as well as fiber content is already accurately set by the manufacturer and high fiber contents can easily be realized. There is a great potential for automatization due to its simple handling. The long shelf life means that structurally optimized, complex lay–ups are easily achieved. However, process temperatures and pressures are high and the materials and tooling needs to be resistant. Autoclaves are usually required, making the process expensive and slow due to long operation times. Typical applications are in the aerospace industry for structural components, and in motor sport or general sports equipment like tennis rackets and skis. Figure 1.25 summarizes the manufacturing process.

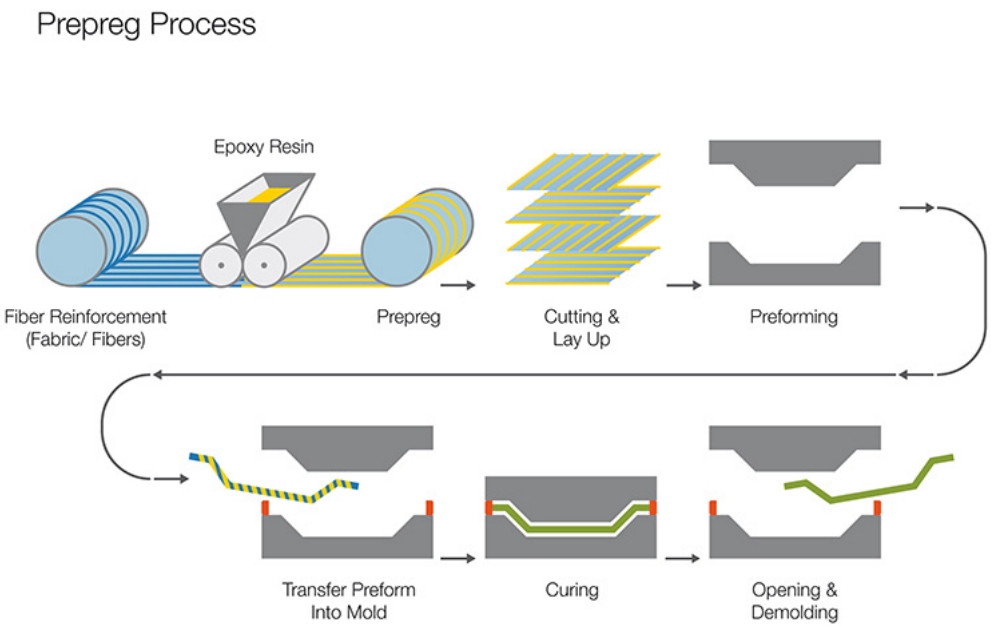

Figure 1.25.: Manufacturing process of prepregs and a prepreg based composite material.[87]

2 Scope

The scope of this work is to introduce the by–product material lignin of the industrial pulping process in a completely new value chain of fiber reinforced polymers. Lignin is one of the most abundant bio–resources with a yearly volume of about $5 - 36 \cdot 10^8$ t per year with 50 million t of lignin in the pulp and paper industry and simultaneously a major by–product material of the paper industry.[88,89] Due to its natural origin the use of lignin in conventional applications is limited because of process impurities such as sulfur contamination, chemical inhomogeneities arising from a non-uniform feedstock and the complexity of its characterization. However, lignin presents a renewable source for bulking agents which possess manifold possibilities compared to conventional wooden derivatives such as wood flour or wood fibers.

It is possible to adjust fusibility, glass transition temperatures and solubility by the variation of the molecular weight of the lignin. In addition, the chemical functionality of lignin can be specifically defined as required for an application. Searching for new valuable markets for lignin, fiber reinforced polymers were found to be of particular interest. Especially epoxy based thermosets seem highly promising due to their applications in the upper price segment. On the one hand, the value of lignin would be increased by the development of new properties, on the other hand with high loaded lignin resins of lignin in epoxy as bulking agent would mean price savings due to less needed epoxy resin material. Yet another advantage is owed to the newly understanding of sustainability. To address this issue, cellulose fiber mats were provided to increase the content in the fiber reinforced polymer materials. An easy and inexpensive method to produce fiber reinforced plastics is the wet lay–up process. This technique combined with newly developed lignin filled epoxy resins provides a new set of materials with interesting properties. To achieve this, several considerations must be taken into account. Due to the complexity of lignin, it is

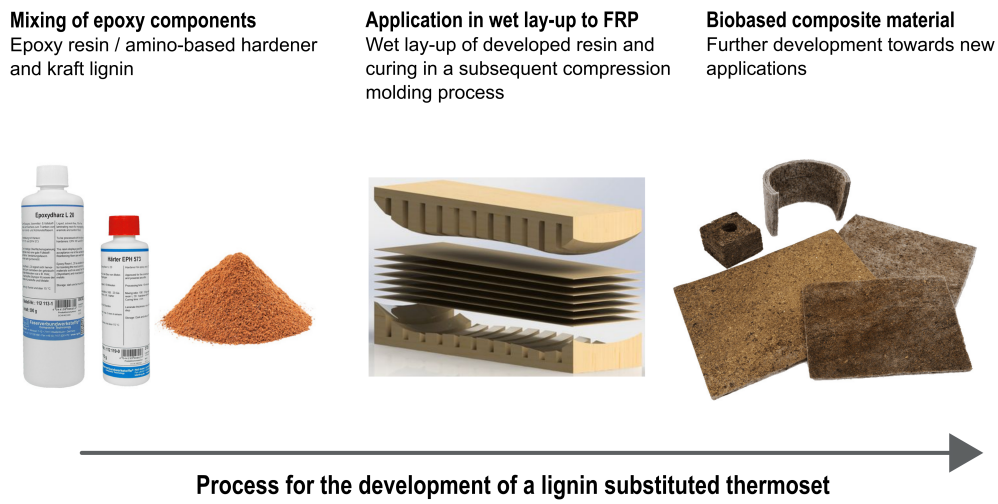

Figure 2.1.: The underlying process for the epoxy formulation developed in this work. Beginning with a lignin substituted thermoset and its characterization and optimization to the assembly in a wet lay–up process resulting in a natural fiber reinfored polymer.

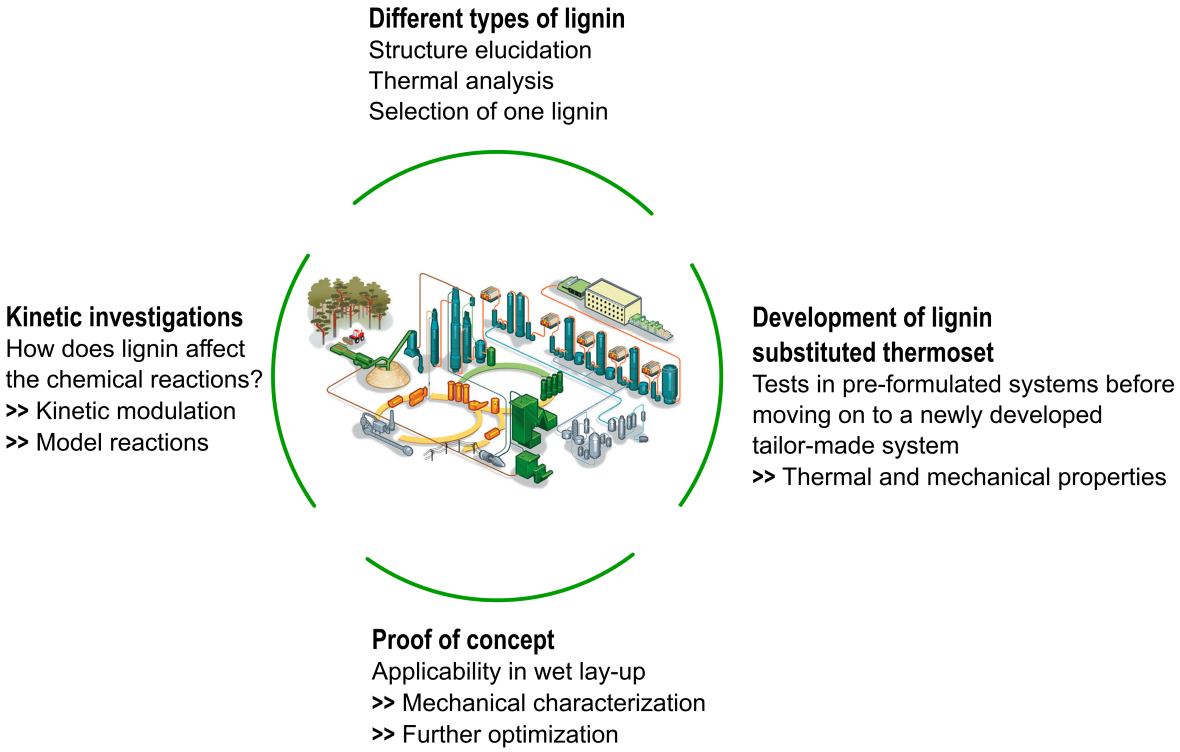

Figure 2.2.: The outlined concept of this work starting with the raw material lignin through the stages of formulation development to its applicability in the composite material. Besides the engineering aspect a further important pillar is the mutual understanding of the reactions taking place.

crucial to assess the different types of lignin available as well as to identify certain positive and negative features.

The aim is to develop a suitable lignin substituted epoxy based thermoset for fiber reinforced polymers which can be applied through wet lay–up processing as summarized in Figure 2.1. First, the chemical characterization and thermal behavior of different types of kraft lignin is paramount. Only with this knowledge a further approach to a biobased thermoset is possible. Thereafter, preliminary experiments with commercial pre–formulated epoxy systems have to be carried out to identify the influence of different types of lignin onto the curing reaction of the epoxy based resin with an amino–based curing agent. Further, the most promising type of lignin from both the chemical as well as the economical point of view has to be selected. For investigations in detail, the development of an entirely new epoxy formulation is necessary. Therefore, an epoxy formulation has to be developed and the influence of lignin on the phase morphology as well as the chemical interaction with the epoxy formulation components have to be studied. Hence, the type of amino–based curing agent, lignin content and the curing conditions have to be varied and optimized. For this type of studies differential scanning calorimetry (DSC) has proven to be a feasible method. During the process of development proofs of concept with regard to the final natural fiber reinforced composite material are important for further characterization and optimization. Therefore, the lignin substituted thermoset has to be introduced in a typical wet lay–up process and tested to ascertain their mechanical and thermal characteristics.

Besides the engineering aspect a further important pillar of this work is to develop a mutual understanding of the chemical processes and influence of lignin onto the different processes of polymerization.

Therefore, kinetic studies have to be carried out utilizing established differential scanning calorimetrical methods as well as a newly derived kinetic model fitted for a lignin substituted epoxy resin. Further, the chemical reactions taking place have to be investigated on molecular level using small molecules as model components for a more thorough and easier characterization regarding the complexity of the highly inhomogeneous lignin molecule. These main aspects are outlined in Figure 2.2.

3 Characterization of Kraft Lignin

The structural and thermal analysis of lignin is important for this work. Generally, analytic characterization of lignin is mostly carried out with spectroscopic methods such as Fourier transform infrared (FT–IR) spectroscopy and nuclear magnetic resonance (NMR) spectroscopy as well as thermal analysis methods like dynamic scanning calorimetry (DSC) and thermogravimetric analysis (TGA).

Due to the availability of a large variety of different lignins, each with a certain set of features, it is important to narrow down the selection with regard to the properties required in the final composite material. Table 3.1 shows the different types of kraft lignins provided for this work. Kraft lignins 1 – 3, an extra purified kraft lignin and an acid washed kraft lignin are all extracted by the same kraft pulping process with only differences in the purifying treatment. However, enzymatic hydrolysis lignin is isolated from the enzymatic hydrolysis residues of the biomass. Acetylated kraft lignin is a modified kraft lignin obtained from the reaction of the OH–moieties of lignin with acetic anhydride. For a simplified representation the types of lignin are assigned abbreviations.

By means of their origin and the manner of the extraction process used, lignins show a large variety of material properties. Regarding the origin of the wood, the composition of the monomeric building blocks coumaryl alcohol, coniferyl alcohol and sinapyl alcohol determine the overall content of OH–moieties. Since NMR spectroscopy has proven to be a reliable method in the domain of wood chemistry, this was also used to characterize the provided lignins. A method using ^{31}P NMR spectroscopy, based on Granata and Argyropolous, was used for quantitative determination of the present different hydroxyl groups.[90] Therefore, the phosphitylation of hydroxyl groups using 2–chloro–4,4,5,5–tetramethyl–1,3,2–diaxophospholane (TMDP) was necessary. A typical ^{31}P NMR spectrum for kraft lignin is shown in Figure 3.1.

With this method the content of aliphatic and phenolic hydroxyl groups as well as the total OH content could be determined. For the determination of the number average molecular weights M_n and weight average molecular weights M_w, gel permeation chromatography (GPC) has been used. Using these values the polydispersity index (PDI $= \frac{M_w}{M_n}$) has been calculated. Residues of the inorganic substances potassium, sodium and sulphur have been determined by elementary analysis. Those properties of the different types of lignin, measured and analyzed in cooperation with UPM, are summarized in Table 3.2.

Table 3.1.: The seven different types of lignins provided for this work: Three kinds of kraft lignin (KL_1 – KL_3) and additionally four different post–treated lignins xpKL, awKL, EHL and acKL.

Type of Lignin	Abbreviation
Kraft Lignin 1	KL 1
Kraft Lignin 2	KL 2
Kraft Lignin 3	KL 3
Extra purified kraft Lignin	xpKL
Acid washed kraft Lignin	awKL
Enzymatic Hydrolyzed Lignin	EHL
Acetylated kraft Lignin	acKL

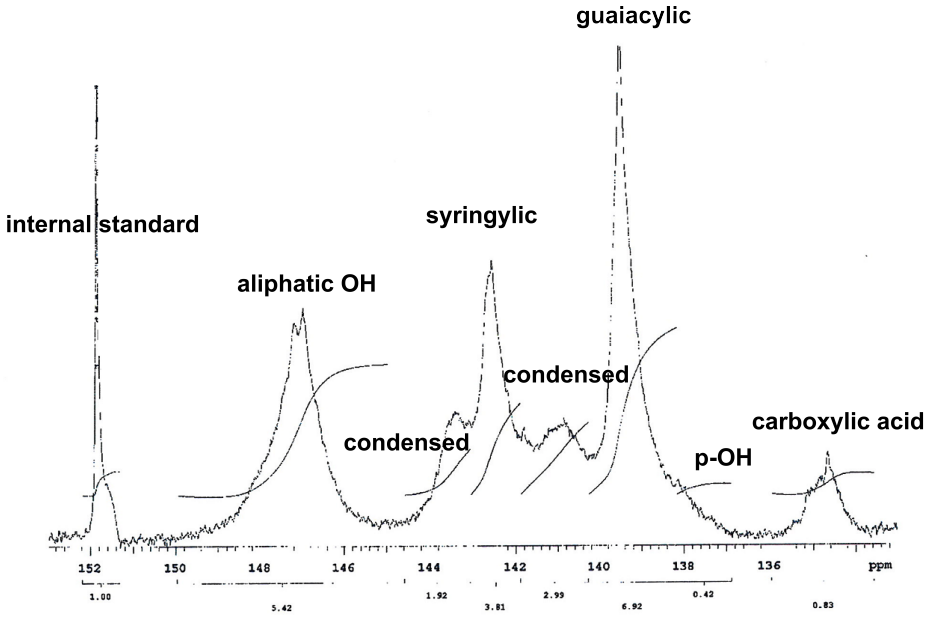

Figure 3.1.: Exemplary ^{31}P–NMR spectrum of kraft lignin derivatized with 2–chloro–4,4,5,5–tetramethyl–1,3,2–diaxophospholane and its assignment to the different OH-moieties and functional groups. Kindly supplied by UPM.

The available lignins show a very broad range of average molecular weight distributions resulting in kraft lignins with mediocre PDIs of around 3.0 like KL 1 – KL 3 as well as xpKL and awKL. On the contrary, EHL shows a fairly high PDI of 6.3. This results from the different pulping method used for EHL in which the carbohydrates are broken down before the fragmentation of lignin, resulting in higher molecular weights. This differences can also be seen in the content of the aliphatic and phenolic hydroxyl groups. Whereas the kraft lignins extracted with the standard kraft process show a nearly identical amount of aliphatic and phenolic OH groups, EHL shows a large share of carbohydrates with even six times the quantity compared to KL 1. Regarding the inorganic substances potassium and sodium significant differences comparing the further purified kraft lignins to KL 1 – 3 become visible. In the following the exemplary characterization of KL 1 is shown and the accompanying difficulties are addressed and discussed.

Increasing molecular weight broadens the resonance due to reduced relaxation times. However, lignin with its highly random and heterogeneous structure further complicates the assignment of chemical shifts and coupling constants. Figure 3.2 shows an example for a ^{1}H–NMR spectrum of kraft lignin (solvent THF–d8). Besides the two major peaks of the solvent THF–d8, three regions can be assigned to structural components present in the kraft lignin. Between the signals of 6.0–9.5 ppm aromatic protons appear, whereas aliphatic protons appear in the region between 0.5–3.0 ppm. The most distinctive signal in the area between 3.0–6.0 ppm can be correlated with protons in the chemical environment of oxygen or sulfor atoms in lignin. The acquired signals are shown in Table 3.3 with their assignment to the structural components of lignin.

The different functional groups can be identified, however, the precise structure can only be presumed. For further characterization of the chemical structure fourier–transform infrared (FTIR) spectroscopy was used. Figure 3.3 presents the FTIR spectrum of KL 1. The broad band at 3390 cm^{-1} is assigned to the OH groups in the phenolic and aliphatic structures of lignin as well as residual water. The 3000 cm^{-1} –

Table 3.2.: Mean number and weight average molecular weights M_n and M_w for the different lignins as well as the calculated PDI and content of OH–groups and inorganic compounds.

	Unit	KL_1	KL_2	KL_3	KL_{xp}	KL_{aw}	KL_{eh}
M_n	[g/mol]	1 244	983	718	1 160	1 340	1 276
M_w	[g/mol]	4 224	2 624	2 306	4 178	4 322	7 999
PDI		3.4	2.7	3.2	3.6	3.2	6.3
Total OH	[mmol/g]	5.2	4.8	5.6	5.4	-	4.2
Aliphatic OH	[mmol/g]	1.1	1.1	1.1	1.0	-	1.3
Phenolic OH	[mmol/g]	3.8	3.4	4.3	3.9	-	1.6
Carbohydrates	[mg/g]	7.6	6.9	0.0	7.4	5.4	42.5
Potassium	[mg/kg]	455	519	106	87	87	144
Sodium	[mg/kg]	2 330	3 954	4 061	90	408	5 923
Sulphur	[mg/kg]	22 867	23 060	9 110	18 546	22 099	1 539

Table 3.3.: Chemical shifts and integration regions for kraft lignin by ^1H–NMR.

Chemical shift	Assignment
1.18	$–CH_3$, $–CH_2–$
1.62	$–CH_2–$
2.55	H_2O, $–CO–CH_2–$
3.54-3.80	R-OH, $–O–CH_3$, secondary alcohols, $–C–SH$
6.61-6.77	Alenes, aromats, phenols

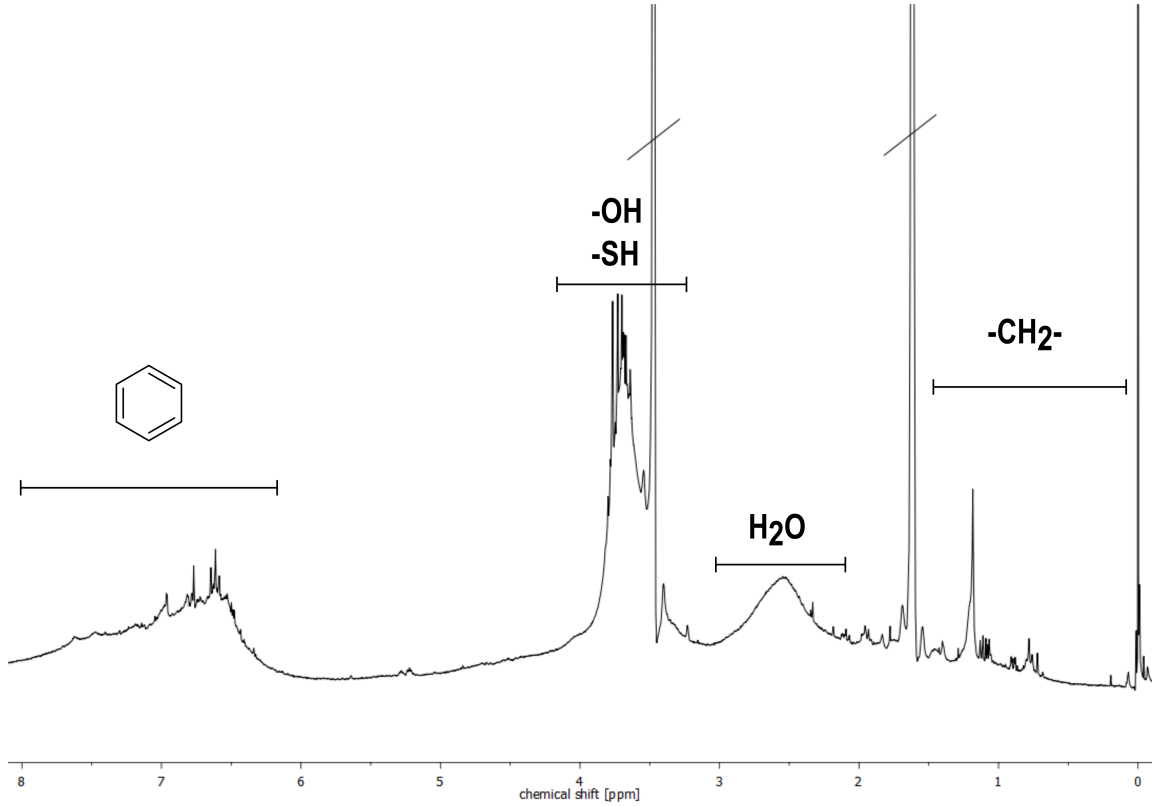

Figure 3.2.: ^1H–NMR spectrum of kraft lignin in THF–d8 and its assignment to structural components.

2800 cm^{-1} region of the predominantly $C-H$ stretching is attributed to methoxyl groups and in methyl and methylene groups in the side chains. At 1700 cm^{-1} a weak carbonyl stretching vibration is observed. Aromatic skeleton vibrations at 1595 cm^{-1} and 1514 cm^{-1} and the C—H deformation combined with aromatic ring vibration at 1456 cm^{-1} are observed. The region below 1400 cm^{-1} contains vibrations specific to the different monolignol units. The spectrum shows the characteristic vibrations for the guaiacyl unit: 1267 cm^{-1} for the ring and C=O stretch, 1143 cm^{-1} for CH in–plane deformation and 846 cm^{-1} and 831 cm^{-1} for the C–H out–of–plane vibrations in position 2, 5 and 6 of guaiacyl units. The assignments are summarized in Table 3.4.

Table 3.4.: Assignment of the wavelength ν to the vibrational states of kraft lignin KL_1.

ν [cm^{-1}]	Vibration	Assignment
3390	OH stretching vibration	$–OH$, H bridges
2939; 2836	CH stretching vibration	$–CH_3$, $–CH_2–$
1700	C=C, C=O vibration	–C=O
1595; 1514	aromatic skeletal vibrations	aromats
1456	CH bending vibration aromatic ring vibration	CH, aromats
1267-1027; 1143; 846;831	aromatic CH bending vibration complex C–O, C–C and C–OH vibrations	

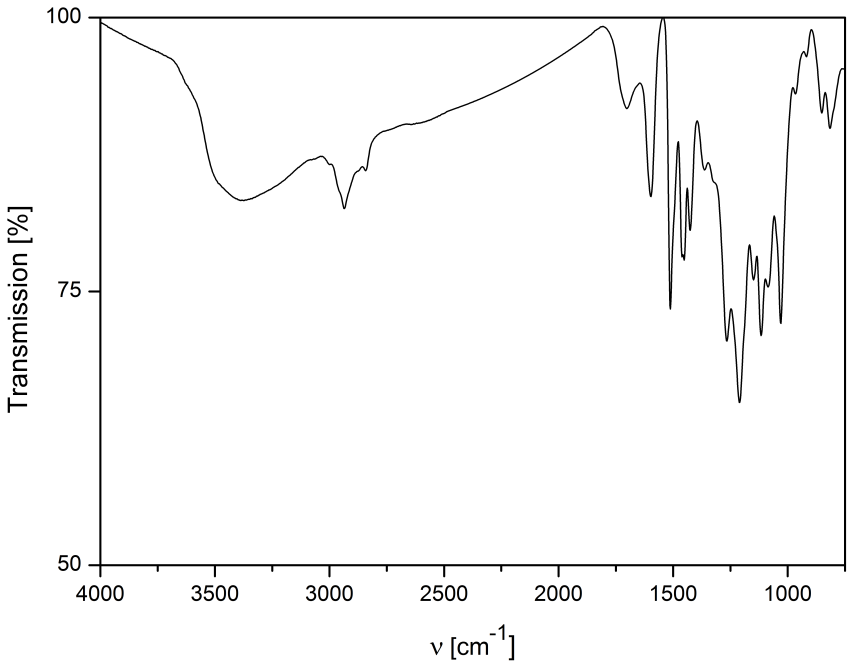

Figure 3.3.: FTIR spectrum of kraft lignin KL_1.

For the introduction of kraft lignin in organic resins and curing agents as well as in solvent aided processing methods like the prepreg process it is necessary to investigate the solubility of lignin in organic and aqueous solvents.

The ability of a solvent to dissolve or swell lignins is affected by the hydrogen–bonding capacities and its solubility parameters. Lower molecular weight fraction of lignin show an easier solubility regarding solvents with a broad range of hydrogen-bonding capacities and its solubility parameters in contrast to the high molecular weight fractions. As 1 g of lignin was diluted in the selected solvent leading to the results shown in Figure 3.4.

As already described in literature, it can be noted that an entire solubility is observed in NaOH, acetone-water (1:1), dioxane, THF and DMSO whereas kraft lignin in toluene and water is completely insoluble. In methanol, ethanol and acetone just a small amount of lignin dissolved in the solution. Regarding this result it can be assumed that the provided kraft lignin is composed of different fractions with varying molar mass and thus the fractions with small molar mass are easily dissolved. Further, the organic solvents THF and dioxan with their relatively low boiling points are suitable for following processing. However, it would be interesting to use fractionated lignin with a uniform molar mass to open up a larger range of available solvents.

3.1 Preparation of Acetylated Lignin

In order to ensure a higher solubility in the hydrophobic epoxy resin and to determine the influence of the OH–moieties on the curing reaction of the epoxy resin with kraft lignin, the hydrophobicity of the lignin needs to be increased. Therefore, the lignin was acetylated with acetic anhydride according to

Figure 3.4.: Solubility of different lignins in selected solvents. From left to right: 1M NaOH, water-acetone (1:1), dioxane, methanol, THF, DMSO, acetone, ethanol, toluene and pure water.

the following procedure: A weighted amount of dried lignin was dissolved in the fourfold amount of dried pyridine. Subsequently, a stoichiometric amount of acetic anhydride is added and stirred at room temperature over night. Methanol was used to quench the remaining acetic anhydride. Afterwards, the solvents were removed through distillation. The crude product was washed with the fivefold quantity of toluene. Finally, the product was dried at 60 °C under vacuum. A brown crystalline solid was obtained with yields around 90 – 95 %. Figure 3.5 shows the reaction mechanism of the acetylation of kraft lignin. [73,91]

Figure 3.6 shows the NMR spectrum of the acetylated kraft lignin (acKL). Compared to the unmodified kraft lignin a significant change in the aromatic range at around 7 ppm as well as strong signals at 2 ppm is present. The singulett at 2.28 ppm results from the introduced methyl group of the acetate ester. If the unconverted educt acetic anhydride had been present as by–product, a singulett at 2.10 ppm would have been present as well as another singulett at 9.48 ppm. The NMR spectrum shows that the acetylated lignin obtained with the selected reaction route is pure and for further measurements usable. Further assignment to the molecular structure (cf. Figure 3.6) is outlined in Table 3.5.

The FTIR spectrum shown in Figure 3.7 illustrates the comparison of the educt kraft lignin with the acetylated lignin which show a significant difference. The obtained signals can be matched to the vibrations of acetylated lignins described in literature. [91,92] Due to the vanishing of the OH stretching vibration at 3390 cm^{-1} it can be assumed that the OH–moieties have been fully transformed. In addition, the intensity of the carbonyl signal at 1700 cm^{-1} increases due to the aromatic and aliphatic stretching vibrations. Apart from this, the signals remained consistent, which indicates that the acetylation reaction

Table 3.5.: Chemical shifts and integration regions for acetylated kraft lignin by ^1H–NMR assigned to the right hand structure.

Chemical shift	Assignment
1.18	-CH_3, -CH_2-
1.92-1.99	$-COCH_3$, -CH_2-
	CH_3 of acetic anhydride
2.21-2.28	H_2O, -CO-CH_2-, CH_3-OOR
3.59-3.82	-O-CH_3, secondary alcohols, -C-SH
6.93-7.20	Alenes, aromats, phenols

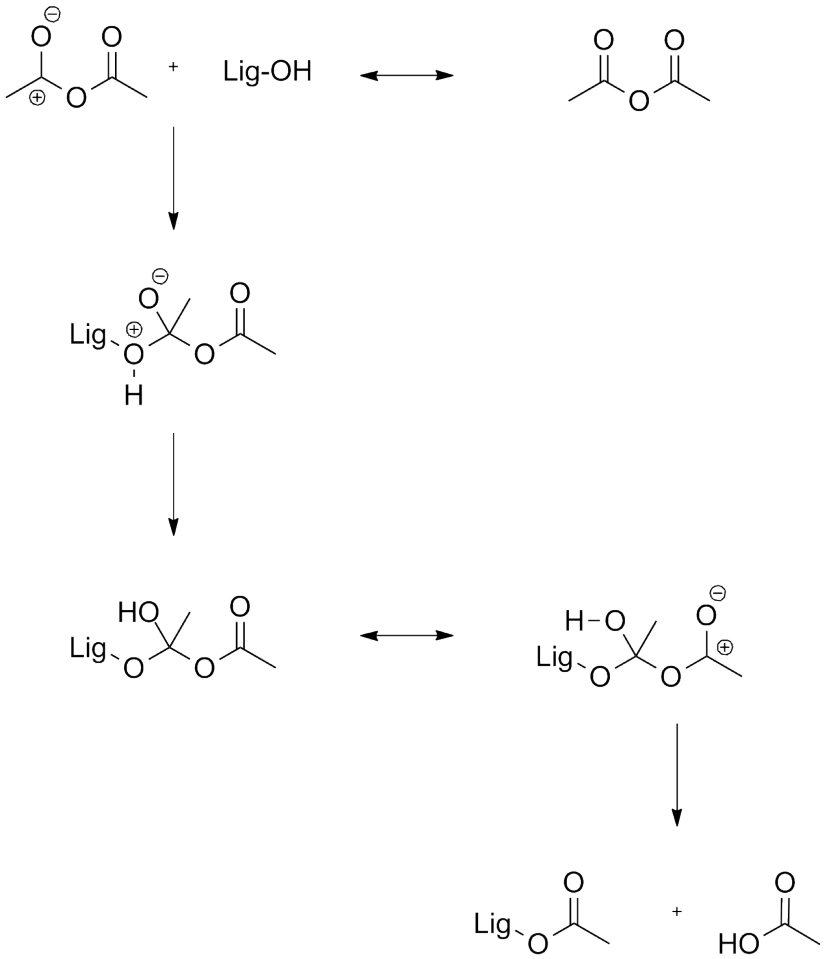

Figure 3.5.: Mechanism of the reaction of acetic anhydride with lignin resulting in acetylated lignin.

took place at the OH–moieties exclusively. From the results of the NMR and FTIR spectra it can be shown that a pure acetylated lignin could be prepared.

After the preparation, the solubility of acetylated lignin was tested as well. Figure 3.8 shows the acetylated lignin dissolved in the selected solvents. Just like kraft lignin, the acetylated lignin dissolves in acetone and THF as well. In water-acetone (1:1) the solution is slightly turbid resulting from dispersed

Table 3.6.: Assignment of the wavelength ν to the vibrations of acetylated kraft lignin.

ν [cm^{-1}]	Vibration	Assignment
2937; 2850	CH stretching vibrations	$-CH_3$, $-CH_2-$
1759; 1741	C=O vibration	$-C=O$ aliphatic and aromatic
1595; 1508	aromatic skeletal vibrations	aromats
1462; 1423		$-CH_2-$, $-CH_3$
1367	aliphatic $C-C-$	
1188; 1128	aromatic CH deformations	$C-O$, $C-H$, $C=O$
1036; 1014	complex $C-O$, $C-C$	
1036	$C-O$	alcohols

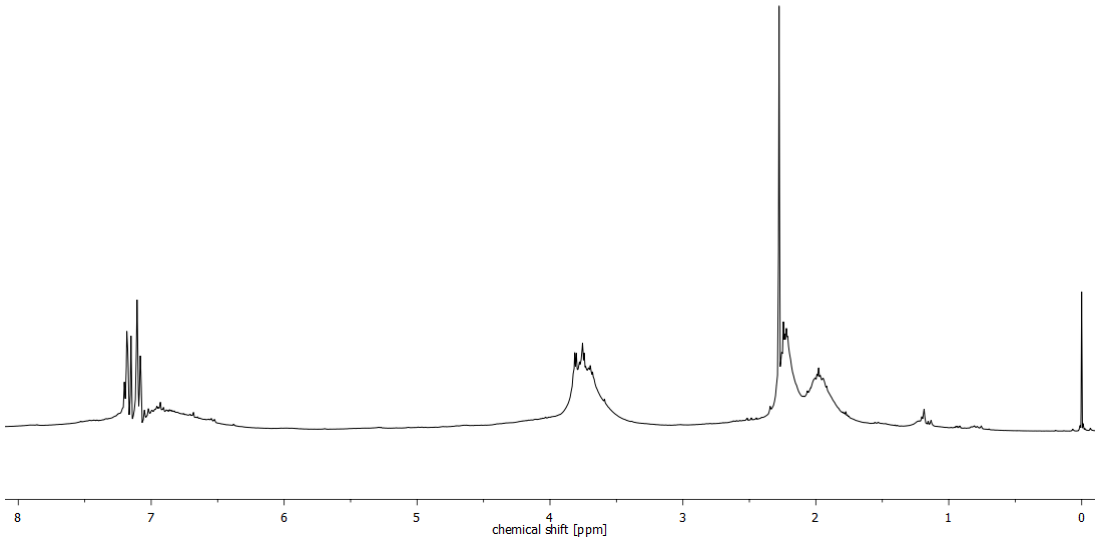

Figure 3.6.: ^1H–NMR spectrum of acetylated kraft lignin.

lignin. A complete insolubility is obtained in ethanol and water. The solubility of acetylated lignin in epoxy resin and curing agent was tested as well resulting in complete insolubility in both components.

3.2 Thermal Characterization

In order to understand the thermal behavior of lignin to define processing temperature and time in the final composite, the available kraft lignins were characterized by dynamic scanning calorimetry, thermogravimetric analysis as well as pyrolysis GC/MS. The results are discussed in more detail in the following.

The dynamic scanning calorimetry measurements were carried out to study general properties like moisture content, T_g as well as the behavior of lignin under recurring variations of temperature. Due to the extraction process of the pulp, different degrees of depolymerization are achieved affecting the molar mass and thus the T_g. In the first heating run of an unaltered sample of kraft lignin (Figure 3.9a) a broad endothermic peak reveals the presence of a large amount of water. This relatively high moisture content compared to other polymers is a common property of lignin due to its hygroscopic nature.

The second heating runs are shown in Figure 3.9b presenting the glass transition temperatures of all available lignins. The glass transition temperatures are all in a broad temperature range as expected for kraft lignin. As for the standard kraft lignins $KL_1 - KL_3$ (Figure 3.9b, left) the T_g increases clearly with increasing molecular weight, differing from the shortest kind of lignin KL_3 with a T_g of 111.1 °C and M_w of 1422 g/mol to a T_g of 154.2 °C of KL_1 with M_w of 4224 g/mol.

Regarding the altered lignins KL_{aw}, KL_{xp}, KL_{eh} and KL_{ac} (Figure 3.9b, right) the trend continues: with an increasing M_w a higher T_g is obtained. Both, the KL_{xp} and KL_{eh}, show a very broad and small

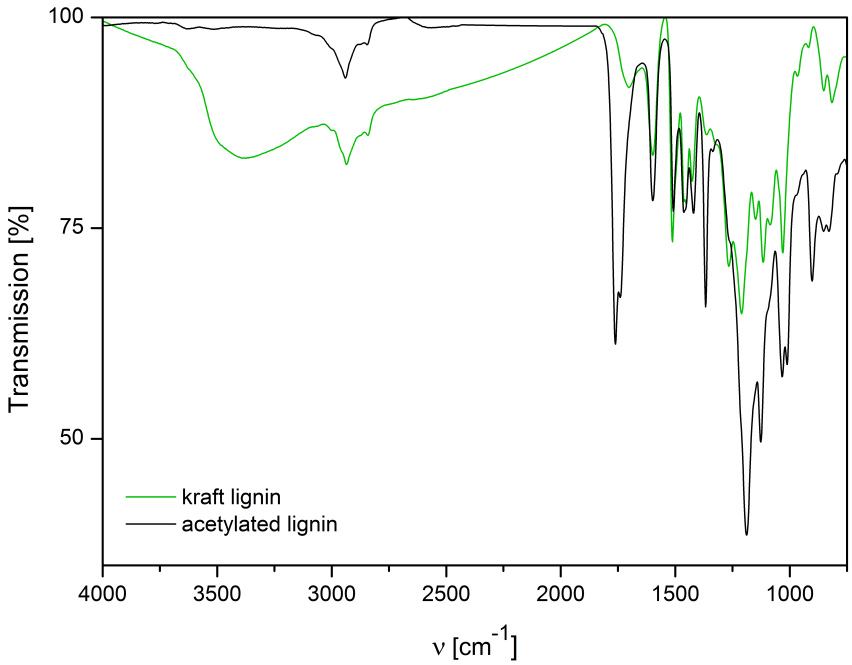

Figure 3.7.: FTIR spectrum of acetylated kraft lignin.

Figure 3.8.: Solubility of different lignins in selected solvents. From left to right: Acetone, THF, DGEBA resin and curing agent as well as ethanol, water, acetone-water (1:1).

pronounced glass transition compared to the other lignins. Solely the acetylated lignin shows a distinct glass transition at a much lower temperature at 104 °C. The glass transition temperatures as well as the weight average molecular weight of the various types of lignins are summarized in Table 3.7.

Table 3.7.: Glass transition temperatures for various lignins determined by DSC measurements.

Lignin	M_w [g/mol]	T_g [°C]
KL_1	4224	154.2
KL_2	2624	149.8
KL_3	1422	111.1
KL_{xp}	4178	154.2
KL_{aw}	4322	144.4
KL_{eh}	7999	163.7
KL_{ac}	-	104.0

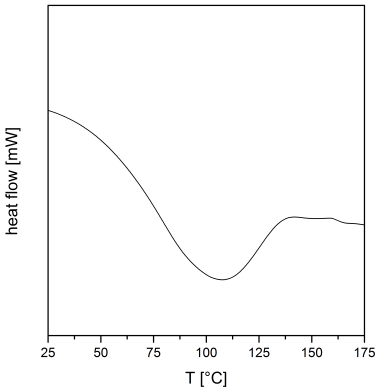

(a) Exemplary DSC thermogram of the first heating cycle of unaltered kraft lignin.

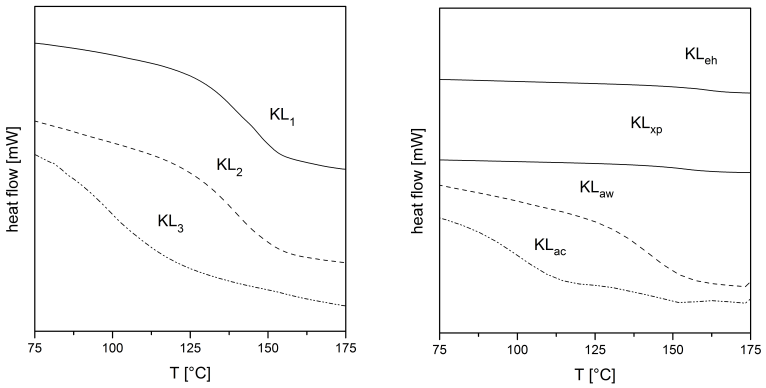

(b) DSC thermograms of the standard kraft lignins KL 1 - 3 and modified kraft lignins KL_{aw}, KL_{xp}, KL_{eh} and KL_{ac} used in this work.

Figure 3.9.

Since most polar amorphous solids absorb a significant amount of water from their surroundings, the identical behavior is to be expected for lignin as already seen in the first heating cycle in Figure 3.9a. To determine if a hygroscopic effect occurs, the kraft lignin was dried completely before the measurement. To remove water absorbed on the lignin surface as well as the bound water, different strategies were tried. The most successful route proved to be azeotropic distillation with toluene and handling the dried lignin samples under inert atmosphere.

Figure 3.10 shows the absorption capacity of dried lignin under atmospheric conditions at room temperature after removal from inert conditions over a period of 24 h. It is obvious that the absorption of water proceeds rapidly in an exponential manner. The major part of water is absorbed in the first 2.5 h with a weight increase of 4 % and approaches saturation after 5 h with a total weight increase of 4.5 %. This means, that the moisture content of lignin has to be taken into account during processing of the final composite material. Since the moisture might lead to preliminary failure and void formation, the processing has to be adapted since drying the lignin beforehand and handling under inert conditions would mean a significant cost and time factor.

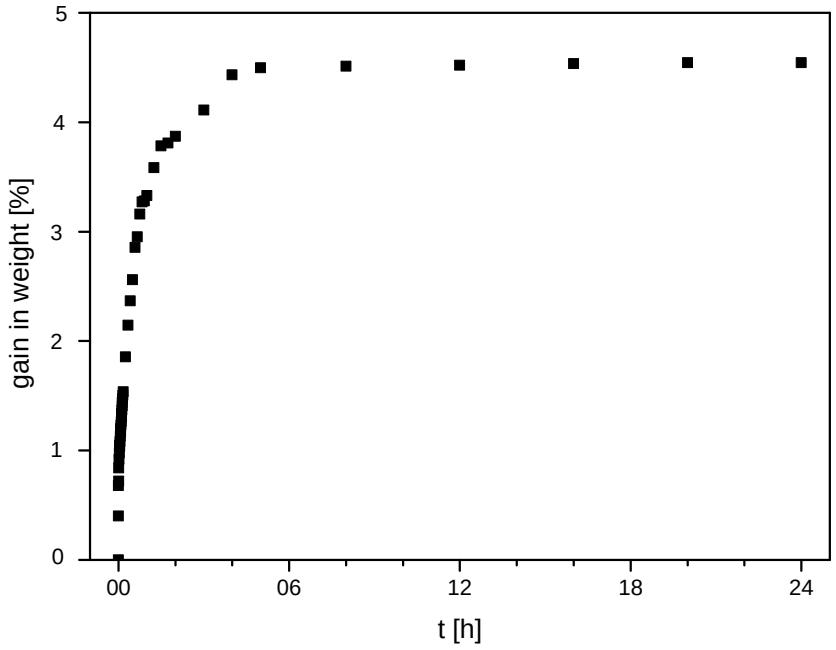

Figure 3.10.: Total moisture absorbance of 4.5 % water of kraft lignin after 24 h under atmospheric conditions.

Composite materials are generally processed at elevated temperatures. In order to incorporate lignin into those materials, it is essential to know how the unaltered lignins themselves degrade at higher temperatures. Therefore, thermogravimetric analysis (TGA) and pyrolysis GC/MS (Py-GC/MS) were used to investigate the thermal degradation and stability of lignin.

TGA studies on eight samples of lignin were carried out from 20 °C up to 600 °C with 10 K/min under inert as well as atmospheric conditions. The mass loss curves for the different lignins are presented in Figure 3.11. An initial mass loss between 20 °C and 150 °C is attributed to loss of inter– and intramolecular bound water. The prominent stage of decomposition stretches from 200 °C to 600 °C and can be divided into two main stages. The sample KL_1 shows clearly the first stage at 100 °C to 420 °C resulting as known from literature from CO_2, CO, formaldehyde, alcohols and phenols due to the cracking and reforming of thermolabile carboxyl, carbonyl and ether groups in the phenylpropane side chain. The second stage spreads from 420 °C to 600 °C and is explained by the continuous formation of CO_2, CO and the release of CH_4.[93] The formation of CO at high temperatures of over 500 °C is ascribed to the breaking of diaryl ether groups and secondary pyrolysis volatiles. Generally, the reactions responsible of the release of volatiles are due to the instability of the propyl chains, of linkages between monomer units and of the methoxy substituents of the aromatic rings.[14,16] It is obvious that KL_1, KL_2 and xpKL have a higher initial decomposition temperature compared to EHL. Depending on several studies, those differences occur due to the differences in the origin of the lignin and in the method used for their extraction. Therefore, EHL with its high carboxy content is prone to early decomposition due to the carboxy's thermolability.[94,95]

For further thermal characterization, KL_1 was exemplary analyzed with pyrolysis GC/MS. With this method, it is possible to simultaneously separate and identify lignin components which are volatile

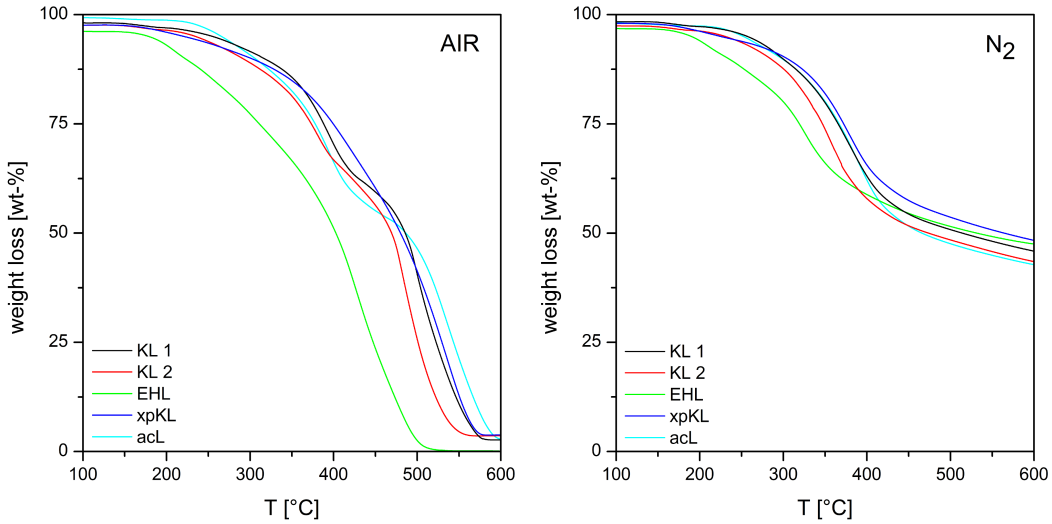

Figure 3.11.: TGA thermograms of KL_1, KL_2, xpKL and EHL as well as the acetylated kraft lignin acKL.

enough to be observed by gas chromatography (GC) and mass spectroscopy (MS). In Figure 3.12 the gaschromatogram of KL_1 measured with evolved gas analysis technique is shown. Therefore the sample was pyrolyzed at 600 °C with 10 K/min. The results confirm the TGA measurements: the release of moisture happens at temperatures up to 100 °C and the degradation of lignin starts at around 220 °C. However, the inhomogeneous structure of lignin makes this method not feasible for further characterization.

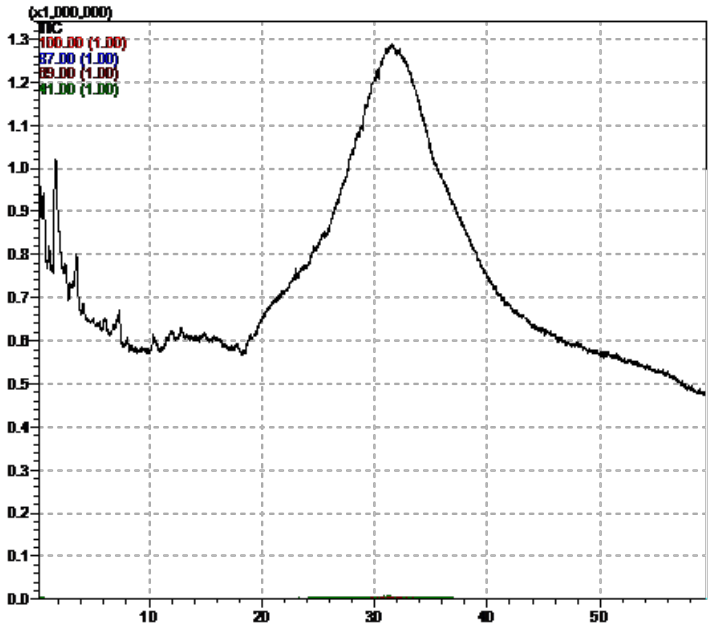

Figure 3.12.: Evolved gas analyzed Py-GC/MS elugram of kraft lignin.

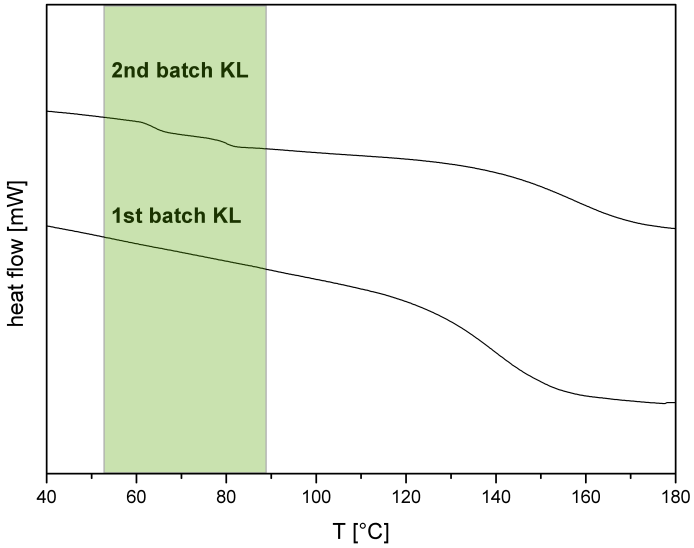

Figure 3.13.: Differences between the first and second batch of extracted kraft lignin due to the large–scale pulping process of wood which is a challenge with regard to inhomogeinities in the lignins.

3.3 Pretreatment of Lignin

Due to the large-scale pulping process of wood and the extraction of lignin it is a challenge to guarantee uniform properties for different batches of lignin. Inhomogeneity due to the wide molecular weight distribution of lignin as well as inorganic impurities resulting from process chemicals such as NaOH and Na_2S cause severe problems like toxicity and odor development during thermal treatment. [96,97] Figure 3.13 shows DSC thermograms of two different batches of kraft lignin which demonstrates the problem of inhomogeneity more precisely: Batch 1 shows the typical single T_g of lignin at 154.2 °C whereas batch 2 has three T_g values in total, two below 100 °C and the known T_g at 152.9 °C suggesting the presence of low-molecular weight fractions of kraft lignin.

Table 3.8.: Overview of the different purification methods as well as used solvents and extraction times.

Solvents	Extraction time
Dialysis	
0.5M NaOH	2 h
0.5M NaOH	24 h
THF	24 h
Ultrafiltration	
THF	24 h
Solvent Extraction	
Ethyle acetate	24 h
Methanol	24 h
Acetone	24 h

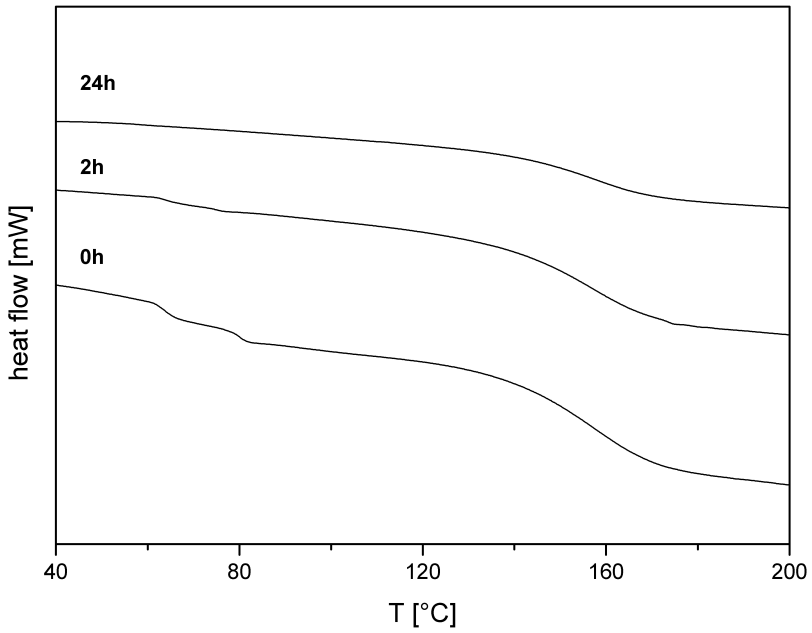

Figure 3.14.: Influence of different extraction times of 0 h, 2 h and 24 h on the T_g values in the purified kraft lignin.

This could lead to different miscibilities, cross-linking densities as well as mechanical properties in the final material. Therefore, different purification methods such as dialysis, solvent extraction and ultrafiltration were applied to investigate the influence of inhomogeneities and impurities on the processability in the resin. The essential values of the three purification processes are presented in Table 3.8. The first two processes, dialysis and ultrafiltration, follow the model of size–exclusion by means of diffusion of solutes and the filtration of the fluid through a semi–permeable membrane. In case of solvent extraction, the kraft lignin was dispersed in a solvent in which lignin is partially soluble. As a result inorganic impurities as well as certain pulping–induced biomass fragments remain in the residue.

Dialysis was carried out with three different extraction times of 2 h, 24 h and 96 h in which kraft lignin was dissolved in a 0.5 M NaOH solution and dialyzed against water (molecular weight cutoff 12-14 kDa; Medicell International Ltd). Every 12 h the NaOH phase is removed and replaced with a fresh NaOH solution. Afterwards, the purified kraft lignin was freeze–dried and analyzed. To investigate the influence of the dialysis time on the T_g DSC measurements were carried out, the obtained results are shown in Figure 3.14.

It is evident that with increasing extraction time the T_g values 63.7 °C and 80.1 °C decrease and vanish after 24 h. Thus, it can be assumed that the low–molecular weight fractions of the kraft lignin have been removed with this pretreatment step. Further, the T_g at 159 °C is not displaced by dialysis which indicates that the treatment did not affect the overall structure of lignin. Therefore, dialysis is a feasible tool to size exclude undesired molecular weights with regard to maintain product quality and properties.

Dialysis was especially efficient with the separation of low molecular weight fractions of kraft lignin whereas ultrafiltration and solvent extraction do not lead to desired results. Figure 3.15 illustrates the

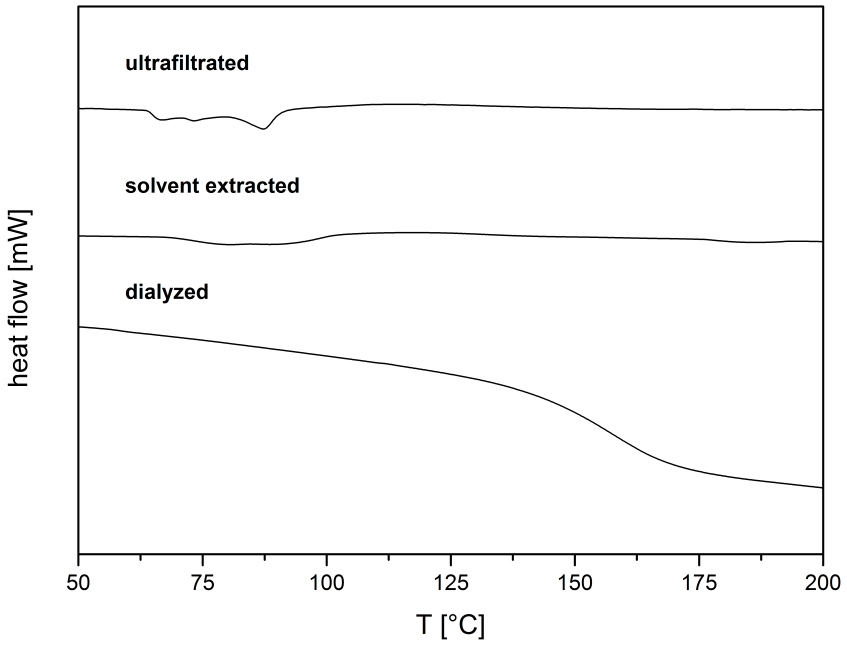

Figure 3.15.: DSC thermograms of the lignin samples purified with ultrafiltration, solvent extraction and dialysis. The second heating run is shown.

effects of the used purification methods on the glass transition temperature(s). It is evident, that the residue after ultrafiltration shows multiple glass transitions comparable to those already seen in the second batch of KL in Figure 3.13 resulting of low-molecular weight fractions of lignin. In comparison, the dialyzed sample shows a single glass transition temperature in at a slightly higher temperature. In between those methods falls the solvent extracted lignin which shows glass transition temperatures of low-molecular weight fractions as well as the well pronounced glass transition of the high-molecular weight fraction leading to no satisfactory purification product.

Table 3.9 presents the results of the elemental analysis with regard to sulfur content compared to the crude lignin. Crude kraft lignin contained 2.16 % sulfur which could not be removed by dialysis. This means, that the sulfur compounds are either insoluble in NaOH solution or the sulfur is chemically bound in the lignin molecule. The sulfur content decreased after purification minimally. As already shown in

Table 3.9.: Comparison of determined sulfur content with elemental analysis with regard to different purification methods, solvents and extraction times.

Sample	Solvent	Time [h]	S [%]
KL1-crude	-	-	2.16
KL1-dialyzed	NaOH	2 h	2.08
KL1-dialyzed	NaOH	24 h	2.02
KL1-dialyzed	NaOH	96 h	2.01
KL1-extraction residue	Ethyl acetate	24 h	2.18
KL1-extracted lignin	Ethyl acetate	24 h	1.58

Figure 1.10, sulfur is bound in the lignin molecule in form of mercaptans which are prone to remain in the final product. In contrast, solvent extraction showed best results by decreasing the sulfur content below 2 %. Hence, solvent extraction proves to be the method of choice for lignin pretreatment with regard to sulfur reduction.

4 Preliminary Studies with Commercial Pre–formulated Epoxy Resins

After the first characterization and pretreatment steps of the crude kraft lignin, the behavior of kraft lignin within the epoxy resin is investigated. To this purpose, a readily available 2–component epoxy formulation, which is typically used in the targeted applications, was used. Preliminary testing helped narrow down fundamental parameters, such as the most suitable type of kraft lignin and content. Both alter the thermal and mechanical properties of the epoxy resin. Based on these considerations the laminating resin MGS® L285 with the corresponding hardener MGS® L285 were selected. The individual components and their weight share in the resin and hardener respectively are listed in Table 4.1. [98]

The L285 resin consists of a typical bisphenol A based diglycidyl ether (DGEBA) with an average molecular weight of 700 g/mol and glycerol diglycidyl ether as reactive diluent primarily to reduce the high viscosity. The main compound of the L285 hardener is 3–Aminomethyl–3,5,5–trimethylcyclohexylamine, commonly abbreviated as Isophorondiamine (IPDA). Benzylalcohol as well as nonylphenol are accelerators which increase the reaction rate of the epoxy resin.

4.1 Thermal characterization

The processing takes place in the range of $20-40\,^{\circ}C$ to reach an optimum pot life of 40 min up to 4 h and a final curing temperature of $50-55\,^{\circ}C$. Typical processing methods are pressure and injection molding, pultrusion and wet lay–up. The formulation meets the requirements for high static and fatigue strength. Properties which are important in composite materials.

First of all, the mixing behavior of the different kinds of lignins as well as different filler amounts of 10 %, 20 %, 40 %, 60 % and 80 % kraft lignin were investigated to study the handling of the lignin filled epoxy resin. The preparation of the formulation batches was carried out in a laboratory dissolver with adapted vacuum vessel. The dispersion time chosen was 15 min at a stirring rate of 3500 rpm. As expected, the dispersability decreased with an increase of the lignin share. However, a dramatic increase in viscosity was noticeable with lignin shares higher than 40 %.

It was observed that the dipersability of the standard kraft lignins KL_1, KL_2 and KL_3 decreased with decreasing average molecular weight. As for KL_3, which shows the lowest molecular weight, the dispersion of lignin in the epoxy was already with loads of 20 % lumpy and barely pourable. On the

Table 4.1.: Commercial epoxy formulations used for preliminary tests with kraft lignin.

Substance	Content
MGS® L285 resin	
Bisphenol A diglycidyl ether	50 – 70 %
Glycerol diglycidyl ether	50 – 70 %
MGS® L285 hardener	
3–Aminomethyl–3,5,5–trimethylcyclohexylamine	70 – 90 %
Benzylalcohol	7 – 10 %
Nonylphenol	1 – 2 %

contrary KL_1 and KL_2 showed a very good dispersability in the epoxy resin even at very high loads. However, at 60 % lignin share and above small aggregates became visible. Regarding the modified kraft lignins, they show identical behavior as the unmodified KL_1 and KL_2. Since the processability of a lignin substituted thermoset with cellulose fibers via wet lay–up methods is intended, an important criterion is the viscosity. Therefore, Table 4.2 shows the suggested amount of lignin which is still properly processable with wet lay–up methods regarding their suitable rheological properties.

Subsequently, the curing behavior of the neat L285 resin as well as L285 resin filled with 10 %, 20 %, 40 %, 60 % and 80 % kraft lignin were investigated. Therefore the samples were prepared and cured according to manufacturers advice at 55 °C for 24 h. DSC measurements were carried out to investigate the thermal behavior of these samples compared to the neat L285 resin.

Figure 4.1 presents the resulting DSC thermograms of the first and second heating run for the neat L285 as well as the kraft lignin filled L285 resin. The neat L285 resin shows a glass transition at 81.2 °C after the curing and a final glass transition at 93.9 °C after the second heating run. However, apparently a minimal degree of postcuring occurred during the first heating run since the T_g values are slightly increased in the second heating run. Therefore, it can be assumed that the cross-linking reaction is mostly finished after the initial curing reaction resulting in a typical T_g value of around 88.2 °C. [98]

With the addition of 10 – 40 % kraft lignin the thermal behavior of the cured samples remains approximately the same resulting in a slightly higher glass transition at 95.8 °C. With amounts of 60 % and 80 % kraft lignin a distinctive shift of the glass transition temperatures to lower values in the first heating run is visible. Up to 40 % kraft lignin share, the first heating run does not present a residual exothermic peak and therefore the curing reaction appears complete. Yet for the 60 % and 80 % kraft lignin filled L285 resin an exothermic reaction is observed at 120 °C. This explains the reduced glass transition temperature in the first heating run since the cross-linking reaction has not been completed after curing at 55 °C.

These tendencies are also demonstrated in Figure 4.2. The left hand graphic shows the behavior of the glass transition with the addition of lignin as they were obtained in the first heating run. Up to loads of 40 % kraft lignin the T_g remains constant, however increasing the loads further to 60 % and 80 % the T_g drops rapidly suggesting the engagement of kraft lignin in the cross–linking process of the epoxy reaction. It can be assumed that high loads of lignin affect the cross–linking reaction between DGEBA and IPDA by extending the diffusion path between the educts resulting in incomplete cross-linking by reaching the gel point. This is being further confirmed by the second heating run: heating up over the current T_g, the unreacted educts become mobile and are able to react leading to full conversion. [99–101]

Table 4.2.: Processability of different types and concentrations of lignin in epoxy resin. √ = processable ∅ = non–processable.

Type of Lignin	10 %	20 %	40 %	60 %	80 %
KL_1	√	√	√	∅	∅
KL_2	√	√	√	∅	∅
KL_3	√	∅	∅	∅	∅
KL_{eh}	√	√	∅	√	∅
KL_{aw}	√	√	√	√	∅
KL_{xp}	√	√	√	√	∅

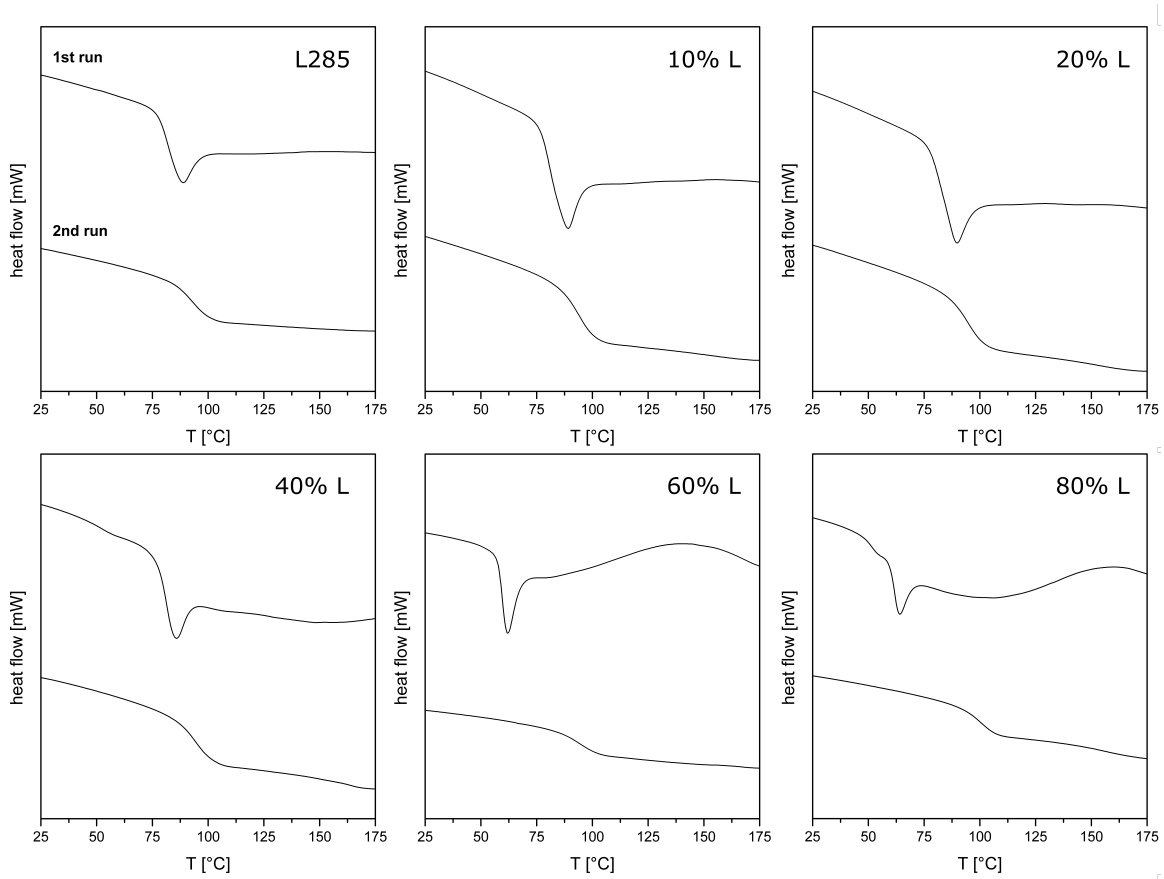

Figure 4.1.: DSC thermograms of the neat L285 as well as samples filled with 10 %, 20 %, 40 %, 60 % and 80 % kraft lignin. Each sample was cured at 55 °C for 24 h.

As shown in Figure 4.2 (right) the glass transition values increase clearly with increasing lignin share. The increase in T_g may be attributed to the loss of mobility of the chain segments of the epoxy resin resulting from the interaction between lignin and matrix. Hence, it can be assumed that the impeded chain mobility results from a homogeneous dispersion of lignin in the epoxy resin. Another important aspect is the presence of one or several T_g from which conclusions about the existing phase separation of the material can be drawn. The DSC thermograms of 10 % and 20 % kraft lignin filled L285 resin present a single distinctive glass transition in the range of the neat L285 resin at around 80 °C. This transition indicates the miscibility of lignin in the epoxy network resulting in a homogeneous system. Regarding the samples with a lignin share of 40 %, 60 % and 80 %, however, a weakly pronounced second glass transition at 166.8 °C, 165.1 °C and 155.2 °C is visible, respectively. It is a clear indication of the immiscibility of kraft lignin with increasing share in the epoxy resin. In the event of a glass transition temperature of lignin in epoxy resin being higher than its glass transition in its neat form, this might result due to the solubility of the low–molecular weight fractions of lignin in the epoxy resin resulting in the formation of a phase solely consisting of high–molecular weight fraction of lignin being immiscible.

Although the curing temperature of 55 °C is recommended by the manufacturer, the behavior of kraft lignin in the epoxy at elevated temperatures was investigated since the previous investigations showed a participation of the lignin in the curing reaction. Furthermore, curing at elevated temperatures results in higher cross–linking densities which would be interesting for further applications. Consequently, multiple

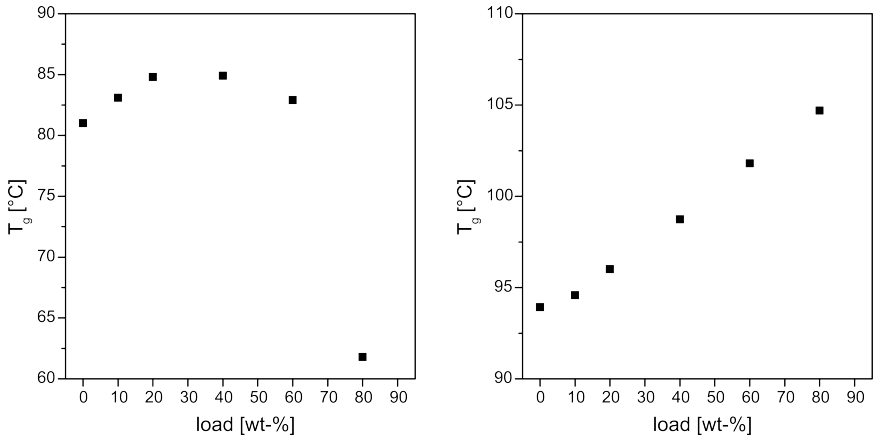

Figure 4.2.: Glass transition temperatures determined for the first heating run (left) and the second heating run (right) for different kraft lignin loads.

series of 10 % lignin filled L285 were cured for 24 h at 55 °C, 25 °C, 75 °C and 100 °C respectively. DSC measurements were carried out for all four curing temperatures for the neat L285 epoxy formulation as well as for a 10 % lignin filled L285 formulation. The effect of the curing temperature on the T_g is presented in Figure 4.3. It is apparent that the lignin filled L285 resin compared to the neat L285 resin shows just minor differences at all curing temperatures. Moreover, increasing the curing temperature over the recommended 55 °C is unnecessary due to the complete curing and the constant T_g which indicates complete cross–linking.

4.2 Mechanical characterization

Besides thermal characterization, the investigation of the mechanical properties is another important aspect. In general, the mechanical performance of a FRP depends not only on the strength and modulus of the reinforcing fiber material, but also on the strength and toughness of the matrix. It is essential for the incorporation of lignin into the epoxy network to strive for a balance of optimum mechanical performance with a maximum amount of lignin. In order to determine the mechanical properties, a positive Teflon mold was designed for the preparation of test specimens. As shown in Figure 4.4 negative molds could be prepared by casting a liquid 2–component heat resistant impression silicone rubber (ADDV M 4641) into the mold. By casting the low–viscous lignin filled epoxy resin into the mold, test specimens could be crafted easily. Due to the flexibility of the silicon mold the brittle specimens could be removed without damages. For the tensile strength measurements a test series consisted of six dog–bone shaped test specimens which were prepared and analyzed according to norm DIN EN ISO 527–4. The stress–strain curves shown are the measurement which achieved the best properties of each series unless otherwise stated.

Tensile strength measurements allow studying mechanical properties such as Young's modulus E, strain ε_b and stress σ_b at break. It is well known that for fillers with a size in the range of micrometers or larger, the stiffness increases on the one hand, but on the other hand the strain and stress at break is reduced by the increasing amount of filler.[102,103]

Figure 4.5 shows the effect of different amounts of kraft lignin on the mechanical properties compared to the neat L285 resin. The tensile strength of the neat L285 epoxy polymer was measured to be 87.8 MPa

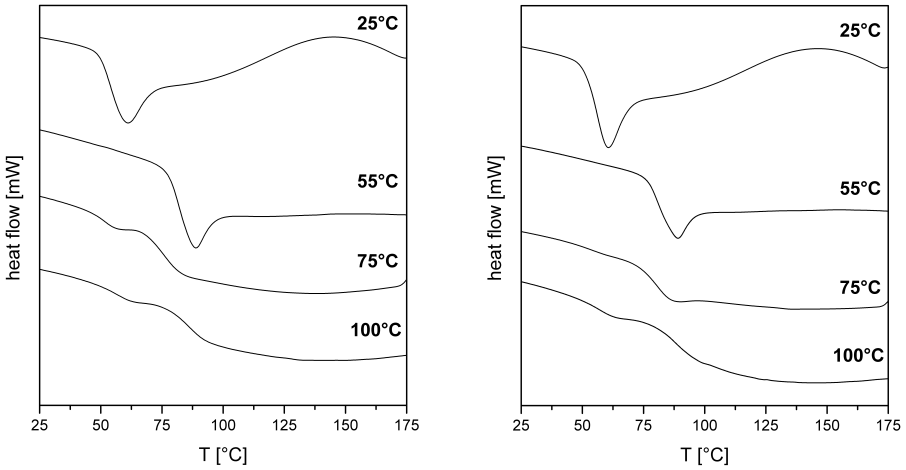

Figure 4.3.: DSC thermograms of the neat L285 formulation (left) and a 10 % lignin filled L285 formulation (right). Each sample was cured at the corresponding temperature for 24 h. Samples containing 10 % and 20 % lignin indicate miscibility in the epoxy network showing a single glass transition tempperature whereas higher amounts of lignin present a weakly pronounced second glass transition indicating a phase separation.

which is in good accordance to tensile strengths of approximately 81 — 83 MPa which typically measured for a DGEBA based epoxy polymer. [104–106]

The addition of lignin has a significant influence on the tensile strength of the resin. With addition of kraft lignin the value drops even with low kraft lignin loads of only 10 % to 73.2 MPa. With further addition of more kraft lignin the value decreases continually to 50.5 MPa for a lignin share of 60 %. Increasing the lignin share to 80 % yields a constant value at 50.6 MPa. In total, a difference of 26.8 MPa and total loss of 44.5 % is measured compared to the neat L285 resin. The continuous decrease of the tensile strength is evidence for the poor lignin matrix interaction which is a result of the inability of the particles to carry any part of the external load. Hence, the tensile strength cannot be higher than the neat epoxy matrix. [103]

With regard to the strain at break, low lignin loads of 10 % and 20 % already cause a decrease of 7.0 % to 10.4 %. However, with lignin loads exceeding 40 %, the strain at break remains constantly at 4.8 % which results in a total decrease of 50 %. Due to the rigidity of the lignin most of the deformation comes from the epoxy matrix so that the deformation experienced by the epoxy is much larger than the measured deformation of the sample. This means that the lignin filled epoxy resin reaches the strain limit at a lower total deformation. Another important aspect is related to the dispersability of the lignin in the epoxy resin. With increasing lignin loads the dispersability of the lignin is increasingly difficult so that more voids and porosities are produced which also lead to reduced stress and strain. Also the formation of agglomerates would lead to crack propagation and failure. [7,107,108]

Figure 4.6 presents the above discussed parameters and trends with their standard deviation. The Young's modulus E as the ratio of stress and strain was calculated from the slope of the linear elastic portion ($\varepsilon \to 0$) of the stress–strain curve in order to determine the stiffness of the lignin filled epoxy. Figure 4.6 (bottom) depicts the Young's moduli calculated for the neat L285 epoxy as well as with lignin

Figure 4.4.: Manufacturing of test specimens. Preparation of a silicon mold by using a Teflon positive form. Casting of lignin filled specimens into the mold resulting in a dog–bone shaped specimen.

loads of 40 %, 60 % and 80 %. Young's modulus of all lignin containing resins is higher than that of the neat L285 and increases to a maximum value at a load of 80 % lignin. The increase of the Young's modulus by the addition of fillers is influenced by the interaction between the epoxy and the filler phase. This means, that the polymer chain mobility and deformation is restricted by the filler due to the depth of the atomic bond energy resulting in both higher tensile strength and Young's modulus.[109]

The phase morphology of the measured specimens were further studied with SEM imaging. Figure 4.7 shows the SEM micrographs for the lignin filled epoxy resin with 20 %, 40 %, 60 % and 80 % lignin load. Low lignin loads of 20 % show a partially smooth surface surrounded by lignin–rich areas, as indicated by arrows. Increasing lignin loads results in increasing lignin–rich areas until the surface shows a complete mixed lignin–epoxy surface at 60 % lignin load. However, crack propagation becomes obvious only at 80 % load as indicated by arrows. In general, lignin remains well dispersed in the epoxy resin even at high loads.

In order to obtain an overview of the influence of different types of lignin stress–strain measurements were carried out. Therefore, samples with 40 % of the provided standard kraft lignins KL_1, KL_2 and KL_3 as well as the modified kraft lignins KL_{eh}, KL_{aw} and KL_{xp} were prepared and measured according to the previous measurements. Figure 4.8 (left) illustrates the effects of the standard kraft lignins on the tensile strength and strain on the neat L285 epoxy resin. Each kraft lignin shows lower tensile strength as well as strain than the neat L285 resin. With an initial tensile strength of 87.8 MPa the value decreased almost by half to 59.7 MPa which is a result of poorly–bonded lignin.

However, the tensile strength as well as the Young's modulus increase with increasing average molecular weight of the kraft lignin. From a tensile strength of 59.8 MPa with an average molecular weight of 1244 g/mol to 35.4 MPa for KL_3 which has the lowest average molecular weight of 718 g/mol. This is a decrease of 42.3 %. This trend also shows with respect to the Young's modulus. This is quite unexpected behavior since smaller–sized fillers show better mechanical properties than bigger ones.[110] However,

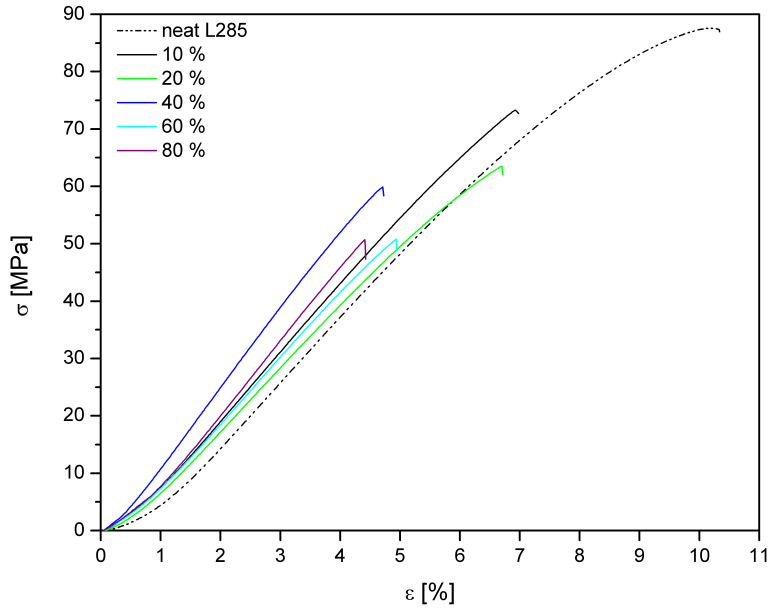

Figure 4.5.: Comparison of the tensile–strength experiments with different lignin content of 10 %, 20 %, 40 %, 60 % and 80 % in the L285 formulation.

DSC measurements proved the integration of lignin into the epoxy network. Since larger lignin molecules contain a higher amount of functional groups, those might cause a higher local cross–linking density surrounding lignin phases.

Strength strongly depends on the stress transfer between fillers and the matrix. Therefore, it can be assumed that larger lignin phases reduce stress transfer, which is an important factor which strongly influences Young's modulus, strength and fracture toughness.[111] Regarding the modified lignins presented in Figure 4.8 (right) a similar trend occurs for the tensile strength but no significant differences between the kind of after–treatment and molecular weight are observed for the Young's modulus.[112,113]

At last, samples containing acetylated kraft lignin have been prepared to determine the influence of an unpolar modified lignin as a filler on the mechanical properties. As seen before acetylated kraft lignin shows no solubility in the resin as well as in the curing agent. Therefore, specimen preparation was challenging due to the poor dispersability of the acetylated kraft lignin. Surprisingly, the results for the stress–strain experiments (Figure 4.9a) show that compared to the crude kraft lignin filled epoxy resin the values are nearly identical. However, regarding the SEM micrographs in Figure 4.9b, a significant

Table 4.3.: Stress, strain and Young's modulus of 40 % KL_1, KL_2 and KL_3 as well as the modified kraft lignins KL_{eh}, KL_{aw} and KL_{xp} in L285 resin.

Sample	M_n [g/mol]	Stress [MPa]	Strain [%]	Young's Modulus [MPa]
KL_1	1244	59.8	4.7	1350
KL_2	983	45.1	4.1	1170
KL_3	718	35.4	3.8	990
KL_{aw}	1340	51.1	5.4	1090
KL_{eh}	1276	46.0	4.4	1180
KL_{xp}	1160	39.1	4.2	1010

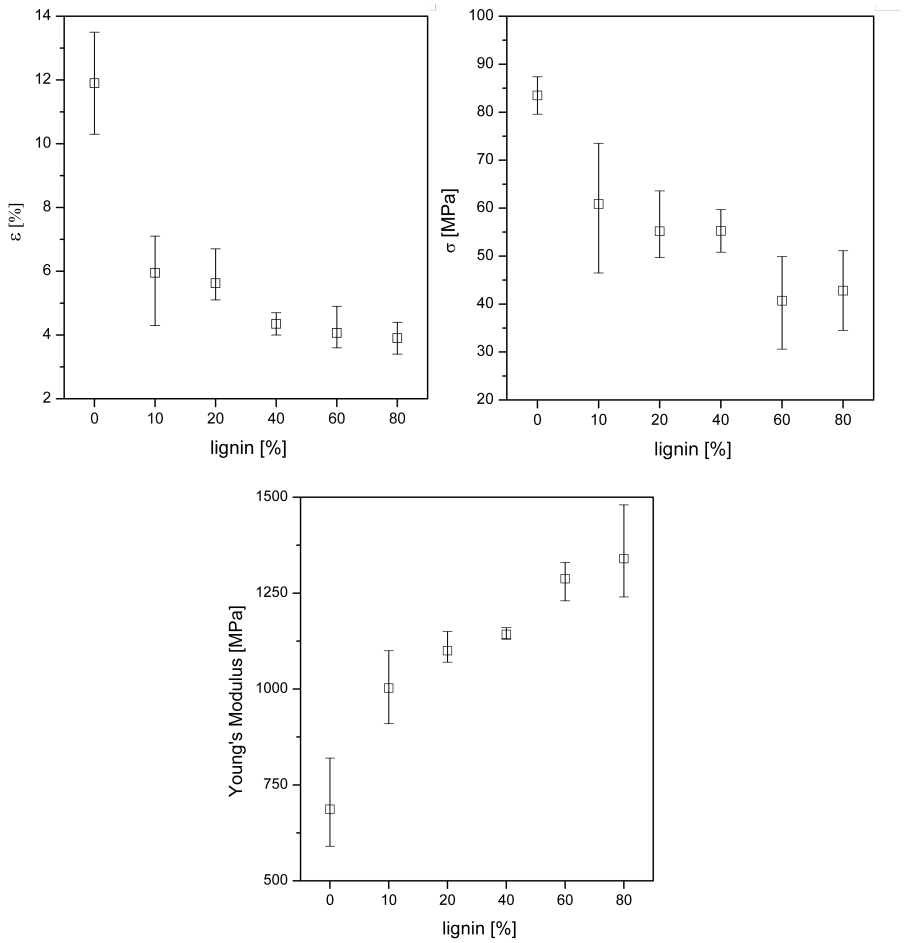

Figure 4.6.: Determined mechanical properties of the L285 formulation with lignin content of 10 %, 20 %, 40 %, 60 % and 80 %. Strain at break (top left) and strength at break (top right) as well as the Young's modulus (bottom) of the lignin filled epoxy formulation.

difference between both kraft lignin types is clearly visible. Whereas crude kraft lignin is well dispersed in the matrix, acetylated kraft lignin shows a complete phase separation due to its immiscibility with the resin. Therefore, the results of these experiments clearly indicate that the aspect ratio of the lignin particles is the most important factor for the mechanical properties since changing lignins polarity shows no effect on the characteristic values. However, due to the poor manufacturing properties of the acetylated lignin, only contents up to 20 % were investigated. Consequently, no final conclusion can be drawn due to lack of comparison with higher amounts of lignin.

4.3 Selection of a Suitable Lignin as Filler for Epoxy Resins

The main focus of this work is to study and develop a new kind of biobased epoxy formulation for composite materials and to gain a better understanding of the influence of lignin on the chemical processes of curing. Therefore, at one point of the development process it was necessary to determine the most suitable type of kraft lignin on which the final epoxy formulation should be based on. This lignin should meet the following criteria:

- Processability

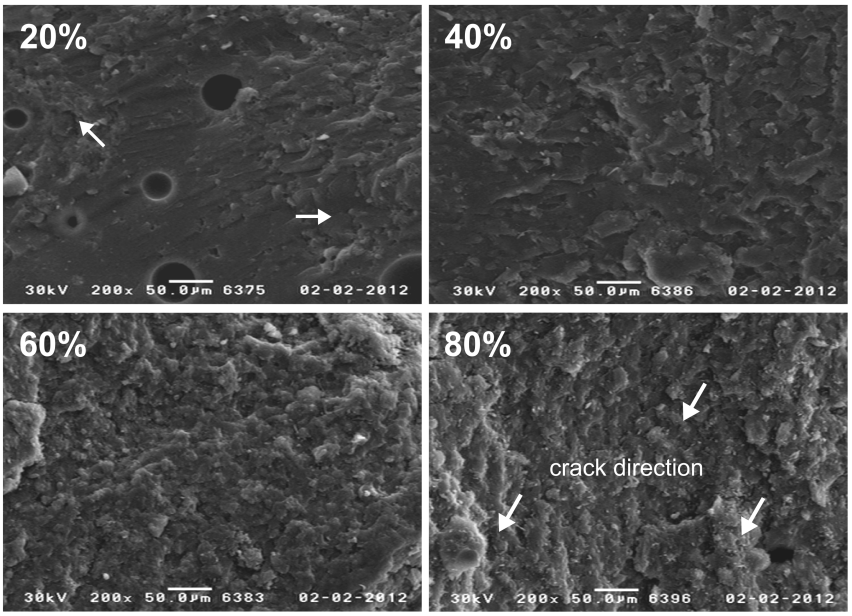

Figure 4.7.: SEM micrographs of freeze fractured lignin filled epoxy with 20 %, 40 %, 60 % and 80 % lignin share.

- Optimal mechanical performance with maximum amount of lignin
- Thermal stability
- Consideration of the lignin cost and availability

Six different kinds of kraft lignin were investigated to analyze their behavior in a commercial available epoxy resin. The processability of the different kinds of kraft lignin available showed that all kraft lignins despite KL_3 were easily pourable as well as dispersable without forming larger aggregations up to an amount of 40 %. Further, the measurements illustrated that 40 % of KL_1 yielded very good results in the mechanical tests compared to any other lignin by increasing the Young's modulus from an initial value of 990 MPa to 1160 MPa as well as reasonable tensile strength and strain compared to the neat epoxy resin. In considering the lignin cost and availability it can be stated that KL_1 shows very good properties without using expensive pulping techniques like KL_{eh} or further purification methods like KL_{aw}, KL_{xp}. Regarding those results KL_1 was selected as the most suitable kraft lignin compound for the system to be developed and is further used throughout the remaining work.

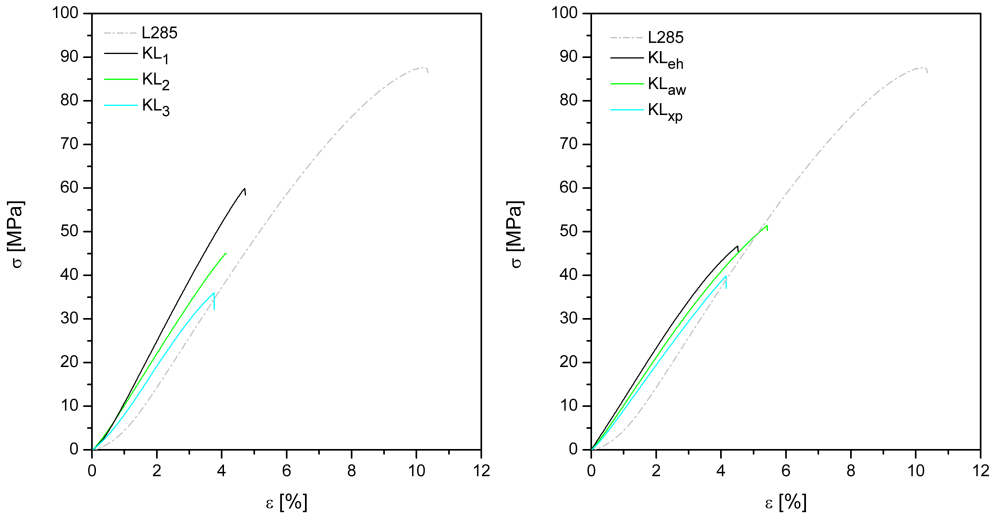

Figure 4.8.: Comparison of the stress–strain experiments of 40 % KL_1, KL_2 and KL_3 (left) as well as the modified kraft lignins KL_{eh}, KL_{aw} and KL_{xp} (right) in the L285 resin.

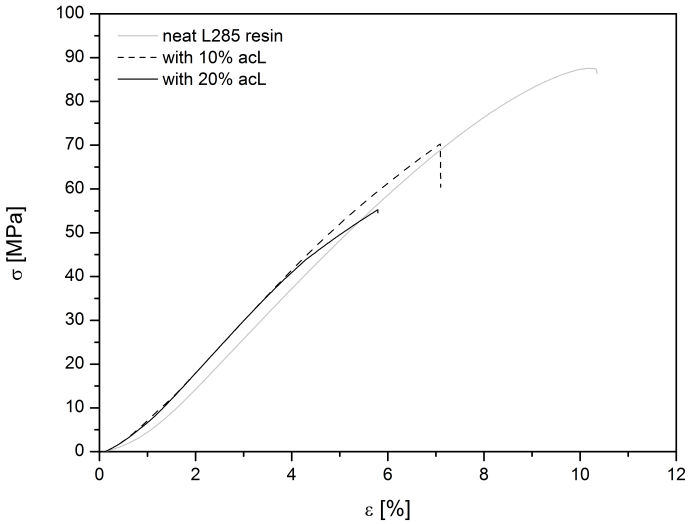

(a) Stress-strain experiments of the neat L285 resin compared with two different amounts of acetylated kraft lignin acL of 10 % and 20 %.

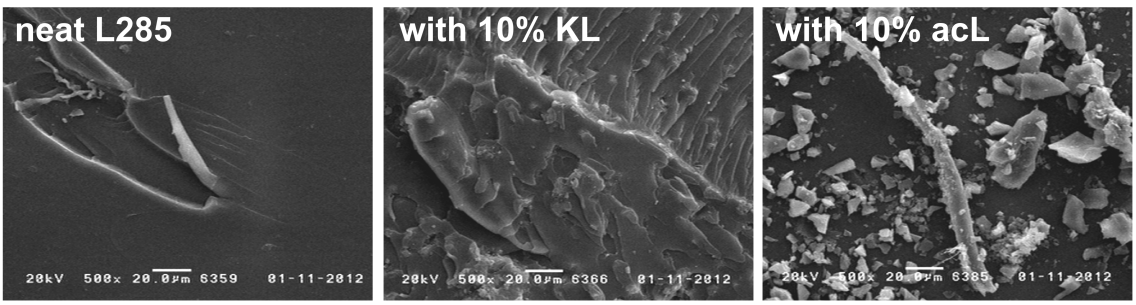

(b) SEM micrographs of freeze fractured lignin filled epoxy with 10 % of KL and KL_{ac} compared to the neat L285 resin.

Figure 4.9.

5 Formulation of a Biobased 2–Component Epoxy Resin

In the previous chapter it became evident that kraft lignin can be incorporated easily into a commercial epoxy resin with just minor losses in tensile strength and strain in spite of high amounts of lignin. Moreover, a stiffening effect with increasing lignin share occurred. A considerable disadvantage in the use of a commercial epoxy resin for research purposes is the addition of multiple additives to the epoxy resin as well as the curing agent. With further addition of reactive diluents, accelerators and stabilizers the investigations of the behavior of kraft lignin with both the epoxy resin and curing agent proves to be difficult due to the occurrence of multiple possible side reactions. Therefore, the complexity was reduced to the formulation's basic educts: the DGEBA resin and curing agent.

This chapter focuses on the incorporation of lignin into a 2–component epoxy formulation based on a DGEBA resin with commonly used amino–based curing agents and the subsequent thermal and mechanical investigations. As mentioned above, the diglycidyl ether of bisphenol A (DGEBA) shown in Figure 5.1a was used throughout the remaining work. This choice was made due to several reasons. First and foremost the commercial availability was the most important criterion. Introducing the biobased epoxy resin in large scale applications would require major quantities with an attractive price/performance ratio only a high–volume produced resin can meet. Further, the viscosity of the resin is another aspect to guarantee a good dispersability of the lignin as well as an easy processability. Therefore a DGEBA resin with a low molecular weight of $M = 381.0$ g/mol and a medium dynamic viscosity of $\mu = 9000 - 13000$ MPas was chosen. The properties of the DGEBA resin are summarized in Table 5.1.

In a two component epoxy formulation a liquid curing agent is required. On this premise two different multifunctional amino–based curing agents were chosen which are commonly used for epoxy curing. Figure 5.1b shows the selected curing agents: diethylenetriamine (DETA; Figure 5.1b, left) and isophorondiamine (IPDA; Figure 5.1b, right).

Both, the aliphatic DETA and the cycloaliphatic IPDA, react with the epoxy resin at room temperature. Due to their molecular structure, they feature a high temperature resistance and mechanical strength as well as good chemical and moisture resistance. Moreover, IPDA permits the production of materials with higher performances compared to aliphatic amines while its toxicity is much lower than aromatic amines.[114] However, both generate a large quantity of heat and have a relatively short pot life. Table 5.2 shows the properties of the used curing agents.

With the help of preliminary solubility experiments the behavior of kraft lignin in the single components was investigated. Achieving a good solubility is a requirement for good mechanical properties since

Table 5.1.: Chemical and rheological properties of the DGEBA resin used in this work.

Chemical Properties	Value	
Dynamic Viscosity μ	9 000 – 13 000	MPas
Density ρ	154.2	g/cm^3
Molecular Weight M	381.0	g/mol
Epoxy Equivalent Weight EEW	182 – 192	g

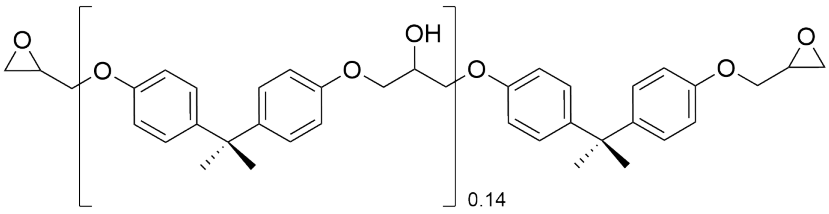

(a) Chosen low molecular weight diglycidyl ether of bisphenol A (DGEBA) resin with a repeating unit of n = 0.14.

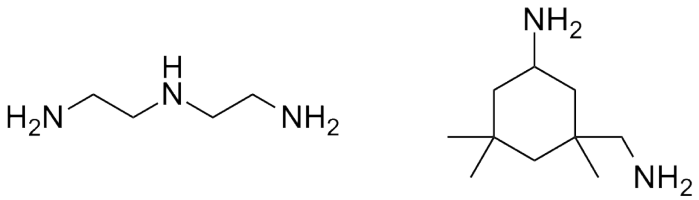

(b) Chosen multifuntional amino–based curing agents diethylenetriamin (DETA, left) and isophorondiamine (IPDA, right)

Figure 5.1.

agglomerations would induce untimely failure and the processing would be more difficult since the wettability of the fiber mats would be insufficient with major inhomogeneities. The preparation of the formulation batches was carried out in a laboratory dissolver with adapted vacuum vessel. The dispersion time chosen was 15 min at a stirring rate of 3500 rpm. Figure 5.2a presents the solubility of kraft lignin in the DGEBA resin as well as the curing agents IPDA and DETA. 10 % Kraft lignin was added to vials with the resin compounds and vigorously stirred to ensure good dispersion. The result was that kraft lignin is partially soluble with DGEBA showing finely dispersed lignin as well as partial agglomerations. With regard to the curing agents, DETA shows a high solubility towards lignin with no visible lignin particles left whilst IPDA shows just a partial solubility with a well–dispersed lignin distribution and no particle agglomeration observed at 10 % kraft lignin share.

However, after mixing the components DGEBA/KL and curing agent a phase separation occurred almost immediately for the 10 % filled DGEBA/DETA sample, resulting in large solid agglomerations as shown in Figure 5.2b. Along with the phase separation an immediate exothermic reaction, accompanied by a significant heat development of the reaction mixture occurred. This means, that kraft lignin causes a possible side reaction with either DGEBA or DETA and might accelerate the reaction between DGEBA and DETA.

In order to study the curing kinetics of the epoxy resin DSC measurements were carried out to evaluate the temperature range in relation to their respective curing reaction by the presence of the exothermic

Table 5.2.: Chemical and rheological properties and curing behavior of DETA and IPDA.[115,116]

Chemical Properties	DETA	IPDA	
Dynamic Viscosity μ	4	19 – 20	mPas
Density ρ	0.96	0.94	g/cm^3
Molecular Weight M	103.17	170.30	g/mol
Epoxy Equivalent Weight EEW	20.63	42.58	g

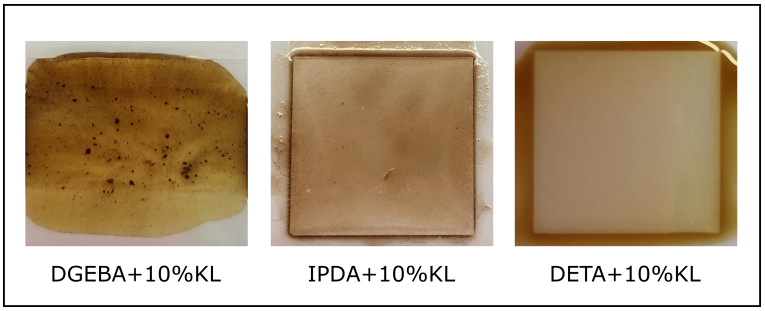

(a) Solubilities of kraft lignin in DGEBA resin (left) as well as IPDA (middle) and DETA (right) curing agents

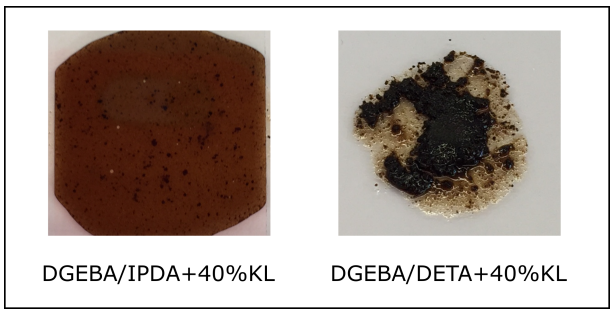

(b) Solubilities of kraft lignin in the DGEBA/IPDA (left) and DGEBA/DETA system (right).

Figure 5.2.

reaction peak in the first heating run. The DGEBA resin was mixed stoichiometrically with the curing agent at room temperature and measured immediately following a predetermined heating rate. The typical DSC curve displaying heat flow $^{dH}/_{dt}$ against temperature T is shown in Figure 5.3 for DGEBA/IPDA (left) and DGEBA/DETA (right). Several information about the curing reaction can be obtained directly from these measurements: the onset temperature T_i, the peak temperature T_p and the terminal temperature T_e as well as the values of $^{dH}/_{dt}$. In the case of the IPDA cured epoxy resin, the reaction starts just over room temperature and ranges up to 160.3 °C. The use of DETA in place of IPDA results in a faster curing process with a heating range from 129.3 °C for the IPDA cured system to 109.2 °C for DETA. The peak temperature shows a slight decrease of about 10 °C.

Since lignin is introduced as a filler into an epoxy resin, it is important to understand how the lignin influences the curing reaction of the resin and the resulting phase morphology. Figure 5.4 shows the DSC measurements of the lignin filled epoxy formulations. Introducing kraft lignin to the binary epoxy formulation results in an unaltered onset temperature. However, the peak temperature as well as the terminal temperature of the reaction decrease with higher loads of lignin. As a result the curing range for the cross–linking process decreases by 17.5 % from initially 129.3 °C to 106.6 °C. At the same time the enthalpy decreases from 19.0 J/g for DGEBA/IPDA to 7.3 J/g for 40 % lignin share but increases again for the 80 % filled epoxy. This could be attributed to agglomerations of kraft lignin restricting its reactivity towards the resin components whereas with 40 % lignin share the well–dispersed kraft lignin lowers the enthalphy of the whole system.

The introduction of 40 % kraft lignin in the DGEBA/DETA system is shown in Figure 5.5. Interestingly, the temperatures T_i, T_p and T_e are not altered by the presence of lignin, however the reaction enthalpy is

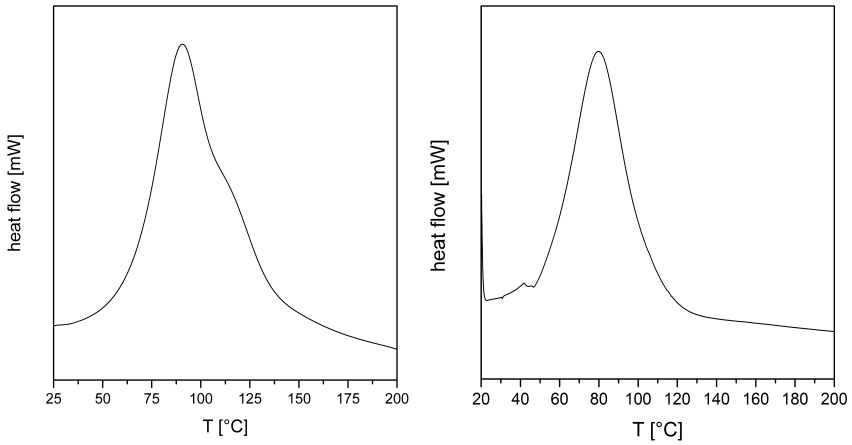

Figure 5.3.: DSC thermograms showing the heat of reaction in the first heating run of DGEBA cured with IPDA (left) and DETA (right).

almost increased by half. This coincides with the observations made while preparing the samples with DETA and lignin which led to a considerable development of heat during mixing. Therefore, the loss in exothermic energy of the DGEBA/DETA system filled with 40 % kraft lignin must have been occurred initially while mixing. This supports the theory of the participation of lignin in the curing process.

A further indication of the high reactivity of kraft lignin towards the resin is the formation of a glass transition at −15.8 °C which can be seen in the first heating run in Figure 5.5. This transition is evidence for the presence of an already cross linked network. After the exothermic reaction, a second glass transition is visible which can be assigned to the agglomerated kraft lignin fraction. This suggests the reaction of the low molecular weight fraction of kraft lignin which leads to an increase in the T_g of the neat kraft lignin. Therefore, DETA as curing agent was excluded from further testing because of strongly limited processabilty as well as incomparability with the IPDA system.

In general, for the 40 % lignin filled epoxy a bimodal peak assigned to two separate cross–linking reactions occur. This means that cross–linking of the epoxy filled with 40 % kraft lignin requires high curing temperatures ($T_c > 200$ °C) to obtain a full consumption of the three compounds. The total enthalpy was calculated by integration of the complete signal.

Table 5.3.: Curing characteristics such as the onset temperature T_i, the peak temperature T_p and the terminal temperature T_e as well as the curing range, heat of reaction and the glass transition temperatures of the neat and lignin filled DGEBA/IPDA and DGEBA/DETA systems.

Sample	T_i [°C]	T_p [°C]	T_e [°C]	Curing range [°C]	ΔH [J/g]	T_g [°C]
DGEBA/IPDA	31.0	90.3	160.3	129.3	19.0	164.0
+ 10 % KL	31.0	88.2	152.6	121.6	8.7	99.0
+ 40 % KL	31.0	82.7	144.0	113.0	7.3	118.8
+ 80 % KL	31.0	82.5	137.6	106.6	11.34	128.8
DGEBA/DETA	28.0	79.7	137.2	109.2	16.0	81.3
+ 40 % KL	25.0	83.5	132.0	107.0	8.5	121.3

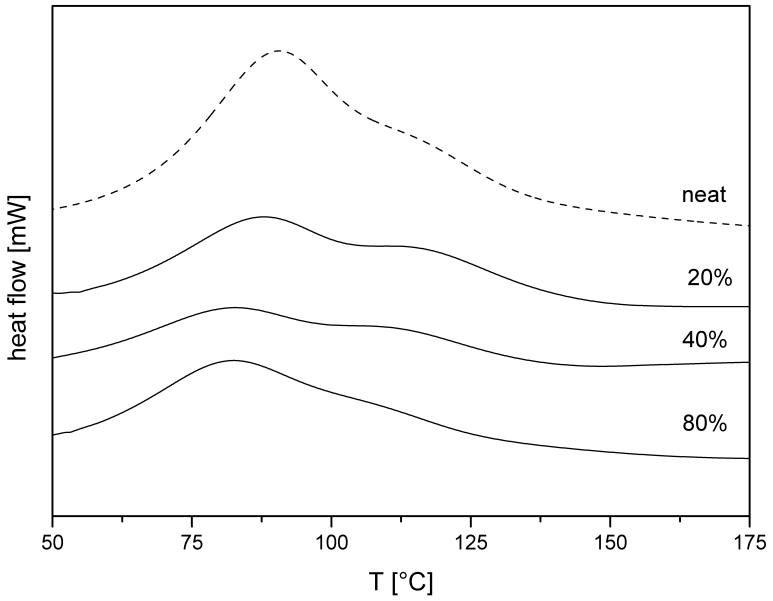

Figure 5.4.: Curing reaction observed in the first heating run with 20 % KL, 40 % KL and 80 % KL compared to the neat DGEBA/IPDA mixture.

To evaluate the curing behavior of the neat DGEBA/IPDA resin, different curing temperatures were chosen to determine the overall progress of the cross–linking reaction and the influence on the T_g. Samples were cured in alumina pans at 20 °C, 60 °C, 100 °C and 120 °C for 24 h. The same procedure was repeated with DGEBA/IPDA resin with a load of 40 % KL. DSC measurements of the samples were carried out immediately after curing. Figure 5.6a depicts the degree of cure obtained from the first heating run of the loaded epoxy resin compared to the neat DGEBA/IPDA. The degree of cure was determined with regard to a postcuring reaction occurring in the first heating run due to an incomplete curing reaction.

It is obvious that for the DGEBA/IPDA system with rising curing temperature the degree of cure increases revealing postcuring effects up to 120 °C. Interestingly, the lignin filled DGEBA/IPDA system achieves higher cross–linking degrees at lower curing temperatures compared to the neat system which is a further indication for the participation of kraft lignin in the curing reaction. Further, the glass transition temperatures of the neat DGEBA/IPDA system as well as with 40 % lignin share obtained from the first heating run are shown in Figure 5.6b. According to this results the glass transition temperatures increase due to further cross–linking with a final T_g at 160 °C. Moreover, starting from a curing temperature of 60 °C a phase separation occurs resulting in two T_g values. This might be easily described by the Flory–Huggins theory for the mixing behavior of polymer blends with regard to the free energy of binary polymer mixtures. The model which was independently derived by Flory and Huggins was initially employed for solvent–solvent and polymer–solvent solutions and is described in Equation 5.1. V is the total volume, R the gas constant, ϕ_i the volume fraction of component 1, M_i the molecular weight of component i, ρ the density.

$$\frac{\Delta G_m}{V} = \rho RT \cdot \left[\frac{\phi_1}{N_1} \ln \phi_1 + \frac{\phi_2}{N_2} \ln \phi_2 \right] + B_{1,2} \phi_1 \phi_2 \tag{5.1}$$

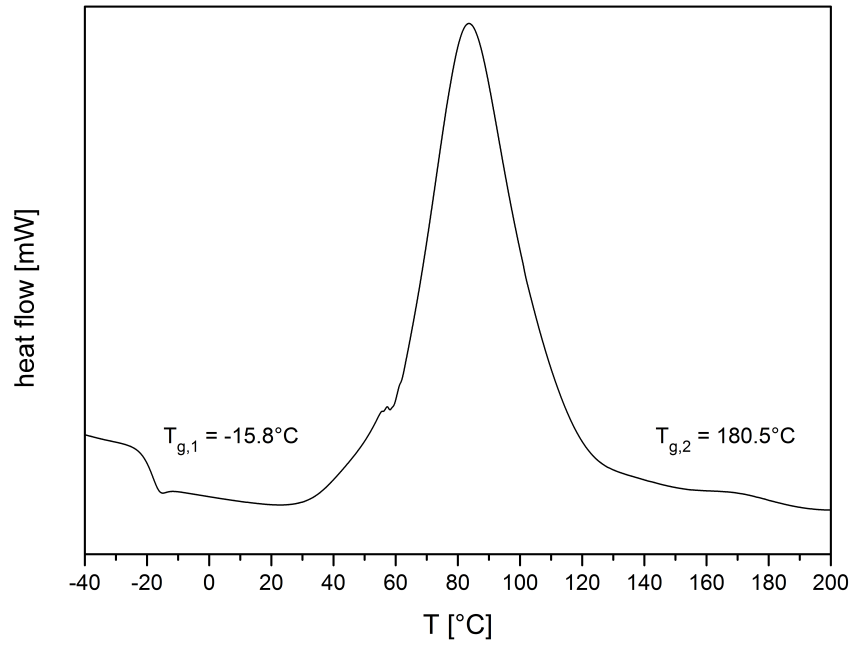

Figure 5.5.: First heating run of DGEBA/DETA with 40 % KL share showing two different glass transition temperatures at −15.8 °C and at 180.5 °C and an exothermic curing reaction.

The binary interaction parameter B is defined as shown in Equation 5.2, which takes the Flory–Huggins interaction parameter $\chi_{1,2}$ into account.

$$B_{1,2} = \chi_{1,2} \cdot RT \tag{5.2}$$

The first part of Equation 5.1 is the combinatorial entropy of mixing. Increasing molecular weight of the components leads to negative value inherent with this expression becomes infinitesimal. With high molecular weight polymers the enthalpy of mixing term ($B_{1,2}\phi_1\phi_2$) determines the phase behavior of the polymer blend. This leads for polymer–polymer mixtures to a phase separation at high conversions due to increasing incompatibility.

Figure 5.7 shows the stress–strain measurements of the lignin loaded DGEBA/IPDA system compared to the neat DGEBA/IPDA system cured at three different temperatures. Obviously, the loss in both strain and stress values for the lignin filled DGEBA/IPDA system is dramatic. The summarized values for stress, strain as well as Young's modulus of the measurements are shown in Table 5.4. As a result of the incorporation of lignin the values for stress and strain at break decrease nearly by half compared to the neat DGEBA/IPDA system. As described in Section 4.2: the rigidity of lignin means that the majority of the deformation is caused by the epoxy matrix, so that the deformation experienced by the sample is much higher than the measured deformation of the sample. This means that the lignin filled epoxy resin reaches the strain limit at a lower total deformation.

Interestingly, the best results are achieved for the neat and the lignin filled system at a curing temperature of 90 °C. This might be induced by the rapid increase of viscosity due to the higher curing

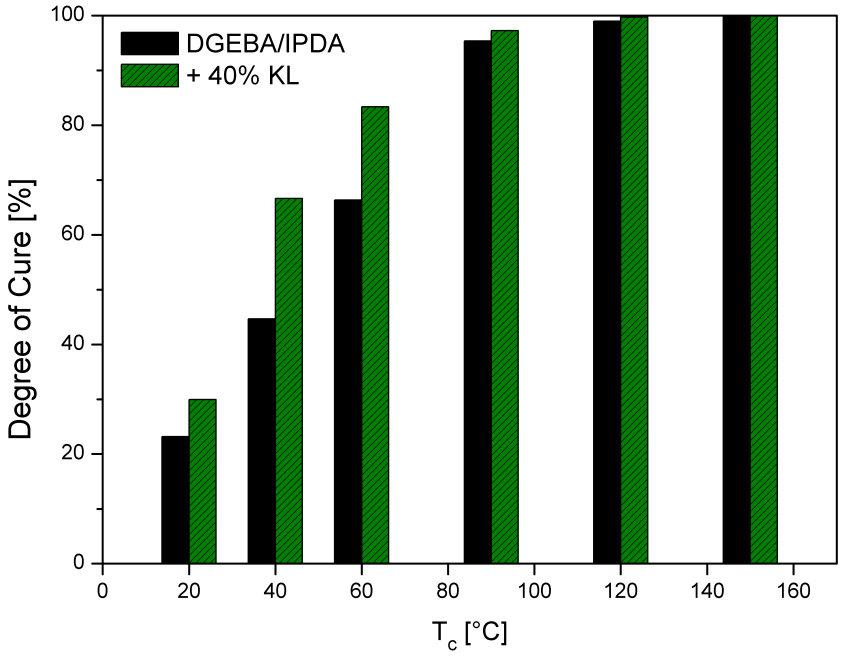

(a) Comparison of the degree of cure of the neat DGEBA/IPDA system with the system loaded with 40 % KL at different curing temperatures.

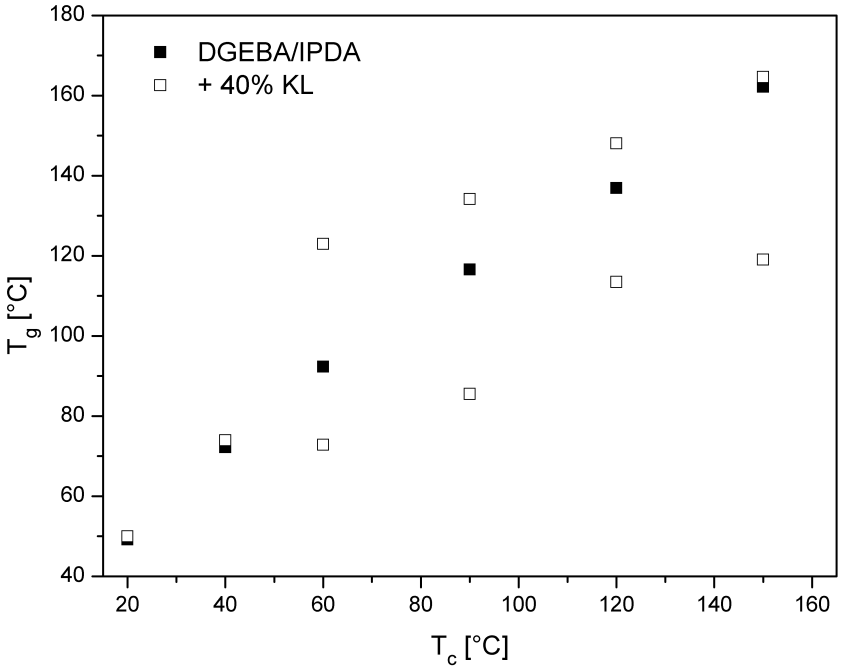

(b) Comparison of the T_g values of the neat DGEBA/IPDA system with the system loaded with 40 % KL at different curing temperatures.

Figure 5.6.

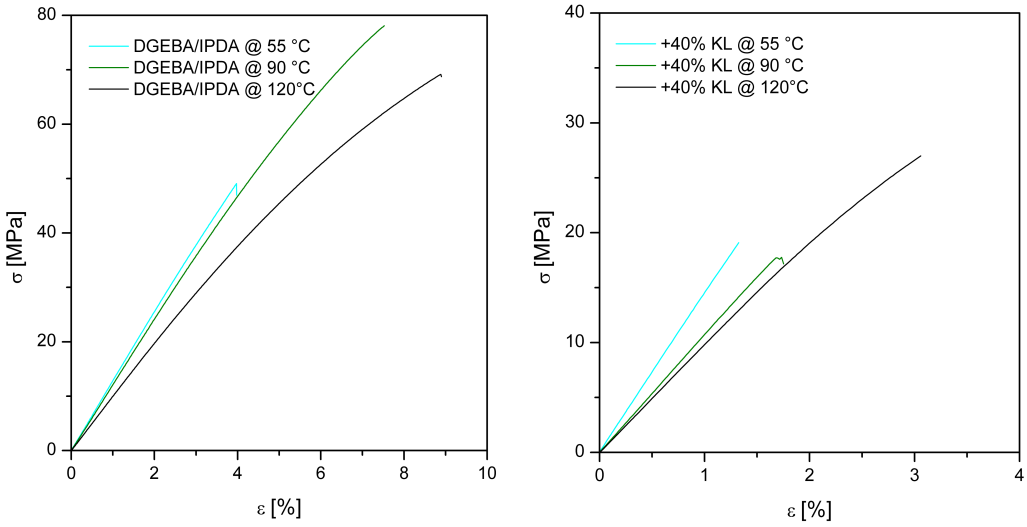

Figure 5.7.: Comparison of the stress-strain measurements of the DGEBA/IPDA system (left) and DGEBA/IPDA with 40 % KL (right) cured at 55 °C, 90 °C and 120 °C.

temperature, causing inhomogeneities as well as voids being more prone to failure as with lower degrees of cure. With regard to the Young's modulus, the stiffness of the resulting lignin filled epoxy did not change at all.

5.1 Isothermal DSC Measurements for the Determination of Kinetic Parameters

Incorporating lignin in the present epoxy resin alters the curing behavior of the neat epoxy resin. To gain a more in–depth understanding of the elapsing curing reactions of the neat and the modified epoxy resin, first a kinetic model is derived. After that, experimental measurements are carried out in order to estimate the kinetic parameters. The resulting kinetic model is than validated against measured data for both, neat epoxy resin as well as for samples with 40 % kraft lignin.

Table 5.4.: Stress at break, strain at break and Young's modulus for the neat DGEBA/IPDA system and the DGEBA/IPDA system filled with 40 % KL with regard to different curing temperatures of 55 °C, 90 °C and 120 °C.

Sample	T_c [°C]	σ_b [MPa]	ϵ_b [%]	Young's Modulus [MPa]
DGEBA/IPDA	55	40.3 ±7.5	3.2 ±0.6	1239 ±15
DGEBA/IPDA	90	70.8 ±6.7	7.2 ±0.7	1131 ±29
DGEBA/IPDA	120	40.5 ±7.4	3.0 ±0.4	963 ±35
+ 40% KL	55	15.3 ±4.3	1.0 ±0.4	1400 ±69
+ 40% KL	90	21.7 ±3.7	2.1 ±0.4	1129 ±16
+ 40% KL	120	18.6 ±5.6	2.1 ±0.6	968 ±1

5.1.1 Deriving a Kinetic Model

Reaction kinetics describe the chronological sequence of a chemical reaction. The reaction rate ν_R is the temporal change of the concentration of educts and products Δc_i in a defined time period Δt. Shown exemplary for a reaction of the type $A + B \longrightarrow C$ in (5.3).

$$\nu_R = -\frac{\Delta c_A}{\Delta t} = -\frac{\Delta c_B}{\Delta t} = \frac{\Delta c_C}{\Delta t} \tag{5.3}$$

The change of concentration is referred to as the conversion of the reaction α, or in case of epoxy curing often described as the degree of cure. Therefore (5.3) can be simplified to:

$$\nu_R = \frac{\mathrm{d}\alpha}{\mathrm{d}t}$$

Curing kinetic models for epoxy reactions are typically obtained by thermal analysis techniques. Under the assumption that the heat of reaction released during reaction correlates with the total heat of reaction ΔH_{tot}, the reaction rate ν_R corresponds to the ratio of the released heat flow $\dot{q}$ and the maximum heat flow that can be released at maximum conversion q_T:

$$\frac{\mathrm{d}\alpha}{\mathrm{d}t} = \frac{\dot{q}}{q_T} \tag{5.4}$$

The curing reaction and therefore the reaction process can be easily determined using DSC, which proves as a valuable tool to obtain the heat of reaction ΔH_{tot}. By integration of Equation 5.5 it is possible to calculate the degree of cure α over time via the measured heat flow $\dot{q}$.[117]

$$\alpha = \int \frac{\dot{q}}{q_T}\,\mathrm{d}t \tag{5.5}$$

Kamal et al. established a phenomenological kinetic model for the description of amine–cured epoxy systems based on isothermal cure curves as shown in Equation 5.6.[118,119]

$$\frac{\mathrm{d}\alpha}{\mathrm{d}t} = (k_1 + k_2\alpha^m)(1-\alpha)^n \tag{5.6}$$

Where α is the fractional conversion at time t, k_1 and k_2 are the rate constants with two different activation energies and m, n are the kinetic exponents of the reaction and $m + n$ gives the overall reaction order. Setting the initial rate $\alpha = 0$, the reaction rate of the initial reaction is k_1. α subsequently follows an exponential decay function.

$$\alpha = A_1 \cdot \exp\left(-\frac{t}{a}\right) + A_2 \cdot \exp\left(-\frac{t}{b}\right) + y_0 \tag{5.7}$$

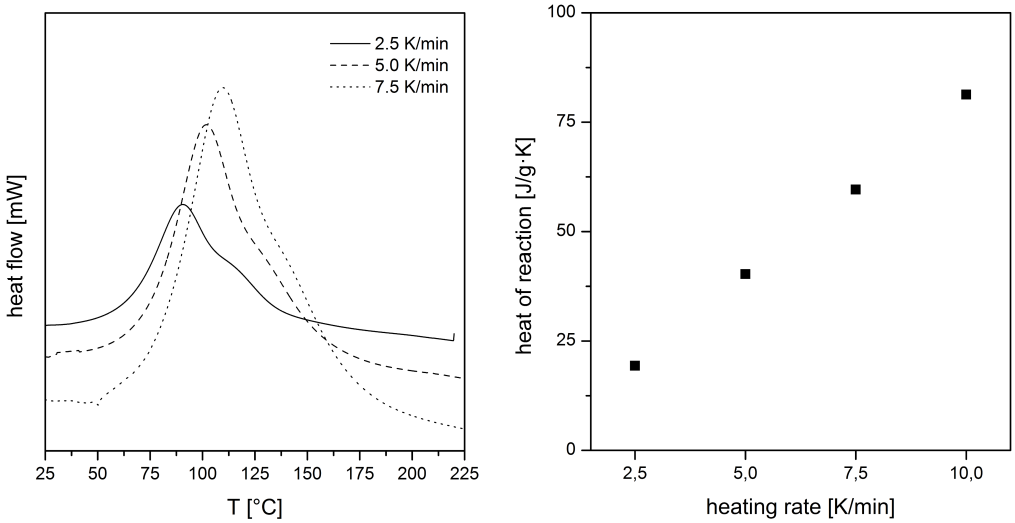

Figure 5.8.: Dynamic DSC measurements at 2.5, 5.0 and 7.5 K/min of the neat epoxy resin (left) and the dependency of the heat of reaction with respect to the heating rate (right).

Inserting Equation 5.7 into the Kamal-Sourour expression in Equation 5.6 yields Equation 5.8.

$$\frac{\mathrm{d}\alpha}{\mathrm{d}t} = \left(k_1 + k_2 \cdot \left(A_1 \cdot \exp\left(-\frac{t}{a}\right) - A_2 \cdot \exp\left(-\frac{t}{b}\right) + y_0\right)^m\right) \cdot \left(1 - \left(A_1 \cdot \exp\left(-\frac{t}{a}\right) - A_2 \cdot \exp\left(-\frac{t}{a}\right) + y_0\right)\right)^n \quad (5.8)$$

The kinetic constants k_1 and k_2 depend on temperature according to Arrhenius law (Equation 5.9).

$$k_i = A_i \exp \frac{-E_{ai}}{RT} \quad (5.9)$$

A_i is the pre exponential constant, E_{ai} is the activation energy, R the gas constant and T is the absolute temperature. [120]

5.1.2 Determination of Degree of Cure α

For the calculation of the kinetic parameters from Equation 5.8 the first step is the determination of the degree of cure α. As seen above, α can be determined using DSC, by integrating over the measured heat flow (Equation 5.5).

DSC provides two different strategies for determination of curing kinetics: dynamic mode and isothermal mode measurements. [19,121–124] The overall heat of reaction ΔH_{tot} is measured using dynamic DSC, in which the temperature in the measuring cell varies according to a preassigned temperature profile. The neat epoxy resin was measured with three different heating rates, 2.5, 5.0 and 7.5 K/min to obtain an average total heat of reaction ΔH_{tot}. The dynamic heating rate curves and the resulting heat of reaction for the neat epoxy resin are shown in Figure 5.8.

The peak maximum of the exothermic reaction shifted towards lower temperatures as the heating rate decreases (Figure 5.8, left). Further, the heat of reaction increases linearly with increasing heating rate from $\Delta H_{tot} = 19.36$ J/gK for 2.5 K/min up to $\Delta H_{tot} = 81.32$ J/gK for 10 K/min (Figure 5.8, right).

Figure 5.9a presents the degree of cure over time obtained for the neat epoxy resin determined using Equation 5.5 for each heating rate. A higher degree of cure is achieved more quickly by lowering the heating rate. A degree of cure of 50 % is achieved at 94.3 °C for the lowest heating rate of 2.5 K/min to 106.8 °C at 5 K/min and 114.8 °C for the maximum of 7.5 K/min.

From these three values an average degree of cure can be calculated which is shown as the red line depicted in Figure 5.9a. The average degree of cure at 50 % was 105.7 °C. This procedure was applied to all measurements to provide a basis for comparison.

To evaluate the behavior of lignin in the epoxy resin, samples with different lignin content were prepared and measured as described. Figure 5.9b shows the average degree of cure (DoC) of epoxy filled with 10 %, 40 % and 80 % lignin compared to the neat epoxy. Considering the initial curing reaction, it is obvious that with increasing the lignin content to at least 40 %, a higher DoC is obtained at the same temperature. This suggests that lignin affects the cross-linking reaction of the epoxy resin with isophorondiamine which is in accordance with the results from the DSC measurements in the former section.

Regarding higher temperatures, only the epoxy containing 80 % lignin reaches 100 % conversion whilst the epoxy containing 40% changes at approximately 96 °C towards lower degree of cure values than the neat epoxy. This change in the reactivity of the lignin filled epoxy is caused by a change in the reaction sequence.

5.1.3 Determination of Kinetic Parameters

Isothermal measurements were taken in order to determine the kinetic parameters by means of an autocatalytic model. Therefore, samples were cured in the preheated DSC cell at preset temperatures in the range of $90 - 150$ °C. The temperature was hold for 60 minutes in order to ensure complete curing. After the isothermal cure was completed, the sample was cooled to RT and a second heating cycle with 10 K/min was carried out to determine the corresponding T_g.

Figure 5.10b shows the resulting isothermal curves for 90 °C, 120 °C and 150 °C of the neat epoxy to determine the specific heat flow in function of the curing time. Each curve shows a sharp increase of the heat flow reaching a peak maximum after 60 s for the sample cured at 120 °C and 150 °C. The sample cured to 90 °C peaked after 300 s.

For each sample the peak maximum is followed by an exponential decay resulting in a completed reaction after 360 s for the samples cured at 120 °C and 150 °C. In contrast, the sample cured at 90 °C reaches a total conversion after 3000 s, which is five times greater than the samples cured at higher temperatures.

To determine the degree of cure α the first derivation of the heat flow curves was calculated and further normalized as shown in Figure 5.10a. The rate constant k_1 can be easily determined from the initial gradient of the measured curves shown in Figure 5.10b.

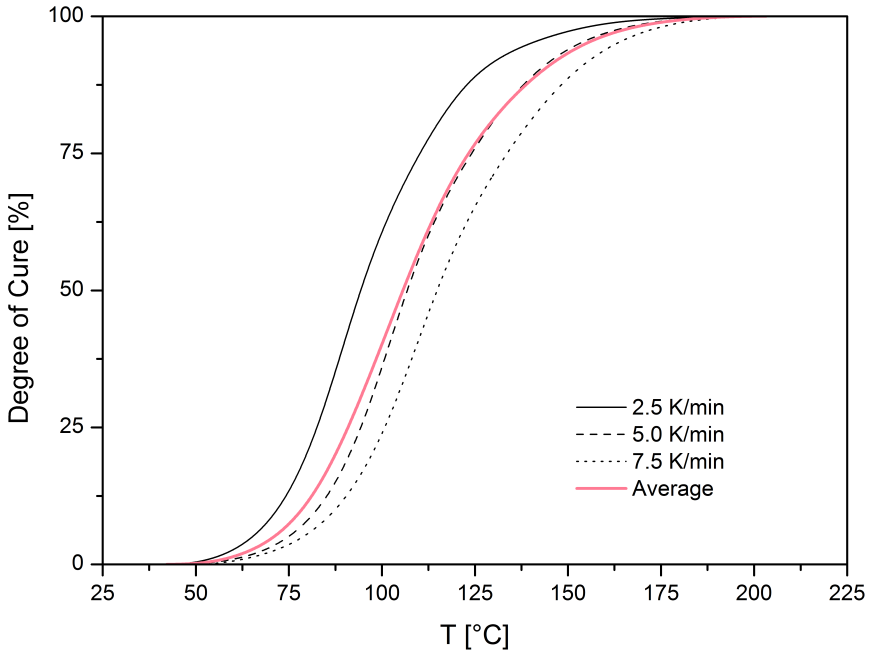

(a) Degree of cure for different heating rates determined for the neat epoxy resin as well as the calculated average value.

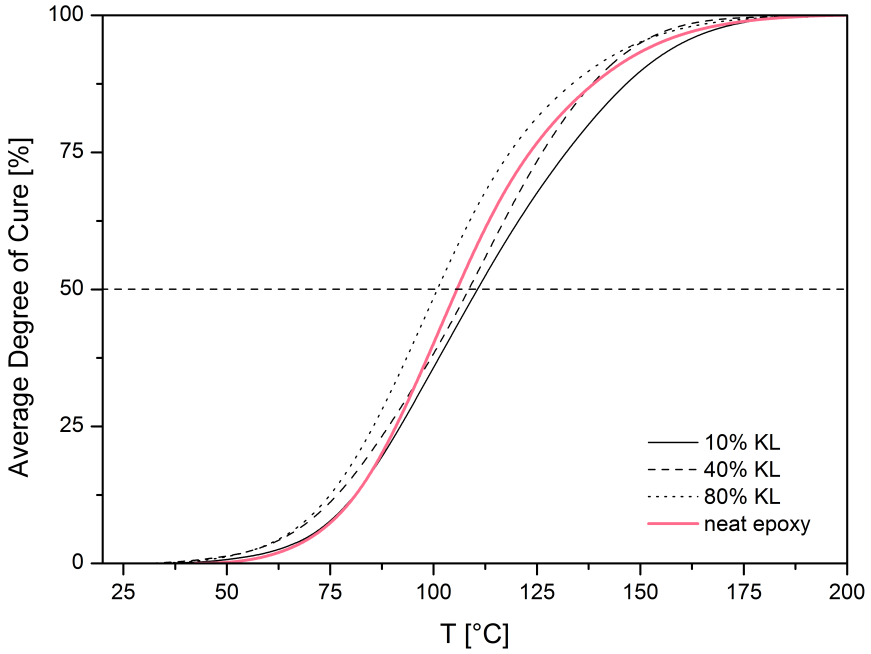

(b) Average degree of cure of lignin filled epoxy compared to the neat epoxy.

Figure 5.9.

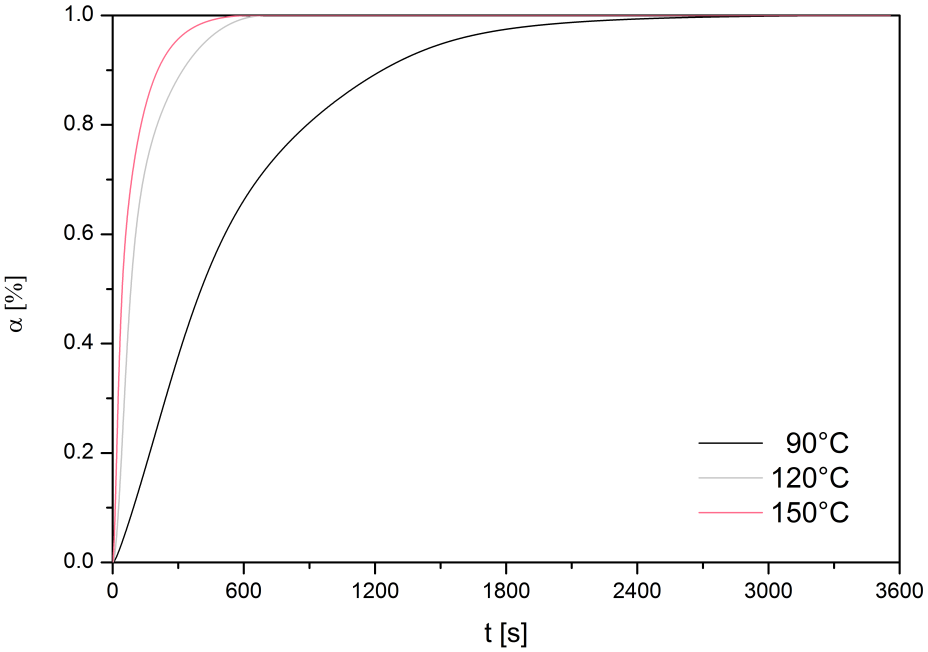

(a) Degree of cure for the neat epoxy cured at 90 °C, 120 °C and 150 °C, determined by calculating the first derivation of the heat flow curves and further normalized.

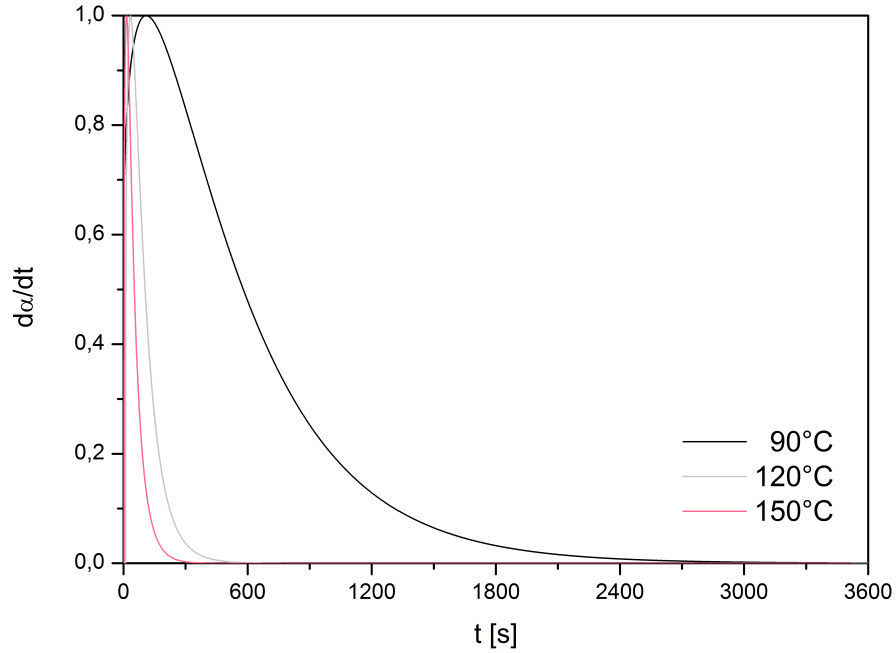

(b) Heat flow curves of the neat epoxy cured isothermally at 90 °C, 120 °C and 150 °C.

Figure 5.10.

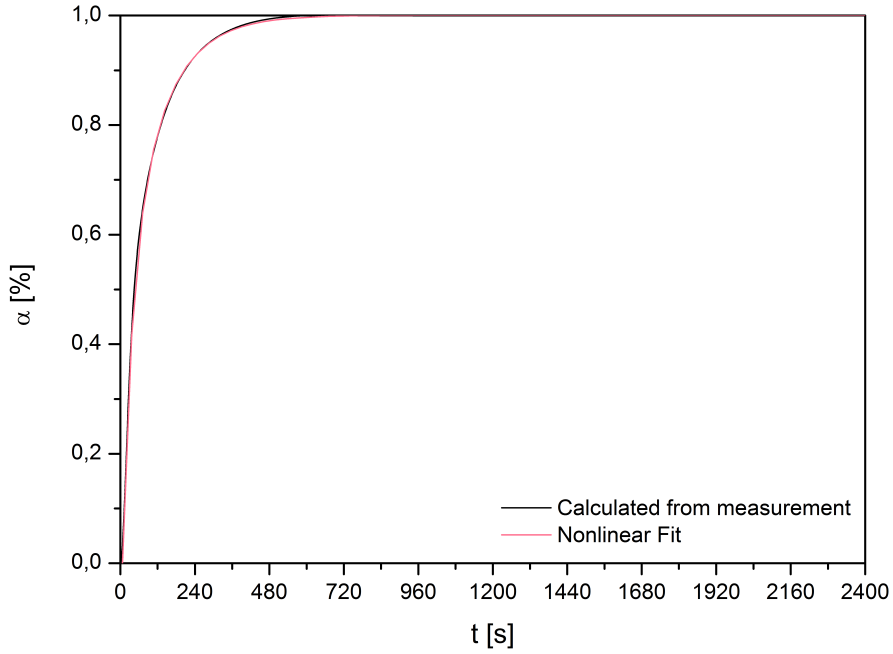

Figure 5.11.: Nonlinear fit for the normalized conversion α of the neat epoxy resin.

In order to estimate the parameters A_1, A_2, a, b and y_0, Equation 5.7 is fitted to the experimental data. Figure 5.11 shows exemplary the sample cured at 150 °C with the applied non–linear fit. The calculated curve fits the measured curve nicely ($\chi^2 = 0.998$) and applies for the other measurements as well.

The resulting parameters of the Kamal–Sourour functions for the neat epoxy samples compared to the actual measured data are shown in Figure 5.12. Best results were obtained at the lowest curing temperature, 90 °C, where just a small shift of the peak maximum as well as the exponential decay occurs. The peak amplitude is higher than measured for 120 °C and slightly lower for 150 °C. Also, higher temperatures show a steeper exponential decay. This is generally to be expected with amino–cured epoxy if the degree of cure—and therefore the cross–linking density—is high enough. The system than undergoes vitrification (when $T_g = T_c$). The molecular movement is drastically reduced so that the system runs from a chemical controlled into a diffusion controlled curing mechanism.

The calculated reaction parameters are summarized in Table 5.5. The reaction order for the initial reaction m as well as for the following auto catalytic reaction n increase as expected with increasing curing temperature. By increasing the curing temperature from 90 °C to 150 °C, the reaction order m is almost doubled from 0.51 to 0.98. The same behavior occurs with the parameter n. Starting from 1.27 at a curing temperature of 90 °C to 2.43 at 150 °C.

k_1 shows just a slight increase of the reaction rate from 8.0 up to 10.5 suggesting that the initial reaction rate is nearly temperature independent. Regarding k_2 the reaction rate is almost tripled. This shows the strong temperature dependency of the auto catalytic reaction. However, in the later stages of the cure reaction when higher conversions are achieved, the obtained data of the model predictions differ slightly from the experimental data. Therefore, the reaction was controlled in the later stages of cure by diffusion mechanisms rather than by kinetic parameters.

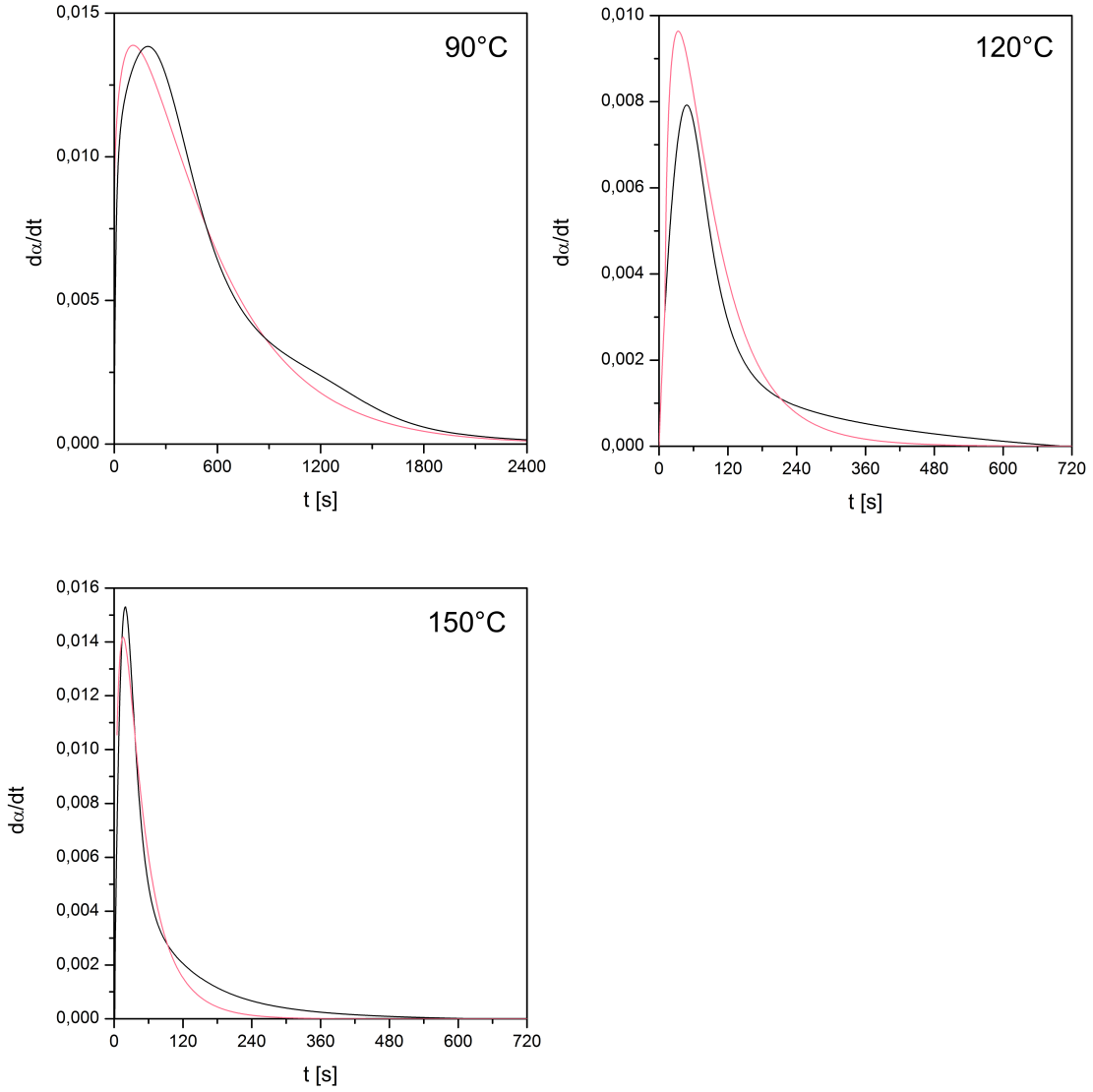

Figure 5.12.: Determination of kinetic parameters for the neat epoxy at 90 °C, 120 °C and 150 °C. Black = Measurement, Red = Calculated with parameters using the fit of Kamal–Sourour.

Differences between measured and model data are greater at higher cure temperatures. This is due to the T_g of the fully cured material. If the curing temperature is close to the T_g, the free volume is reduced leading to higher cross–linked structures making the reaction diffusion controlled.

This is also reflected in the overall reaction order which is increased up to 3.41. This is attributed to a trimolecular mechanism when few of the hydroxyl groups in the epoxy chain participate in the cross–linking reaction. However, this cure reaction cannot be described as a standard n^{th} order reaction. At elevated temperatures, the hydroxyl group in the molecular chain is able to become a proton donor, which is able to participate in the reaction following a trimolecular mechanism. Therefore, the overall reaction order $m + n$ increases with increasing temperatures. [125]

However, up to these limitations, the calculated parameters are in very good agreement for neat epoxy compared to parameters known from literature. [126,127] Since the model predictions of the neat epoxy resin proved to be in good agreement with experimental data as well as with literature, these results can be used as benchmarks in comparative studies with lignin.

Therefore, samples containing 40 % kraft lignin were prepared and measured according to the neat samples. The representative plots of the experimental data and the data obtained by the autocatalytic model by Kamal and Sourour are shown in Figure 5.13a. At all curing temperatures, the data of the model predictions compared to the experimental data are in good agreement at low conversions. With increasing curing temperature, diffusion control of the further cross-linked epoxy system increases as described for neat epoxy resin.

However, deviations to the model predictions are less pronounced with lignin as with neat epoxy. Hence, apparently the cross–linking of the tertiary reaction system is mainly kinetically controlled and less affected by diffusion control due to the presence of kraft lignin. Figure 5.13b presents the comparison of the model predictions of the neat epoxy resin with the 40 % filled epoxy.

At all temperatures the reaction still follows the same reaction scheme. While the peak maximum values remain approximately the same, the exponential decay is affected by the lignin at all temperatures with an increase in the reaction rate. Since the reaction sequence is not influenced with the presence of lignin in the epoxy, it is possible to apply the kinetic model used for neat epoxy as well. Table 5.6 shows the calculated reaction parameters for the lignin filled epoxy compared with the parameters for the neat epoxy.

Compared to the neat epoxy there is an obvious shift of both of the reaction orders. Especially m shows a reversed type of behavior. While for the neat epoxy the values increase from 0.51 to 0.98 the values for 40 % epoxy start with an order of 2.0 falling to 0.49. In case of the second reaction order n the values show a stronger increase than the neat epoxy starting with a much lower reaction order of 0.29 compared to value for the neat epoxy of 1.27.

Table 5.5.: Reaction orders m and n as well as rate constants k_1 and k_2 determined by Kamal–Sourour. [118]

T °C	m	n	$m+n$	$k_1 \cdot 10^{-3}$ $[min^{-1}]$	$k_2 \cdot 10^{-3}$ $[min^{-1}]$
90	0.51	1.27	1.78	8.0	23.9
120	0.63	1.98	2.61	9.3	39.1
150	0.98	2.43	3.41	10.5	66.7

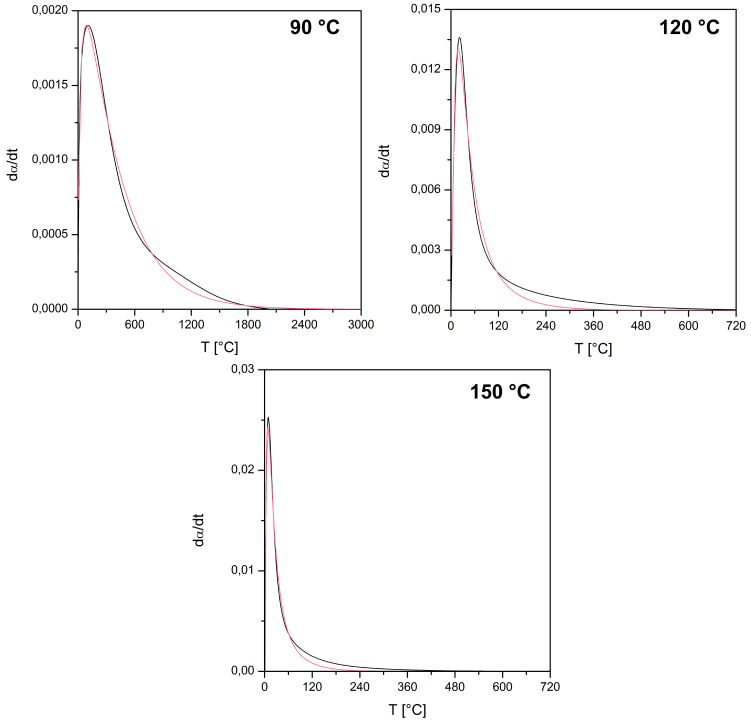

(a) Comparison of the model prediction with the experiment for a 40 % lignin filled epoxy resin at curing temperatures of 90 °C, 120 °C and 150 °C.

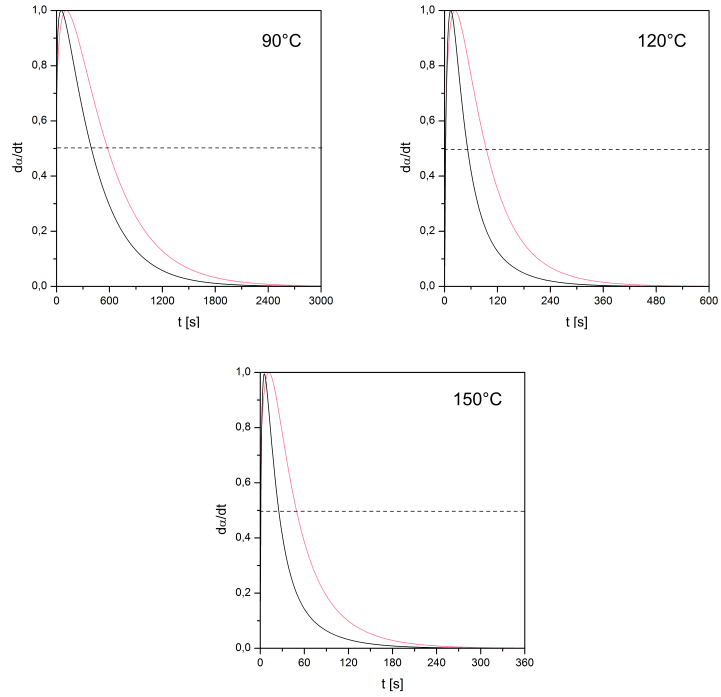

(b) Comparison of the neat epoxy (red) with 40% KL (black) at the curing temperatures 90 °C, 120 °C and 150 °C.

Figure 5.13.

The calculated reaction rates are strongly influenced by the lignin k_1 and k_2 as well (cf. Figure 5.14). k_1 shows at each curing temperature reduced values by almost one third whereas k_2 shows the opposing trend with higher values for the 120 °C and 150 °C cured systems.

Regarding the initial step of the reaction, there is a significant drop of the reaction rate with the addition of lignin. It is almost one forth slower than the neat epoxy resin. This means that at this point the lignin hinders the reaction between the epoxy and amino moieties. This can be explained by the increasing diffusion path of the epoxy and hardener molecules when the bulk material lignin is present.

The overall reaction order $(m + n)$ offers another interesting indicator for the participation of kraft lignin in the cross–linking reaction. At the lowest curing temperature of 90 °C an overall reaction order of 1.22 is achieved. This is lower than the neat epoxy resin occurring from the deceleration of the initial reaction. However, increasing the curing temperature results in an overall reaction order of around 3 which means that a trimolecular reaction occurs at around 120 °C. There are two possible causes: either kraft lignin accelerates the reaction of the hydroxyl groups in the molecular chain or kraft lignin acts as a participant itself.

Interestingly, the overall reaction order decreases to 2.85 with increasing the curing temperature to 150 °C, however this can be explained regarding the single reaction orders m and n. With a reaction order of $n = 2.35$, the value of the autocatalytic reaction is similar to the neat epoxy system. This means, that a temperature of 120 °C shows the strongest effect of kraft lignin towards the cross–linking reaction.

With two rate constants k_1 and k_2 two activation energies are possible. On the basis of these results the two activation energies $E_{a,1}$ and $E_{a,2}$ as well as the pre exponential constants A_1 and A_2 can be calculated by applying an Arrhenius plot. Therefore the Arrhenius law shown in Equation 5.9 is brought into its linear form:

$$\ln k_i = -\frac{E_{a,i}}{R} \cdot \frac{1}{T} + \ln A_i \tag{5.10}$$

whereas $\ln k_i$ is plotted against $\frac{1}{T}$ and the activation energy $E_{a,i}$ can be calculated by Equation 5.11 in which m is the slope of the line

$$E_{a,i} = -m \cdot R \tag{5.11}$$

Table 5.6.: Reaction orders m and n as well as rate constants k_1 and k_2 determined by Kamal–Sourour.

T	m	n	$m+n$	$k_1 \cdot 10^{-3}$ $[min^{-1}]$	$k_2 \cdot 10^{-3}$ $[min^{-1}]$
Neat epoxy					
90	0.51	1.27	1.78	8.0	23.9
120	0.63	1.98	2.61	9.3	39.1
150	0.98	2.43	3.41	10.5	66.7
+ 40 % KL					
90	2.0	0.29	1.22	2.0	1.9
120	0.79	2.60	3.04	2.57	69.0
150	0.49	2.35	2.85	3.35	79.0

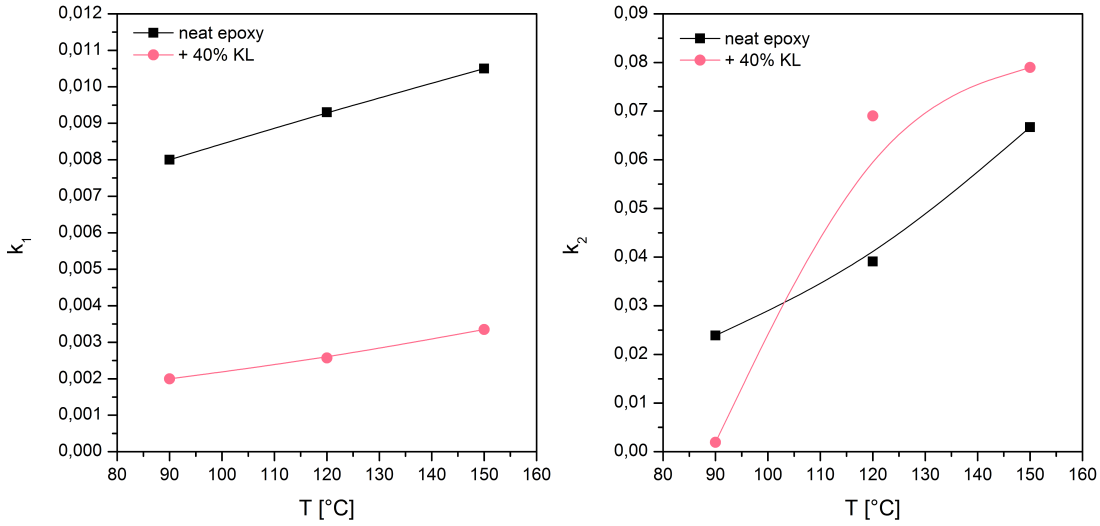

Figure 5.14.: Comparison of the rate constants k_1 and k_2 determined for the neat DGEBA/IPDA epoxy resin as well as for the epoxy resin with 40 % kraft lignin share. Calculated measuring points are connected for better illustration.

and the pre exponential factor A_i by Equation 5.12 is given by the intercept with the y-axis:

$$A_i = \ln k_i \tag{5.12}$$

Figure 5.15 shows both Arrhenius plots for the neat epoxy as well as the Arrhenius plots for the lignin filled epoxy resin which provided linear slopes $-E_{a,1}/R$ and $-E_{a,2}/R$ as well as the intercepts $\ln A_1$ and $\ln A_2$, respectively. Table 5.7 lists the parameters obtained for the neat and lignin filled epoxy resin. The lignin filled system exhibited higher activation energies compared to the neat resin. This means that lignin as a stiff filler will definitely obstruct the cross–linking reaction between the epoxide and curing agent.

With this study using isothermal DSC mode of measurements at 90 °C, 120 °C and 150 °C it has been proven that the kinetic model of Kamal and Sourour can be applied to a lignin filled epoxy system and the reaction parameters have been obtained successfully. Further it could be shown that kraft lignin participates in the cross–linking reaction of the tertiary system. However, further investigations have to be made to explain the exact part of lignin in the reaction. This will be addressed subsequently in Chapter 8.

Table 5.7.: Activation energies $E_{a,1}$ and $E_{a,2}$ and pre exponential factors A_1 and A_2 for the neat epoxy and the lignin filled epoxy system.

Parameter	neat epoxy	+ 40 % KL
$E_{a,1}$	5.90 kJ/mol	11.7 kJ/mol
$E_{a,2}$	21.8 kJ/mol	79.2 kJ/mol
A_1	2.91	2.37
A_2	3.46	20.03

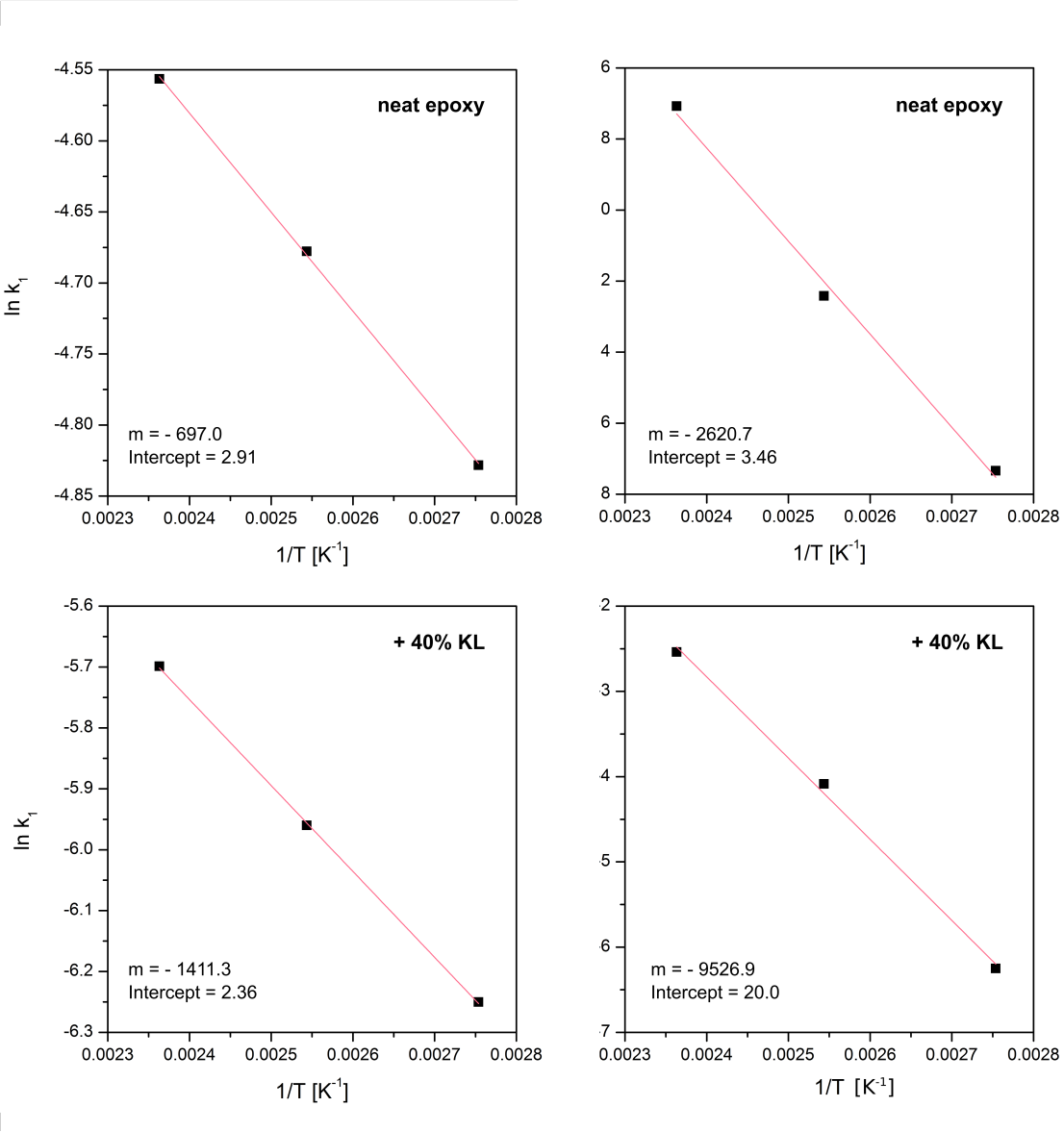

Figure 5.15.: Arrhenius plots for k_1 and k_2 to determine the activation energy $E_{a,i}$ and pre exponential constant A_i for the neat epoxy and the lignin filled epoxy resin.

5.2 Introducing a Reactive Diluent in the Lignin Filled DGEBA/IPDA System

In the previous section, the incorporation of lignin yields an improved Young's modulus due to the presence of rigid lignin particles. However, the increasing viscosity proves to be a major challenge in the processabilty of fiber reinforced polymers. To counteract the increase of viscosity as well as to improve toughness and elasticity, reactive diluents have been considered as a feasible additive. They enable to tailor the physical and mechanical properties of the epoxy system, allowing them to be suitable for different applications. [128,129] Additionally, a lower viscosity gives better wetting and impregnation of fibers and permits higher filler loading without substantial decrease in thermal stability and curing rate. [130]

Generally, reactive diluents serve on one hand as a solvent for the epoxy compounds and on the other hand are able to react with oligomer monomers to build a network. Hence, reactive diluents are

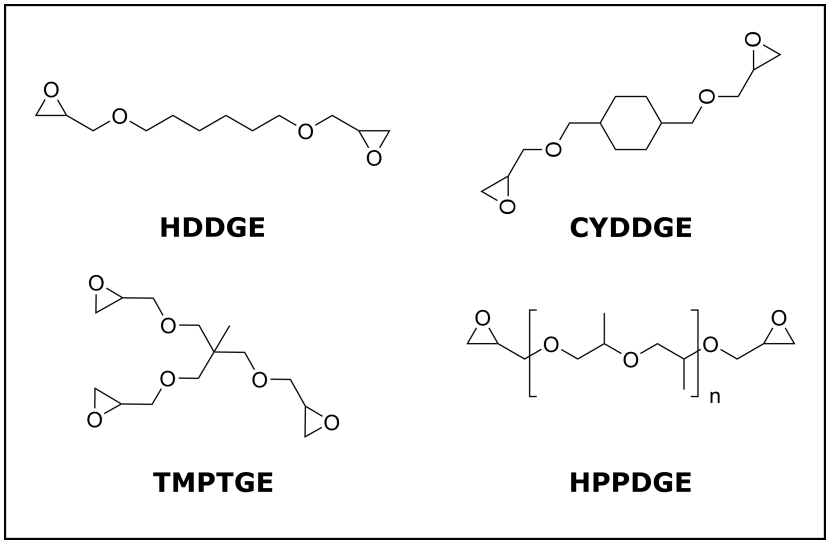

Figure 5.16.: Chemical structures of reactive diluents based on aliphatic diglycidyl and triglycidyl ethers which were chosen for further investigation.

usually low in viscosity with functionalities which are either able to react with the oxiran moieties or are compatible with the curing agent.

A further important issue is the phase morphology of the lignin filled epoxy system. As seen previously, the lignin content as well as the curing temperature causes the system to split–up into a phase separated system. Therefore, the solubility of lignin in the reactive diluent might result in an improvement of the interfacial interaction between epoxy resin and lignin.

Reactive diluents are generally glycidyl ethers, sometimes glycidyl esters, of aliphatic or aromatic structure. In some epoxy systems, diluents with several epoxy groups can be used as resin instead. Figure 5.16 shows the chemical structures of the diglycidyl ether based reactive diluents which were chosen due to their chemical reactivity towards the amino–based curing agent as well as their commercial availability. The aliphatic reactive diluents include both cycloaliphatic and non–cyclic aliphatic diglycidyl ethers.

At first, the different types of lignin were mixed into the four reactive diluents to understand the solubility as well as dispersability of the various lignins in the diluents. Therefore, lignin–diluent samples were prepared containing 10 % weight fraction of lignin. They were mixed until complete dispersion was achieved and were allowed to settle for 2 h. Table 5.8 shows the results for the dispersability of lignin in the reactive diluents.

Lignin which had not sedimented was either dispersed or dissolved in the reactive diluent. Except for HDDGE, sedimentation of lignin occurred in all other samples. It could be observed that a major fraction of lignin dissolves in the HDDGE reactive diluent. These results can be allotted to the polarities of the reactive diluents. Since lignin dissolves in solvents with high polarity, complete dissolution is not expected in reactive diluents. As for the sedimentation of lignin in the reactive diluents, the low dispersabilty is due to the particle size of the lignins. Therefore, the good results in HDDGE are associated with the interaction of good solubility and dispersabilty.

Due to the positive results with HDDGE, mechanical tests were performed only with HDDGE. Samples with 0 %, 20 %, 40 % and 60 % lignin share were prepared as described in the previous chapter. While

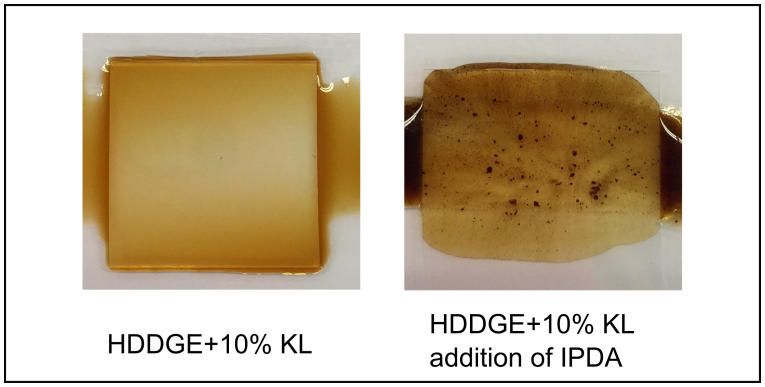

Figure 5.17.: Solubility of kraft lignin in reactive diluent HDDGE (left) and with addition of IPDA (right).

the dispersability as well as solubility remained constant with the presence of DGEBA the addition of IPDA proved to be difficult with the immediate precipitation and agglomeration of lignin as shown in Figure 5.17.

Therefore, the preparation of homogeneous and void free samples was challenging. The results of the stress–strain measurements for samples with 0 %, 20 %, 40 % and 60 % lignin share are shown in Figure 5.17.

The addition of the reactive diluent to the neat DGEBA/IPDA resin system causes a significant change of the mechanical behavior. Instead of brittle fracture, the material starts to flow after reaching a yield point at a yield stress of $\sigma_y = 35$ MPa then the stress decreases rapidly to a minimum drawing stress $\sigma_d = 22.8$ MPa.

With the addition of kraft lignin plastic deformation is suppressed and brittle fracture occurs at a stress increased by 30 % compared to the unfilled sample. The Young's moduli of the lignin filled samples increase with higher lignin loads from initially 780 MPa to 935 MPa for the sample with 60 % lignin share. Table 5.9 summarizes the obtained measured values for stress, strain and Young's modulus.

In order to investigate the influence of HDDGA on the curing behavior as well as the resulting glass transition temperature DSC measurements were carried out. Figure 5.19 show the first and second

Table 5.8.: Dispersability of different kraft lignins in four different diglycidyl ether–based reactive diluents HDDGE, CYDDGE, TMPTGE and HPPDGE.

	HDDGE	CYDDGE	TMPTGE	HPPDGE
KL_1	partially soluble	partially sedimented viscous dispersion	no dispersion viscous dispersion	no dispersion
KL_2	partially soluble	partially sedimented	partially sedimented	partially sedimented
KL_3	partially soluble	mostly sedimented	mostly sedimented	no dispersion
KL_{aw}	partially soluble	partially sedimented cloudy solution	partially sedimented	no dispersion
KL_{xp}	partially soluble	partially sedimented	partially sedimented	partially sedimented
KL_{eh}	no dispersion	no dispersion	no dispersion	no dispersion

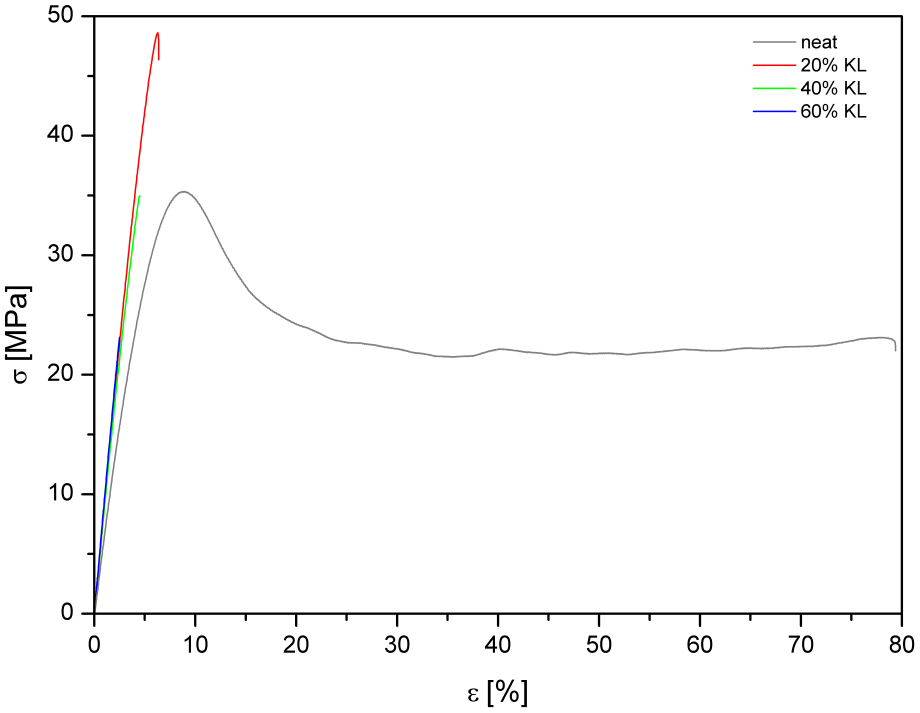

Figure 5.18.: Stress-strain measurements for samples with 0 %, 20 %, 40 % and 60 % lignin share containing 10 % reactive diluent HDDGE.

heating run of the neat DGEBA/IPDA/HDDGA system and the system filled with 40 % kraft lignin load. The kraft lignin has no direct influence on the required initial curing temperature T_i, peak temperature T_p or the end of curing T_e.

However, the heat of reaction is decreased by around 50 % for the lignin filled DGEBA/IPDA/HDDGA system. This might be explained by the agglomeration of lignin in the formulation and therefore the decreased reactivity towards the resin components. The T_g decreased from 164.0 °C for the neat DGEBA/IPDA system to 48.7 °C for the HDDGA diluted formulation. Despite its agglomeration effects, kraft lignin has a strong influence on the glass transition, which increases to 93.5 °C and clearly indicates the reactivity of the residual solved or dispersed lignin.

The experiments with reactive diluents showed that mechanical properties as well as the glass transition temperature are easily adaptable parameters for specific requirements. However, the agglomeration of kraft lignin with the addition of IPDA is an undesired effect which aggravates the handling as well as the processability in the wet–lay up method. Further, studies proved that reactive diluents, especially

Table 5.9.: Stress at break, strain at break and Young's modulus for of DGEBA/IPDA/HDDGA system filled with 20 %, 40 % and 60 % KL.

Sample	σ_b [MPa]	ϵ_b [%]	Young's Modulus [MPa]
DGEBA/IPDA/HDDGA	31.9 ±2.8	70.1 ±34.8	780 ±34
+ 20% KL	40.0 ±7.6	5.0 ±1.1	840 ±44
+ 40% KL	26.3 ±6.7	3.7 ±0.7	880 ±70
+ 60% KL	22.3 ±0.7	2.4 ±0.1	935 ±4

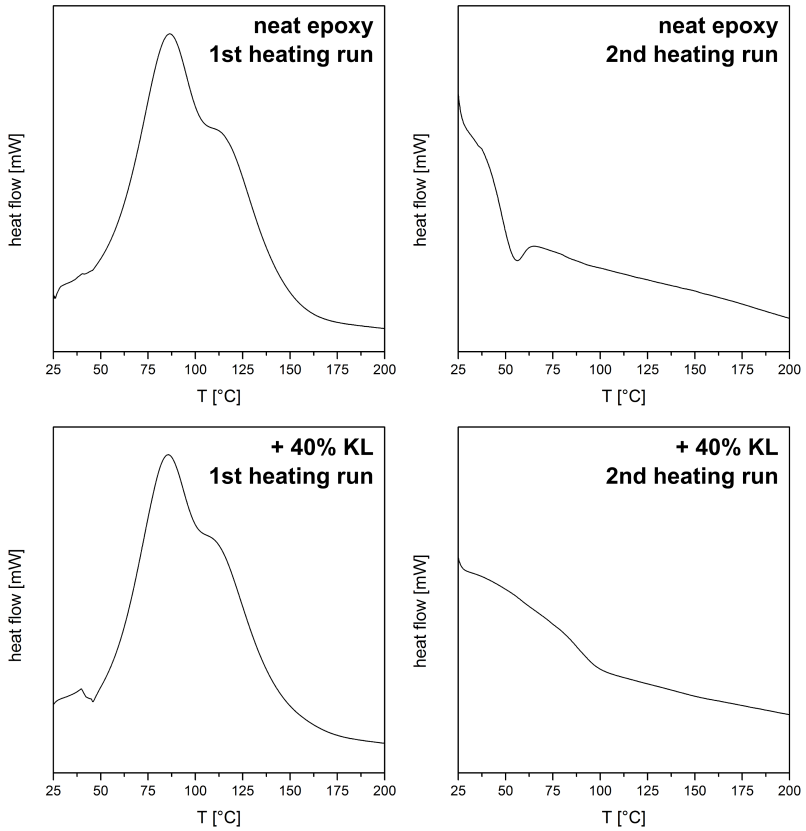

Figure 5.19.: First and second heating run of DGEBA/IPDA/HDDGA (left) and DGEBA/IPDA/HDDGA +40 % kraft lignin (right).

aliphatic diglycidyl ehters like HDDGA, constitute a serious health risk leading to severe contact allergic reaction.[131] Therefore, further experiments with reactive diluents have been discontinued.

Table 5.10.: Curing characteristics such as the onset temperature T_i, the peak temperature T_p and the terminal temperature T_e as well as the curing range, heat of reaction and the glass transition temperatures of the DGEBA/IPDA system compared to the systems with added reactive diluent.

Sample	T_i [°C]	T_p [°C]	T_e [°C]	Curing range [°C]	ΔH [J/g]	T_g [°C]
DGEBA/IPDA	31.0	90.3	160.3	129.3	19.0	164.0
+ HDDGA	28.3	86.7	175.0	146.7	13.7	48.7
+ 40 % KL	26.0	86.2	176.8	150.8	10.0	93.5

6 Introducing the Lignin-Epoxy Blend in Composite Materials

The previous chapters focused on the development as well as thermal and kinetic characterization of a 2–component kraft lignin based epoxy formulation consisting of DGEBA and IPDA. At this point of this work it became necessary to investigate the processability and curing behavior to validate the developed lignin filled epoxy formulation towards the FRP and to study the influence of the reinforcing component.

In collaboration with the Fraunhofer Institute for Structural Durability and System Reliability LBF as well as Darmstadt University of Applied Science the processability of the wet–lay up procedure was tested in pilot scale.[132,133] Additionally, the curing behavior of the newly developed biobased epoxy formulation as well as basic mechanical properties were investigated.

The main objective was to create an epoxy based FRP with maximum bio share. Therefore, not only lignin was introduced into the resin, a large quantity of the bio share stems from the fiber component as well. Cellulose fibers have been chosen due to their high availability. Different fibers as well as the optimal type, length, orientation and processing have been selected, tested and analyzed in cooperation with Technical University of Darmstadt's department of Paper Technology and Mechanical Process Engineering (PMV). Additionally, for maximum bio share lignin was brought into the cellulose fiber mats as well and tested according to the neat cellulose fiber mats. The optimized parameters were used for the production of cellulose fiber mats.[134–136]

Figure 6.1a demonstrates the individual steps of the paper making process. In the first step 50 g cellulose fibers and, in the case of lignin–filled cellulose mats, lignin are beaten in 2 L water to obtain an even distribution of the fibers, then the water-soaked fibers are filled in a mixing chamber with a stirrer (a) and vigorously suspended in 22 L water. In the next step, a defined amount of the suspension is transferred to a Rapid Köthen sheet former consisting of a riser pipe which can be folded back (b) having a fine mesh on its bottom. After starting the sheet, former water is pumped automatically into the chamber and at a level of 4 L the prepared suspension is added (c). Subsequently, the water is drained and the fibers deposits on the mesh surface (d). The resulting wet fiber mat is placed between two paper sheets and in a vacuum assisted press dried at 90 °C for 15 min (e). Finally, cellulose fiber mats are obtained with 4.8 g per sheet.

The manufacturing process of the FRP and test specimens respectively is based on several consecutive processing steps: Laminating, pressing and tempering of the FRP followed by cutting with a diamond belt saw into test specimens. To prevent overheating of the specimens, which could lead to changes in the material, the blade was cooled with water. The specimens were dried at 30 °C and 0.5 % RH for 12 h. To avoid surface defects through the cutting procedure, it is essential to polish sides and edges since even small notches could cause preliminary failure.

It is important to use just enough resin to impregnate the fibers without soaking since tearing of the paper sheets during handling might occur. For easier processing the formulations were warmed to 30 °C to decrease viscosity. After completing the first layer a second fiber mat is placed on top and strongly pressed with a metal disc drum onto the first layer. This process is repeated until 9 layers of paper mats are stacked. Slipping of the paper sheets is avoided by fixation with needles. Finally the outer surface is coated in resin as well.

Afterwards, the prepared fiber mats are assembled in a vacuum bag which consists of 4 different layers as shown in Figure 6.1b (left): The outermost layer is foil, then a felt cloth to absorb excess resin and the peel ply for easy removal of the finished composite, the perforated foil acts as protection against sticking together of both layers. The vacuum bag is sealed with sealing tape and applied to vacuum for 30 min.

Vacuum is applied for several reasons, on the one hand to remove excess resin and voids as well as to ensure complete wetting of the fibers and on the other hand specially in this case to remove excess moisture of kraft lignin (Figure 6.1b, right). Afterwards, the paper is pressed. The pressing plates are preheated to 90 °C and after introduction of the FRP a pressing force of 50 kN is applied for 5 h. In order to guarantee complete cross–linking, the paper was tempered at 60 °C and 50 % relative humidity for 10 h in a climatic chamber.

For the determination of the material–specific parameters at tensile load, tests were conducted according to DIN EN ISO 527–4 "Test conditions for isotropic anorthotropic fibre-reinforced plastic composites" which restricts the shape of the test specimen.[137] Adapted Type II specimen according to the norm were prepared as illustrated in Figure 6.2a. The specimen's dimensions are summarized in Table 6.2b. All tests were conducted at 2 mm/min test speed and standard atmosphere (23 °C, 50 % relative humidity).

With regard to the significance of the measurements, five specimen were attempted to be measured per series. However, dismissal problems such as slipping of specimens out of the clamping jaw, failure or break of the material within the clamping jaw (up to 10 mm from the jaw) and obvious defects like delamination occurred. Therefore, depending on the series, the number of valid measurement for analysis is between three and seven.

Due to the parallel structure of the specimen no predetermined breaking point is given, which mimics realistic material behavior. Within the scope of this project, the increase of the bioshare in the final FRP is paramount importance. Therefore, introducing kraft lignin not just in the epoxy formulation, but also as filler in the fiber mats was attempted. The experimental design is shown in Table 6.1. Samples with 0 %, 20 % and 40 % kraft lignin share in the fiber mats were prepared as well as an epoxy formulation with 0 % and 40 % kraft lignin content and compared to the reference.

Tensile measurements of the prepared specimen were carried out at Darmstadt University of Applied Science and the results are summarized in Table 6.1. The standard deviation of each series of measurements is relatively small in a range of $60 - 300$ MPa which suggests a high quality and homogeneity of the manufactured specimens.

Table 6.1.: Calculated density and measured Young's modulus, stress and strain at break of the manufactured FRP with regard to different kraft lignin share in the paper mats and resin resulting in different fiber volumes.

	KL in [%]		Fiber volume	ρ	E	σ	ϵ
	paper	resin	[%]	[g/cm^3]	[MPa]	[MPa]	[%]
0	0	0	38	1.12	5189 ± 206	100 ± 2.4	3.3 ± 0.2
1	40	0	81	1.17	7581 ± 415	69.4 ± 6.0	1.8 ± 0.2
2	40	40	49	1.11	6512 ± 153	61.4 ± 2.1	2.0 ± 0.1
3	20	40	51	1.14	7557 ± 259	74.3 ± 4.3	2.1 ± 0.2
4	0	40	35	1.19	7035 ± 306	79.4 ± 4.3	2.7 ± 0.2

As illustrated in Figure 6.3, the samples with 20 % kraft lignin in the fiber mats and 40 % kraft lignin load in the epoxy formulation show the highest values for Young's modulus. This might result from a synergistic effect of the kraft lignin in both components achieving a higher stiffness. However, increasing the share of kraft lignin in a fiber/resin ratio of 40 % / 40 % results in a loss of stiffness, tensile strength and strain. This shows the importance to find the optimum ratio of kraft lignin in fiber and resin.

Compared to the reference, kraft lignin shows an overall positive effect on the Young's modulus with values around 6500 — 7500 MPa compared to 5189 MPa of the reference. By means of tensile strength and strain lower values with increasing amount of kraft lignin are noticeable. This effect is explained by the nature of filling materials which tend to strengthen the final material. In very rare cases they cause a deterioration of the values resulting in increasing amounts of voids with higher filler loads. Nonetheless, good results for the tensile strength were achieved with kraft lignin.

Besides the tensile measurements, SEM imaging of the kraft lignin fiber/resin ratios 0 / 40, 20 / 40 and 40 / 40 were carried out to determine fracture mechanisms and fiber–matrix adhesion as shown in Figure 6.4. Although the fracture surface does not describe the behavior of the material for the unloaded case, it is still feasible to deduce adhesion results.

The shown fracture surfaces are formed after exposure under tensile load. To provide a general overview of the FRP micrographs over the whole thickness of the specimen were taken. The alternating layers of fiber mats and epoxy resin are clearly visible. The appearance of the black cavities is caused by the applied tensile load. Due to the deformation of the FRP, cracks and delamination can occur. Moreover, torn fibers over the entire fracture surface are visible. It is interesting to note that these delamination effects occur more heavily with kraft lignin filled fibers compared to the neat fiber sheets. Magnification of the fractured samples shows that void formation of the resin layers and missing matrix in the fibrous structure is influenced by kraft lignin load in the fiber sheets as well.

Even more interesting is the apparent segregation of the kraft lignin loaded epoxy resin within the ratios 20 / 40 and 40 / 40. This might result from low molecular weight fractions of kraft lignin in the reinforced paper which is able to dissolve in the liquid epoxy resin and hardener even more at elevated temperatures causing this segregation.

As mentioned at the beginning of this chapter biobased FRP highly loaded with kraft lignin in both components, reinforcement and matrix, are in the spotlight of the current work. On one hand, kraft lignin was successfully introduced into the epoxy compound as shown in the previous chapters. On the other hand, kraft lignin was introduced as filler into the cellulose fiber sheets to increase the biocontent even more. The previous results showed the positive effect by increasing Young's modulus with only a small decrease in tensile strength and strain.

The combination of kraft lignin in the fiber sheets and epoxy resin shows good results, however, the SEM micrographs prove a segregation of the epoxy components due to an increasing amount of kraft lignin in the epoxy resin. This increase reduces the mechanical properties which are higher in a homogeneous system.

Furthermore, additional challenges in the manufacturing process (e. g. a short pot life) emerged. These extended the requirement profile of the novel biobased FRP. Therefore, a different approach was chosen which combines the positive influence of kraft lignin in the DGEBA–based epoxy resin as well as to adapt to a new field of application.

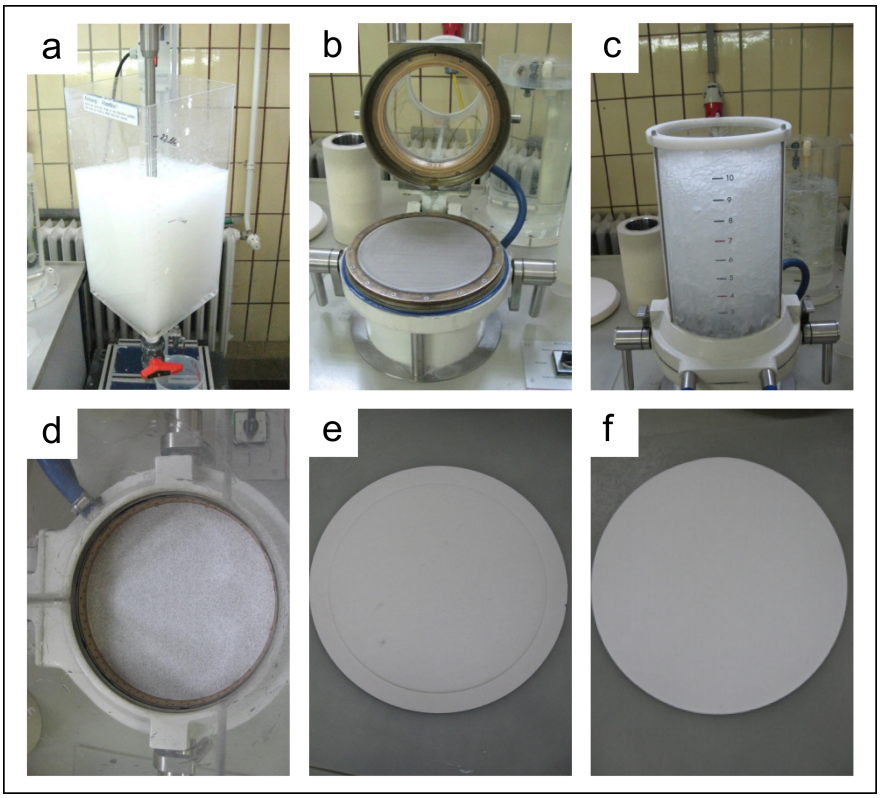

(a) Different stages of the paper making process for fiber mats used as reinforcement material for biobased composites.

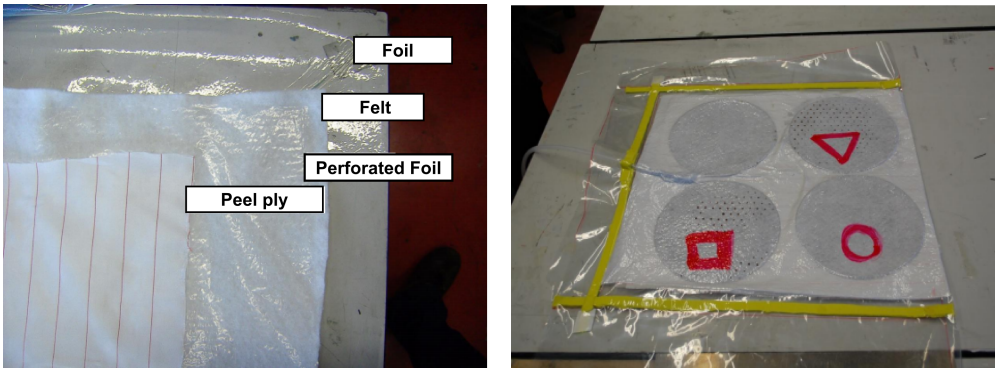

(b) Vacuum process for composite manufacturing: Several layers of materials such as peel ply, (perforated) foil and felt are applied between the FRP and vacuum foil prior to vacuumization to ensure a flawless material.

Figure 6.1.: Different steps of the paper making process (a) and further their introduction into the FRP (b).

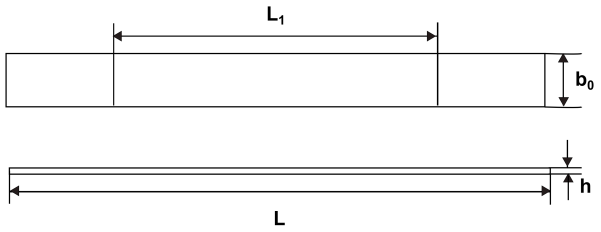

(a)

Test specimen		Type II
Total length	L	250 mm
Thickness	h	$2-3$ mm
Width	b_1	$25-50$ mm
Initial Distance	L_1	150 mm

(b)

Figure 6.2.: Dimensions of the test specimens manufactured according to DIN EN ISO 527–4.

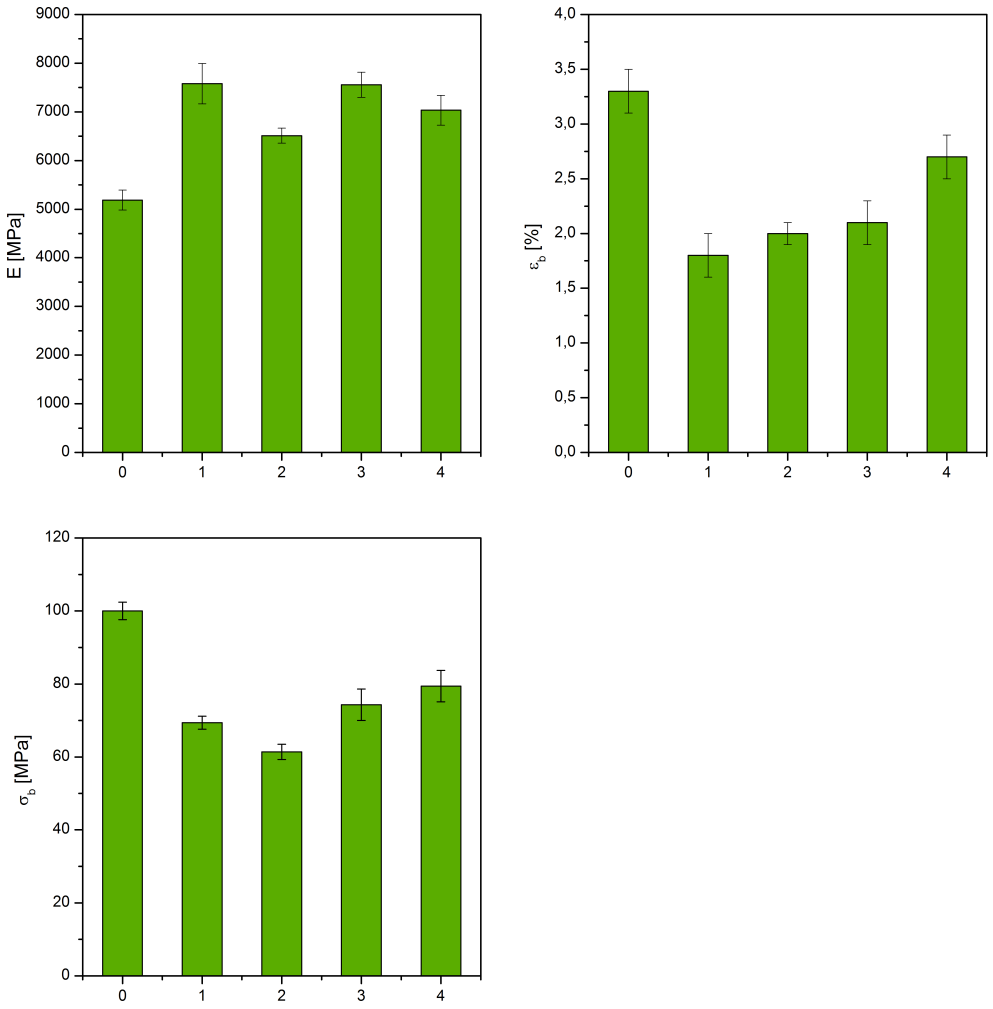

Figure 6.3.: Results of Young's modulus (top left), strain at break (top right) and stress at break (bottom) for the neat FRP (0) compared to FRP samples with different loads of lignin of 40 %/0 % (1), 40 %/40 % (2), 20 %/40 % (3) and 0 %/40 % (4). (KL in paper/resin in %)

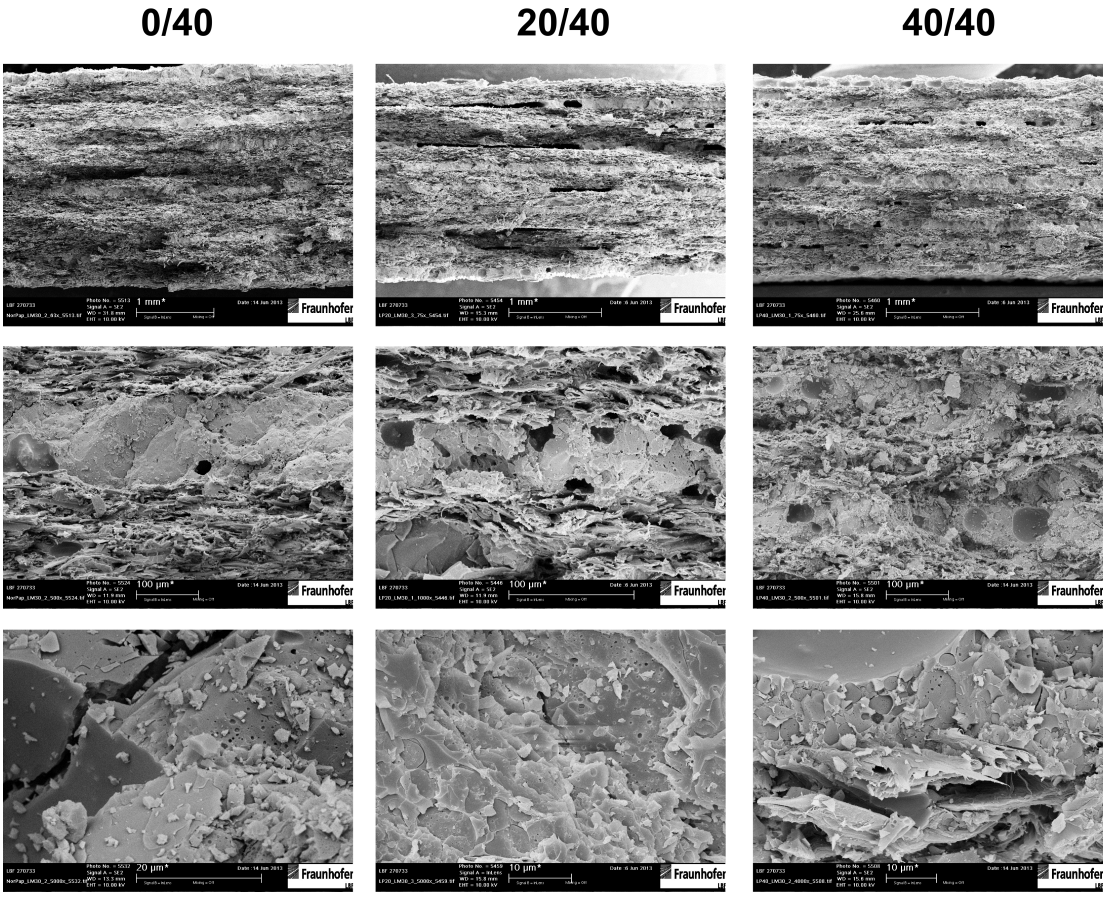

Figure 6.4.: SEM micrographs of the kraft lignin reinforced FRPs with kraft lignin fiber/resin ratios of 0 %/40 %, 220 %/40 % and 40 %/40 %.

7 Introducing Dicyandiamide for a 1–Component Epoxy Resin

In the previous chapter it was investigated how a 2–component epoxy formulation filled with kraft lignin can be incorporated in composite manufacturing. Due to the results of Chapter 6 which extended the set of requirements for the FRP, a different DGEBA–based epoxy formulation had to be developed and investigated. In particular, a pre–impregnated composite fiber (pre–preg) approach was followed. The pre–preg approach imposes several requirements towards the epoxy formulation which are listed below.

Curing time: Since the pre–preg needs to be produced in a continuous fashion, it is important that the curing time is fast to achieve a semi cross–linked—so called B–stage—epoxy resin.

Curing temperature: The curing temperature needs to be higher than the storage temperature to achieve a partially cured B–stage epoxy resin.

Tackiness: Tackiness denotes a measure of the adhesion quality of the pre–preg. It increases with the amount of resin, the extent resin curing to the B–stage and by slightly increasing the ambient temperature.

Shelf life: A shelf life of several weeks at lower temperatures is required to avoid a completely cured system. This is traditionally achieved by the use of a solid curing agent with a high melting point.

In contrast to the previously described 2–component system which is composed of a liquid curing agent and a resin mixed prior to use and cures at RT, 1–component systems require a curing agent which cures at elevated temperatures. This provides a long pot life with no reactivity towards the epoxy moieties when mixed. Dicyandiamide (DICY) is one of the first curing agents used for 1–component epoxy systems since their commercialization in the late 1950s. DICY is a solid with a melting point at $209-212\,^{\circ}\mathrm{C}$ which provides the required latency due to the insolubility in epoxy resins at RT.[138,139] A reaction with the epoxy occurs only at elevated temperatures of 180 °C and above. To achieve reactivity at lower curing temperatures, the addition of an accelerant is needed. In this chapter the thermal and mechanical behavior as well as the shelf life of lignin filled 1–component epoxy systems are investigated and discussed.

7.1 Investigation of the Curing Behavior

The structure of DICY, which belongs to the group of cyanamides, is shown in Figure 7.1. It has a functionality of 4 towards epoxy resins depending on the presence of four NH–bonds. It is assumed

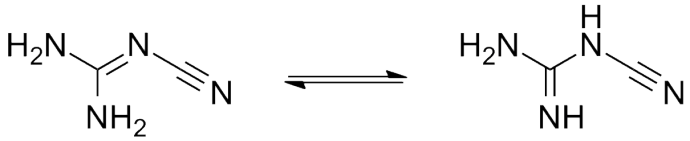

Figure 7.1.: The amino–based curing agent dicyandiamide (DICY) with its two tautomeric structures. Since its high melting point, DICY is a preferred curing agent for 1–component epoxy formulations.

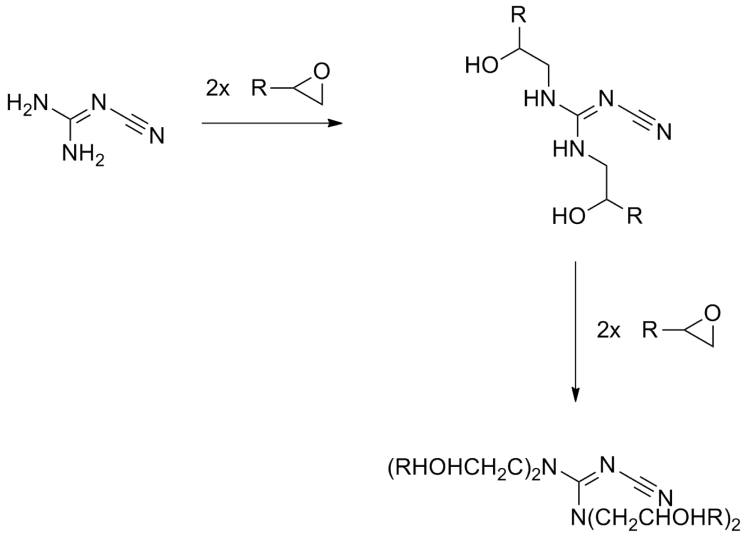

Figure 7.2.: Reaction of the NH_2–moieties with the glycidyl ether.

that the cyano moiety shows also a reactivity towards the epoxy ring. The curing mechanism of the epoxy/DICY system is quite complex and involves several simultaneous reactions. The mechanism has been investigated extensively and a various number of reaction pathways were suggested. [140–143]

As is the case with IPDA, The first reaction step is the addition of the glycidyl ether to the NH_2–moieties of the DICY as shown in Figure 7.2. Since DICY shows two tautomeric structures two different pathways of the attack of the NH_2–moieties onto the glycidyl ether are possible.

In order to investigate the effect of DICY on the curing behavior of the DGEBA resin and compare it to the characteristics of the 2–component systems of the previous chapter, DSC measurements were carried out. Figure 7.3 (left) shows a sharp exothermic peak of the curing reaction starting at 160 °C with its peak maximum at 195 °C. At around 206 °C an endothermic reaction peak indicates a melting point which correlates with the melting point of DICY at 209 °C. This suggests that DICY shows a reduced reactivity towards the epoxy moieties resulting in still existing educt. This is a problem in so far, that on one hand the curing time and temperature is increased and on the other hand when T_c is far below melting point just a low degree of polymerization can be achieved resulting in poor mechanical properties.

In order to increase the reactivity, a micronized variety of DICY (μDICY) with a maximum grain size of 6 µm was chosen. This ensures a higher dispersability in the epoxy resin and through its smaller grain size a higher volume to surface ratio which affects reactivity. Figure 7.3 (right) shows the corresponding DSC thermogram. It clearly shows the increased reactivity of the μDICY towards the glydicyl ether in form of the disappearance of the melting point at 206 °C and a completed reaction at 220 °C.

In order to investigate the effect of kraft lignin on the DICY cured DGEBA, samples with different amounts of kraft lignin were prepared. The dispersabilty of kraft lignin in the DGEBA resin with an additional particulate solid curing agent proved to be good with no sedimentation of either. Due to the catalytic behavior of lignin observed during the investigations with the 2–component DGEBA/IPDA and DGEBA/DETA system respectively, DSC samples were measured shortly after preparation to ensure no

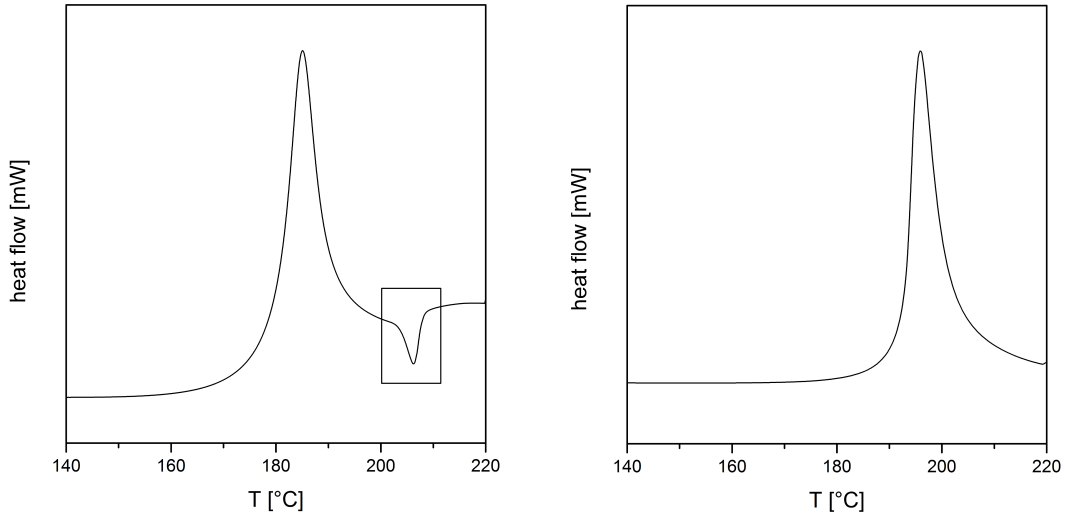

Figure 7.3.: DSC thermogram of neat DGEBA/DICY (left) and DGEBA/μDICY with a maximum grain size of 6 µm (right) showing the impact of the curing agents particle size onto the curing reaction.

premature curing. Figure 7.4 shows the resulting DSC thermograms of the neat DGEBA/DICY system compared to kraft lignin loads of 20 %, 40 % and 80 %.

Kraft lignin has a tremendous impact on the cross–linking reaction of the DGEBA/DICY system. Two different effects occur: the incorporation of kraft lignin induces not only a broadening of the distinct reaction peak of the neat DGEBA/DICY, it causes also the segregation into a multimodal system. Even with small amounts of 20 % kraft lignin the initial curing temperature can be decreased around 64 °C from 174.0 °C to 108.6 °C. The initial temperature decreases further with the addition of more kraft lignin: below 100 °C for the 80 % filled DGEBA/DICY.

Further, the distinct exothermic reaction peak of DGEBA/DICY also shifts to lower temperatures. However, due to the apparent multiple reactions the curing range increases naturally. In practice, this means that a reduction of the curing temperature of 50 °C with the addition of kraft lignin is beneficial for the epoxy curing and therefore positive for the processability.

Table 7.1.: Curing characteristics such as the onset temperature T_i, the peak temperature T_p and the terminal temperature T_e as well as the curing range, heat of reaction and the glass transition temperatures of the neat DGEBA/DICY system compared to DGEBA/DICY with different lignin share.

Sample	T_i [°C]	T_p [°C]	T_e [°C]	Curing range [°C]	ΔH [J/g]	T_g [°C]
DGEBA/DICY	174.0	195.8	223.3	49.3	13.1	148.8
+ 20 % KL	108.6	175.1	203.1	94.5	16.5	142.1
+ 40 % KL	104.7	168.2	193.8	89.1	13.4	145.9
+ 80 % KL	90.4	144.1	187.0	96.9	10.3	142.8
neat KL	-	-	-	-	-	149.8

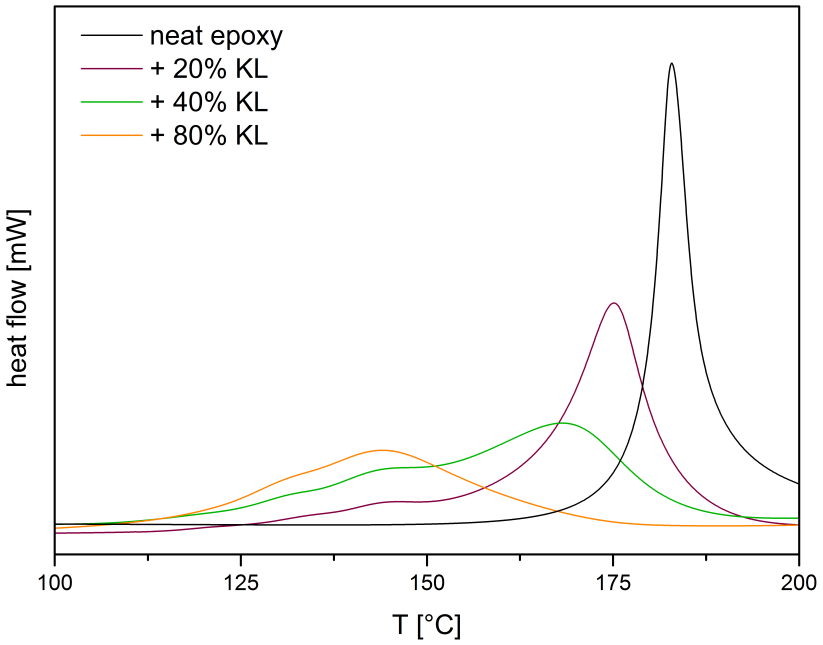

Figure 7.4.: Comparison of the curing behavior of the neat epoxy with epoxy filled with 20 %, 40 % and 80 % kraft lignin. The increasing lignin share shows a tremendous effect on the curing reaction by reducing curing temperatures.

With regard to natural fibers as a main component of the FRP this may have an impact on the preservation of the fiber fabric during curing at elevated temperatures. ΔH for DGEBA/DICY is lower than the sample with 20 % lignin share. However, with higher lignin share ΔH decreases. This indicates that large quantities of kraft lignin are able to transfer heat and may act as a heat storage in the composites. Figure 7.5 shows the monitoring of the heat development during the curing reaction, which confirm this assumption. Therefore, a type K thermocouple was introduced in the reaction mixture and the temperature was observed during the curing.

In comparison to the neat DGEBA/DICY system, the 40 % lignin filled epoxy resin heats up at lower temperatures with a temperature difference of around 20 °C. Further, the inflection point, which indicates that the heat development of the exothermic reaction leads to self–acceleration, is reached 30 °C earlier for the lignin filled system as well. Self–acceleration is always combined with a significant temperature leap which is clearly demonstrated in Figure 7.5.

Whereas the neat DGEBA/DICY system shows a temperature leap of nearly 129 °C in a time span of 20 s, the lignin filled epoxy resin shows a temperature leap of 47 °C over a broad time span of 3.5 min. This behavior of lignin is caused by its phenylpropanoid structure, which serves a specific role in energy dissipation and radical scavenging.[144,145] K. Bahl showed, that filler, networks and agglomeration strongly influence energy dissipation: poor dispersion of the filler as well as large particle sizes increase the dissipation of energy. Moreover, when surface polarity of the filler and matrix material matches this, the compatibility and hence the energy dissipation is improved.[146]

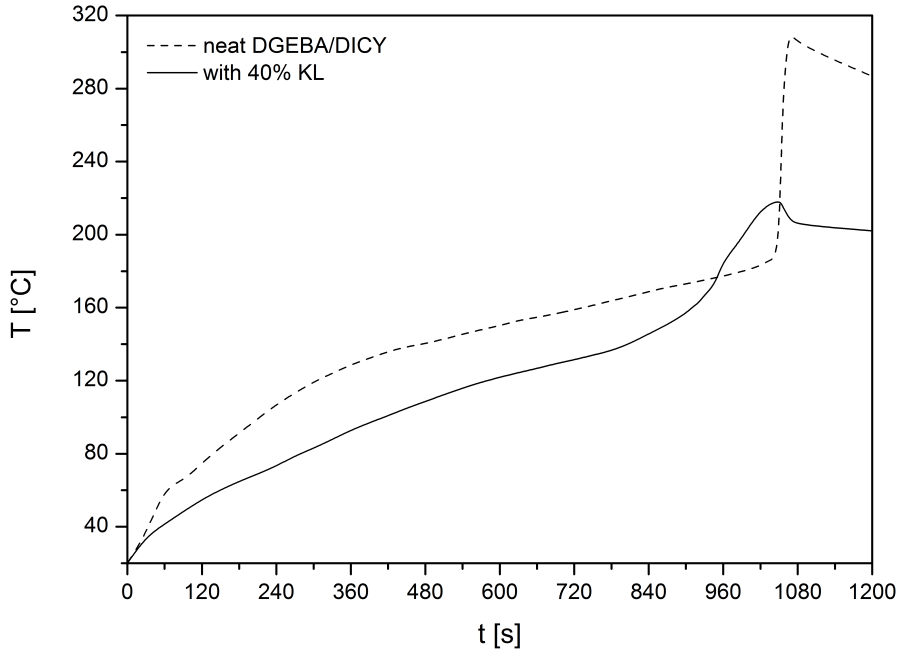

Figure 7.5.: Heat development of the neat DGEBA/DICY and the 40 % lignin filled epoxy resin during curing. Measured with a type K thermocouple introduced in the reaction mixture.

From these assumptions several conclusions can be drawn. Due to the polar structure of lignin in contrast to the unpolar molecular structure of the bisphenol–A based diglycidyl ether the compatibility is low. Further, particle sizes of lignin ranges in micrometer scale which reduces energy dissipation as well. Therefore, lignin declines the heat dissipation during curing, which means that lignin might prove to be effective preventing the runaway of the chemical reaction of the epoxy systems.

The earlier described segregation into a multimodal system is illustrated in Figure 7.6 for DGEBA/DICY with 40 % kraft lignin load. The multimodal exothermic peak can be divided into four segments. Segment IV can be assumed as the distinct reaction peak originating from the reaction of DGEBA with DICY. The newly emerged segments $I - III$ must stem from side–reactions with kraft lignin. Table 7.2 summarizes the development of the particular peak maxima. Interestingly, segments $I - III$ show regardless of the kraft lignin share similar peak temperatures. Only segment IV shifts to lower temperatures and diminishes completely for 80 %. This key issue of the chemical behavior of the kraft lignin towards the reactive moieties of the DGEBA/DICY system will be addressed in detail in Chapter 8.

The glass transition temperatures remained the same as shown in Table 7.1, which is important for the application of kraft lignin as a filler. Just a single T_g is present as illustrated in Figure 7.7 by the 40 % lignin filled DGEBA/DICY. Since the T_g values for both the neat DGEBA/DICY as well as kraft lignin are very close, it cannot be assumed that a homogeneous morphology was achieved.

To gather further evidence, SEM micrographs of freeze–fractured, fully cured samples were obtained. Figure 7.8 shows an overview at the magnification of 500 µm and a close–up at 5 µm of the neat epoxy compared to the epoxy filled with 40 % kraft lignin. Comparing the neat epoxy with the lignin filled epoxy at a magnification of 500 µm it is obvious, that the 40 % lignin filled epoxy shows no lignin fragments

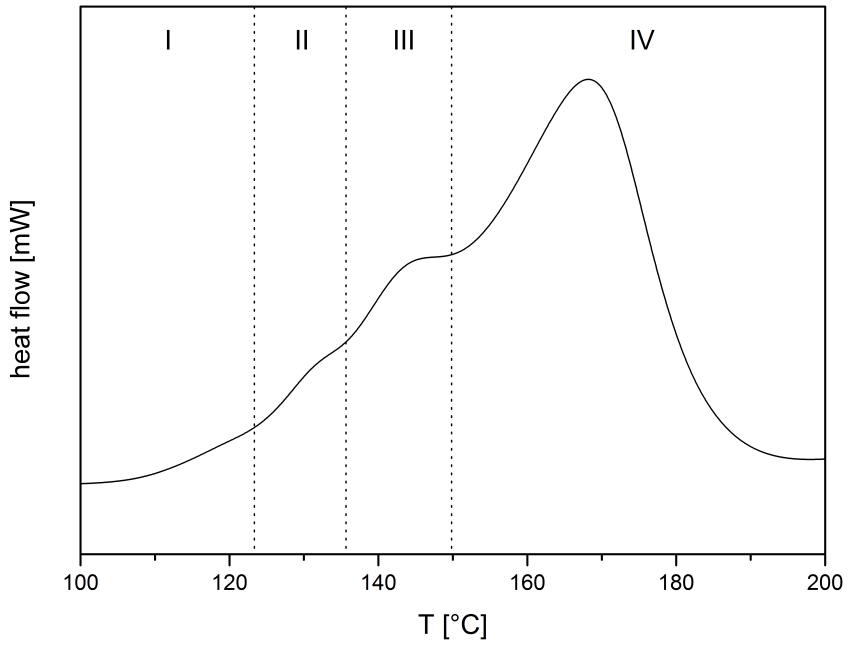

Figure 7.6.: DSC thermogram of epoxy filled with 40 % kraft lignin which shows a multimodal distribution divided into segments. Segment IV can be assumed as the distinct reaction peak originating from the reaction of DGEBA with DICY whereas segments $I—III$ must stem from side–reactions of the epoxy system with kraft lignin.

on the smooth surface as well as on the breaking edge. The higher magnification of 5 µm shows small differences in the character of the surface. While the neat epoxy shows a very smooth surface, the lignin filled epoxy shows a slightly scaly surface, which indicates the brittleness of the material.

The SEM micrographs are in good agreement with the DSC measurements which both show a homogeneous phase morphology resulting in very good dispersability of kraft lignin in the DGEBA/DICY system. Due to the absence of large lignin agglomerations, the DGEBA/DICY system filled with kraft lignin is well suited for the wet lay–up process since a sufficient penetration of the fibers can be guaranteed. Large agglomerations would cause a filtration effect with the fiber fabric since they would not be able to pass through the porous structure. This might cause premature failure and reduced mechanical properties.

Table 7.2.: Peak temperatures of the segments $I-IV$ of the multimodal distribution of the lignin filled DGEBA/DICY system.

Sample	T_I [°C]	T_{II} [°C]	T_{III} [°C]	T_{IV} [°C]
DGEBA/DICY	-	-	-	195.8
+ 20 % KL	122.2	134.4	145.4	175.1
+ 40 % KL	120.9	131.8	145.1	168.2
+ 80 % KL	119.0	131.6	144.8	-

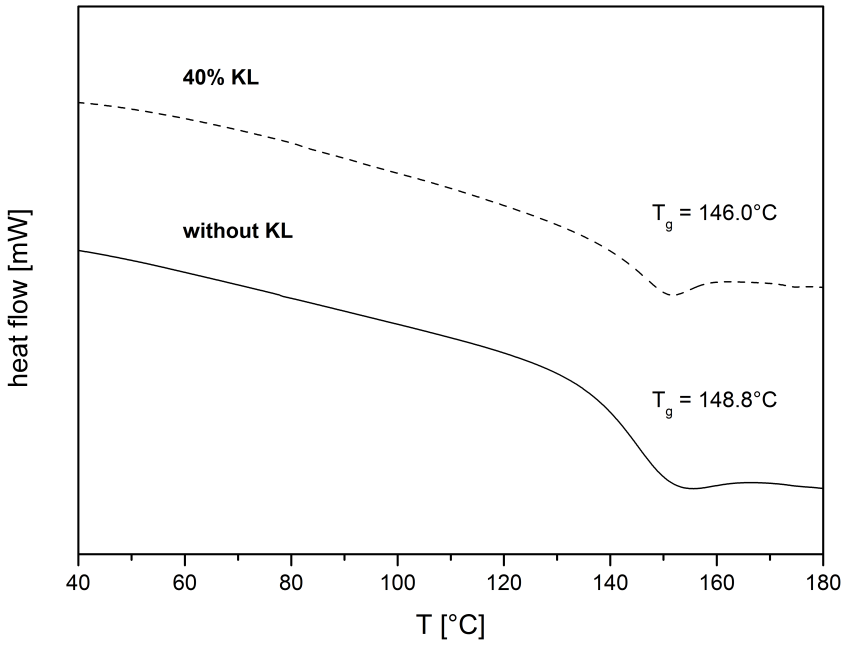

Figure 7.7.: Determination of the glass transition temperature for the neat DGEBA/DICY and with 40 % load presenting both a single T_g.

As seen in the previous experiments, the participation of kraft lignin in the curing process as a reactant is fairly obvious. However, the incorporation into the cross–linked polymer network suggests that kraft lignin can be regarded as a cross–linking agent due to the multiple reactive moieties present in the lignin molecule. Therefore four samples with different amounts of DICY and one blank test with just DGEBA and kraft lignin were prepared. Each with a load of 40 % kraft lignin. Figure 7.9 shows the progress of the released exothermic energy obtained from the first heating run as well as the resulting glass transition temperatures.

As assumed, exothermic energy is released even without the addition of the curing agent resulting in a material with a glass transition temperature of 54.8 °C. Therefore, it can be assumed that kraft lignin reacts with the epoxy moieties of the DGEBA resin. With increasing amounts of DICY the DGEBA/DICY/40 % kraft lignin system experiences a noticeable increase in heat development as well as higher T_g values as compared to the system without kraft lignin. In other words, kraft lignin is able to partially replace the curing agent DICY. This reduces the costs of an expensive curing agent, especially when aiming for materials with a lower T_g. The required amount of DICY can be reduced by almost one-quarter.

7.2 Comparability of Kraft Lignin to Industrial Used Accelerators

Due to the high melting point of DICY and curing temperatures of around 180 °C, it is common practice to add an accelerator to the epoxy formulation to achieve lower curing temperatures. This is highly important towards the processing of the pre–pregs on one hand to minimize production cost due to the

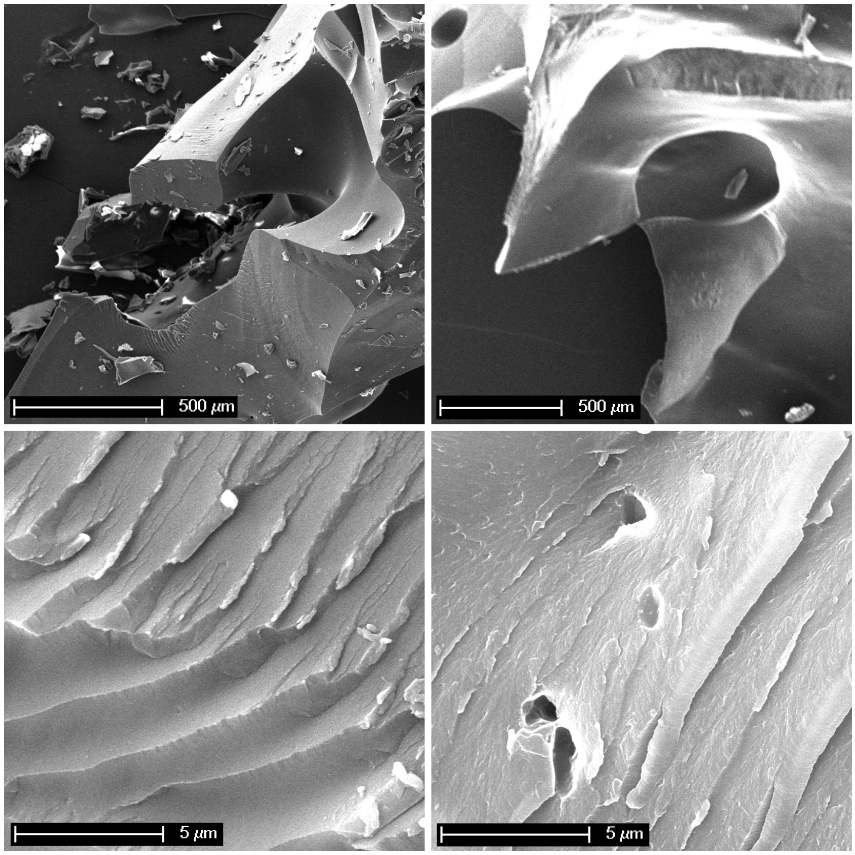

Figure 7.8.: SEM micrographs of neat epoxy (left) and epoxy filled with 40 % kraft lignin (right) are in good agreement with DSC measurements. For both systems a homogeneous phase morphology is achieved resulting in very good dispersability of kraft lignin in the DGEBA/DICY system.

conservation of energy and on the other the thermal stability of sensible natural fibers which decompose fast at elevated temperatures.

Common latent accelerators for epoxy systems are either urone– or imidazole–based. Typically urone–based accelerators are 1,1–dialcyl–3–arylureas with a hydrated or substituted aromatic ring. It releases dimethylamine and isocyanate at elevated temperatures. These show a synergistic accelerating effect towards DICY: dimethylamine reacts with the epoxy moiety to give a tertiary amine that catalyzes the reaction of DICY with the epoxy moieties whereas the isocyanate reacts with the other epoxy unit to give an 1,3–oxazolidin–2–one as shown in Figure 7.10a. [147]

The dissociation temperature is dependent on the type of substituent. Tertiary amines in general are anionic initiators, which are commercially accepted as accelerators for epoxy resins. It was proposed by S.K. Ooi, that for 1–methyl imidazole and 2–methyl imidazole two different reaction mechanism are involved. [149]

The catalytic effect of 2–methyl imidazole is presented in Figure 7.10b (Scheme 1). The catalytic effect of 2–methyl imidazole and 1,3–unsubstituted imidazoles (with no substitution on nitrogen atoms) emanates through the attack on the epoxy moiety of DGEBA by the pyridine–type nitrogen to form the 1:1 adduct. In the second reaction step the generated pyridine–type nitrogen attacks a second epoxy moiety to produce the 1:2 adduct. For 1–methyl imidazole it was suggested that in addition to the reaction

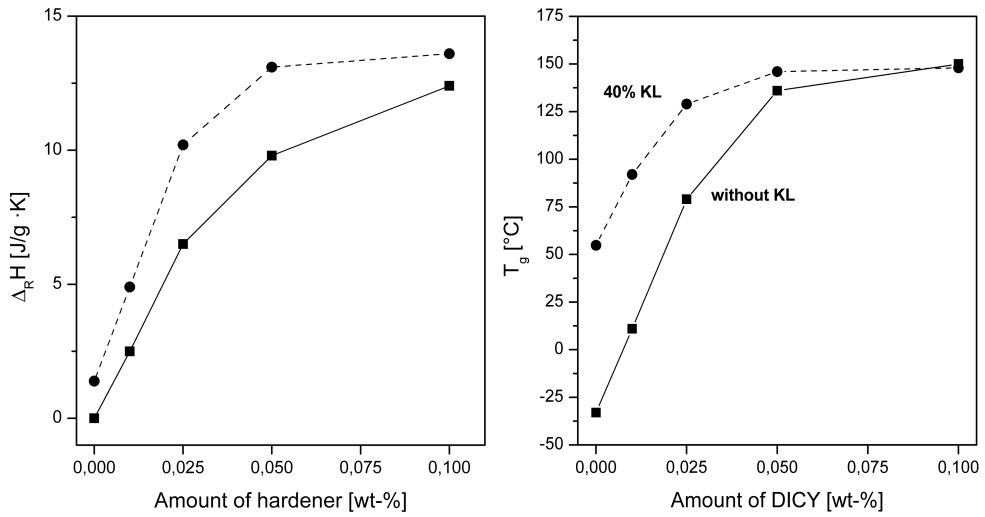

Figure 7.9.: Development of the exothermic energy (left) and glass transition temperatures (right) of the DGEBA/40 %KL system with different amounts of DICY.

mechanism shown in Figure 7.10b (Scheme 1a) the lone pair of electrons positioned at the 1–substituted nitrogen can attack the epoxy moiety as well (Scheme 2).[148–151]

For the investigation of the effect of the type of accelerator five accelerators according to Figure 7.11 were considered. Therefore, three urone based accelerators as well as two imidazole based accelerators were used. As for the imidazole based accelerators 1–methyl imidazole (1–MI) and 2–methyl imidazole (2–MI) are chosen. The urones 1,1–dimethyl–3–phenylurea (UR–1), 1,1'–(4–methyl–1,3–phenylene)bis(3,3–dimethylurea) (UR-2) and 3–(3,4–dichlorophenyl)–1,1–dimethylurea (UR-3) are able to decrease the initial curing temperature to room temperature if necessary and were kindly provided by AlzChem. Samples with a constant amount of 1 wt–% accelerator with and without the addition of kraft lignin were prepared and the cure behavior studied by DSC.

Figure 7.13a (top) shows the results obtained from the DSC experiments for the neat DGEBA/DICY system with 1 wt–% UR–1, the bifunctional UR–2 and chloro–substituted UR–3 (left) as well as 1–MI and 2–MI (right). Curing characteristics of the accelerated formulations are shown in Table 7.13b.

Urones and imidazoles sharply decrease curing temperatures as expected. Each mole of urone funcionality consumes two mole of epoxy moieties due to the isocyanate and dimethylamine reactions. The bifunctionality of UR–2 leads to maximum catalytic activity towards the epoxy reaction with a decrease by 71.2 °C from 174.0 °C to 102.8 °C. The unsubstituted UR–1 and UR–3 substituted with chlorine moieties show both a similar catalytic effect with a reduction of around 50 — 55 °C.

T_g measurements show that the addition of any type of urone based accelerator to the DGEBA/DICY system reduces the T_g. The bifunctionality of UR–2 results in additional cross–linking which explains the higher T_g value than UR–1 and UR–3. 1–MI and 2–MI show broader peaks and initial curing temperatures of 64.0 °C and 87.2 °C, respectively. In comparison, the peaks cured with urones are narrow and started at higher temperatures but finish at the same temperature of about 160 — 170 °C. The curing range of 1–MI is almost doubled compared to the neat DGEBA/DICY system and urone accelerators.

In both cases it is obvious, that the initial curing temperature of kraft lignin is fairly comparable with the urone accelerated system. As seen before, the effect of kraft lignin on the peak temperature is substantial

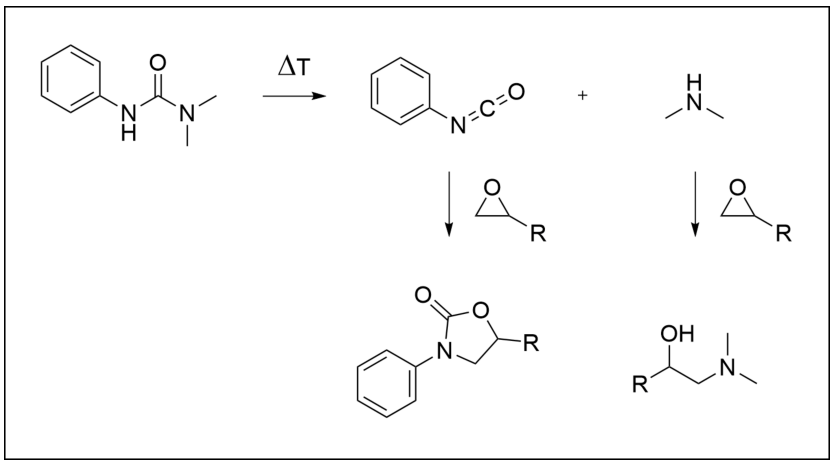

(a) Mechanism of the urone/epoxy reaction. Dimethylamine reacts with the epoxy moiety to give a tertiary amine that catalyzes the reaction of DICY with the epoxy moieties whereas the isocyanate reacts with the other epoxy unit to give 1,3–oxazolidin–2–one. [147]

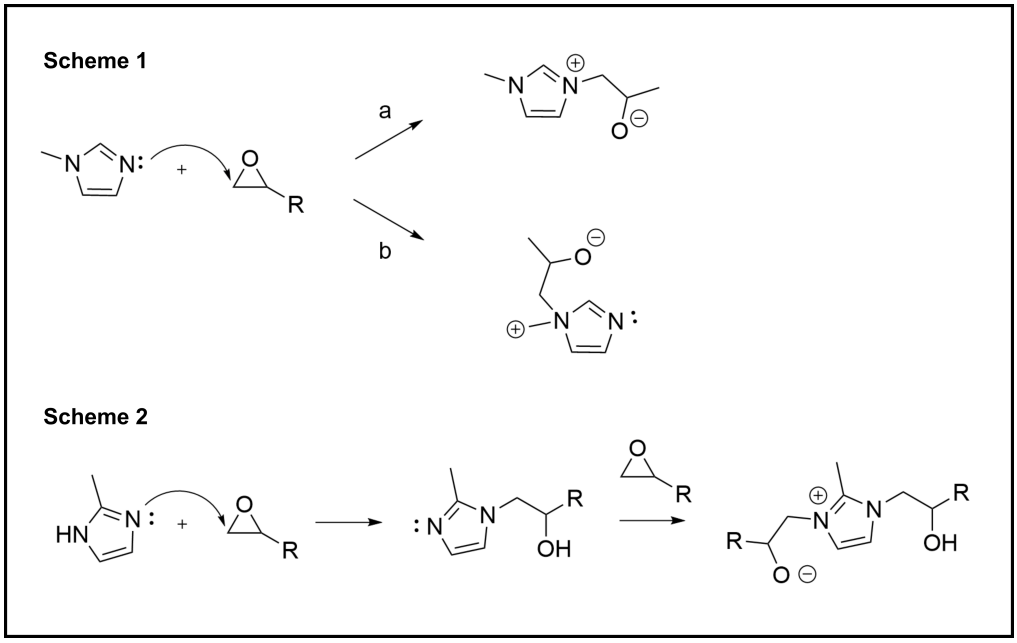

(b) Proposed mechanism of the 2-methyl imidazole/epoxy reaction. Attack of the epoxy moiety of DGEBA by the pyridine–type nitrogen forming an 1:1 adduct. The generated pyridine–type nitrogen attacks the second epoxy moiety to produce the 1:2 adduct. (Scheme 1) For 1–methyl imidazole the lone pair of electrons positioned at the 1–substituted nitrogen can attack the epoxy moiety as well. (Scheme 2) [148–151]

Figure 7.10.

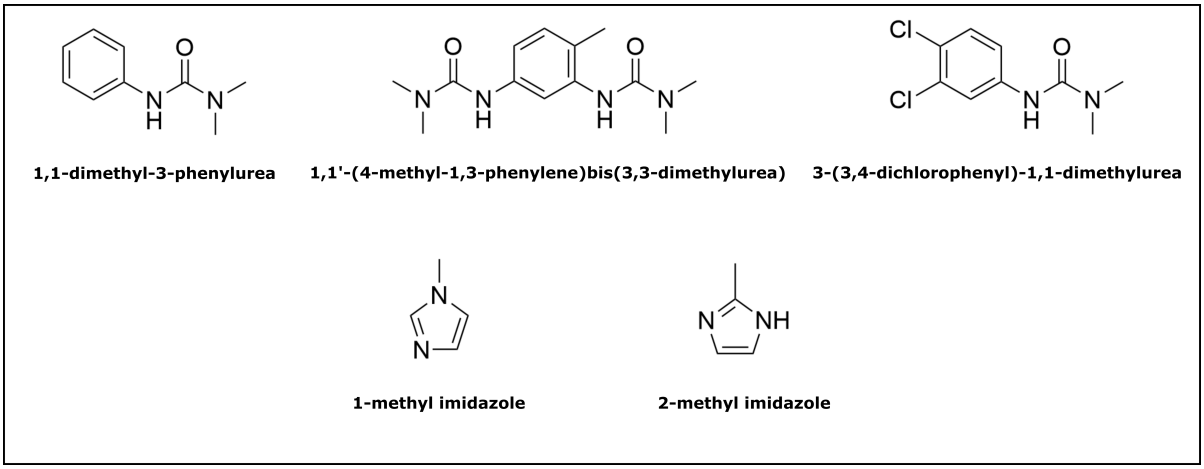

Figure 7.11.: Accelerators used in this work: Urone based (top) UR-1 (UR300); UR-2 (UR500) and UR-3; Imidazole based (bottom) 1-methyl imidazole, 2-methyl imidazole.

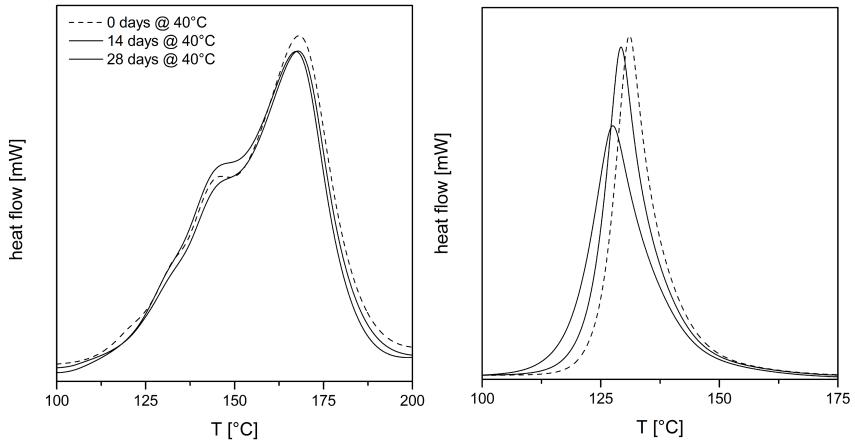

Figure 7.12.: Shelf life tests conducted for 0, 14 and 28 days at 40 °C for the 40 % KL filled DGEBA/DICY system (left) and the UR–1 accelerated DGEBA/DICY system (right). The kraft lignin filled epoxy resins remain constant with no shifting of the reaction peak whereas the UR–1 accelerated sample shows a significant shift and decrease of heat of reaction proving an already occurred cross–linking.

and is with $15-20$ °C slightly higher for the urone accelerated DGEBA/DICY system. Disadvantageous is that the end of the curing reaction is barely affected by the presence of lignin increasing the overall temperature range.

In contrast, the imidazole accelerated systems show merely a comparability in contrast to the lignin filled DGEBA/DICY system. Since it could be shown that kraft lignin has a substantial impact on the cross–linking reaction of the epoxy with DICY, it is quite interesting to investigate the behavior of the lignin filled epoxy with the addition of an accelerator. According to the previous experiment samples with 1 wt–% accelerator and 40 % kraft lignin were prepared and measured. Figure 7.13a shows the urone–accelerated epoxy with 40 % kraft lignin. Interestingly, the epoxy filled system with 40 % kraft lignin shows exactly the same reduction of the curing temperature as the systems with the addition of accelerator. However, with addition of accelerator the epoxy–DICY reaction is catalyzed, since the reaction peak shifts towards lower temperatures.

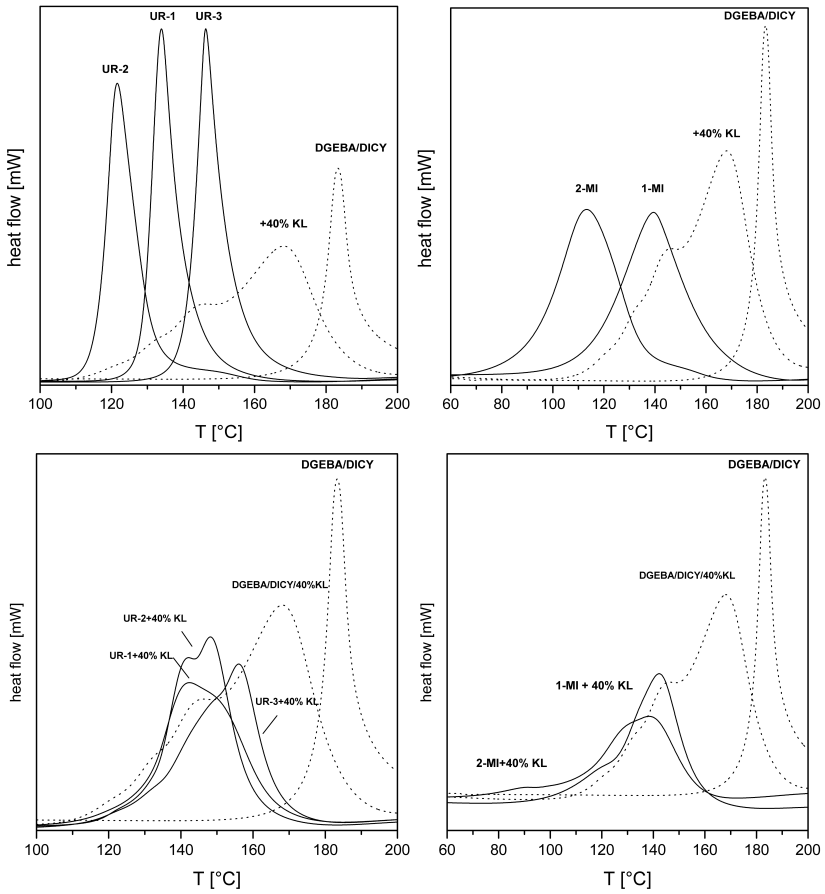

(a) Top: Imidazole accelerated DGEBA/DICY system compared to DGEBA/DICY/+40 % KL (left) and the combination of 1 wt-% accelerator with 40 % kraft lignin (right). Bottom: Urone accelerated DGEBA/DICY system compared to DGEBA/DICY/+40 % KL (left) and the combination of 1 wt-% accelerator with 40 % kraft lignin (right).

Sample	T_i [°C]	T_p [°C]	T_e [°C]	Curing range [°C]	ΔH [J/g]	T_g [°C]
neat epoxy	174.0	195.8	223.3	49.3	13.1	148.8
+ 40 % KL	104.7	168.2	193.8	89.1	13.4	145.9
UR-1	118.1	133.9	171.1	53.0	14.4	134.4
UR-2	102.8	121.6	160.0	57.2	13.7	145.2
UR-3	126.8	146.4	180.0	53.2	13.8	140.2
1-MI	64.0	113.0	169.5	105.5	18.9	
2-MI	87.2	113.3	170.1	82.9	18.8	153.3
UR-1 + 40 % KL	105.6	142.6	180.2	74.6	-	142.0
UR-2 + 40 % KL	108.4	148.1	178.9	70.5	-	-
UR-3 + 40 % KL	112.3	156.1	180.5	68.2	-	-
1-MI + 40 % KL	100.0	142.3	177.5	77.5	-	-
2-MI + 40 % KL	60.9	139.1	165.4	104.5	-	-

(b) Curing characteristics such as the onset temperature T_i, the peak temperature T_p and the terminal temperature T_e as well as the curing range, heat of reaction and the glass transition temperatures of the accelerated DGEBA/DICY and DGEBA/DICY + 40 % kraft lignin system.

Figure 7.13.

A further object of interest is the shelf life of these formulated epoxy resins containing accelerators. Usually, a disadvantage of using accelerators is that they do not only increase the reactivity during the curing reaction, they tend to decrease the storage stability as well. Therefore, shelf life tests were performed to investigate the storage stability of the DGEBA/DICY system using UR–1 as accelerator and the 40 % accelerated system. To this end, those formulations were stored at a temperature of 40 °C to emulate extreme temperature conditions for 28 days and measured with DSC.

Figure 7.12 shows the exothermic reaction peaks of the normalized samples for both systems measured after 0, 14 and 28 days. It is evident, that the kraft lignin filled epoxy resin remains constant with no shifting of the reaction peak whereas the UR–1 accelerated sample clearly shows a significant decrease of the heat of reaction which proves of an already occurred reaction. Therefore, kraft lignin brings an advantageous balance of reactivity and storage stability towards the DGEBA/DICY epoxy system.

This chapter showed, that lignin clearly takes part in the reaction with DGEBA and the amino–based hardener and, additionally, it interferes in the reaction of the accelerator with the epoxy system. To understand these observations, it is important to comprehend the fundamental reaction of the epoxy moieties of the resin with the multi–functional lignin. This will be addressed in the following chapter.

8 Preparation of an Epoxy-Lignin Prepolymer

As seen in the previous chapters, kraft lignin is able to interfere in the cross linking reaction of DGEBA resin and the curing agent. DSC measurements showed that the addition of lignin splits up the single peak of heat release into a broadened multimodal signal.

Since the peak of the neat DGEBA/DICY is reproduced in the tertiary DGEBA/DICY/KL system, DICY was omitted to prevent the cross–linking reaction for the determination of the side reactions. To this end samples of DGEBA with different amounts of 5 %, 10 % 20 % and 40 % kraft lignin were prepared and measured according to the previous measurements. Figure 8.1 presents the results obtained from these measurements.

With increasing amount of kraft lignin, an exothermic peak is increasingly visible. With an amount of 40 % the formation of a bimodal peak begins. This confirms the assumption of the reactivity of kraft lignin towards the epoxy moieties. On the basis of the previously described lignin structure, the reactivity of lignin is given by different functional groups: mainly hydroxyl groups, both aliphatic and cyclic, as well as double bonds. As proposed by Aniceto et al. the oxylpropylation reaction (Figure 8.2) using basic or acid catalyst is possible to occur. [152]

For this purpose samples of different types of kraft lignin with varying amount of hydroxyl–content were prepared and measured with DSC (Table 8.3a). To evaluate the obtained results with regard to the influence of hydroxyl groups, acetylated kraft lignin with a total amount of 0.3 mmol/g OH-moieties as blank sample was measured for comparison. The results of the measurements are shown in Figure 8.3b and the curing characteristics are summed up in Table 8.3c.

A shift of the exothermic peak to higher temperatures occurs which correlates with the amount of total hydroxyl moieties. Hence, acetylated kraft lignin with a bare minimum of hydroxyl moieties shows no reaction towards the epoxy. Interestingly, KL_{eh} shows the highest heat of reaction ΔH and connected glass transition temperature of the measured kraft lignins with 118.8 °C. The acetylated kraft lignin shows,

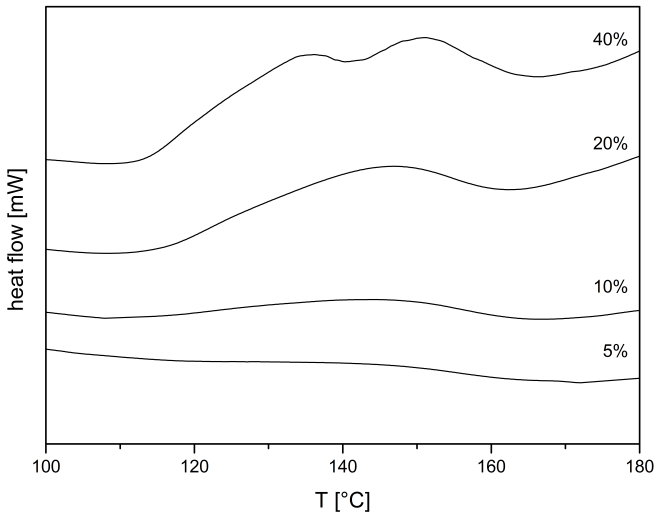

Figure 8.1.: Formation of a prepolymer during the exothermic reaction of DGEBA resin at different kraft lignin shares of 5 %, 10 %, 20 % and 40 %.

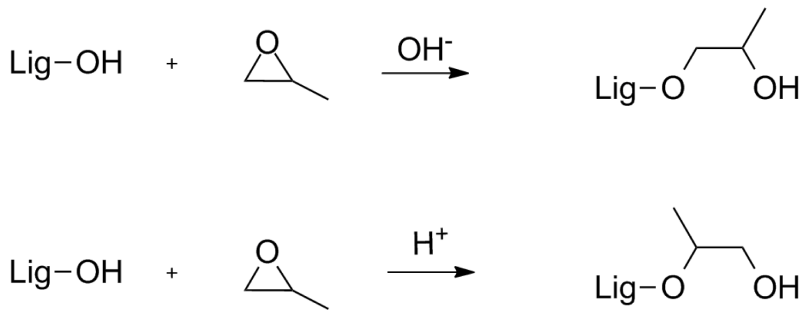

Figure 8.2.: Basic or acid catalyzed oxypropylation reaction proposed by Aniceto et al. of lignins hydroxl moieties with the epoxy ring.[152]

despite the fact that no reaction peak occurred during the measurement, a glass transition temperature even higher than KL_1 and KL_2. This might be caused by the fact, that the acetylated kraft lignin is swollen with epoxy resin. Therefore, the epoxy resin acts as a plasticizer, which is most commonly used in industrial relevant polymers such as PVC, in which a plasticizer is introduced to reduce the glass transition temperature to obtain different polymer properties. This is supported through the fact, that the initial glass transition temperature of acetylated kraft lignin is with 104 °C much higher than the resulting glass transition temperature after swelling.

Since kraft lignins in general come from a versatile pulping and purification process, it is possible to obtain lignins precipitated at different pH values. This results in a different degree of deprotonation of the hydroxyl groups which results in different reactivity towards the epoxy moieties due to the negative charge of the phenolates. Therefore, three samples of kraft lignin precipitated at pH values of 3, 8 and 10 were tested towards their reactivity. The results of the DSC measurements are shown in Figure 8.4. The DSC thermograms confirm clearly the assumptions made. The reactivity increases dramatically with the amount of deprotonized hydroxyl groups. The increasing glass transition temperature from 39.7 °C to 102.8 °C of the lignins precipitated at different pH (3–10) are reflecting this as well. This clearly highlights the increase of the cross–linking density and the dependency of the degree of deprotonation on the overall reactivity of KL with DGEBA.

For further identification of the reaction products, samples of DGEBA with 40 % KL_1 cured to different degrees of cross–linking were prepared and extraction tests have been carried out. Samples were cured for 24 h in alumina pans either at one of the two onset temperatures $T_{O1} = 100$ °C and $T_{O2} = 142$ °C or at one of the peak temperatures $T_{P1} = 124$ °C and $T_{P2} = 188$ °C which were determined with regard to the DSC experiment shown in Figure 8.3b.

The sample cured at 100 °C was highly viscous and still sticky. The sample cured at 124 °C was still soft to the touch after removing from the oven but hardened significantly after cooling to room temperature which indicates that a glass transition value over room temperature was achieved. The samples cured at 142 °C and 188 °C appeared cured. Figure 8.5 shows the prepolymer obtained at 188 °C which appears as a brittle solid. With the exception of the sample cured at 100 °C, the removal of the KL/DGEBA prepolymer out of the reaction vessel was easy and showed no indication of residual kraft lignin. As a

OH moiety	KL_1	KL_2	KL_{EHL}	KL_{acKL} [mmol/g]	$pH3$	$pH8$	$pH10$
Aliphatic	1.1	1.1	1.3	0.1	0.9	0.8	1.0
Condensed	1.1	0.5	0.3	0.1	1.0	0.8	0.9
Syringil	1.0	2.2	0.2	0.0	0.7	0.8	0.5
Guaiacyl	1.7	0.7	0.6	0.0	1.3	1.3	1.1
p-Hydroxyl	0.1	0.0	0.6	0.0	0.0	0.1	0
Phenolic Total	3.8	3.4	1.6	0.1	3.0	3.1	2.5
Total	5.2	4.8	4.2	0.3	4.0	4.3	3.6

(a) Aliphatic and phenolic hydroxyl content in different types of lignin (condensed also includes syringil).

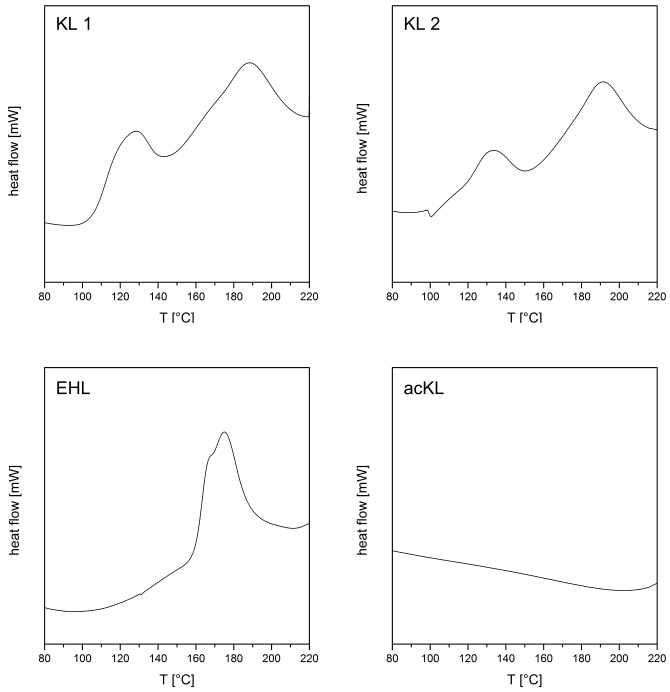

(b) First heating runs of different types of kraft lignin incorporated in DGEBA resin with 40 % lignin share.

Sample	T_1 [°C]	T_2 [°C]	ΔH [J/g]	T_g [°C]
KL1	128.1	188.6	1.23	44.7
KL2	133.3	191.3	2.01	55.8
EHL	167.8	175.3	2.29	118.8
acKL	-	-	0.00	68.2
pH 3	multiple		14.3	102.8
pH 8	123.3	218.7	1.70	99.8
pH 10	119.0	136.3	0.30	39.7

(c) Curing characteristics such as the peak temperatures T_1 and the T_2 as well as the heat of reaction and the glass transition temperatures of different types of kraft lignin incorporated in DGEBA resin with 40 % lignin share.

Figure 8.3.

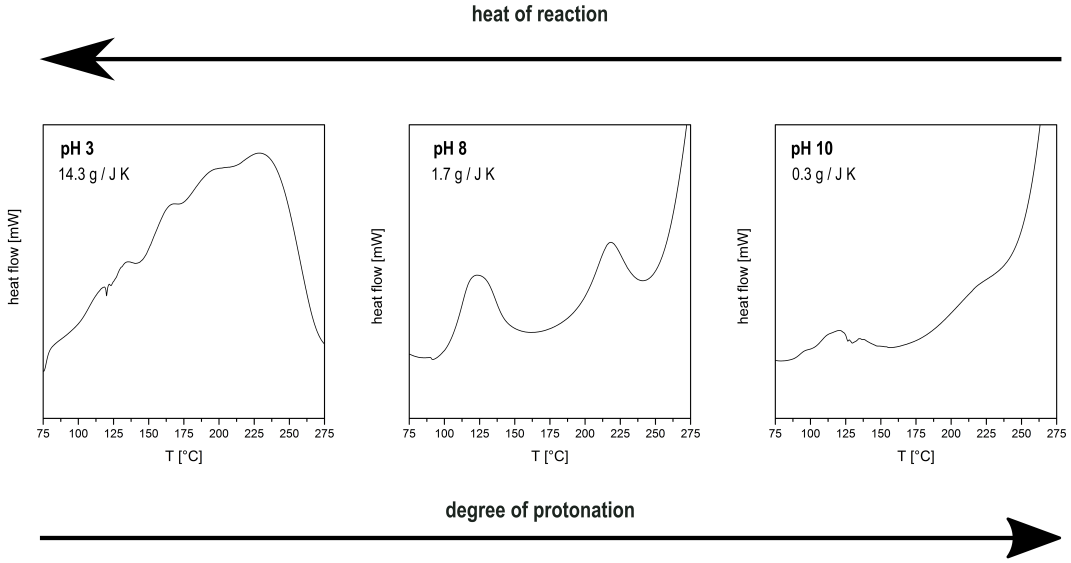

Figure 8.4.: Dependency of the degree of protonation with lignins precipitated at three different pH values (3,8,10) with the total heat of reaction.

Figure 8.5.: DGEBA/KL prepolymer samples cured at 188 °C. A brittle but fully cured sample could be obtained.

distinctive proof if a cross–linking reaction and not a simple caking of the mixture took place, a simple solubility test was performed due to the fact that a cross–linked system is entirely insoluble.

Therefore, each sample was refluxed for 24 h at the boiling point of the respective solvent. As solvents a 1*M* NaOH solution as well as THF were used. The resulting residue was separated from the dissolved kraft lignin and dried in vacuum at 40 °C. As for the kraft lignin dissolved in THF, the solvent was subsequently removed by distillation. Figure 8.6 shows the obtained supernatants after extraction in 1*M* NaOH solution with regard to the chosen curing temperatures. It is obvious, that up to the curing temperature of 142 °C less and less lignin can be removed by extraction obtaining at 188 °C a colorless liquid with no traces of dissolved lignin. Therefore it can be concluded, that at 188 °C the integration of lignin into the cross-linked system is complete.

With increasing curing temperature, the amount of kraft lignin that can be removed from the cross–linked epoxy network decreases rapidly. This is a clear proof that lignin has to be bound covalently in the formed network. Further, this trend can be seen with the residual polymer as well. After extraction the samples cured at 100 °C and 124 °C they showed small swollen particles the size of around $1-2$ mm. In

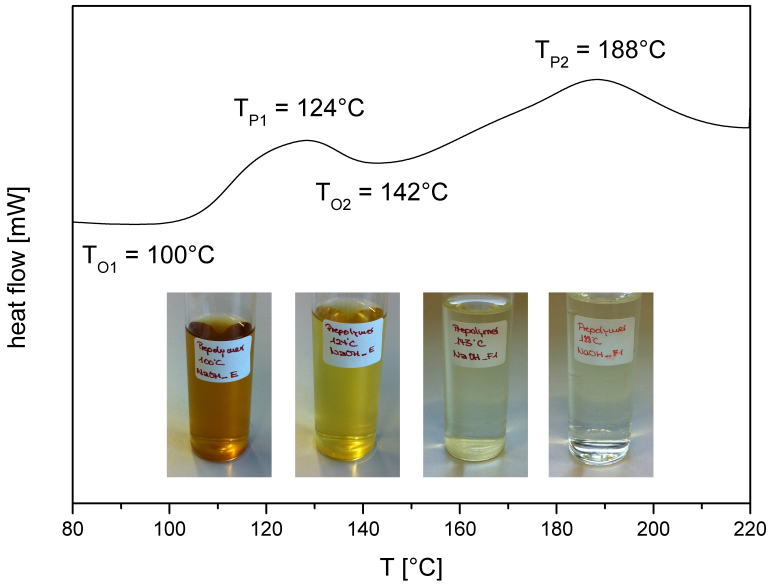

Figure 8.6.: First heating run of a DGEBA sample containing 40 % KL with assignment of peak temperatures and solubility of residual not cross–linked lignin.

contrast, the samples cured at higher temperatures showed neither signs of swelling nor fraying of the polymer. Moreover, samples of the extracted polymers were measured with DSC to determine the glass transition temperatures with regard to the degree of cross–linking. Figure 8.7 shows the obtained glass transition values.

Each sample shows two glass transition temperatures, one of the cross–linked DGEBA/KL prepolymer and the other of residual kraft lignin, which show an opposing trend: on one hand, the first T_g increases with rising curing temperatures from 49.1 °C for the 100 °C cured sample to 92.8 °C for curing at 188 °C. On the other hand the second T_g is reduced slightly from 136.4 °C to 124.8 °C. The latter is an indication of the predominant assembling of the low–molecular weight fractions of kraft lignin into the epoxy network.

For a better understanding of the results obtained in extraction tests and DSC measurements, freeze fractured samples were investigated in SEM. Figure 8.8 shows micrographs of the fractured surfaces of the samples cured at 124 °C, 142 °C and 188 °C. The overview images indicate a smooth surface with minor irregularities. The close–ups show, that the increase in curing temperature reduces these surface irregularities which are still clearly visible in (a). Moreover, no large kraft lignin agglomerations and fragments are visible. This indicates a homogeneous phase morphology contradicting the results of the DSC measurements.

This could also be visualized by the THF extraction experiments. They indicate what that kraft lignin is capable of forming a prepolymer with the epoxy moieties of the DGEBA resin which might be of great interest with regard to new materials. The development of a partially cured prepolymer is especially promising for commercial applications due to the simplified handling of the powdery kraft lignin which tends to become electrically charged.

With respect to FRPs, it would be interesting to aim for a certain degree of postcuring where the final stage of curing would be initiated with the addition of curing agent. In this case, it is vital to maintain addressable epoxy moieties for further cross–linking.

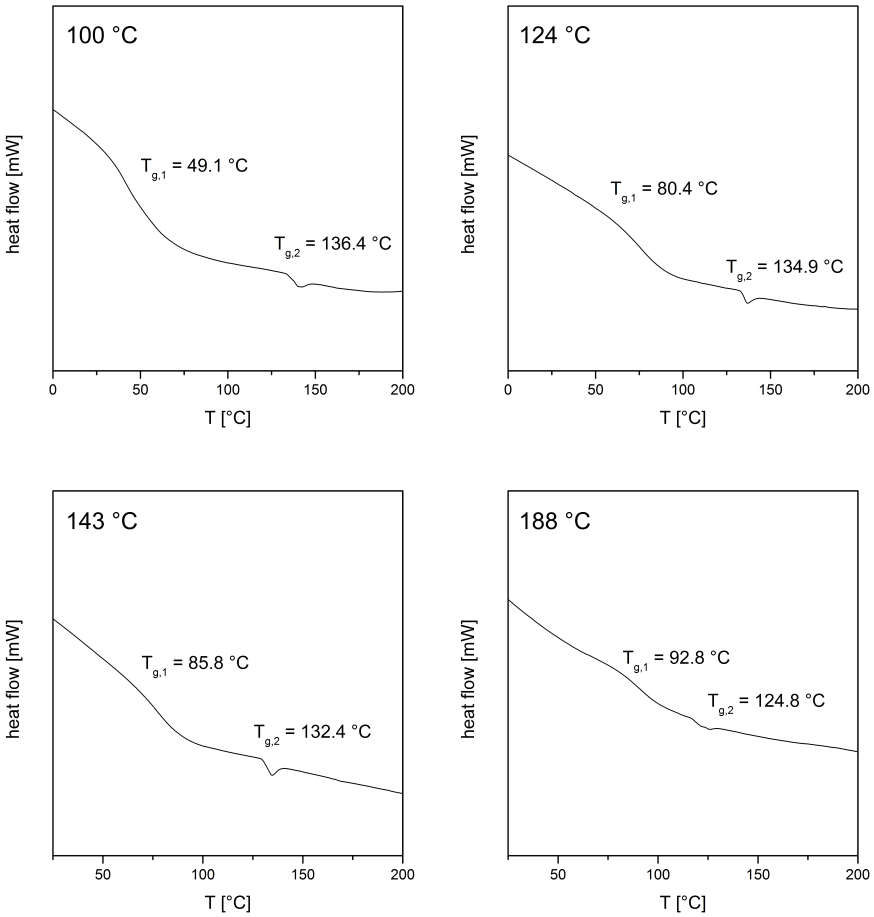

Figure 8.7.: Obtained glass transition temperatures of NaOH extracted samples of the prepolymer cured at 100 °C, 124 °C, 143 °C and 188 °C.

To this end, experiments with the 188 °C cured polymer have been carried out to investigate the behavior of the precured polymer with further addition of curing agent. In order to achieve a maximum contact of the interfaces the prepolymer was prepared by finely grinding it into a fine powder with pestle and mortar followed by drying in vacuum at 40 °C. Samples were mixed vigorously to ensure complete wetting and contact with the amine–equivalent of IPDA and DICY respectively. Finally, it was measured via DSC to keep track of a possible reaction.

Figure 8.9 shows the results of these measurements. In both cases an exothermic reaction takes places followed by a shift of the glass transition temperatures to a single T_g with a value similar for both curing agents of around 160 °C. This means further curing takes place exceeding the glass transition temperatures of the conventional cured samples by 20 °C. More specifically, a higher network density is achieved, caused by the fact that the conventional system shows competing reactions of the single components whereas the reactions in the prepolymer cured system takes place step–by–step.

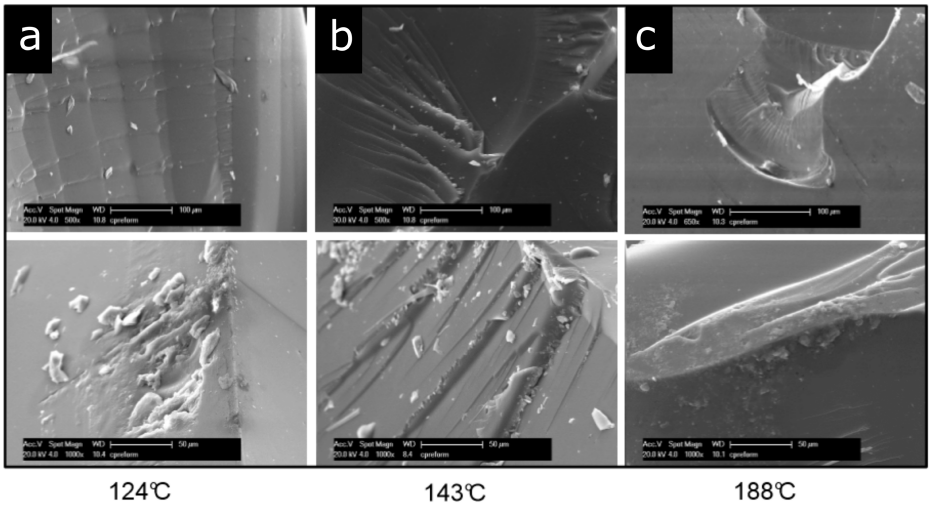

Figure 8.8.: Micrographs of freeze fractured samples cured at (a) 124 °C, (b) 142 °C and (c) 188 °C.

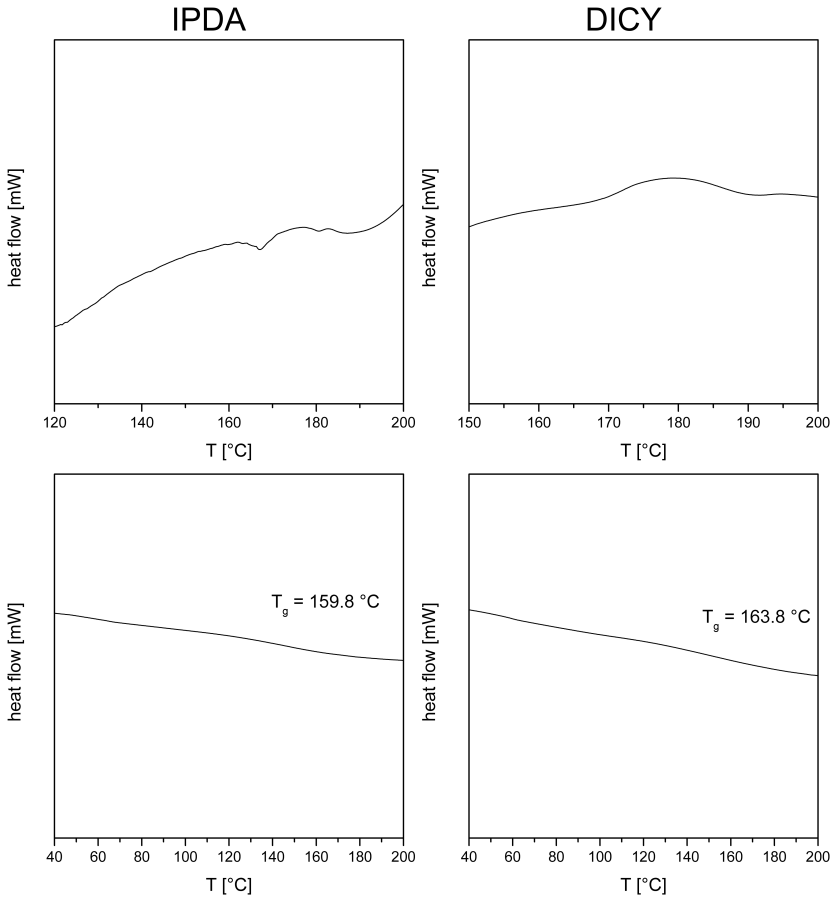

Figure 8.9.: Further conversion of the KL/DGEBA prepolymer with the addition of curing agents IPDA (left) and DICY (right). Top row shows first heating run and the bottom row the second heating run with the determination of the T_g.

8.1 Determination of Kraft Lignins Functional Groups Involved in the Curing Reaction

As seen previously, kraft lignin strongly effects and influences the curing reaction of the DGEBA/DICY system. Further, the existing hydroxyl moieties are responsible for the exothermic reaction as can be seen in the DSC measurements. However, due to the shift of glass transition temperature of the acetylated kraft lignin it is safe to assume that not only the hydroxyl moieties but rather several functionalities participate.

Figure 8.10 shows a fragment of the kraft lignin macromolecule with reactive functionalities such as hydroxyl groups, aliphatic and phenolic as well as internal double bonds. Analytic investigations are limited due to the complexity of the kraft lignin macromolecule as well as the behavior of (partially) cured epoxy resins model compounds were introduced into the epoxy system, which mimic the lignin functionalities.

Therefore, several small molecules (cf. Figure 8.11) were chosen which include one or two of the required functionalities: hydroquinone (1) has two phenolic hydroxyl groups. Cinnamyl alcohol (2) with an internal double bond as well as the aliphatic hydroxyl group and coniferyl alcohol (3) containing the phenolic and aliphatic as well as the internal double bond. Coniferyl alcohol is the most interesting small molecule of those since it combines not only all important functionalities, it is also considered as one of the monomers kraft lignin is build of.

As a result of the high price of (3) of around 100 € per 100 mg the model compound was synthezied in a two–step procedure following Figure 8.12. Following published synthetic procedures[153] ferulic acid **5** (9.38 g, 47.9 mmol) was dissolved in a mixture of ethanol (500 mL) and acetyl chloride 50 mL. The mixture was stirred for 24 h at room temperature resulting in a yellow solution. Afterwards the solvent was removed under vacuum at 40 °C. The obtained yellow oil was crystallized from ethylacetate/cyclohexane (1:1, 6 mL) resulting in a light pink solid. Ethyl ferulate **6** was obtained in 89 % yield (9.48 g, 42.7 mmol). At 0 °C ethyl ferulate **6** (2 g, 8.9 mmol) was dissolved in dry toluene (100 mL). Under nitrogen atmosphere, DIBAL–H in toluene (37.8 mL, 37.8 mmol, 4.2 equiv.) was added drop wise

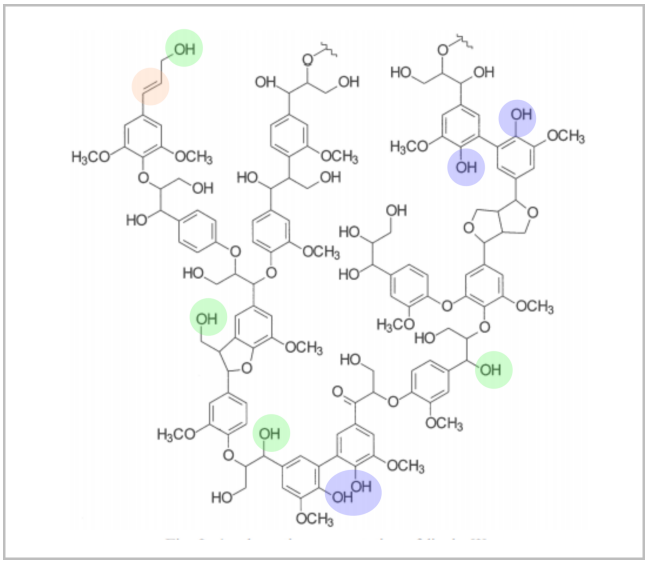

Figure 8.10.: A cutout of lignins structure with its different functionalities: phenolic (blue) and aliphatic (green) hydroxyl groups as well as internal double bonds (red).

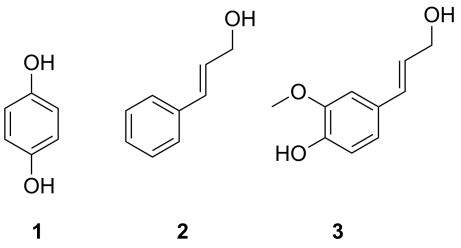

Figure 8.11.: Chemical structures of the model compounds utilized for the investigation of the reactivity of kraft lignin: hydroquinone (1), cinnamyl alcohol (2) and coniferyl alcohol (3).

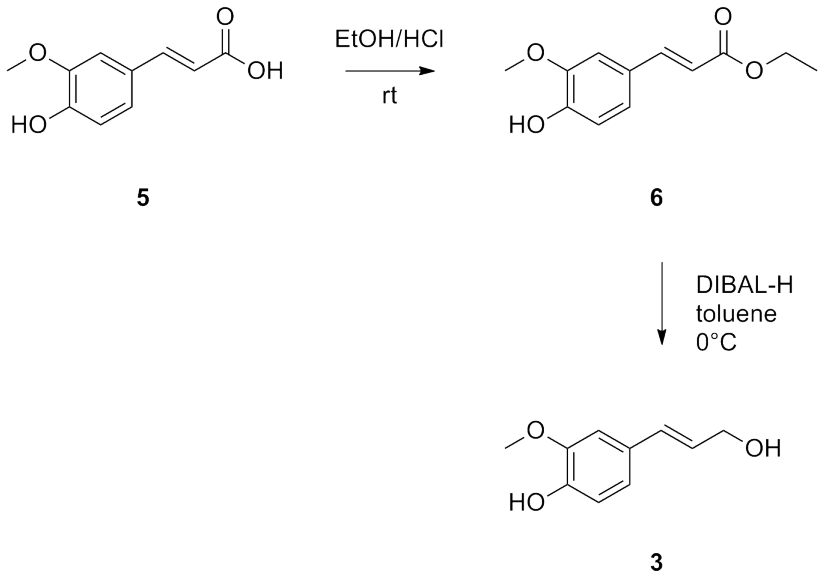

Figure 8.12.: Reaction mechanism of coniferyl alcohol. In the first step, ferulic acid **5** reacts with acetyl chloride to Ethyl ferulate **6**. In the second step DIBAL–H is added as reducing agent for the formation of coniferyl alcohol **3**.

via syringe over 30 min and stirred for an additional 1 h. The reaction mixture was carefully quenched with 10 mL ethanol. The solvent was partially removed under vacuum at 40 °C. Water (50 mL) was added and the resulting mixture was extensively extracted with ethyl acetate (4 × 150 mL). The combined organic layers were dried over Na_2SO_4, filtered, and the solvent removed under vacuum at 35 °C. The yield of the resulting pale yellow highly–crystalline coniferyl alcohol **3** was 73.2 % (1.2 g, 6.59 mmol).

For the investigation of the reactivity of the model compounds each compound was thoroughly mixed stoichiometrically with the DGEBA epoxy resin as well as with the curing agents DETA, IPDA and DICY and cured at elevated temperatures. Table 8.1 shows whether viscosity increased after mixing and heating. The table shows that hydroquinone showed no reactivity towards DGEBA as well as DETA but an increase in viscosity could be proven for the curing agents IPDA as well as DICY. Coniferyl alcohol showed a cross–linking reaction with DGEBA, IPDA and DICY. The utilization of cinnamyl alcohol proved to be difficult due to the condensation of a yellowish oil besides the increase of viscosity. It emerged that cinnamyl alcohol decomposes with increasing conversion. Therefore, it is unsuitable as a model compound for kraft lignin. Due to these results, hydroquinone as well as coniferyl alcohol were further analyzed.

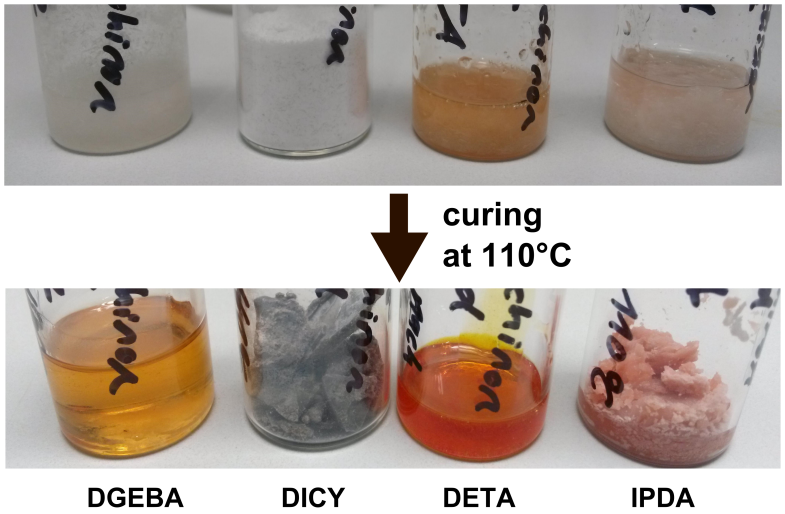

Figure 8.13.: Curing reaction of hydroquinone with DGEBA, DICY, DETA and IPDA (from left to right).

8.1.1 Investigations of the Reactivity of Hydroquinone

Figure 8.13 shows the reaction products of hydroquinone with DGEBA, DICY, DETA and IPDA. As seen previously (Table 8.1) no cross–linking reaction takes place with the DGEBA resin and the DETA curing agent. However, significant changes are visible with DICY and IPDA. With DICY the former white mixture transforms into a brittle concrete like solid. With IPDA a pink soft solid was obtained.

To further investigations of the cross–linked network, NMR spectroscopy, FT–IR spectroscopy and DSC measurements were conducted. However, in all cases the insolubility of the cross–linked hydroquinone gave direct evidence of a successful partial conversion into a cross-linked network. This was confirmed by ^{1}H– and ^{13}C–NMR–spectra of the soluble oligomeric compounds. They showed signals of unconverted hydroquinone which can still be removed from the cross–linked network.

The FT–IR spectrum of hydroquinone with DICY compared with neat DICY is shown in Figure 8.14a. The area around $3000 - 3500\ \mathrm{cm}^{-1}$ is of particular interest since the OH stretching vibrations of hydroquinone are located at $3150\ \mathrm{cm}^{-1}$ whereas several splitted peaks resulting from the N–H stretching vibrations of DICY are located at $3146\ \mathrm{cm}^{-1}$ and around $3332\ \mathrm{cm}^{-1}$. Compared to the cured hydroquinone/DICY mixture the signal changes to a less splitted peak. Due to its topology, this can be assumed as the N–H stretching vibrations. This means a change of the bonding character of the nitrogen atoms resulting from the cross–linking formation of a primary amine.

Table 8.1.: Reactivity of different model compounds towards the DGEBA epoxy resin and the three curing agents DETA, IPDA and DICY. √ indicates a successful reaction.

Model compound	DGEBA	DETA	IPDA	DICY
Hydroquinone			√	√
Cinnamyl alcohol				
Coniferyl alcohol	√		√	√

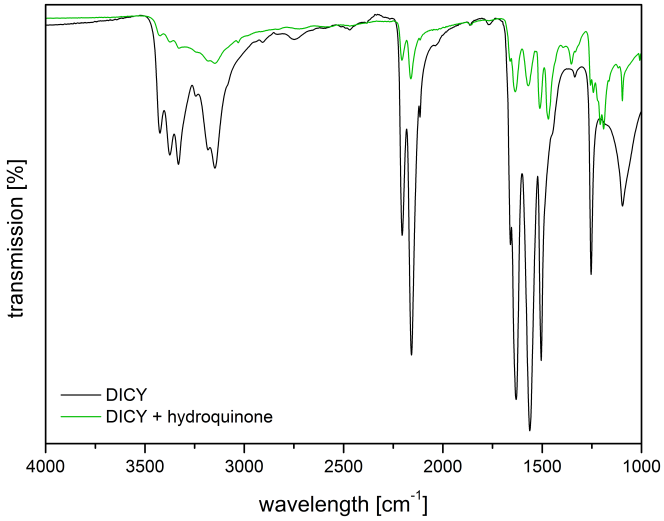

(a) FT–IR spectra of DICY and hydroquinone cured with DICY.

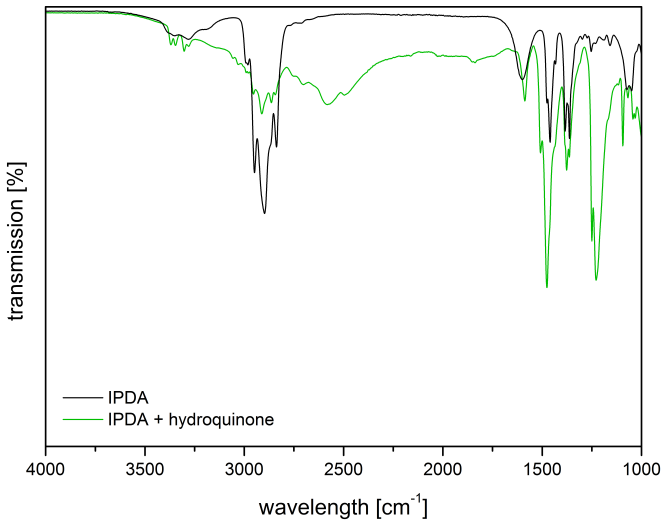

(b) FT–IR spectrum of IPDA and the product of IPDA and hydroquinone.

Figure 8.14.

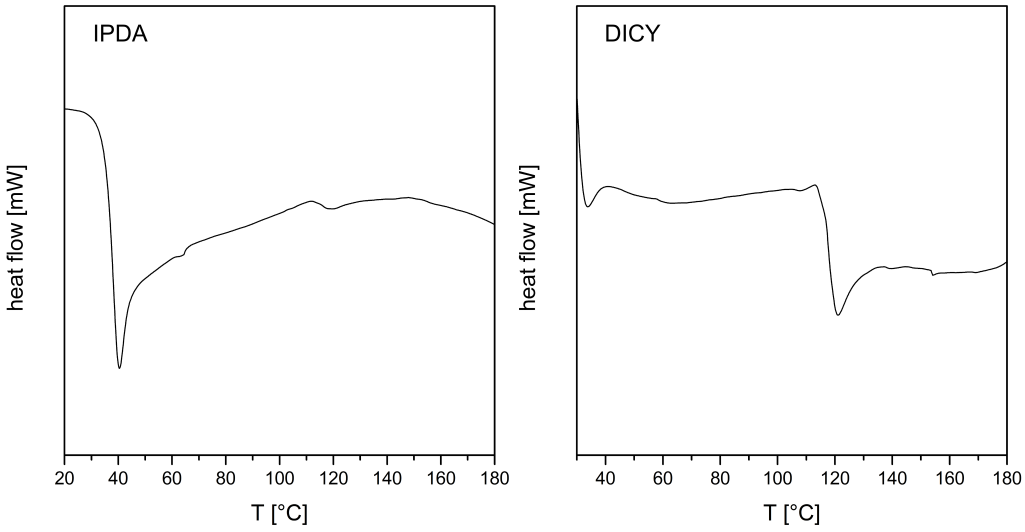

Figure 8.15.: DSC thermograms of the products of hydroquinone/IPDA (left) and hydroquinone/DICY (right).

Regarding the reaction of hydroquinone with IPDA the results of the FT–IR spectroscopy are shown in Figure 8.14b. Neat IPDA shows stretching vibrations of both of its amine moieties located at 3100 cm^{-1} as well as C–H stretching vibrations at around 2890 cm^{-1}. After conversion, similar to the reaction with DICY, an alteration of the vibrational bands of both is visible. This is an indicator for the cross–linking and thus the formation of a primary amine.

The cured samples of hydroquinone/IPDA and hydroquinone/DICY were measured with DSC to investigate changes of glass transition values. Figure 8.15 shows clearly that a reaction took place due to the formation of multiple glass transition temperatures. With IPDA a significant glass transition temperature at 40.3 °C and a weak one at 118.8 °C occurs. DICY shows similar glass transition temperatures but with opposed intensities. Interestingly, the assumed glass transition temperature at around 118.8 °C is almost identical with the melting point of 1,4–benzoquinone which is located at 115 °C which might occur from the oxidation of hydroquinone.

In combination with the resulting second glass transition temperature at 40.3 °C it can be assumed that a partial cross–linked product as well as the formation of 1,4–benzoquinone took place. Based on this knowledge a closer look into the FT–IR spectrum of hydroquinone and IPDA reveals that the vibrational bonds at 3345 cm^{-1} as well as the the vibrational bonds at 1479 cm^{-1} and 1229 cm^{-1} can be assigned to 1,4–benzoquinone.

Due to the oxidation into 1,4–benzoquinone, hydroquinone is not suitable as a model compound for these investigation. However, a cross–linking reaction has been observed with FT–IR and DSC measurements and with regard to FT–IR the mechanism presented in Figure 8.16 can be assumed.

8.1.2 Investigations of the Reactivity of Coniferyl Alcohol

As described previously, coniferyl alcohol is the most promising model compound, because it contains the three most important functional groups also included in kraft lignin: phenolic and aliphatic hydroxyl

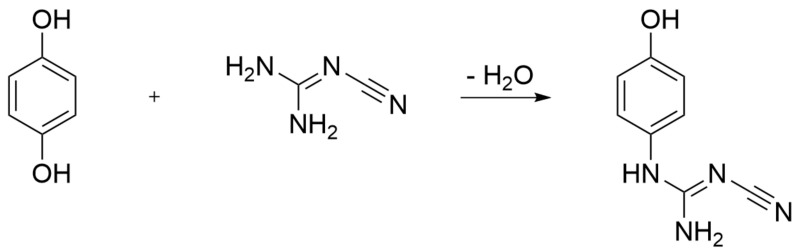

Figure 8.16.: Proposed mechanism of the reaction of hydroquinone with DICY under release of water.

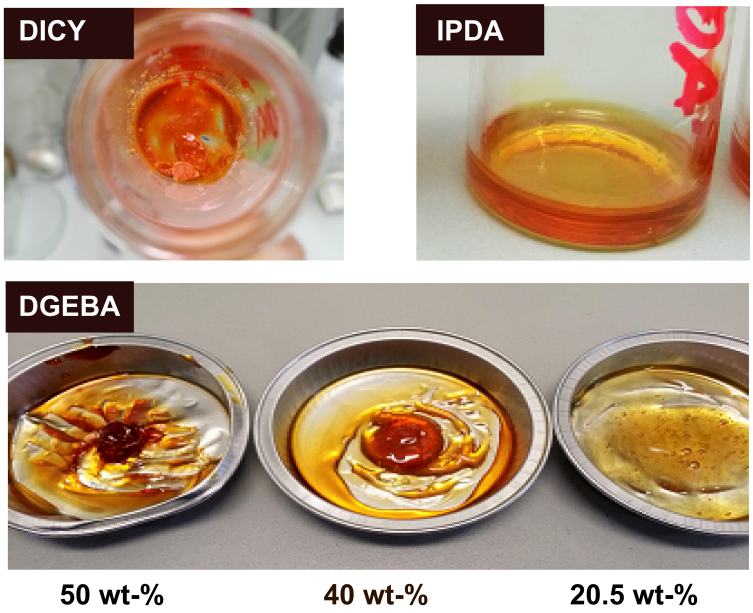

Figure 8.17.: Reaction mixtures of coniferyl alcohol with DICY and IPDA (top) as well as DGEBA resin (bottom) cured at elevated temperatures.

moieties as well as internal double bonds. Figure 8.17 shows the prepared samples of coniferyl alcohol in the curing components DICY and IPDA as well as in the DGEBA resin.

In each case a cross–linking reaction took place resulting in orange solids as for DICY and IPDA as well as a yellowish high viscous mixture for DGEBA with 20 % coniferyl alcohol and brown solids for higher coniferyl alcohol concentrations of 40 % and 50 %.

As before IR measurements were conducted to determine the functional groups involved in the cross–linking reaction. Figure 8.18a shows the IR spectrum of coniferyl alcohol, DGEBA and the reaction product of both. The range of $2500 - 3500\ cm^{-1}$ is of particular interest because of vibrational bands of the hydroxyl moieties. A significant change in the band structure of the reaction product is evident. The band at $3462\ cm^{-1}$ and $3233\ cm^{-1}$ disappears in favor of a broad peak at $3454\ cm^{-1}$. The appearance of this broad band, which is not present in DGEBA as well, might be induced of the formation of hydroxyl groups in the cross–linked polymer due to the ring–opening of the epoxy moieties.

The prepared samples of coniferyl alcohol cross–linked with the curing agents IPDA and DICY are shown in Figure 8.18b. In both cases the IR bands are difficult to assign to their specific functionalities due to a major overlap of the signals. Only the band at $2157\ cm^{-1}$ for the DICY cross–linked coniferyl

alcohol (bottom) shows a significant change in comparison to the educts. Clearly, the vibrational modes of the NCN–group of DICY, which are located at 2154 cm^{-1} and 2203 cm^{-1}, decrease with the formation of a new peak at 2475 cm^{-1}. Therefore, it can be assumed that a new bond structure has been developed.

For further identification of the reaction products, ^{1}H and ^{13}C NMR spectroscopy as well as mass spectrometry (MS) were conducted. Figure 8.19a presents the ^{1}H NMR spectrum of the product of coniferyl alcohol and IPDA. It can be seen that coniferyl alcohol is present as unreacted educt as well as cross–linked product. This is obvious due the presence of the dublett of the methylene groups at 4.22 ppm (educt) and its high–field shift because of the direct neighborhood to the newly formed amino group (product). Further, the singuletts of the aliphatic hydroxyl group at 5.05 ppm and phenolic hydroxyl group, which showed a singulett at 9.55 ppm, disappear completely. It appears that IPDA reacted entirely with the coniferyl alcohol due to the lack of signals of the NH_2 moieties at around 8 ppm. Therefore, both NH_2 moieties of IPDA seem to react with the hydroxyl moieties of coniferyl alcohol resulting in excess coniferyl alcohol since two molecules alcohol react with one molecule IPDA. Moreover, the presence of the protons at the ethylenic double bond at 6.21 and 6.5 ppm suggest that this functional group does not participate in the reaction.

Based on these results, the reaction mechanism shown in Figure 8.20 can be assumed. As proof of the condensation reaction is the strong singulett of H_2O obtained in the ^{1}H–NMR spectrum at 4.8 ppm as a result of the release of water during the reaction.

Figure 8.21 shows the ^{1}H–NMR spectrum of the reaction product of coniferyl alcohol and DICY. At 4.7 ppm and 3.2 ppm signals resulting from the hydroxyl moieties are present which indicate a not completely converted coniferyl alcohol. At a chemical shift of 2.2 ppm a singulett can be assigned to the newly formed bond between the aliphatic hydroxyl group and the amine groups of DICY. Further, peaks of the DICY NH_2 groups, usually visible at around 8 ppm, are not present. This is evidence of the complete consumption of DICY which is in good agreement with the FT–IR results. Therefore it can be assumed, that in order to achieve complete consumption both hydroxyl moieties are involved in the cross–linking reaction. The recorded ^{13}C–NMR spectrum proves that according to the reaction with IPDA a condensation reaction takes place during the formation of the new C–N bond.

As further confirmation of this products mass spectrometry experiments were conducted to evaluate the resulting fragmentation pattern. Samples of the reacted coniferyl alcohol/IPDA and coniferyl alcohol/DICY systems were measured up to a temperature of 300 °C. Because of the complicated mixture of the samples consisting of educts and cross–linked products with different degree of polymerization, only the peak of molecule ion is observed.

The MS spectrum of coniferyl alcohol/IPDA shows the peak of coniferyl alcohol at 180 m/z. The peak of molecule of IPDA is not present. Both values are consistent with the results of the NMR spectrum. The reaction product assumed with IR and NMR measurements with a molar mass of 494 m/z could be identified (cf. Figure 8.19b). This product is shown in Figure 8.22 (top) in two possible isomeric structures.

As for the reaction of coniferyl alcohol and DICY, product fragments with 312, 474 und 636 m/z are visible besides the peaks of coniferyl alcohol at 180 m/z and DICY at 84 m/z. The assignment of the products is shown in Figure 8.22 (bottom) and gives evidence of the condensation reaction. With fragmentation temperatures of 300 °C a degree of polymerization of $n = 2$ can be observed. In both cases

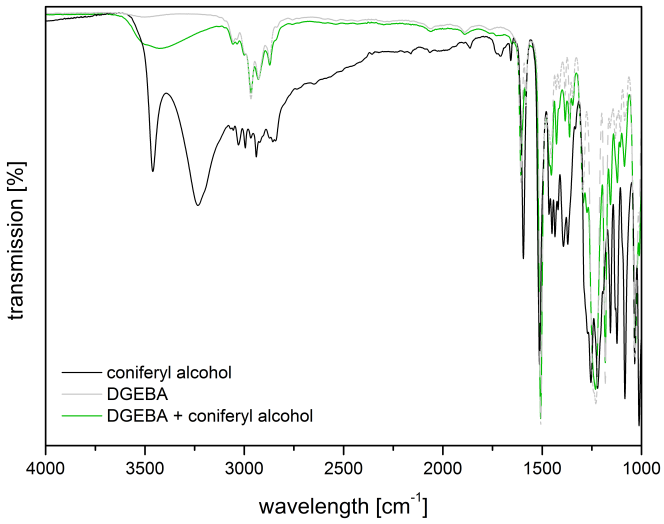

(a) FT–IR spectrum of coniferyl alcohol and DGEBA.

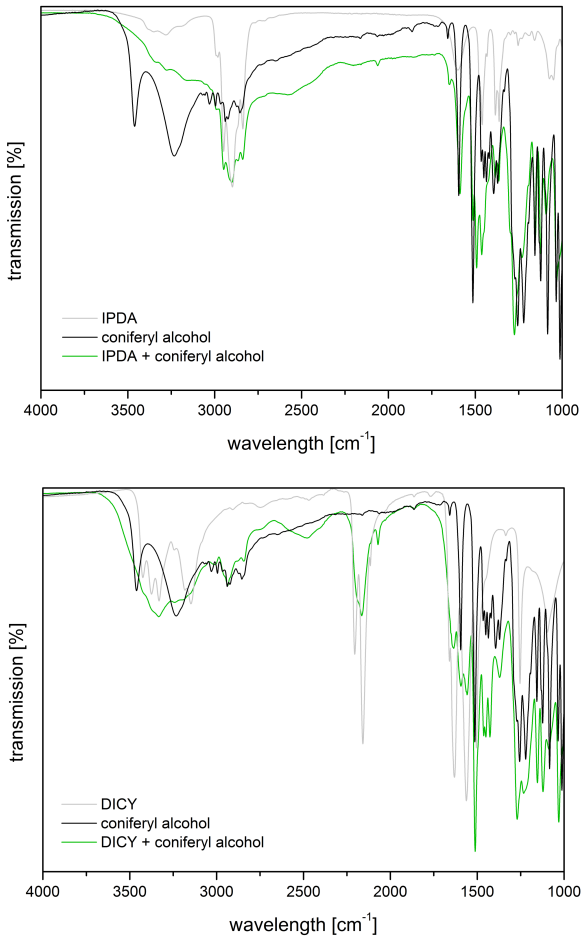

(b) FT–IR measurements of coniferyl alcohol cured with IPDA (top) and DICY (bottom) compared to their educts.

Figure 8.18.

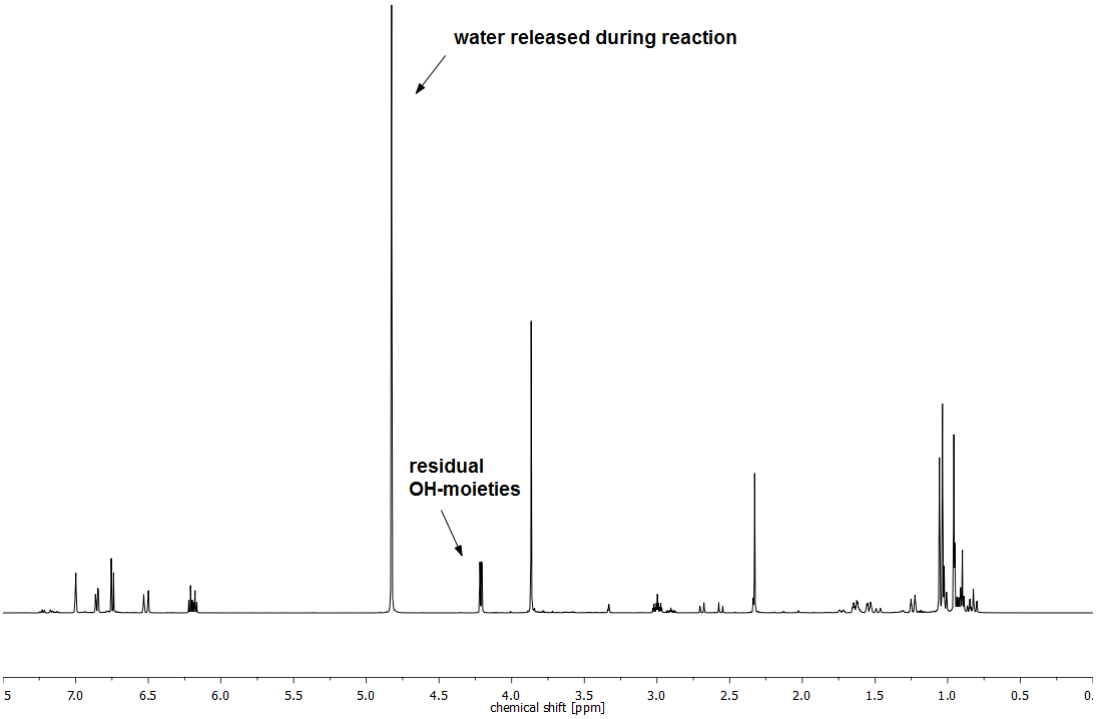

(a) NMR spectrum of the reaction product of coniferyl alcohol and IPDA.

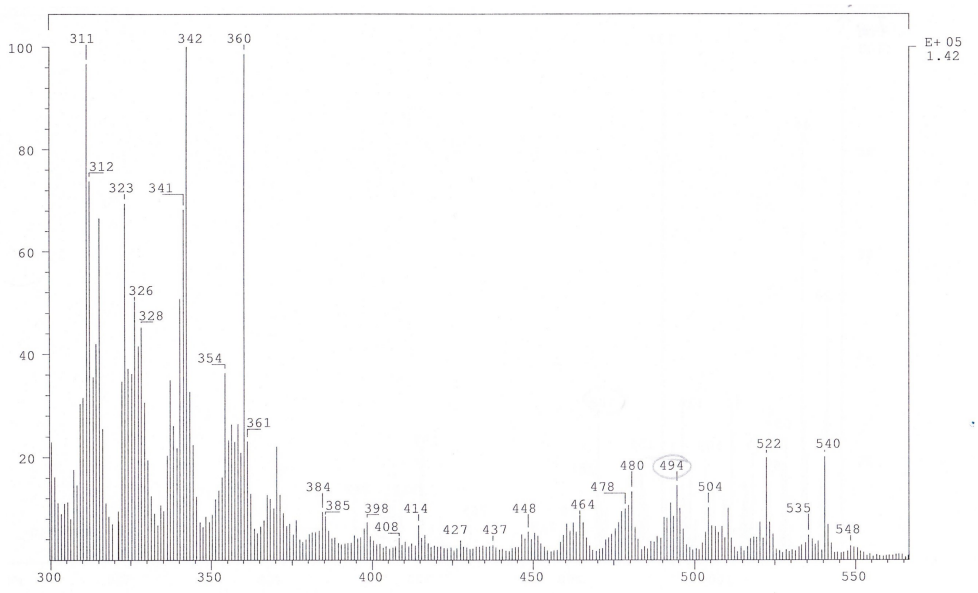

(b) Mass spectrum of the reaction product of coniferyl alcohol and IPDA.

Figure 8.19.: NMR and mass spectrum of coniferyl alcohol and IPDA

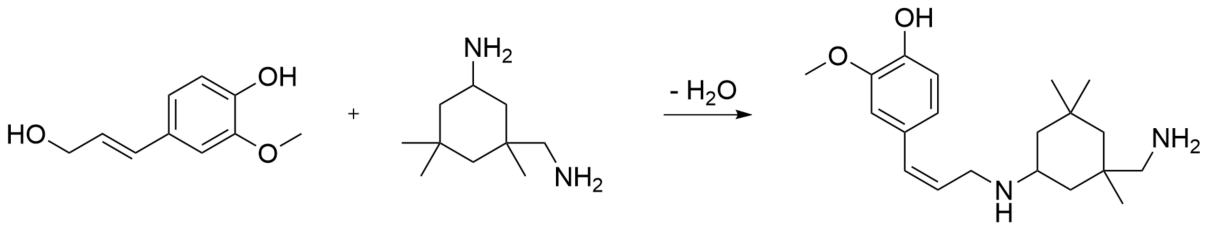

Figure 8.20.: Proposed mechanism of the reaction of coniferyl alcohol with IPDA under the release of water.

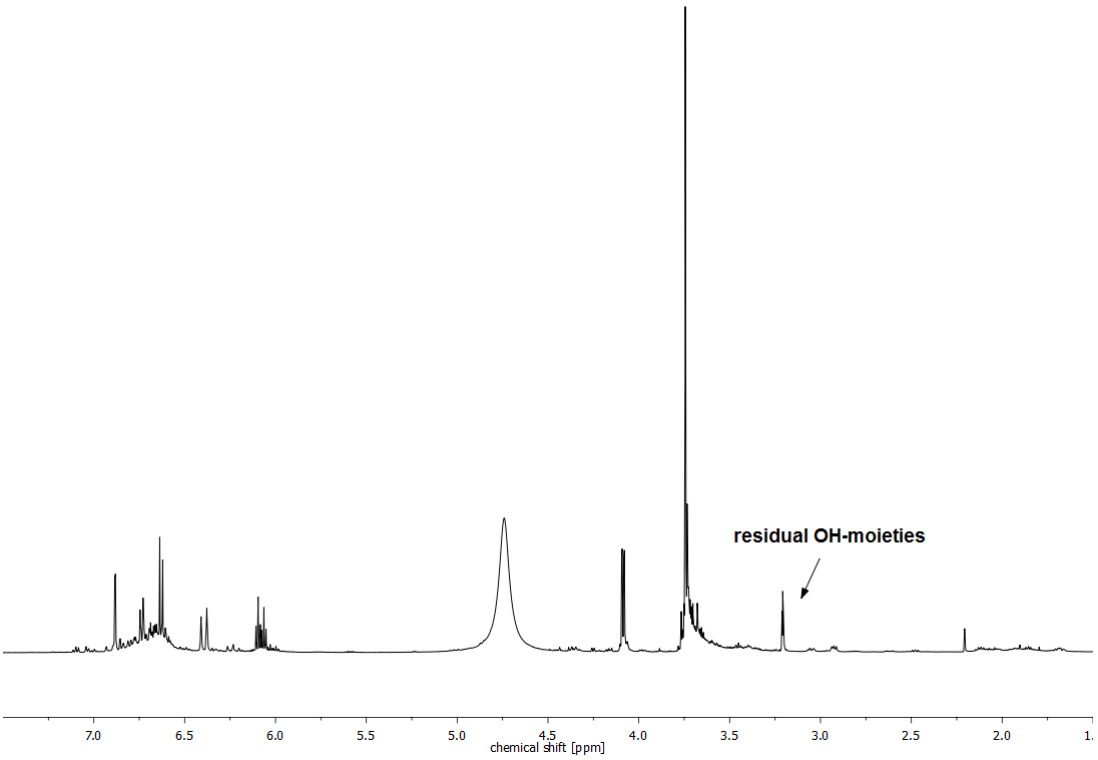

Figure 8.21.: ^{1}H–NMR spectrum of the reaction product of coniferyl alcohol and DICY

the fragmentation pattern shows a high temperature resistance of the products and with an increase of the fragmentation temperature higher polymerization grades are expected and also could be proven.

Finally, DSC measurements of the reaction products were conducted to obtain information whether a polymer could be achieved for coniferyl alcohol and the curing agents IPDA as well as DICY and the DGEBA resin. The formation of a polymer will be reflected in the development of a visible glass transition temperature. The results of these experiments are presented in Figure 8.23. With both amino–based curing agents glass transition temperatures could be obtained, which leads to the conclusion that polymers with higher degrees of polymerization with increasing amount of coniferyl alcohol have been build.

The coniferyl alcohol/IPDA system shows a T_g of 92.8 °C, whereas with DICY a slightly higher glass transition of 118.8 °C could be obtained. Further, samples of DGEBA with different concentrations of coniferyl alcohol have been cured and measured as well to prove the reactivity of coniferyl alcohol towards the epoxy moieties and therefore the adjustability of the cross–linking density. It is evident that the increase of the concentration of coniferyl alcohol in the epoxy resin shows a significant increase of the

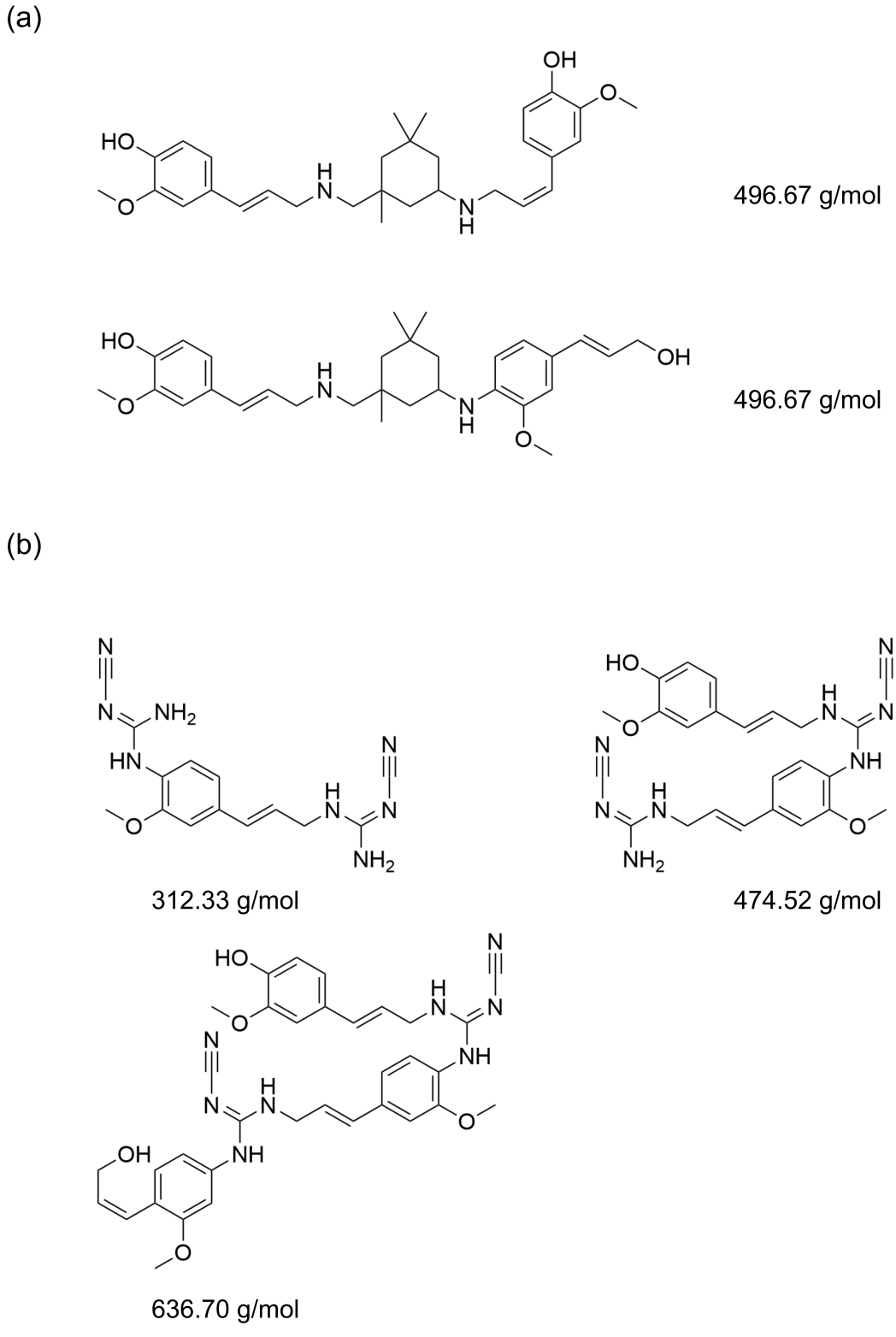

Figure 8.22.: Possible structures of the fractions of the products from the reaction of coniferyl alcohol with (a) IPDA and (b) DICY.

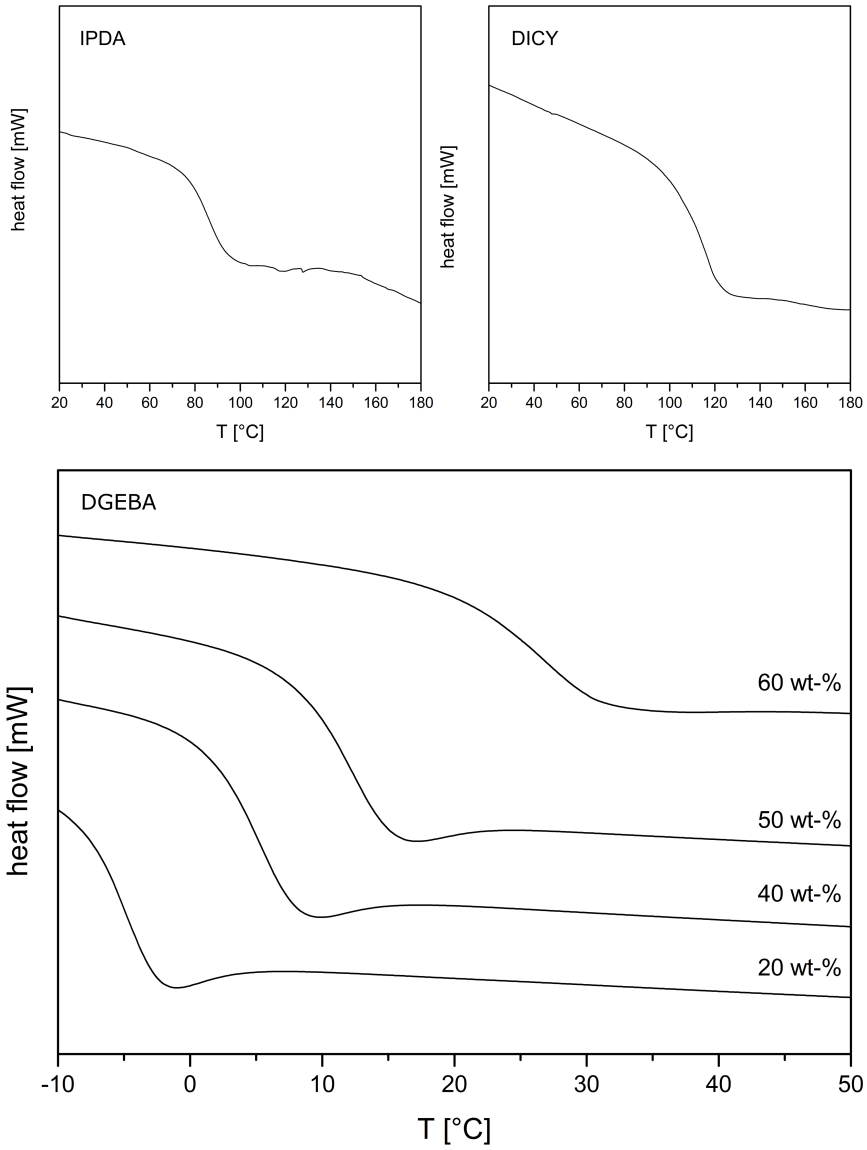

Figure 8.23.: Determination of the glass transition temperature of the reaction product of coniferyl alcohol with IPDA (top, right), DICY (top, left). Samples with different concentrations of coniferyl alcohol in DGEBA were investigated as well (bottom). $T_{g,20wt-\%}$ = −5.3 °C, $T_{g,40wt-\%}$ = 4.4 °C, $T_{g,50wt-\%}$ = 11.6 °C and $T_{g,60wt-\%}$ = 28.8 °C.

glass transition temperature from −5.3 °C for 20 wt-% towards 28.8 °C for a content of 60 wt-% coniferyl alcohol.

Both, hydroquinone as well as coniferyl alcohol, react with the curing agents IPDA and DICY. The synthezised molecular compound coniferyl alcohol showed also a high reactivity towards the epoxy moieties of the DGEBA resin. Transferring the findings, made with the model compounds, towards the lignin macromolecule leads to the following conclusions. On one hand, the hydroxyl moieties of the aliphatic and phenolic part are able to react with the amine moieties of the curing agents under the release of water to secondary amines. Therefore, the mechanism of the reactivity of kraft lignin towards the epoxy compounds, namely the DGEBA resin as well as the curing agents IPDA and DICY, is resolved.

9 Lignin as a Feasible Alternative for Commercially Used Accelerators

Up to this point in this work, it became evident that kraft lignin can be a substantial part of a bio–based epoxy formulation. It does not only serve for the purpose of cost reduction, it also has proven to be a feasible alternative to commercially used accelerators as well. Kraft lignin provided a temperature reduction of almost 80 °C compared to the neat unaccelerated DGEBA resin. The performance of common accelerators showed a performance similar to kraft lignin with lignins advantage of an extended shelf life compared to urone–based accelerators.

9.1 Assembly of a Biobased Lignin–Epoxy Reinforced Prepreg Material

For processing in the wet–lay up prepreg process epoxy formulation with and without kraft lignin and accelerator were prepared, respectively, as described in Chapter 6. Fiber mats consisted of cellulose or glass fibers, respectively. The processing conditions are summarized in Table 9.1. It is quite noticeable that even with additional accelerator the composites without kraft lignin are not fully cured, whereas each composite containing kraft lignin appears fully cured and solid at 120 °C–even the one with no additional accelerator added. This reveals that kraft lignin is not only competitive with commercial accelerators with regards to the curing behavior, lignin proves to be a more feasible substitute. This is a significant result regarding the history of lignin as waste material.

With regard to the applicability for fiber reinforced polymers it is imperative to achieve a high content of fibers in a finished composite material. In Table 9.2 the fiber mass fraction Ψ is calculated using

$$\Psi = \frac{m_f}{m_{composite}} \tag{9.1}$$

in which m_f is the fiber mass and $m_{Composite}$ the overall mass of the composite. It is evident that without lignin slightly higher fiber mass fractions are obtained. This is the result of a higher epoxy resin content, due to the slightly higher viscosity of the kraft lignin filled epoxy. To increase the fiber content, the resin

Table 9.1.: Manufacturing conditions of the composite material and their properties after molding.

Sample	Accelerator	t_c [min]	T_c [°C]	p [kN]	Properties
1	-	4	120	15	wet
2	-	4	180	15	tacky, yellow, burned smell
3	1 wt-% UR-2	4	120	15	tacky
4	1 wt-% 2-MI	4	120	15	tacky, small particles
With 40 % KL					
5	-	4	120	15	solid
6	-	4	180	15	solid
7	1 wt-% UR-2	4	120	15	solid
8	1 wt-% 2-MI	4	120	15	solid

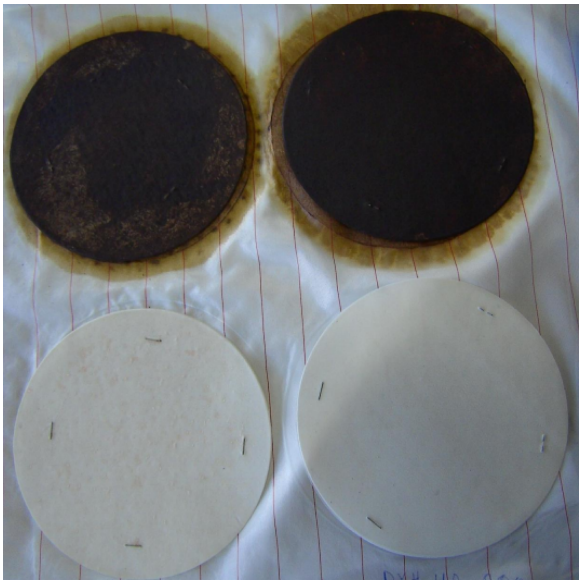

Figure 9.1.: Manufactured FRP with the neat DGEBA/DICY system as well as with the addition of 40 % kraft lignin as accelerator.

needs to be preheated to decrease its viscosity or the use of reactive diluents. This step enhances the permeability of the kraft lignin filled epoxy throughout the porous fiber mats. Figure 9.1 shows the cured samples of a 40 % lignin filled FRP compared to the neat fiber reinforced epoxy. In all cases, cured samples could be obtained with no visible delamination effects.

Another important factor for the mechanical properties of the composite is not only whether the kraft lignin filled epoxy is fully cured, but also whether the kraft lignin and DICY are homogeneously distributed throughout the composite. This ensures a full conversion of the epoxy moieties and avoids sedimentation of the DICY particles and kraft lignin on top of the fiber mats (filter effect).

In order to verify this, a sample of the cured composites have been cut out of the cured composite materials and DSC measurements to investigate the phase morphology were conducted. The DSC measurements (Figure 9.2) proved that the kraft lignin filled epoxy shows no alterations such as a split

Table 9.2.: Calculated fiber mass fraction Psi using Equation 9.1 of samples without lignin (1–4) and with a 40 % lignin share (5–8).

Sample	m_f [g]	$m_{Composite}$ [g]	Ψ [%]
1	14.82	29.67	50
2	14.64	26.49	55
3	14.66	28.78	51
4	14.95	29.39	51
With 40 % KL			
5	14.69	36.62	40
6	15.20	37.54	40
7	14.70	38.18	38
8	14.85	36.32	41

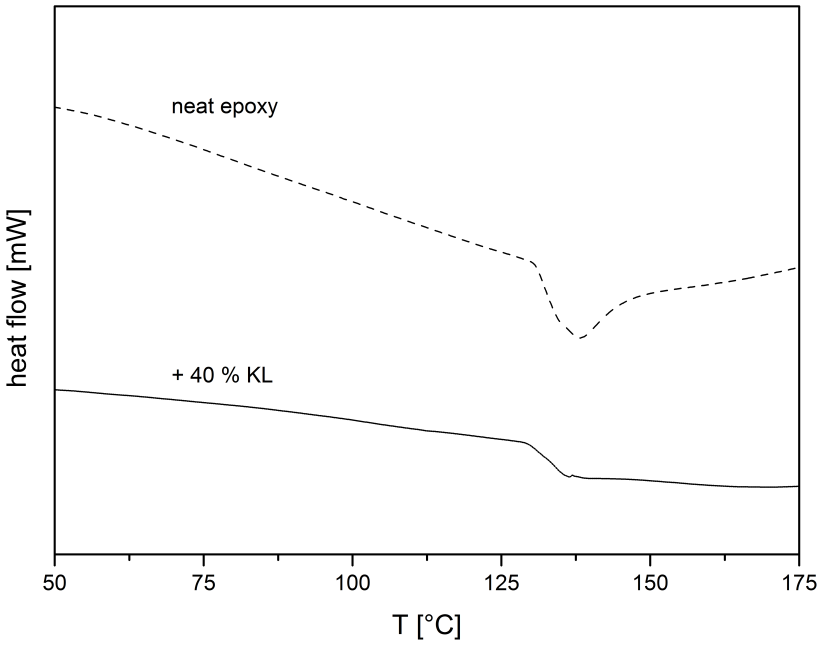

Figure 9.2.: DSC thermogram of the neat composite and the kraft lignin filled composite. A single T_g of the lignin filled composite proves that no sedimentation of lignin particles on top of the fiber layers occurs.

into two glass transition temperatures which would indicate agglomerations. Further, the same glass transition temperature as the neat DGEBA/DICY cured composite was measured proving complete curing.

A very important aspect in this work is the total bio–content Φ of the resulting composite material. This ratio can be calculated by

$$\Phi = \frac{m_f + m_L}{m_{composite}} \tag{9.2}$$

with m_f and m_L denoting the mass of the fiber and kraft lignin mass respectively and $m_{Composite}$ denoting the total composite mass. Table 9.3 shows that the produced composite material with the newly developed kraft lignin filled epoxy resin has a total bio–content of almost 60 %. This proves that the desired biobased material has been successfully introduced into a new value chain for FRPs suitable for both, wet-lay up as well as prepreg processing. To even further increase the biopolymer content, it is possible to incorporate kraft lignin in the fiber mats as well. Therefore, a defined amount of kraft lignin can be introduced in the first step into the fiber-water suspension (Figure 6.1a a).

Especially at this stage of designing and dimensioning of the final material, knowledge of the material behavior and performance is required. In the following sections the basic mechanical properties are discussed in particular.

9.2 Mechanical Characterization of Cellulose Fiber Reinforced Composites

To determine the mechanical properties of the fiber reinforced polymers tensile tests were carried out. In collaboration with the Fraunhofer Institute for Structural Durability and System Reliability LBF a series of experiments with 14 different samples was designed. The aim was to evaluate the influence of the different curing parameters and components on the mechanical properties as well as the manufacturing process. [154]

Curing time and temperature as well as the manufacturing setup were tested with kraft lignin reinforced resin and paper sheets. However, for some samples poor material quality due to a too low curing temperature or curing time and therefore insufficient properties were immediately obvious, therefore no characterization was made. Table 9.4 shows the parameters of the most promising samples 9–14 which were analyzed subsequently with tensile tests, dynamic mechanical thermal analysis (DMTA) and SEM imaging. In order to assure comparability to reference values, the samples of the newly developed resin were cured at 180 °C despite the fact that the lignin containing epoxy resin shows complete curing even at 120 °C.

The results of the tensile tests for Young's modulus and tensile strength are shown in Figure 9.3. Regarding the stiffness of the material (left), an increasing curing temperature and lignin share yields an increase of the modulus. This behavior is observed for the tensile strength as well. However, in general, no significant difference between the kraft lignin filled epoxy resin and the neat epoxy resin is observable.

It is important to note that those results were obtained in a special setup: due to the hygroscopic properties of lignin and cellulose the development of moisture during manufacturing in press at elevated temperature proved to be a challenge. Figure 9.4 shows the resulting condensed water inside the vacuum bag which resulted in FRPs with low cross–linking densities, delamination of fiber sheets and matrix, and low mechanical properties due to void formation in the resin. Therefore a new technique was used, in which the vacuum setup normally used before transferring the composite into the press was used during pressing as well, reducing the amount of water tremendously.

Additionally, DMTA of selected samples was carried out to determine the temperature–dependent visco–elastic properties and determines the storage modulus G', loss modulus G'', and the damping values by applying an oscillating force to the sample. Figure 9.5 shows the results for G' and G'' for the samples 12,13 and 14 cured at 180 °C for 8 min.

The samples with kraft lignin show a homogeneous progress of the storage modulus which decreases monotonously. However, the neat FRP shows the highest storage modulus at low temperatures but reacts more sensible to changes in temperature with a significant drop at 110 °C of G'.

Table 9.3.: Calculated biopolymer content for the lignin based composite materials using Equation 9.2.

Sample	m_f [g]	$m_{Composite}$ [g]	m_L [g]	Φ [%]
5	14.69	36.62	6.18	57
6	15.20	37.54	6.38	57
7	14.70	38.18	6.99	55
8	14.85	36.32	6.13	58

Both lignin samples show a stable loss modulus up to 140 °C compared to the neat FRP. The loss modulus is much more pronounced with the 40 % kraft lignin sample due to the enhanced solid content which produces additional friction in the material resulting in a higher dissipation energy.

For further comparison, the loss factor $\tan\delta$ was calculated which equals the ratio of G' and G'' and provides a representative basis of valuation. The comparison in Figure 9.6 shows that the sample with 20 % kraft lignin has a low loss factor of 0.1. The 40 % sample shows a distinctive damping behavior and a loss factor of 0.16 which is caused by an increased loss modulus G''. The neat FRP shows at lower temperatures a higher stiffness but compared to the lignin samples a significant rise of the loss factor with increasing temperature. Moreover, a second peak at around 190 °C is visible which results from a drop of the storage modulus.

The SEM micrographs in Figure 9.7 reveal that fiber pull–out appears on the raw edge for both lignin filled FRP. This results from the low tensile strength which is caused by insufficient transmission throughout the total fiber length and poor fiber–resin adhesion.

Table 9.4.: Design of experiments executed for optimization and characterization of the developed composite material.

Sample	KL resin [wt-%]	KL paper [wt-%]	Acc [wt-%]	t_c [min]	T_C [min]
1	20	0	0	8	150
2	40	0	0	8	150
3	20	20	0	8	150
4	40	20	0	8	150
5	20	0	0	8	120
6	40	0	0	8	120
7	20	20	0	8	120
8	40	20	0	8	120
9	20	0	0	4	180
10	40	0	0	4	180
11	0	0	1	4	180
12	20	0	0	8	180
13	40	0	0	8	180
14	0	0	1	8	180
15	20	0	0	6	180
16	40	0	0	6	180
17	20	20	0	6	180
18	40	20	0	6	180
19	20	0	0	8	180
20	40	0	0	8	180
21	20	20	0	8	180
22	40	20	0	8	180
22	0	0	1	8	150
23	0	0	1	8	120
24	0	0	0	6	180
25	0	0	0	8	180

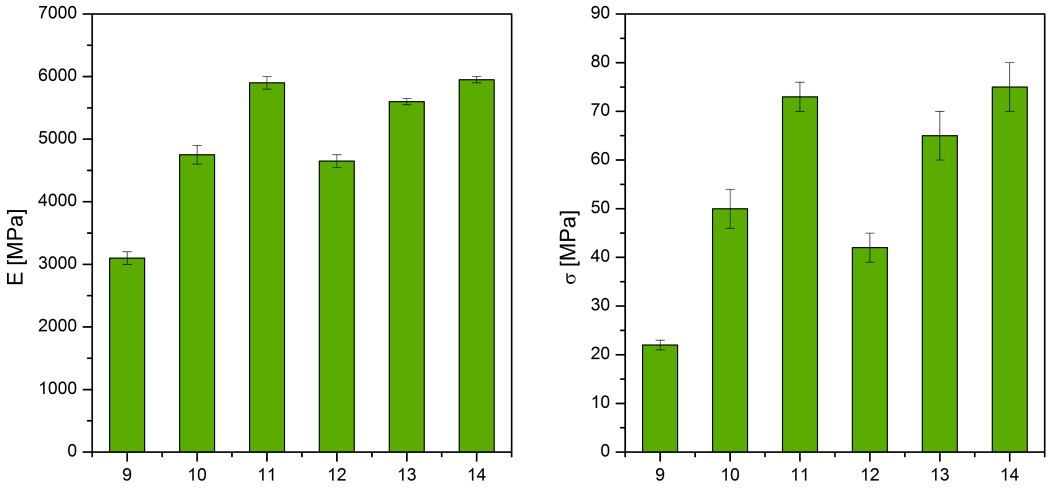

Figure 9.3.: Young's modulus (left) and tensile strength (right) of the developed cellulose–fiber reinforced composite materials. Samples 9 – 11 were cured at $180\ ^{\circ}\mathrm{C}$ for $4\ \mathrm{min}$ with 20 % (9), 40 % (10) and 0 % (11) kraft lignin content. Samples 12 – 14 were cured at $180\ ^{\circ}\mathrm{C}$ for $8\ \mathrm{min}$ with 20 % (12), 40 % (13) and 0 % (14) kraft lignin content. Samples 11 and 14 containing 0 % kraft lignin contained 1 % accelerator as references.

Figure 9.4.: Moisture development during vacuum molding (left). New technique (right): Vacuum tube inserted during the curing and pressing step to reduce moisture development and therefore void content in the final material. This simple procedure led to superior quality with regard to delamination effects compared to samples produced without the new set–up.

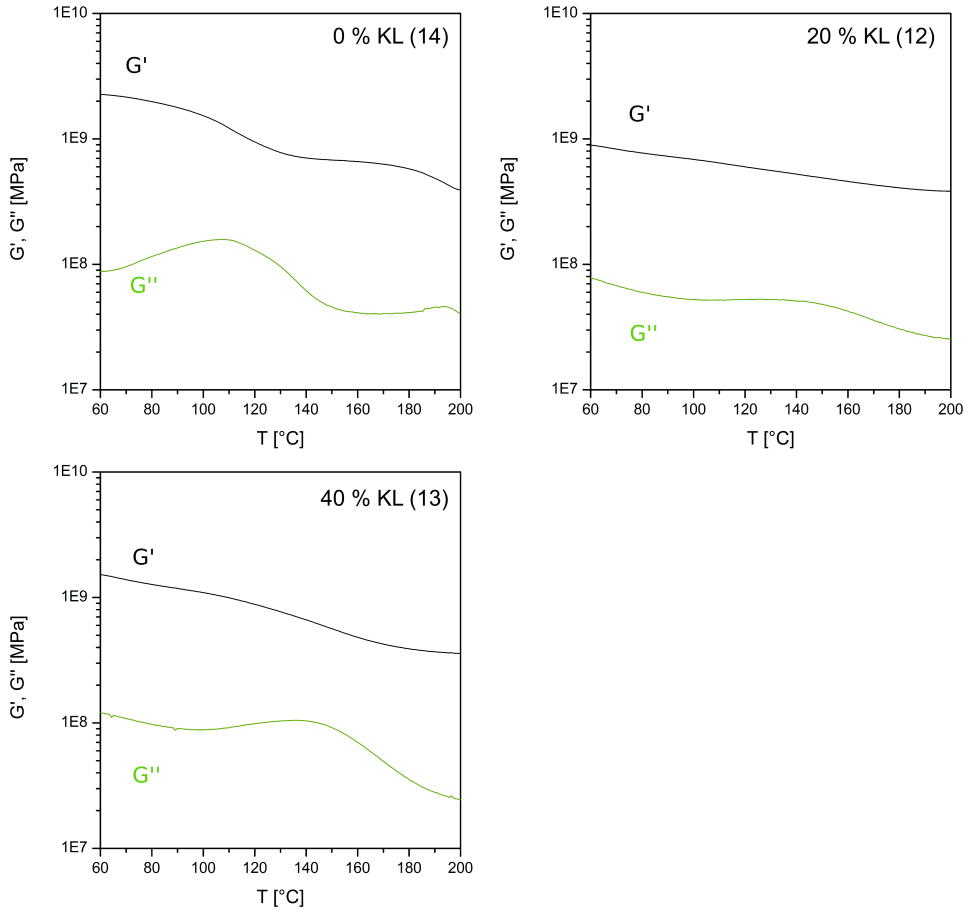

Figure 9.5.: DMTA results for the storage modulus G' and loss modulus G'' for samples without kraft lignin (14, top left), 20 % kraft lignin (12, top right) and 40 % kraft lignin (13, bottom).

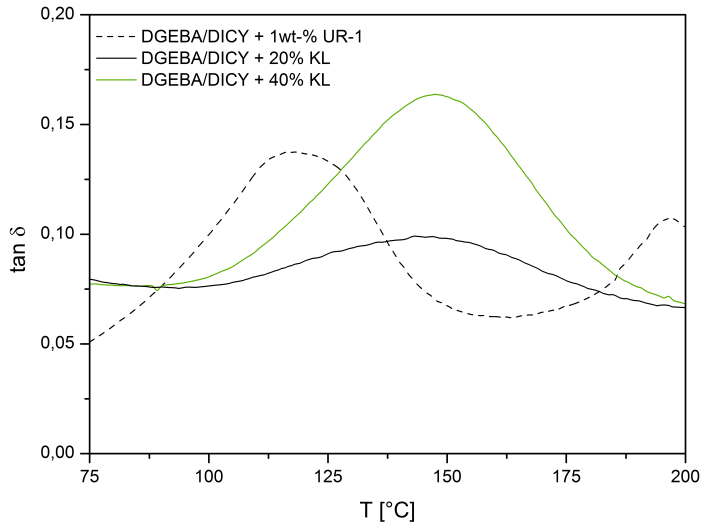

Figure 9.6.: Comparison of the loss factor $\tan\delta$ of the neat DGEBA/DICY/UR-1 sample with the lignin filled samples.

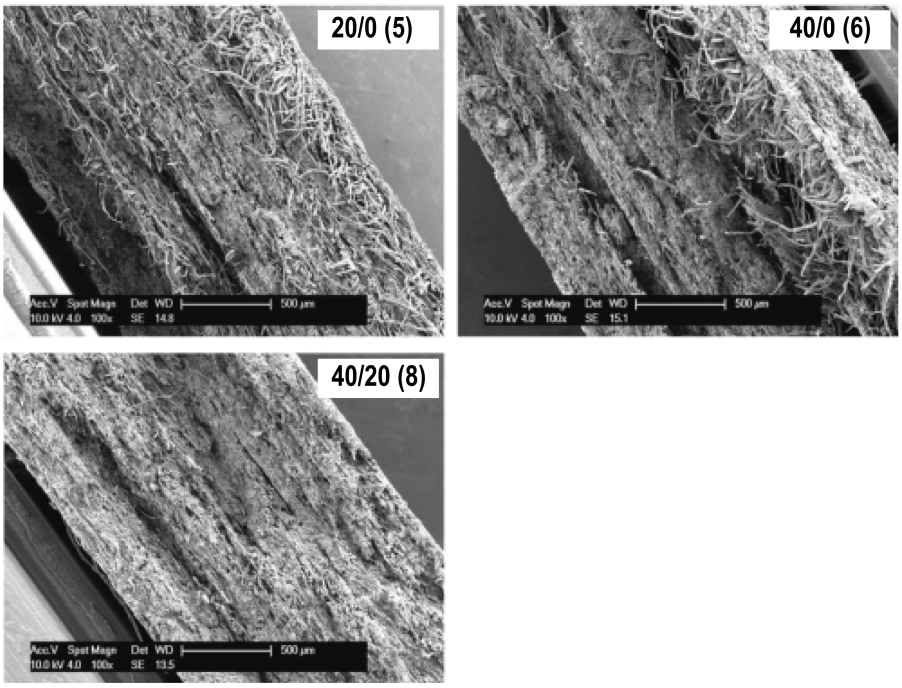

Figure 9.7.: SEM micrographs of the manufactured lignin filled FRP samples with lignin/paper ratio of 20/0 (5), 40/0 (6) and 40/20 (8) revealing fiber pull–out. This results from low tensile strength which is caused by insufficient transmission throughout the total fiber length and poor fiber–resin adhesion.

9.3 Mechanical Characterization of Glass Fiber Reinforced Composites

The previous section discussed the reinforcement of cellulose sheets with the developed kraft lignin filled epoxy resin. It could be seen that the release of moisture during the manufacturing process became a huge challenge resulting in poor material properties. To evaluate the properties of the developed epoxy resin itself, FRPs with commercially used glass fiber sheets were manufactured to decrease moisture content from the cellulose fibers. The design of experiments is shown in Table 9.5.

This test series investigates the developed resin with 20 % and 40 % lignin share and compares to two references with and without accelerator. The non–accelerated neat epoxy resin was included to determine the potential of time saving during processing of the kraft lignin accelerated resin. The manufacturing was carried out according to the paper reinforced composites with random laid glass fiber mats. An example of the kraft lignin filled GFC is shown in Figure 9.8.

Figure 9.9 shows the resulting tensile strength and Young's modulus of the manufactured FRPs. The tensile strength of the samples 1–3 and 5–7 is around 160 — 170 MPa and shows no significant differences.

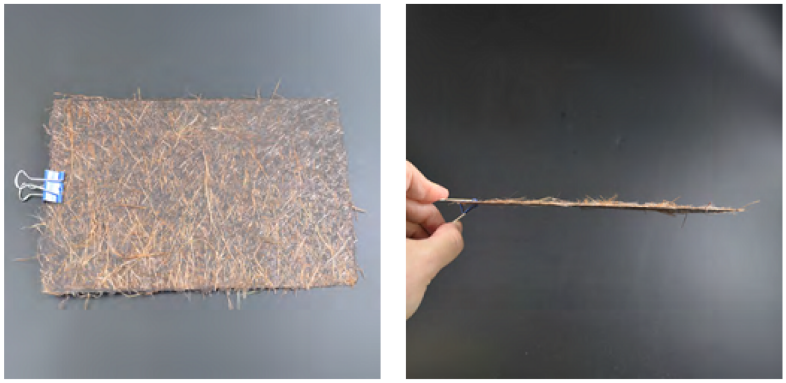

Figure 9.8.: GRP manufactured with the developed kraft lignin filled DGEBA/DICY resin.

Table 9.5.: Design of experiments executed for optimization and characterization of the glass fiber reinforced composite material.

Sample	KL resin [wt-%]	Acc [wt-%]	t_c [min]	T_C [min]
1	20	0	2	180
2	40	0	2	180
3	0	1	2	180
4	0	0	2	180
5	20	0	4	180
6	40	0	4	180
7	0	1	4	180
8	0	0	4	180
9	20	0	8	180
10	40	0	8	180
11	0	1	8	180
12	0	0	8	180

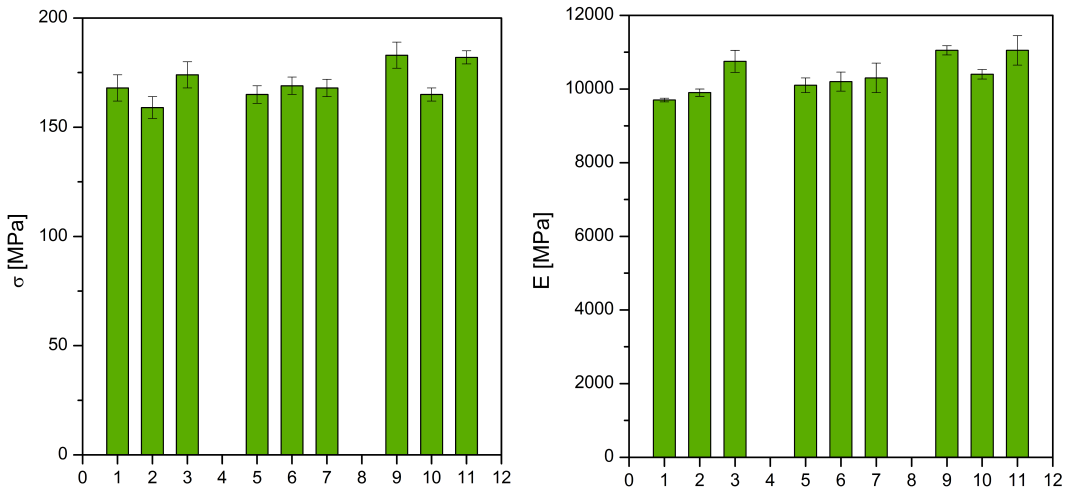

Figure 9.9.: Tensile strength (left) and Young's modulus (right) of the developed glass–fiber reinforced composite materials. Mechanical properties of the manufactured glass fiber FRPs. Samples 1 – 3 were cured at 180 °C for 2 min with 20 % (1), 40 % (2) and 0 % (3) kraft lignin content. Samples 5 – 7 were cured at 180 °C for 4 min with 20 % (5), 40 % (6) and 0 % (7) kraft lignin content. Samples 9 – 11 were cured at 180 °C for 8 min with 20 % (9), 40 % (10) and 0 % (11) kraft lignin content. Samples 3, 7 and 11 containing 0 % kraft lignin contained 1 % accelerator as references.

However, sample 9 shows a pronounced value of 185 MPa. An increase of the stiffness of the samples containing 20 % kraft lignin (samples 1, 5, 9) with extended curing time is obvious. The same pattern is recognizable with 40 % lignin share (samples 2, 6, 10).

Interestingly, the neat epoxy resin with no accelerator added, shows at curing times of 2 and 4 minutes no curing and at 8 minutes solely a lower level of curing compared to the lignin containing samples.

Unlike paper fibers, glass fibers are able to conduct the heat throughout the material which contributes to the curing process. During manufacturing the different amount of kraft lignin showed no difference in the preparation of the FRPs as well as in the curing behavior. These experiments showed that the lignin filled epoxy resin has proved to be a feasible alternative to typical epoxy resins with consistent mechanical properties compared to reference samples.

The potential as accelerator regarding the process efficiency is tremendous. The unmodified resin showed complete curing only after 20 min hence the time saving is around 18 min which corresponds to a reduction of 90 %.

Figure 9.10a shows the results of the DMTA measurements to determine the storage and loss modulus G'/G''. The storage modulus G' is less pronounced in the lignin samples than in the neat epoxy resin ones. However, the peak maximum is higher which makes the kraft lignin filled resin less sensible to temperature changes due to the higher cross–linking density. This is confirmed through the glass transition temperature of the neat FRP which is distinctively lower than the kraft lignin filled FRP. The single glass transition proves a homogeneous phase morphology with no filter effect of the glass fiber sheets as well.

Figure 9.10b shows the calculation of the loss factor $\tan\delta$. The loss factor of the 20 % kraft lignin filled FRP of 0.1 at 115 °C shows an increased stiffness compared to the neat FRP with a value of 0.28. The higher solid content in the sample containing 40 % kraft lignin results in an increased dissipation

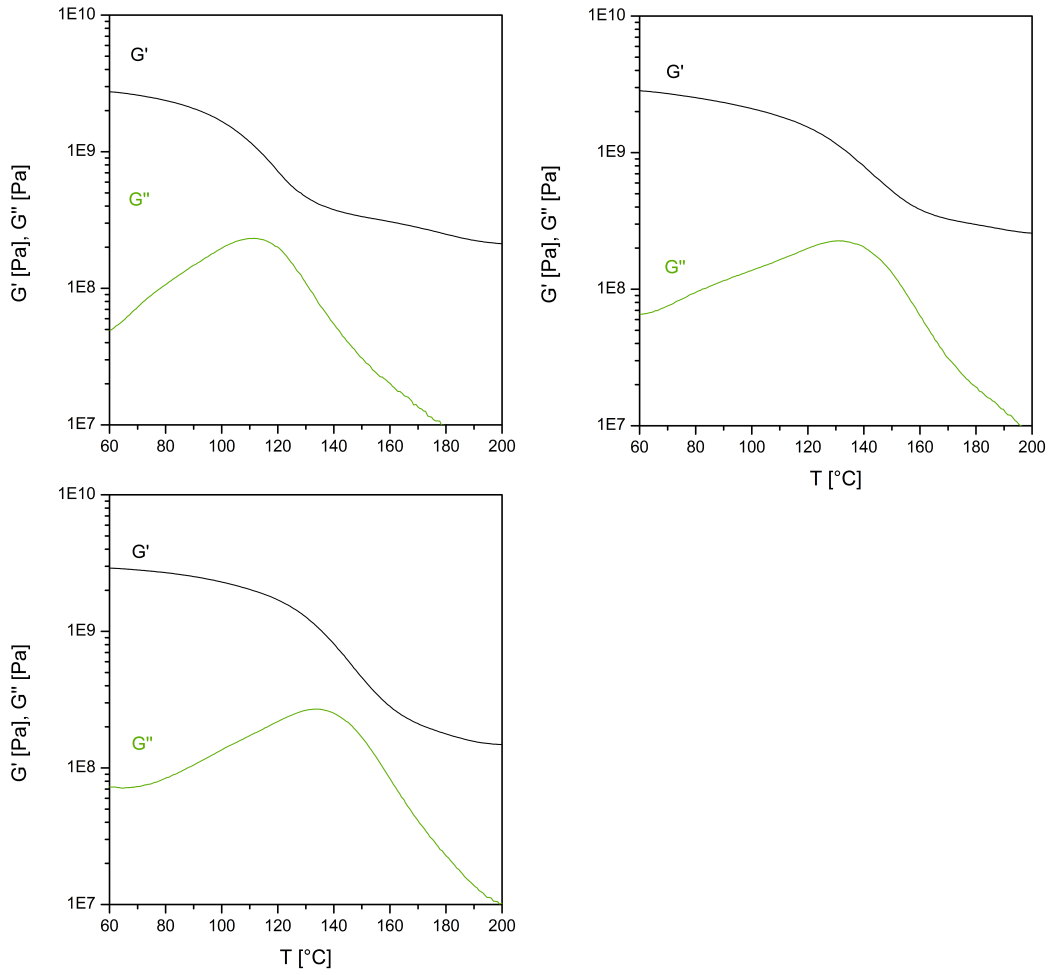

(a) DMTA results for the storage modulus G' and loss modulus G'' for FRP samples without kraft lignin (top left), 20 % kraft lignin (top right) and 40 % kraft lignin (bottom).

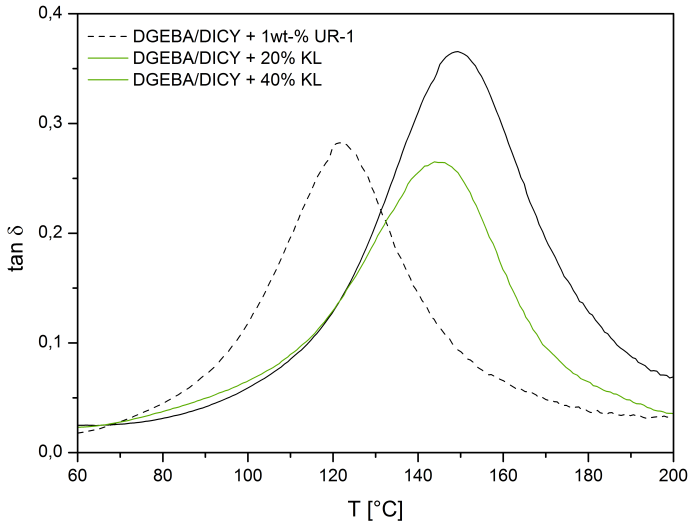

(b) Comparison of the loss factor tan δ of the neat epoxy resin and with lignin loads of 20 % and 40 %.

Figure 9.10.

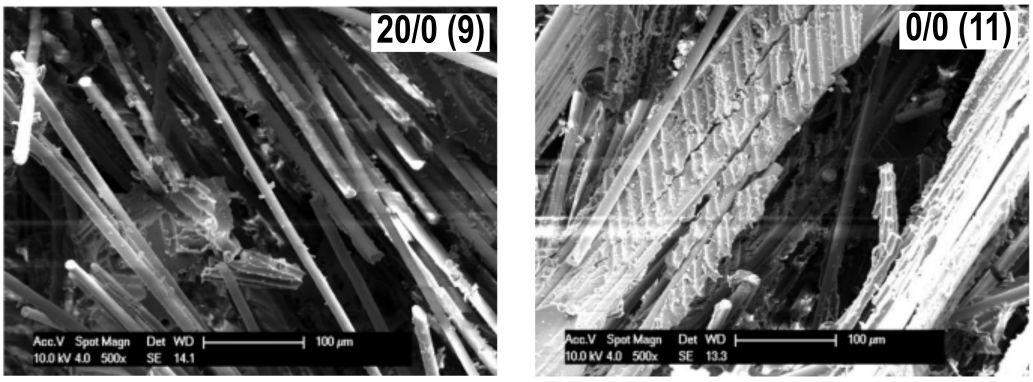

Figure 9.11.: SEM micrographs of the manufactured glass fiber reinforced polymers with lignin/paper ratio of 20/0 (9) compared to the neat sample (11) which shows in both cases a low degree of adhesion due to bare fibers.

energy which raises the loss factor. By means of peak width, an increased damping behavior is evident for the 40 % kraft ligin FRP along with a larger loss of stiffness compared to 20 % kraft lignin. Significant differences of the peak maxima are obvious resulting of different pronounced glass transition temperatures and therefore the storage modulus G'. The measurements showed that the storage modulus of the neat FRP decreases early compared to the lignin FRPs resulting in an earlier drop in stiffness for the neat FRP.

SEM micrographs of sample 9 with 20 % kraft lignin and the neat FRP sample 11 of the breaking edges reveal that in both cases a low degree of adhesion is achieved due to bare fibers. No further significant differences in quality are visible. Generally, it can be assumed that optimal fiber adhesion is achieved in neither specimen. This shows that kraft lignin has in general no impairing influence towards the matrix.

9.4 Conclusion

It could be shown that kraft lignin offers an incentive as filler as well as an active component in an epoxy resin formulation for the manufacturing of FRPs. As a feasible accelerator kraft lignin offers the same effect on the curing behavior as commercial available accelerators at a much lower price. It has been proven that the newly developed kraft lignin based epoxy resin can be used with traditional glass fiber reinforced composites as well as renewable biocomposites with cellulose as fiber material. This makes also an attractive economical advantage with $350-730$ € per ton of kraft lignin (depending on form) compared to almost 14 000 € for commercial accelerators for epoxy systems.[155] Further, the epoxy resin includes 20 – 40 % kraft lignin which contributes to further price savings. Even with 1 – 4 % accelerator content compared to 20 – 40 % kraft lignin, using kraft lignin is often profitable.

Assuming a price of 730 € per ton for kraft lignin, production of a ton of the epoxy resin with the use of 20 % kraft lignin (i. e. 200 kg) or 40 % kraft lignin (i. e. 400 kg) costs 146 € and 292 € respectively. In contrast, the use of 1 % accelerator (i. e. 10 kg) costs 1440 €. This yields savings of around 1000 € per ton. Moreover, further investigations regarding kraft lignin as inactive filler a price comparison with competing fillers is useful.

10 Summary and Outlook

Within this work,various types of kraft lignin have been analyzed chemically as well as thermally. Spectroscopic methods such as NMR and IR spectroscopy proved to be feasible methods for the characterization of the molecular structure. By phosphitylation of lignin with TMDP it was possible to determine the OH–content of lignin through 31^P–NMR measurements which is an important parameter for the reactivity of lignin with epoxy resin compounds. Thermal analysis such as DSC and TGA were carried out to study general properties like moisture content, glass transition temperatures and decomposition temperatures. These properties are important since they later determine the kind of epoxy resin used as well as the properties of the final FRP. It was shown that the glass transition temperature correlates strongly with the molecular weight of lignin, by which an increasing molecular weight in a higher T_g results.

DSC measurements and moisture uptake measurements revealed the hygroscopic nature of lignin. This means, that the moisture content of lignin has to be taken into account during the assembly and processing of the final FRP. TGA measurements showed the high thermal stability of the different types of lignins which is slightly different due to their extraction method. Further, from TGA it can be concluded that lignin is processable at high curing temperatures up to 350 °C.

Due to large-scale pulping of wood and the extraction of lignin, inconsistencies with regard to the glass transition temperature between different batches of lignin became visible. This could lead to different miscibilities, cross–linking densities as well as mechanical properties in the final FRP. Therefore, three different pretreatment methods, dialysis, ultrafiltration and solvent extraction, were analyzed in terms of their feasibility of the removal of inhomogeneities. Dialysis proved to be the method of choice with regard to size exclude undesired molecular weight fractions. However, dialysis failed to remove undesired inorganic components and it was shown with elemental analysis, that solvent extraction led to a reduction of the sulfur content below 2 %.

After the first characterization and investigations of pretreatment techniques, the behavior of kraft lignin within the epoxy resin was investigated. Therefore, a commercially available 2–component epoxy formulation, which is typically used in the targeted application, was used to narrow down fundamental parameters. DSC measurements were carried out to determine ideal curing temperatures and the influence of different loads of lignin on the phase morphology.

Tensile tests were performed to determine mechanical parameters such as Young's modulus, tensile strength and strain. Therefore, a teflon mould was designed for simple casting of test specimens. As a result, it was revealed that KL_1 shows the most positive influence on the epoxy formulation compared to other types of lignin leading to good mechanical properties by increasing the Young's modulus by 15 %. The investigations of different loads of lignin showed that up to a lignin content to 40 % resulted in a good dispersability without larger aggregations with is an important factor for the processability and hence the mechanical stability as well.

By introducing an acetylated ligin into the commercial resin, the effect of an unpolar modified lignin could be investigated. Those tests revealed, that the polarity of the filler lignin is a crucial factor for good dispersability and therefore the homogeneity in the epoxy resin. As a result, KL_1 was selected as the most suitable lignin for the application in a FRP and was used throughout the remaining work.

Due to the complexity of an already formulated epoxy system it proved to be difficult to investigate the behavior of lignin with both the epoxy resin and curing agent. Therefore, the complexity was reduced to the formulation's basic educts: the DGEBA resin and curing agent. A low molecular weight DGEBA–based epoxy resin and two amino–based curing agents (IPDA and DETA) were chosen as a starting point for the development of a new biobased epoxy resin. Preliminary solubility experiments showed that kraft lignin is partially soluble with DGEBA resulting in finely dispersed lignin in the DGEBA resin.

Interestingly, the addition of DETA in the presence of lignin led to an initial exothermic reaction with an immediate agglomeration of the mixture whereas IPDA showed a very good solubility of the lignin. This experiments gave evidence, that kraft lignin causes a possible side reaction with either DGEBA or DETA and might accelerate the reaction between those components. This assumption was investigated with DSC measurements which was confirmed with regard to the calculated enthalpy and the resulting glass transition temperatures. This incompatibility and strongly limited processability with regard to the final FRP of lignin with DETA led to the exclusion of the curing agent DETA from further mechanical investigations.

However, with the system DGEBA/IPDA could be shown that kraft lignin has a tremendous effect on the cross–linking reaction. Dynamic and isothermal DSC measurements proved that kraft lignin shows an accelerating effect as well as the participation of lignin in the cross–linking mechanism. Therefore the Kamal–Sourour model for amino–cured epoxy resins has been successfully adopted for lignin filled epoxy resins. Curing parameters such as both rate constants, reaction orders as well as activation energies have been determined which proved lignins accelerating features further.

Mechanical investigations in cooperation with Fraunhofer Institute for Structural Durability and System Reliability LBF as well as the department of Paper Technology and Mechanical Process Engineering PMV of the processed material have revealed that a composite build with a two component epoxy formulation does not result in the mechanical properties as well as processability desired for the aspirated production area. Therefore a one component DGEBA system was developed using the solid curing agent DICY to improve the system towards prolonged pot and shelf life which makes applications such as preimpregnated fibers (prepregs) possible.

It could be shown that kraft lignin shows an even more dramatic accelerating behavior with the one component system which makes it comparable to commercially used accelerators. The applicability of the developed kraft lignin based epoxy resin was tested with glass fiber mats as well as cellulose fiber mats for increased bioshare. It has been shown that with consistent properties compared to neat FRPs the kraft lignin filled FRP showed complete curing after 2 min whereas the neat FRP showed complete curing after a time span of 20 min which corresponds to a total reduction of 90 %.

Economical considerations revealed that with a 40 % kraft lignin share savings of around 1000 € per ton can be achieved which makes lignin a relevant competitor towards commercially available accelerators and filler.

Within this work kraft lignin was successfully introduced into a new value chain of a cellulose based fiber reinforced polymer. Figure 10.1 shows the actual newly developed biobased kraft lignin filled epoxy formulation processed in a prototype of a bicycle seat manufactured at LBF. The bicycle seat stands not just for a successful development and collaboration of many fold expertise throughout the project it presents as well the starting point towards a commercial application.

Figure 10.1.: Paper fiber reinforced bicycle seat using the newly developed kraft lignin filled epoxy formulation manufactured at Fraunhofer LBF.

In the following the developed biobased epoxy resin has to be characterized according to common DIN and ISO norms to establish a basis for industrial manufacturers. Therefore, fundamental processing and characterization methods for epoxy resins have to be applied. Moreover, suitable fields of application have to be determined to further develop the resin formulation with regard to further additivation.

11 Zusammenfassung

Innerhalb dieser Arbeit wurden verschiedene Sorten an Lignin chemisch sowie thermisch analysiert. Spektroskopische Methoden wie z. B. NMR– und IR–Spektroskopie erwiesen sich als sehr gut geeignet zur Charakterisierung der Molekülstruktur. Durch die Phosphorelierung mit TMDP war es möglich die OH–Zahl der Lignine mittels ^{31}P–NMR zu Bestimmen, welche sich als sehr bedeutend für die Reaktivität der Lignine mit den Harzkomponenten herausgestellt hat.

Thermische Analysemethoden wie DSC und TGA wurden zur Bestimmung allgemeiner Eigenschaften wie Feuchtigkeitsgehalt, Glasübergangstemperatur und Zersetzungstemperatur der Lignine durchgeführt. Diese Eigenschaften sind sehr wichtig, da sie die Auswahl des Epoxidharzes einschränken und die Eigenschaften des resultierenden FRP bestimmen. Es wurde gezeigt, dass die Glasübergangstemperatur stark mit den Molekulargewichten der Lignine korreliert, wodurch durch Zunahme des Molekulargewichts eine höhere Glasüberganstemperatur folgt. DSC Messungen und Messungen zur Feuchtigkeitsaufnahme zeigten die hygroskope Natur des Lignins. Dies bedeutet, dass der hohe Wassergehalt des Lignins bei dem Bau und der Verarbeitung des Composite–Materials berücksichtigt werden muss. TGA Messungen zeigten die hohe thermische Stabilität der verschiedenen Ligninsorten, welche sich lediglich leicht durch die verschiedenen Extraktionsprozesse der Lignine unterschieden. Mittels der TGA konnte gezeigt werden, dass hohe Aushärtetemperaturen bis zu 350 °C mit Lignin als Füllmaterial leicht realisierbar sind.

Durch den großtechnischen Papieraufschlussprozess und der daraus folgenden Extraktion des Lignins entsteht eine Inkonsistenz verschiedener Lignin–Chargen im Bezug auf die Glasübergangstemperatur. Dies ist unerwünscht, da es zu verschiedenen Verhalten in der Mischbarkeit, sowie einer anderen Vernetzungsdichte und daraus folgend zu unterschiedlichen mechanischen Eigenschaften im gebauten FRP kommen kann. Daher wurden verschiedene Methoden zur Vorbehandlung des Lignins untersucht, um diese Inhomogenitäten und Unreinheiten zu entfernen. Als Aufreinigungsmethoden wurden Dialyse, Ultrafiltration und Lösungsmittel–Extraktion gewählt. Dialyse zeigte sich als Mittel der Wahl, um störende niedermolekulare Fraktionen des Lignins über Größenauschluss abzutrennen. Jedoch konnten mittels Dialyse nicht die unerwünschten anorganischen Substanzen wie beispielsweise Schwefel abgetrennt werden. Mit der Lösungsmittel–Extraktion hingegen, konnte der Schwefelgehalt auf unter 2 % reduziert werden.

Nach der Charakterisierung und der Anwendung verschiedener Vorbehandlungsmethoden, konnte anschließend das Verhalten der Lignine in Epoxidharz untersucht werden. Für erste Untersuchungen wurde ein kommerziell verfügbares 2–Komponenten Epoxidharz–System gewählt, welches auch üblicherweise bei Composite–Anwendungen genutzt wird. DSC Experimente wurden genutzt um eine ideale Aushärtungstemperatur zu wählen und um den Einfluss verschiedener Lignin–Gehalte auf die Phasenmorphologie im Epoxidharz zu untersuchen. Zug–Dehnungs–Messungen wurden durchgeführt, um mechanische Parameter wie das Elastizitäts–Modul, Zugfestigkeit und Bruchdehnung zu ermitteln. Dazu wurde eine Teflonform konstruiert, um Probekörper zu gießen. Es konnte gezeigt werden, dass das Kraft Lignin KL_1 im Vergleich zu den anderen vorliegenden Ligninsorten die besten mechanischen Eigenschaften zeigte. Somit konnte das Elastizitäts–Modul, als Kenngröße der Steifigkeit eines Polymeren, um 15 % verbessert werden. Weiterhin zeigte sich, dass ein Lignin–Gehalt bis zu 40 % eine gute Dispergierbarkeit ohne große

Lignin–Agglomerate im Harz zeigte. Dies ist ein ausgesprochen wichtiger Faktor bei der Verarbeitbarkeit und der daraus resultierenden mechanischen Stabilität.

Durch das Einbringen des unpolar–modifizierten acetylierten Lignins konnte außerdem ein Vergleich zu den typischerweise polaren Ligninen gezogen werden. Das Verarbeiten des unpolaren acetylierten Lignins in der polare Epoxidharz–Formulierung war nahezu unmöglich, da weder eine gute Löslichkeit noch Dispergierbarkeit erzielt wurde. Demnach ist die Polarität des Füllstoffes im Epoxidharz ein kritischer Faktor der berücksichtigt werden muss.

Durch diese Untersuchungen mit verschiedenen Sorten von Lignin in einem kommerziellen 2–Komponenten Epoxidharz–System resultierte, dass das Kraft Lignin KL_1, zum einen durch die erzielten mechanischen und thermischen Eigenschaften, zum anderen durch die gute Verfügbarkeit zu dem am besten geeigneten Lignin für die Anwendung innerhalb eines FRP ausgewählt wurde. Somit wurde in Verbindung mit der Verarbeitung und des Baus eines FRP ausschließlich KL_1 genutzt.

Durch die Komplexität eines vor–formulierten 2–Komponenten Epoxidharz–Systems, welches generell noch Additive wie Beschleuniger, Reaktionsverdünner und Pigmente enthält, war es schwierig den Einfluss des Lignins auf die einzelnen Bestandteile der Formulierung zu untersuchen. Demnach wurden lediglich die Grundbausteine der Harzformulierung gewählt: das Harz und der Härter. Ein niedermolekulares DGEBA–Harz in der Kombination mit zwei amin–basierten Härtern (IPDA und DETA) wurden als Ausgangspunkt zur Entwicklung des neuen biobasierten Epoxidharzes gewählt. Vorausgehende Löslichkeitstests zeigten, dass das Kraft Lignin sehr gut im Epoxidharz dispergierbar ist und das niedermolekulare Fraktionen des Kraft Lignins im Epoxidharz in Lösung gehen. Interessanterweise stellte sich heraus, dass die Zugabe von DETA zu dem Harz/DETA–Gemisch zu einer sofortigen exothermen Reaktion führt welche mit einer Agglomeration des Lignins einhergeht. Im Vergleich dazu zeigte IPDA sehr gute Ergebnisse in der Löslichkeit des Lignins. Es zeigte sich, dass Kraft Lignin in der Aushärtungsreaktion zwischen DGEBA und DETA eingreifen muss und zur Beschleunigung dieser Reaktion führt. Diese Vermutungen wurden mit DSC Messungen überprüft, welche durch die Berechnung der Reaktionsenthalpien und der Betrachtung der Glasübergangstemperaturen diese Beobachtungen bestätigten. Durch die Unverträglichkeit der Harz/Lignin–Mischung mit DETA, welche zu einer stark beschränkten Verarbeitbarkeit zum FRP resultierend in unzureichenden mechanischen Eigenschaften führt, wurde DETA als Härter ausgeschlossen.

Jedoch konnte gezeigt werden, dass Lignin auf die Vernetzungsreaktion des DGEBA/IPDA–Systems einen enormen Effekt hat. Dynamische und isotherme DSC Messungen bewiesen den beschleunigenden Effekt und die Teilnahme des Lignins in der Vernetzungsreaktion. Dazu wurde das kinetische Modell von Kamal–Sourour erfolgreich für das vorliegende System adaptiert. Daraus konnten die Geschwindigkeitskonstanten, Reaktionsordnungen sowie die Aktivierungsenergien errechnet werden.

Die Realisierbarkeit des biobasierten Lignin–Epoxidharzes wurde in Kooperation mit dem Fraunhofer–Institut für Betriebsfestigkeit und Systemzuverlässigkeit LBF und dem Fachgebiet Papierfabrikation und Mechanische Verfahrenstechnik der TU Darmstadt getestet. Es zeigte sich, dass die Verarbeitung mit einem 2–Komponenten Epoxidharz–Systems für ein Papierfaser–verstärktes Composite–Material in Betracht der Verarbeitung ungeeignet ist. Dies ergab, dass ein 1–Komponenten–System mit dem festen Härter DICY entwickelt wurde um Faktoren wie Verarbeitungszeigt und Haltbarkeit, welche wichtige Parameter für Composite aus dem Prepreg–Verfahren sind, zu erzielen.

Abbildung 11.1.: Faserverstärkter Fahrradsattel bestehend aus der neu–entwickelten Lignin–basierten Epoxidharz–Formulierung. Hergestellt am Fraunhofer LBF.

Mit dem neuen 1–Komponenten System konnte gezeigt werden, dass Lignin innerhalb des DGEBA/DICY–Systems noch einen viel dramatischeren Einfluss auf die Aushärtereaktion hat. So konnte gezeigt werden, dass Kraft Lignin in seiner beschleunigenden Wirkung vergleichbar zu handelsüblichen Beschleunigern ist. Die Verarbeitung wurde mit Papierfasern sowie mit Glasfasermatten getestet. Es zeigte sich, dass bei gleichbleibenden mechanischen Eigenschaften (verglichen zu FRPs ohne Lignin) eine vollständige Aushärtung bereits nach 2 Minuten erfolgte, welches eine Verringerung der Reaktionszeit um 90 % entspricht.

Ökonomisch Betrachtet ergab sich, dass ein Kraft Lignin–Anteil von 40 % zu Preiseinsparungen von ca. 1000 € pro Tonne führen kann, welches Lignin ein relevantes Konkurrenzprodukt zu kommerziell verfügbaren Beschleunigern und Füllstoffen macht.

Innerhalb dieser Arbeit konnte gezeigt werden, dass Kraft Lignin erfolgreich in eine neue Wertschöpfungskette von faserverstärkten Polymeren eingebracht werden konnte. Abbildung 11.1 zeigt die neu entwickelte Lignin–Harz–Formulierung welche in Kooperation mit dem LBF zu einem Fahrradsattel verarbeitet wurde. Dieser Fahrradsattel steht nicht nur für eine erfolgreiche Entwicklungs– und Kollaborationsarbeit vielfältiger Expertise im durchgeführten Projekt, sondern markiert auch den Startpunkt der entwickelten Materialien in Richtung der Kommerzialisierbarkeit.

12 Experimental

12.1 Chemicals

All types of lignin were kindly supplied by UPM-Kymmene. The used epoxy resins and reactive diluents were obtained from Leuna Harze and R and G Faserverbundwerkstoffe GmbH. The curing agents DETA and IPDA as well the imidazole-based accelerators were obtained from Fisher Scientific. DICY and the urone-based accelerators were kindly supplied by AlzChem AG. Organic solvents and further chemicals were obtained from Acros, Fisher Scientific, ABCR and Sigma Aldrich and used without further purification. For NMR measurements deuterated solvents were obtained from the department of NMR at the TU Darmstadt and originate from euriso-top.

12.2 Characterization Methods and Devices

For the determination of analytical data the following devices and methods were used:

Dynamic scanning calorimetry (DSC)

Studies on curing kinetics of epoxy resin were carried out using differential scanning calorimeter (DSC1, Mettler Toledo). Resin and agents were mixed at a stoichiometric epoxide/amine ratio at room temperature, respectively. For dynamic DSC scans, samples (5–30 mg) were sealed in aluminum pans, and heated up to from room temperature at rates of 5 °C/min, 10 °C/min, 15 °C/min and 20 °C/min, respectively. For isothermal curing the prepared samples were introduced into the DSC chamber at the requested temperature and measured at constant temperature of90 °C, 120 °C and 150 °C, respectively. Thermal equilibrium was regained within 1 min of sample insertion, and the exothermic reaction was considered to be complete when the recorder signal leveled off to the baseline. The final baseline was extrapolated to determine the total area under the exothermic curve and the heat of curing. In both cases, nitrogen was purged at rate of 20 mL to minimize oxidation of the sample during the curing. For evaluation each samples was normalized. Before the curing of the samples, two standard materials, indium (99.999% pure) and zinc (99.999% pure), were used to calibrate the temperature and energy axis of the DSC device.

Thermogravimetric analysis (TGA)

TGA measurements were carried out using a thermogravimetric analysis device TGA1 from Mettler Toledo under nitrogen atmosphere with 10 °C/min from $25 - 500$ °C.

Nuclear magnetic resonance spectroscopy (NMR)

NMR measurements were carried out on either 300 (Avance-II/-III, Bruker BioSpin) or 600 MHz spectrometer (DRX 500, Bruker BioSpin). Chemical shifts are shown in parts per million (ppm). Proton signals are relative to tetramethylsilane (TMS) with $\delta = 0$ ppm used as external standard.

Fourier Transformation Infrared spectroscopy (FT–IR)

Fourier transform infrared (FT–IR) spectra were carried out on a Perkin Elmer Instruments Systems One FT–IR spectrometer, coupled to an universal attenuated total reflectance (UATR) unit. Ten scans were registered per spectrum with a resolution of 4 cm^{-1} between wavenumbers of 4000 cm^{-1} and 650 cm^{-1}. The software Spectrum by Perkin Elmer was used for operating the spectrometer and evaluation of recored spectra.

Mass spectroscopy (MS)

EI mass spectra were carried out on Finnigan MAT 95 spectrometer with EI ionization.

Elemental analysis (EA)

Elemental analysis was carried out at Analytische Laboratorien GmbH.

Tensile tests

Tensile tests were carried out on ZwickiLine (BT1 FR2.5TH.D14, Zwick/Roell) with a load cell of 5 kN at room temperature. Evaluation of the results were carried out in textXpert II.

Dynamic mechanical thermal analysis (DMTA)

DMTA measurements were conducted at Fraunhofer LBF.

Scanning electron microscopy (SEM)

SEM micrographs were recorded using a high-resolution scanning electron microscope (HR-SEM) Philips XL30 FEG.

Bibliography

[1] Jari Vartiainen, Mika Vähä-Nissi, and Ali Harlin. Biopolymer films and coatings in packaging applications - a review of recent developments. *Materials Sciences and Applications*, 5(10), 2014.

[2] Ruben Vanholme, Kris Morreel, John Ralph, and Wout Boerjan. Lignin engineering. *Current Opinion in Plant Biology*, 11(3):278 – 285, 2008. Physiology and Metabolism - Edited by Markus Pauly and Kenneth Keegstra.

[3] W. Thielemans, E. Can, S.S. Morye, and R.P. Wool. Novel applications of lignin in composite materials. *Journal of Applied Polymer Science*, 83(2):323–331, 2002.

[4] M. Mngomezulu, M. J. John, V. Jacobs, and Adriaan S. Luyt. Review on flammability of biofibres and biocomposites. *Carbohydrate Polymers*, 111:149–182, 2011.

[5] Bundesministerium für Ernährung Landwirtschaft und Verbraucherschutz BMELV. Neue produkte: Aus natur gemacht; nachwachsende rohstoffe im alltag. *Neue Produkte: Aus Natur gemacht; Nachwachsende Rohstoffe im Alltag*, 2013.

[6] M. Weyrich. Technologien der fertigungsautomatisierung - ausgewählten forschungsthemen der industriellen anwendung. *Technologien der Fertigungsautomatisierung - Ausgewählten Forschungsthemen der industriellen Anwendung*, 2013.

[7] Ruxanda Bodirlau, Carmen-Alice Teaca, and Iuliana Spiridon. Influence of natural fillers on the properties of starch-based biocomposite films. *Composites Part B: Engineering*, 44(1):575–583, 2013.

[8] J. Sarkia, S.B. Hassana, V.S. Aigbodiona, and J.E. Oghenevwetaa. Potential of using coconut shell particle fillers in eco-composite materials. *Journal of Alloys and Compounds*, 509(5):2381–2385, 2011.

[9] Manju Kumari Thakurb Vijay Kumar Thakura and Raju. Review: Raw natural fiber-based polymer composites. *International Journal of Polymer Analysis and Characterization*, 19(3), 2014.

[10] R. Whetten and R. Sederoff. Lignin biosynthesis. *Plant Cell*, 7(7):1001–1013, 1995.

[11] Lucas Montero de Espinosa and Michael A. R. Meier. Plant oils: The perfect renewable resource for polymer science?! *European Polymer Journal*, 47(5), 2011.

[12] Erich Adler. Lignin chemistry: past, present and future. *Wood Science and Technology*, 11(3):169–218, 1977.

[13] Wout Boerjan, John Ralph, and Marie Baucher. Lignin biosynthesis. *Annual Review of Plant Biology*, 54(1):519–546, 2003. PMID: 14503002.

[14] Hyoe Hatakeyama and Tatsuko Hatakeyama. Lignin structure, properties, and applications. In Akihiro Abe, Karel Dusek, and Shiro Kobayashi, editors, *Biopolymers*, volume 232 of *Advances in Polymer Science*, pages 1–63. Springer Berlin Heidelberg, 2010.

[15] Timothy D.H. Bugg and Rahman Rahmanpour. Enzymatic conversion of lignin into renewable chemicals. *Current Opinion in Chemical Biology*, 29:10–17, 2015.

[16] Francois-Xavier Collard and Joel Blin. A review on pyrolysis of biomass constituents: Mechanisms and composition of the products obtained from the conversion of cellulose, hemicelluloses and lignin. *Renewable and Sustainable Energy Reviews*, 38:594–608, 2014.

[17] Xiaopeng Yue, Fangeng Chen, and Xuesong Zhou. Improved interfacial bonding of pvc/wood-flour composites by lignin amine modification. *BioResources*, 6(2), 2011.

[18] Tatiana Dizhbite, Girts Zakis, Anna Kizima, Elena Lazareva, Galina Rossinskaya, Vilhelmina Jurkjane, Galina Telysheva, and Uldis Viesturs. Lignin as a useful bioresource for the production of sorption-active materials. *Bioresource Technology*, 67(3):221 – 228, 1999.

[19] Klaus Hofmann and Wolfgang G Glasser. Engineering plastics from lignin. 21.1synthesis and properties of epoxidized lignin-poly (propylene oxide) copolymers. *Journal of Wood Chemistry and Technology*, 13(1):73–95, 1993.

[20] William O.S. Doherty, Payam Mousavioun, and Christopher M. Fellows. Value-adding to cellulosic ethanol: Lignin polymers. *Industrial Crops and Products*, 33(2):259 – 276, 2011.

[21] S. Kubo and J.F. Kadla. Lignin-based carbon-fibers: Effect of synthetic polymer blending on fiber properties. *Journal of Polymers and the Environment*, 13, 2005.

[22] K. Lindgren, H. Persson, and G. Ziegler. Method of manufacturing a building panel and a building panel, January 15 2015. US Patent App. 14/321,288.

[23] L. Ziegler, H. Nägele, J. Pfitzer, and U. Pohsner. Thermoplastische verarbeitung von lignin. *Chemie Ingenieur Technik*, 86(9):1516–1517, 2014.

[24] H. Nägele, J. Pfitzer, L. Ziegler, E. Kauffmann, W. Eckl, and N. Eisenreich. *Lignin Matrix Composites from Natural Resources – ARBOFORM in Bio-Based Plastics: Materials and Applications*. John Wiley & Sons, Inc., 2013.

[25] E.R. Inone-Kauffmann. Arboform - a lignin-based thermoplastic. *International Sugar Journal*, 111(1321):10–11, 2009.

[26] Laura L. Kosbar, Jeffrey D. Gelorme, Robert M. Japp, and William T. Fotorny. Introducing biobased materials into the electronics industry. *Journal of Industrial Ecology*, 4(3):93–105, 2000.

[27] G. Scholz, J. Lohr, E. Windeisen, F. Tröger, and G. Wegener. Carbonization of hot-pressed arboform-mixtures. *European Journal of Wood Products*, 67:351–355, 2009.

[28] A. Hofenauer. *Development of specific wood based composites for the fabrication of silicon infiltrated silicon carbide ceramic*. PhD thesis, Fakultät Wissenschaftszentrum Weihenstephan, 2005.

[29] S. K. Nune, J. Jeon, L. Zhang, and J. Lutkenhaus. Controlling porosity in lignin-derived nanoporous carbon for supercapacitor applications. *ChemSusChem*, 8(3):409, 2015.

[30] J.-M. Raqueza, M. Deléglisea, and P. Krawczak M.-F. Lacrampea. Thermosetting (bio)materials derived from renewable resources: A critical review. *Progress in Polymer Science*, 35(4):487–509, 2010.

[31] Wim Thielemans and Richard P. Wool. Lignin esters for use in unsaturated thermosets: Lignin modification and solubility modeling. *Biomacromolecules*, 6(4):1895–1905, 2005. PMID: 16004426.

[32] W.G. Glasser, R.A. Northey, and T.P. Schultz. Lignin: historical, biological and materials perspectives. In *ACS symposium series*, 2000.

[33] Benjamin M. Wood, Stuart R. Coles, Steven Maggs, James Meredith, and Kerry Kirwan. Use of lignin as a compatibiliser in hemp/epoxy composites. *Composites Science and Technology*, 71(16):1804 – 1810, 2011.

[34] Wim Thielemans and Richard P. Wool. Butyrated kraft lignin as compatibilizing agent for natural fiber reinforced thermoset composites. *Composites Part A: Applied Science and Manufacturing*, 35(3):327 – 338, 2004. {AIChE} 2002.

[35] Binyuan Zhao, Gang Chen, Yu Liu, Keao Hu, and Renjie Wu. Synthesis of lignin base epoxy resin and its characterization. *Journal of Materials Science Letters*, 20(9):859–862, 2001.

[36] United Nations. *Report of the World Summit of Sustainable Development 2005*, volume A/RES/60/1. 2005.

[37] J. Pope, D. Annandale, and A. Morrison-Saunders. Conceptualising sustainability assessment. *Environmental Impact Assessment Review*, 24(6):595–616, 2004.

[38] Yan Lin and Shuzo Tanaka. Ethanol fermentation from biomass resources: current state and prospects. *Appl. Microbiol. Biotechnol.*, 69:627–642, 2006.

[39] Tomohiro Aso, Keiichi Koda, Satoshi Kubo, Tatsuhiko Yamada, Isamu Nakajima, and Yasumitsu Uraki. Preparation of novel lignin-based cement dispersants from isolated lignins. *Journal of Wood Chemistry and Technology*, 33(4), 2013.

[40] Yanlin Qin, Dongije Yang, Wenyuan Guo, and Xueqing Qiu. Investigation of grafted sulfonated alkali lignin polymer as dispersant in coal-water slurry. *Journal of Industrial and Engineering Chemistry*, 27:192–200, 2015.

[41] P. Estellé, S. Halefadl, and T. Maré. Lignin as dispersant for water-based carbon nanotubes nanofluids: Impact on viscosity and thermal conductivity. *International Communications in Heat and Mass Transfer*, 57:8–12, 2014.

[42] Vijay Kumar Thakur, Manju Kumari Thakur, Prasanth Raghavan, and Michael R. Kessler. Progress in green polymer composites from lignin for multifunctional applications: A review. *ACS Sustainable Chemistry & Engineering*, 2(5):1072–1092, 2014.

[43] Yuejun Pan and Jack N. Saddler. Effect of replacing polyol by organosolv and kraft lignin on the property and structure of rigid polyurethane foam. *Biotechnology and Biofuels*, 6(12), 2013.

[44] Yang Li and Arthur J. Ragauskas. Kraft lignin-based rigid polyurethane foam. *Journal of Wood Chemistry and Technology*, 32(3), 2012.

[45] Sanghamitra Sen, Shrada Patil, and Dimitris S. Argyropoulos. Thermal properties of lignin in copolymers, blends, and composites: a review. *Green Chemistry*, 2015.

[46] J.F. Kadla, S. Kubo, R.A. Vendetti, R.D. Gilbert, A.L. Compere, and W. Griffith. Lignin-based carbon fibers for composite fiber applications. *Carbon*, 40:2913–2920, 2002.

[47] Derek C. Waggoner, Hongmei Chen, Amanda S. Willoughby, and Patrick G. Hatcher. Formation of black carbon-like and alicyclic aliphatic compounds by hydroxyl radical initiated degradation of lignin. *Organic Geochemistry*, 82:69–76, 2015.

[48] Aymerick Eudes, Yan Liang, Prajakat Mitra, and Dominique Loqué. Lignin bioengineering. *Current Opinion in Biotechnology*, 26:189–198, 2014.

[49] Qiao Zhao and Richard A. Dixon. Transcriptional networks for lignin biosynthesis: more complex than we thought? *Trends in Plant Science*, 16(4):227–233, 2011.

[50] Alessandro Gandini. The irruption of polymers from renewable resources on the scene of macromolecular science and technology. *Green Chem.*, 13:1061–1083, 2011.

[51] Edward M. Rubin. Genomics of cellulosic biofuels. *Nature*, 454, 2008.

[52] K. Freudenberg. Beiträge zur erforschung des lignins. *Angewandte Chemie*, 68(16):508–512, 1956.

[53] Fadi S. Chakar and Arthur J. Ragauskas. Review of current and future softwood kraft lignin process chemistry. *Industrial Crops and Products*, 20(2):131 – 141, 2004. 6th International Lignin Institute conference.

[54] Charles H. Ludwig, Bernard J. Nist, and Joseph L. McCarthy. The high resolution nuclear magnetic resonance spectroscopy of protons in compounds related to lignin. *Journal of the American Chemical Society*, 86(6):1186–1196, 1964.

[55] Simon Sarkanen, David C. Teller, Edward Abramowski, and Joseph L. McCarthy. Lignin. 19. kraft lignin component conformation and associated complex configuration in aqueous alkaline solution. *Macromolecules*, 15(4):1098–1104, 1982.

[56] Wolfgang G. Glasser, Charlotte A. Barnett, Peter C. Muller, and Kyosti V. Sarkanen. The chemistry of several novel bioconversion lignins. *Journal of Agricultural and Food Chemistry*, 31(5):921–930, 1983.

[57] Wolfgang G. Glasser. Classification of lignin according to chemical and molecular structure. *Lignin: Historical, Biological, and Materials Perspectives*, 742:216–238, 2000.

[58] A. van Heningen. Converting a kraft pulp mill into an integrated forest biorefinery. *biorefining*, 107(6), 2006.

[59] S.P. Sadtler. Cellulose or wood fibre. *Journal of the Franklin Institute*, 133, 1892.

[60] George Tomlinson. Sulphite pulping process, July 24 1962. US Patent 3,046,182.

[61] George Tomlinson. Sulphite pulping process, June 4 1963. US Patent 3,092,535.

[62] A.K. Eaton, August 9 1870. US Patent 106,143.

[63] A.K. Eaton, September 26 1871. US Patent 119,224.

[64] Carl Ferdinand Dahl. Process of manufacturing cellulose from wood, April 15 1884. US Patent 296,935.

[65] Peder J. Kleppe. Kraft pulping. *Tappi Journal*, 53(1):35–47, 1970.

[66] Herbert Sixta and Gabriele Schild. A new generation kraft process. *Lenzinger Berichte*, 87:26–27, 2009.

[67] Héctor A. Ruiz, Denise S. Ruzene, Daniel P. Silva, Fernando F. Macieira da Silva, António A. Vicente, and José A. Teixera. Development and characterization of an environmentally friendly process sequence (autohydrolysis and organosolv) for wheat straw delignification. *Applied Biochemistry and Biotechnology*, 164:629–641, 2011.

[68] A. Berg, W. Janssen, S. Balle, deceased Rudolf G. Kunz, and W. Klein. Delignification of cellulosic raw materials using acetic acid, nitric acid and ozone, January 31 1995. US Patent 5,385,641.

[69] B. Saake, S. Lummitsch, R. Mormanee, R. Lehnen, and H.H. Nimz. Production of pulps using the formacell process. *Das Papier*, 49(10A):V1–V7, 1995.

[70] O. Jedicke, N. Eisenreich, and H. Dümpert. Aquasolv-process as a multifunctional process for isolated areas. *International Conference on New and Renewable Technologies for Sustainable Development*, 2002.

[71] R. Estermann and B. Schwarzwälder. Life cycle assessment of mater-bi bags for the collection of compostable waste. *COMPOSTO*, 1998.

[72] Lawrence T. Drzal Amar K. Mohanty, Manjusri Misra. *Natural Fibers, Biopolymers, and Biocomposites*. CRC Press, 2005.

[73] A. K. Mohantya, M. Misra, and L. T. Drzalc. Surface modifications of natural fibers and performance of the resulting biocomposites: An overview. *Composite Interfaces*, 8(5), 2001.

[74] L. H. Baekeland. The synthesis, constitution, and uses of bakelite. *Ind. Eng. Chem.*, 1(3):149–161, 1909.

[75] E. Ziegler and A. Zinke. Studien auf dem gebiete der phenol-harze. *European Journal of Lipid Science and Technology*, 52(10):588–592, 2006.

[76] A. Zinke, R. Kretz, E. Leggewie, and K. Hössinger. Zur kenntnis des härtungsprozesses von pheno-formaldehyd-harzen. *Monatshefte für Chemie und verwandte Teile anderer Wissenschaften*, 83(5):1213–1227, 1952.

[77] M.D. Lechner, K. Gehrke, and E.H. Nordmeier. *Makromolekulare Chemie: Ein Lehrbuch für Chemiker, Physiker, Materialwissenschaftler und Verfahrenstechniker*. Springer-Spektrum, 2009.

[78] Bernd Tieke. *Makromolekulare Chemie: Eine Einführung*. Wiley-VCH, 2014.

[79] Walter Brockmann. *Klebtechnik: Klebstoffe, Anwendungen und Verfahren*. Wiley-VCH, 2005.

[80] Gerd Habenicht. *Kleben: Grundlagen, Technologien, Anwendungen*. Springer-Verlag Berlin Heidelberg GmbH, 1996.

[81] Jan-Erik Ehlers, Nelson G. Rondan, Lam K. Huynh, Ha Pham, Maurice Marks, and Thanh N. Truong. Theoretical study on mechanisms of the epoxy–amine curing reaction. *Macromolecules*, 40(12):4370–4377, 2007.

[82] Qipeng Guo, editor. *Thermosets: Structure, properties and application*. Woodhead Publishing, 2012.

[83] M. Balasubramanian. *Composite Materials and Processing*. CRC Press Taylor & Francis Group, 2014.

[84] SwissComposite. Datasheet for aramid fibers. *www.swiss-composite.ch/pdf/I-Aramid.pdf*, 2015.

[85] `http://www.r-g.de/wiki/Datei:Schema_Handlaminat.jpg`. Accessed: 2016-03-14.

[86] George Marsh. Prepregs - raw material for high-performance composites. *Reinforced plastics*, 46(10):24–28, 2002.

[87] `https://www.hexion.com/epoxyphenoliccomposites/automotive/prepreg/`. Accessed: 2016-03-14.

[88] Patricia S.B. dos Santos, Xabier Erdocia, Darci A. Gatto, and Jalel Labidi. Characterisation of kraft lignin separated by gradient acid precipitation. *Industrial Crops and Products*, 55:149–154, 2014.

[89] Fangong Kong, Shoujuan Wang, Jacquelin T. Price, Mohan K.R. Konduri, and Pedram Fatehi. Water soluble kraft lignin–acrylic acid copolymer: synthesis and characterization. *Green Chemistry*, 17:4355–4366, 2015.

[90] Alessandro Granata and Dimitris S. Argyropoulos. 2-chloro-4,4,5,5-tetramethyl-1,3,2-dioxaphospholane, a reagent for the accurate determination of the uncondensed and condensed phenolic moieties in lignins. *J. Agric. Food Chem.*, 43(6):1538–1544, 1995.

[91] Nour-Eddine El Mansouri and Joan Salvado. Analytical methods for determining functional groups in various technical lignins. *Industrial Crops and Product*, 26:116–124, 2007.

[92] Carmen G. Boeriu, Dominique Bravo, Richard J.A. Gosselink, and Jan van Dam. Characterisation of structure-dependent functional properties of lignin with infrared spectroscopy. *Industrial Crops and Products*, 20:205–218, 2004.

[93] Mohd Asmadi, Haruo Kawamoto, and Shiro Saka. Gas- and solid/liquid-phase reactions during pyrolysis of softwood and hardwood lignins. *Journal of Analytical and Applied Pyrolysis*, 92(2):417–425, 2011.

[94] Yanqin Huang, Zhiguo Wei, Zejing Qiu, Xiuli Yin, and Chuangzhi Wu. Study on structure and pyrolysis behavior of lignin derived from corncob acid hydrolysis residue. *Journal of Analytical and Applied Pyrolysis*, 96:153–159, 2012.

[95] E. Jakab, O. Faix, F. Till, and T. Székely. Thermogravimetry/mass spectrometry study of six lignins within the scope of an international round robin test. *Journal of Analytical and Applied Pyrolysis*, 35(2):167–179, 1995.

[96] Yong-Chan Sun, Min Wang, and Runcang Sun. Towards an understanding of inhomogeneities in structure of lignin in green solvents biorefinery. part 1: fractionation and characterization of lignin. *ACS Sustainable Chem. Eng.*, 2015.

[97] Wenwen Fang, Marina Alekhina, Olga Ershova, Sami Heikkinnen, and Herbert Sixta. Purification and characterization of kraft lignin. *Holzforschung*, 2015.

[98] Hexion. Safety sheet laminating resin mgs l 285. *Safety Sheet Laminating resin MGS L 285*, 2006.

[99] Dorel Feldman, Dorina Banu, and Marwan Khoury. Epoxy lignin polyblends. iii. thermal properties and infrared analysis. *Journal of Applied Polymer Science*, 37(4):877–887, 1989.

[100] D. Feldman, D. Banu, C. Luchian, and J. Wang. Epoxy lignin polyblends: Correlation between polymer interaction and curing temperature. *Journal of Applied Polymer Science*, 42(5):1307–1318, 1991.

[101] D. Feldman, D. Banu, A. Natansohn, and J. Wang. Structure-properties relations of thermally cured epoxy lignin polyblends. *Journal of Applied Polymer Science*, 42(6):1537–1550, 1991.

[102] Bernd Wetzel, Frank Haupert, Klaus Friedrich, Ming Qui Zhang, and Min Zhi Rong. Impact and wear resistance of polymer nanocomposites at low filler content. *Polymer Engineering and Science*, 42(9), 2002.

[103] Bernd Wetzel, Frank Haupert, and Ming Qiu Zhang. Epoxy nanocomposites with high mechanical and tribological performance. *Composites Science and Technolog*, 63:2055–2067, 2003.

[104] J. Chen, A.J. Kinloch, S. Sprenger, and A.C. Taylor. The mechanical properties and toughening mechanisms of an epoxy polymer modified with polysiloxane-based core-shell particles. *Polymer*, 54:4276–4289, 2013.

[105] D.J. Bray, P. Dittanet, F.J. Guild, A.J. Kinloch, K. Masania, R.A. Pearson, and A.C. Taylor. The modelling of the toughening of epoxy polymers via silica nanoparticles: The effects of volume fraction and particle size. *Polymer*, 54(26):7022–7032, 2013.

[106] G. Giannakopoulos, K. Masania, and A. C. Taylor. Toughening of epoxy using core–shell particles. *Journal of Materials Science*, 46(2):327–338, 2011.

[107] M. Martin-Gallego, M.M. Bernal, M. Hernandez, R. Verdejo, and M.A. Lopez-Manchado. Comparison of filler percolation and mechanical properties in graphene and carbon nanotubes filled epoxy nanocomposites. *European Polymer Journal*, 49:1347–1353, 2013.

[108] L. Nielsen and R. Landel. *Mechanical properties of polymers and composites*. Marcel Decker, 1994.

[109] Peerapan Dittanet and Raymond A. Pearson. Effect of silica nanoparticle size on toughening mechanisms of filled epoxy. *Polymer*, 53(9):1890–1905, 2012.

[110] M.J. Zaini, M.Y.A. Fuad, Z. Ismail, M.S. Mansor, and J. Mustafah. The effect of filler content and size on the mechanical properties of polypropylene / oil palm wood flour composites. *Polymer International*, 40:51–55, 1996.

[111] Shao-Yun Fu, Xi-Qiao Feng, Bernd Lauke, and Yiu-Wing Mai. Effects of particle size, particle/matrix interface adhesion and particle loading on mechanical properties of particulate–polymer composites. *Composites: Part B Engineering*, 39:933–961, 2008.

[112] Young-Kuk Choia, Koh ichi Sugimotoa, Sung-Moo Songa, Yasuo Gotohb, Yutaka Ohkoshib, and Morinobu Endoa. Mechanical and physical properties of epoxy composites reinforced by vapor grown carbon nanofibers. *Carbon*, 43(10):2199–2208, 2005.

[113] J.B. Bai and A. Allaoui. Effect of the length and the aggregate size of mwnts on the improvement efficiency of the mechanical and electrical properties of nanocomposites—experimental investigation. *Composites Part A: Applied Science and Manufacturing*, 34(8):689–694, 2003.

[114] Elena Mazzon, Amelia Habas-Ulloa, and Jean-Pierre Habas. Lightweight rigid foams from highly reactive epoxy resins derived from vegetable oil for automotive applications. *European Polymer Journal*, 68, 2015.

[115] Huntsman. Technical bulletin deta. *Technical Bulletin DETA*, 2015.

[116] Merck Millipore. Safety data sheet isophorondiamine. *Safety Data Sheet Isophorondiamine*, 2010.

[117] Gerrit Hülder. Reaktionskinetik von verbundmörtelsystemen für tragende anwendungen im bauwesen. *Zeitschrift Kunststofftechnik*, 2010.

[118] S. Sourour and M.R. Kamal. Differential scanning calorimetry of epoxy cure - isothermal cure kinetics. *Thermochimica Acta*, 14(1â€“2):41 – 59, 1976.

[119] V.L Zvetkov. Comparative dsc kinetics of the reaction of dgeba with aromatic diamines i. non-isothermal kinetic study of the reaction of dgeba with m-phenylene diamine. *Polymer*, 42(16):6687 – 6697, 2001.

[120] Bejoy Francis, Geert Vanden Poel, Fabrice Posada, Gabriel Groeninckx, and Sabu Thomas. Cure kinetics and morphology of blends of epoxy resin with poly (ether ether ketone) containing pendant tertiary butyl groups. *Polymer*, 44:3687–3699, 2003.

[121] Mehdy Vafayan, Mohammad Hosain Beheshty, Mir Hamid Reza Ghoreishy, and Hossein Abedini. Advanced integral isoconversional analysis for evaluating and predicting the kinetic parameters of the curing reaction of epoxy prepreg. *Thermochimica Acta*, 557(0):37 – 43, 2013.

[122] Valery L. Zvetkov, Rumen K. Krastev, and Senen Paz-Abuin. Is the kamal's model appropriate in the study of the epoxy-amine addition kinetics? *Thermochimica Acta*, 505(1â€“2):47 – 52, 2010.

[123] V.L. Zvetkov and Veronica Calado. Comparative dsc kinetics of the reaction of dgeba with aromatic diamines. iii. formal kinetic study of the reaction of dgeba with diamino diphenyl methane. *Thermochimica Acta*, 560(0):95 – 103, 2013.

[124] Hongyang Caia, Peng Lia, Gang Suia, Yunhua Yua, Gang Lia, Xiaoping Yanga, and Seungkon Ryub. Curing kinetics study of epoxy resin/flexible amine toughness systems by dynamic and isothermal dsc. *Thermochimica Acta*, 473:101–105, 2008.

[125] Raju Thomas, Christophe Sinturel, Jürgen Pionteck, Harinarayanan Puliyalil, and Sabu Thomas. In-situ cure and cure kinetic analysis of a liquid rubber modified epoxy resin. *Industrial & Engineering Chemistry Research*, 51:12178–12191, 2012.

[126] D. Feldman and Dorina Banu. Kinetic data on the curing of an epoxy polymer in the presence of lignin. *Journal of Polymer Science Part A: Polymer Chemistry*, 26(4):973–983, 1988.

[127] Dorel Feldman and Marwan Khoury. Epoxy-lignin polyblends. part ii. adhesive behavior and weathering. *Journal of Adhesion Science and Technology*, 2(1):107–116, 1988.

[128] S.J. Shaw. *Chemistry and Technology of Epoxy Resins: Additives and modifiers for epoxy resins*. Springer, 1993.

[129] Alejandrina Campanella, Mingjiang Zhan, Paula Watt, Alexander T. Grous, Connie Shen, and Richard P. Wool. Triglyceride-based thermosetting resins with different reactive diluents and fiber reinforced composite applications. *Composites Part A: Applied Science and Manufacturing*, 72:192–199, 2015.

[130] Sushanta K. Sahoo, Smita Mohanty, and Sanjay K. Nayak. Synthesis and characterization of bio-based epoxy blends from renewable resource based epoxidized soybean oil as reactive diluent. *Chinese Journal of Polymer Science*, 33(1):137–152, 2015.

[131] Kristiina Alto-Korte, Outi Kuuliala, Maj-Len Henriks-Eckermann, and Katri Suuronen. Contact allergy to reactive diluents and related aliphatic epoxy resins. *Contact Dermatitis*, 72(6):387–397, 2015.

[132] G. Stenger. Materialcharakterisierung und prozessoptimierung papierbasierter bio-komposite. Master's thesis, Materialentwicklung von Bioadditiven als Beschleuniger in Harzsystemen, 2013.

[133] U. Herge. Basic material characterization of a novel paperbased biocomposite. Master's thesis, Materialcharakterisierung und Prozessoptimierung papierbasierter Bio-Komposite, 2012.

[134] H. Kröling, S. Mehlhase, J. Fleckenstein, N. Nubbo, A. Endres, S. Schabel, and F. Miletzky. Engineering and modelling of the tensile strength of paper-thermoset composites. *International Conference on Composite Materials*, 2013.

[135] H. Kröling, A. Endres, J. Fleckenstein, A. Miletzky, and S. Schabel. Anisotropy of paper and paper based composites and the modelling thereof. *European Conference on Composite Materials*, 2014.

[136] H. Kröning, J. Fleckenstein, N. Nubbo, A. Endres, F. Miletzky, and S. Schabel. Non-woven and paper based epoxy composites. *Science & Technology - Das Papier*, 2014.

[137] ISO. Plastics – determination of tensile properties – part 4: Test conditions for isotropic and orthotropic fibre-reinforced plastic composites. ISO 527–4:1997, International Organization for Standardization, Geneva, Switzerland, 1997.

[138] M.A. Vrana, J.G. Dillard, T.C. Ward, M.D. Rakestraw, and D.A. Dillard. The influence of curing agent content on the mechanical and adhesive properties of dicyandiamide cured epoxy systems. *The Journal of Adhesion*, 55(1-2), 1995.

[139] E. Sacher. Kinetics of epoxy cure: 3. the systems bisphenol-a epoxides/dicy. *Polymer*, 14(3):91–95, 1973.

[140] Michael D. Gilbert, Nathan S. Schneider, and William J. MacKnight. Mechanism of the dicyandiamide / epoxide reaction. *Macromolecules*, 24:360–369, 1991.

[141] T.F. Saunders, M.F. Levy, and J.F. Serino. Mechanism of the tertiary amine-catalyzed dicyandiamide cure of epoxy resins. *Journal of Polymer Science Part A: Polymer Chemistry*, 5:1609–1617, 1967.

[142] M. Fedtke, F. Domaratius, K. Walter, and A. Pfitzmann. Curing of epoxy resins with dicyandiamide. *Polymer Bulletin*, 31:429–435, 1993.

[143] Jocelyne Galy, Daniele Gulino, and Jean-Pierre Pascault. Study on the mechanism of 1-cynoguanidine cure of epoxy resins using model compounds. *Macromolecular Chemistry*, 188:7–19, 1987.

[144] Danuta Solecka and Alina Kacperska. Phenylpropanoid deficiency affects the course of plant acclimation to cold. *Physiologia Plantarum*, 119:253–262, 2003.

[145] Stephen C. Grace and Barry A. Logan. Energy dissipation and radical scavenging by the plant phenylpropanoid pathway. *Philosophical Transactions of the Royal Society of London*, 355(1402), 2000.

[146] Kushal Bahl. *Towards Development of Lignin Reinforced Elastomeric Compounds with Reduced Energy Dissipation*. PhD thesis, Ohio Tech, 2014.

[147] J. Barwich, D. Guse, and H. Brockmann. Curing of epoxy resins with dicyandiamide and monuran. *Adhasion*, 33(5), 1989.

[148] Thomas Günther and Benedikt Hammer. Curing of epoxy resins with dicyandiamide and urones. *Journal of Applied Polymer Science*, 50:1453–1459, 1993.

[149] S.K. Ooi, W.D. Cook, G.P. Simon, and C.H. Such. Dsc studies of the curing mechanisms and kinetics of dgeba using imidazole curing agents. *Polymer*, 41(10):3639–3649, 2000.

[150] H. Brockmann, M. Haufe, and J.O. Schulenberg. Mechanism of the curing reaction of model epoxy compounds with monuron. *Internation Journal of Adhesion and Adhesives*, 20(4):333–340, 2000.

[151] K. Raetzke, M.Q. Shaikh, F. Faupel, and P.-L.M. Noeske. Shelf stability of reactive adhesive formulations: A case study for dicyandiamide-cured epoxy systems. *Internation Journal of Adhesion and Adhesives*, 30(2):105–110, 2010.

[152] José P.S. Aniceto, Ines Portugal, and Carlos M. Silva. Biomass-based polyols through oxypropylation reaction. *ChemSusChem*, 5(8):1358–1368, 2012.

[153] Stephane Quideau and John Ralph. Facile large-scale synthesis of coniferyl, sinapyl, and p-coumaryl alcohol. *Journal of Agricultural and Food Chemistry*, 40(7):1108–1110, 1992.

[154] A. Walger. Materialentwicklung von bioadditiven als beschleuniger in harzsystemen. Master's thesis, Hochschule Darmstadt, Fachbereich Maschinenbau und Kunststofftechnik, 2014.

[155] NNFCC. Marketing study for current and potential market for lignin based materials., 2011.

List of Figures

List of Tables

Erklärung

Sabrina Mehlhase
Buchenlandweg 38
64295 Darmstadt

Darmstadt, den 16. März 2016

Ich erkläre hiermit, dass ich meine Dissertation selbstständig und nur mit den angegebenen Hilfsmitteln angefertigt habe.

Darmstadt, den 16. März 2016

(Sabrina Mehlhase)

Erklärung

Sabrina Mehlhase
Buchenlandweg 38
64295 Darmstadt

Darmstadt, den 16. März 2016

Ich erkläre hiermit, noch keinen Promotionsversuch unternommen zu haben.

Darmstadt, den 16. März 2016

(Sabrina Mehlhase)

Lebenslauf

Persönliche Daten

Name:	Sabrina Mehlhase
Adresse:	Buchenlandweg 38
	64295 Darmstadt
Geburtsdatum:	07. Februar 1985
Geburtsort:	Rüsselsheim
Familienstand:	verheiratet

Bildungsweg

Seit 12/2011	Wissenschaftlicher Mitarbeiter und Promotion: TU Darmstadt, Arbeitskreis Prof. Matthias Rehahn
10/2004 - 09/2011	Studium Chemie, Dipl. – Ing., TU Darmstadt Diplomarbeit: "Thermoplastische Elastomere aus Styrol und Butadien: Pfropf– statt Blockcopolymere"
09/2001 - 06/2004	Gustav–Heinemann–Schule, Rüsselsheim Abschluss: Allgemeine Hochschulreife
09/1995 - 07/2001	Anne–Frank–Schule, Raunheim

Darmstadt, den 16. März 2016

(Sabrina Mehlhase)